UNIVERSITÀ DEGLI STUDI DI PAVIA

DOTTORATO IN SCIENZE CHIMICHE E FARMACEUTICHE E INNOVAZIONE INDUSTRIALE
(XXXVI Ciclo)
Coordinatore: Chiar.mo Prof. Giorgio Colombo

Gaining health and energy from Lombard agrifood waste

Tesi di Dottorato di
Ilaria Frosi

AA 2022/2023

Tutor
Prof.ssa Chiara Milanese

Co-tutor
Prof.ssa Adele Papetti

SUMMARY

The project developed during my doctoral research focused on the valorization of agricultural waste products from the Lombardy region. Three different cereal waste materials (corn cob, rice bran and husk, and wheat production waste) and three vegetable waste materials (pumpkin and melon peels and asparagus bottom parts) were considered as potential sources of nutraceuticals with antiglycation activity and innovative materials for hydrogen storage. The thesis includes an introduction that provides an overview of the current state of the art in food waste utilization. It is then divided into two sections that reflect the two research areas of the project. Section I focuses on the research activities in the field of food. Initially, four different extraction techniques for each of the six matrices were compared to extract polyphenols, the main bioactive compounds found in botanicals. The six best performing extracts obtained for each matrix were tested for antiglycative and antioxidant activity, using different in vitro antiglycation assays that mimic the glycation reaction at various stages and the traditional DPPH and ABTS assays. The extract obtained from rice husk showed the highest overall activity and it was further chemically characterized. A targeted intestinal formulation was then developed for the creation of a rice husk-based ingredient. Section II, on the other hand, concerns to the energy sector, where the same matrices underwent pyrolysis and activation to produce biochar, that was characterized using various complementary physicochemical techniques. The use of a manometric instrument allowed the evaluation of the amount of hydrogen adsorbed and released from the materials and of the reaction kinetics, yielding promising results for each type of waste. The activated material from melon peels was found to be the most promising, with a hydrogen adsorption amount of 4.1 wt% and very rapid sorption kinetics.

Index

LIST OF ABBREVIATION

5-MQ: 5-methylquinoxaline

ABE-1: asparagus bottom parts extract obtained with CSE-HA

ABE-2: asparagus bottom parts extract obtained with MAE-HA

ABE-3: asparagus bottom parts extract obtained with CSE-NaDES

ABE-4: asparagus bottom parts extract obtained with MAE-NaDES

ABE: asparagus bottom parts extract

ABP: asparagus bottom parts

ABTS: 2,2'-azino-bis (3-ehtylbenzothiazoline-6-sulphonic acid) diammonium salt

AC: activated carbons

AFW: agrifood waste

AG: aminoguanidine hydrochloride

AGEs: advanced glycation end products

BBD: Box-Behnken Design

BET: Brunauer-Emmett-Teller

BI: bioaccessibility index

BSA: bovine serum albumine

CBE-1: corn cob extract obtained with CSE-HA

CBE-2: corn cob extract obtained with MAE-HA

CBE-3: corn cob extract obtained with CSE-NaDES

CBE-4: corn cob extract obtained with MAE-NaDES

CBE: corn cob extract

CC: corn cob

CGAs: chlorogenic acids

CPE: citrus peel extract

CQA: caffeoylquinic acids

CSE-HA: conventional extraction with hydroalcoholic solvents

CSE-NaDES: conventional extraction with natural deep eutectic solvents

DE: degree of esterification

DEYPP: de-esterified pectin form yuzu peel

DOE: design of experiment

DPPH: 2,2-diphenil-1-picryzil-hydrazyl

DSC: differential scanning calorimetry

EAE: enzyme-assisted extraction

EC: European community

ECs: electrochemical capacitors

EDX: energy-dispersive x-ray spectroscopy

EE: encapsulation efficiency

ES: emulsion stability

EtOH: ethanol content

EU: Europe

FBC: fat binding capacity

FTIR: Fourier transformation infrared spectroscopy

GHG: greenhouse gases

GLU: glucose

GO: glyoxal

GRAS: generally recognized as safe

HMP: high methoxyl pectin

IR: Infrared spectroscopy

KOH: potassium hydroxide

LC-MS/MS

LC: loading capacity

LMP: low methoxyl pectin

LOD: limit of detection

LOQ: limit of quantification

MAE-HA: microwave-assisted extraction with hydroalcoholic solvents

MAE-NaDES: microwave-assisted extraction with natural deep eutectic solvents

MAE-WA: microwave-assisted extraction with acidic water.

MAE: microwave-assisted extraction

ME: maceration extraction

MGO: methylglyoxal

MM: molecular mass

MP: melon peel

MPE-1: melon peel extract obtained with CSE-HA

MPE-2: melon peel extract obtained with MAE-HA

MPE-3: melon peel extract obtained with CSE-NaDES

MPE-4: melon peel extract obtained with MAE-NaDES

MPE: melon peel extract

Mw: molecular weight

NaDES: natural deep eutectic solvents

NBT: nitrotetrazolium blue chloride

NEPs: non-extractable polyphenols

NRF: Novel food regulation

OPA: orthophtaldialdehyde

OPD: orthophenylene diamine

PCT: pressure-composition-temperature measurements

PHWE: pressurized hot water extraction

Pi: polydispersity index

PLE: pressurized liquid extraction

PP: pumpkin peel

PPE-1: pumpkin peel extract obtained with CSE-HA

PPE-2: pumpkin peel extract obtained with MAE-HA

PPE-3: pumpkin peel extract obtained with CSE-NaDES

PPE-4: pumpkin peel extract obtained with MAE-NaDES

PPE: pumpkin peel extract

PPP: pumpkin peel pectin

RB: rice bran

RH: rice husk

RHE-1: rice husk extract obtained with CSE-HA

RHE-2: rice husk extract obtained with MAE-HA

RHE-3: rice husk extract obtained with CSE-NaDES

RHE-4: rice husk extract obtained with MAE-NaDES

RHE: rice husk extract

RSM: Response surface methodology

SBP: sugar beet pectin

SC-CO_2: supercritical carbon dioxide

SE: Soxhlet extraction

SEC: size exclusion chromatography

SEM: scanning electron microscopy

SFE: supercritical fluid extraction

SGF: simulated gastric fluid

SIF: simulated intestinal fluid

SLE: solid-liquid extraction

SPE: solid-phase extraction

SPI: soy protein isolate

SSA: specific surface area

SSR: solvent to solid ratio

SWE: sub-critical water extraction

T: temperature

t: time

TE: Trolox equivalents

TGA: thermogravimetric analysis

TMC: total metabolite content

UAE: ultrasound-assisted extraction

UAEP: ultrasound assisted extracted pectin

WC: water content

WHC: water holding capacity

WPE-1: wheat processing by-products extract obtained with CSE-HA

WPE-2: wheat processing by-products extract obtained with MAE-HA

WPE-3: wheat processing by-products obtained with CSE-NaDES

WPE-4: wheat processing by-products obtained with MAE-NaDES

WPE: wheat processing by-products extract

WPP: wheat processing by-products

XRPD: powder x-ray diffraction

Y: yield

YP: pectin yield

1. INTRODUCTION

1.1 Food waste: current state of art

Food waste is defined as a decrease in food quality and quantity due from decisions and actions of retailers, food service suppliers, and consumers (FAO, the State of Food and Agriculture, 2019). The main causes of food waste are the huge urbanization of the world population and the general food consumption behavior, which have led to an increase in organic waste production no longer sustainable. The Food Waste Index Report 2021 estimates that food waste globally produces 931 million tons each year, of which 52% from households, 23% from food service, and 23% from retail establishments (United Nations Environment Programm. Food Waste Index Report, 2021).

Today food waste is more than ever a challenge to face due to its nutritional, environmental, and economic impact on our lives. From a nutritional point of view, it still contains proteins, carbohydrates, lipids, vitamins, and phytochemicals which can potentially fulfill nutritional and healthy gaps. A recent review reported that the annual amount of food loss and waste can potentially provide a diet of 2100 kcal per day for 2 billion people (Capanoglu et al., 2022). This data is impressive, considering that FAO estimate 828 million people suffering from hunger in 2021, which were dramatically increased after the COVID-19 pandemic (FAO Global Hunger Report, 2022). Moreover, the disposal of these wastes causes serious environmental hazards, due to the emission of greenhouse gases (GHG) equal to around 3.3 billion tons of CO_2 per year accumulated in the atmosphere, contributing to impair climate emergency. In fact, common incineration of food waste increases air pollution by the production of dioxin, ash, and toxic gases as well as landfill disposal is one of the causes of groundwater contamination (Paritosh et al., 2017). Another crucial point is the economic effect of food wastage, which global cost amount to 1000 billion dollars annually. This quantity is expected to increase up to 2600 billion dollars if environmental costs are ignored. Among commodities, vegetables firstly contribute to the economic cost of food loss and waste (23% of total cost), followed by meat (21%), fruits (19%), and cereals (18%) (FAO, Food Wastage Footprint, 2013). Considering that the global population is expected to increase by about 2 billion persons by 2050 (United Nation site) the management of this problem is a serious and global issue that needs to be addressed. In this contest, Europe, has stated an action plan to prevent and reduce food loss and waste, as part of the 2030 Sustainable Development Agenda of the United Nation (EU Platform on Food Loss and Food Waste). Effectively, in December 2019 the European Commission announced the European Green Deal with the aim to transform the continent in the first climate neutral area by 2050, embracing policy for food waste reduction.

Prevention, reduction, and recycle are the first options to manage the problem. Nevertheless, valorization of food waste has gained increasing attention.

1.2 Valorization of food waste: upcycling

Valorization refers to the practice to convert the waste in value-added products, which became new raw materials. The term "upcycling" was recently born to denote this practice, introducing a new key concept in the circular economy strategy, and it was coined in opposition to recycling, which is generally identified as a "downcycling", the way of giving a second life to waste materials, with increased value and quality than before (Aschemann-Witzel et al., 2022). In food sector, trends report on upcycled food and ingredients predict a huge market potential (Capanoglu et al., 2022).

This is also supported by the recent birth of the Food Upcycled Association (UFA), the first non-profit American association focused on the prevention of food loss and waste across the entire supply chain by growing the upcycling economy (Upcycled Food Association 2022, report). The association gives firstly the definition of upcycled food as "*foods that use ingredients that otherwise would not have gone to human consumption, are procured and produced using verifiable supply chains, and have a positive impact on the environment*". Moreover, UFA gives the possibility to certify a food ingredient or product obtained from food waste, that allows the consumer to recognize an upcycled product with an on-package mark and allows the companies to have guidelines to produce a quality and safe product using food waste (https://www.upcycledfood.org/the-standard-1). This step is crucial to increase consumer acceptability of products made from wastage (Bath et al., 2021; Spratt et al., 2022) and confirms that food upcycling is not just a trend but a realty.

Despite the arousing interest on these products, some issues concerning the reintroduction of recovered agrifood waste (AFW) must be assessed before commercialization, including safety, biological instability, and potential contaminants, such as pesticides, pathogens, and toxins (Vilas-Boas et al., 2021). In Europe, the utilization of food waste and by-products as food ingredients or natural food additives is governed by European Community (EC) Regulation No. 178/2002, Article 2, as well as the guidelines established by Codex Alimentarius. When considering the use of food by-products as natural additives, it is imperative to ensure compliance with the existing regulations. If such by-products do not align with the current regulatory framework, obtaining proper authorization becomes necessary, specifically under Novel Food Regulation (NFR). The Novel Food Regulation (EU) 2015/2283 applies to foods and food ingredients that were not commonly consumed in the EU before May 15th, 1997. If the botanical preparations in question contain agricultural or A ingredients that were not part of

the traditional diet in the EU before this date, they could be considered novel foods. As a result, they would need to undergo a safety assessment and obtain proper authorization in accordance with the Novel Food Regulation before they can be legally marketed and used in food supplements or other food applications within the EU. Compliance with these regulations is essential to ensure the safety and legal status of such products.

1.3 Focus on upcycled polyphenols as new active ingredients for food application

Polyphenols are plant secondary metabolites and constitute the most considerable group of phytochemicals with health benefits. They can be generally classified in flavonoidic and non-flavonoidic compounds. As can be seen in Figure 1, flavonoids are characterized by a basic structure composed of a condensed bicycle with a third aromatic ring and can be divided into flavanols, flavonols, flavanones, flavones, isoflavones, anthocyanidins, and chalcones. The flavonols have a keto group in para in relation to the oxygen atom and are distinguished from flavones by the hydroxyl group in ortho. The isoflavones are isomers of the latter mentioned. Moreover, the anthocyanidins do not have the keto group differently from flavonols. Chalcones are the open-chain form of flavonoids, precursors for flavonoids or isoflavonoids. Considering the non flavonoidic polyphenols, stilbenes and phenolic acids (benzoic and hydroxycinnamic acid derivatives) are the most relevant compounds for healthy properties.

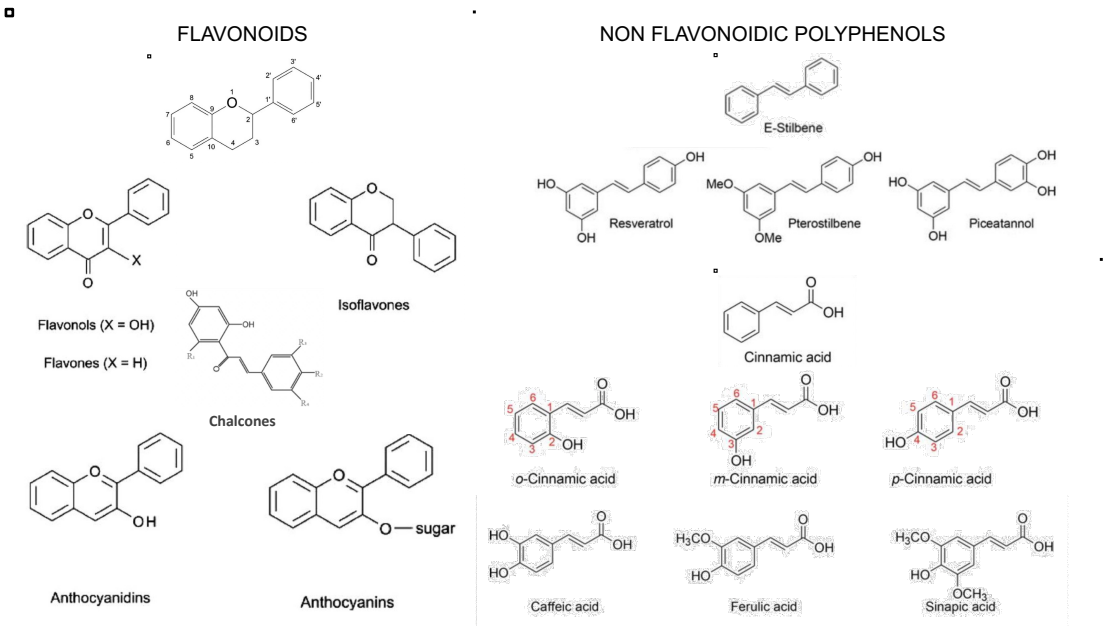

Figure 1. Chemical structures of flavonoidic and non-flavonoidic polyphenols.

Polyphenols are widely known to have different bioactivities which make them the main active ingredients in botanicals, i.e. antioxidant, antiglycative (Velinchova et al., 2023), anticancer, anti-inflammatory, cardio- and neuro-protective capacities (Rana et al., 2022).

Currently, fruit and vegetable peels, seeds, and pomace are widely studied as possible sources of polyphenols that can be used in the nutraceutical sector. The global ranking of waste generation estimates that AFW represents around the 25% of total industrial by-products, mainly coming from the production of wine and olive oil (actual core business of the Southern Europe). Grape pomace, the main by-product of winemaking, is generated in quantities equal to nine million tons per year worldwide. However, the vinification process is able to extract only 30-40% of the total polyphenols present in grapes (Mouritzinos et al., 2019). Several studies have highlighted the presence of various polyphenols in wine residues, including resveratrol, catechins, epicatechins, procyanidin, ellagic acid, quercetin, rutin, myricetin, kaempferol, malvidin, and peonidin, well-known for health benefits. On the other hand, olive pomace represents the main semi-solid waste generated from olive oil production, composed by olive skin, pulp, and bone. It is reported to be rich in polyphenols, such as hydroxytyrosol, tyrosol, oleuropein, caffeic acid, rutin, luteolin, and elenolic acid (Tapia-Quiros et al., 2022).

Additional sources of polyphenolic compounds come from the by-products of fruit juice industries, mainly apple, orange, and pineapple (Mir-cerdà et al., 2023). The main polyphenols present in apple by-products are catechins and proanthocyanins, followed by flavonols, hydroxycinnamates and dihydrochalcones, among which the distinctive phlorizin (Waldbauer et al., 2017). Orange residues are composed of pulp, peel, and seeds, which are still sources of naringenin, naringin, hesperidin, and rutin (Mouritzinos et al., 2019). Considering vegetables by-products, surprisingly onion is at the first position with more than 0.6 tons of waste produced from the European industrial peeling. The most important by-product is part of onion bulb and outer peels, which results to be rich in quercetin and kaempferol glycosides (Kumar et al., 2022).

These data suggest how AFW is still a source of bioactive compounds and can be reused as new raw materials. However, the extraction methods to recover these bioactives and their stabilization under gastrointestinal digestion are crucial aspects to be addressed to effectively exploit their benefits. These important considerations are discussed in the two following sections.

1.3.1 Innovative extraction methods to recover polyphenols from food waste

The choice of the extraction solvent and method are the first key step in successfully extracting metabolites. Temperature, time, and solid to solvent ratio are among the most common variables that affect phenolic recovery form a plant matrix. To optimize the extraction conditions, experimental design approaches (DOE) are powerful tools used to study different variables at the same time, investigating their impact on the extraction yields.

For many decades, solid-liquid traditional extraction (SLE) techniques have been used, which generally exploited the solvent extraction ability and the application of heat and/or mixing (Azmir et al., 2013; Castro-Lopez et al., 2017). SLE includes conventional approaches such as Soxhlet extraction (SE), hot water bath extraction, percolation, and maceration (ME). However, these strategies are quite expensive, due to the excessive consumption of time, energy, and high volume of solvents (Aamer et al., 2017). For these reasons, today they are commonly used as reference approaches to compare innovative methodologies (Azmir et al., 2013, Aamer et al., 2017). Currently, the development of eco-friendly processes to obtain high-value extracts and bioactives from food waste has gained prominence. They involve the use of GRAS (Generally Recognized As Safe) solvents, thus guaranteeing the absence of toxic solvents in the obtained final products, such as hydroalcoholic solvents or the innovative Natural Deep Eutectic Solvents (NaDES).

Some of the most effective techniques are considered, such as microwave-assisted extraction (MAE), ultrasound assisted extraction (UAE), supercritical fluid extraction (SFE), enzyme-assisted extraction (EAE), and pressurized liquid extraction (PLE). MAE is a promising technique to recover polyphenols from AFW because it is a rapid method to obtain high extraction yields with good reproducibility compared to the conventional methods (Aamer et al., 2017, Alara et al., 2019, Garofulic et al., 2020). This is possible because microwaves induce alteration at cellular level in the food matrix, promoting the formation of pores and fractures in cell walls and the subsequent fast release of phytochemicals. This mechanism has been demonstrated by SEM analysis performed after microwave irradiation on pomegranate peel (Kaderides et al., 2019), sunflower by-products (Nathia Neves et al., 2021), and cocoa bean shell (Mellinas et al., 2020). Microwaves generate heating by dipole rotation of polar solvent molecules and ionic conduction, which increase the pressure inside plant cells and cause their rupture (Florez et al., 2014; Vilas Boas et al., 2021). The main factors that affect the process are microwave power, extraction time and temperature, volume and nature of the solvent, and matrix characteristics. The solvent choice is the key step to obtain an efficient extraction process. The capacity of the solvent to absorb the microwave energy is directly linked to its dielectric properties, measured through the dielectric constant and dissipation factor (Florez

et al., 2014). Due to the thermolabile nature of polyphenols, the working temperature is another important parameter to be considered. These compounds are usually susceptible to thermal degradation at temperature above 70 °C in traditional extraction processes, leading to intramolecular isomerization or transesterification (Mouriznos et al., 2019). However, different studies show that the MAE short extraction time allows to use higher temperature without causing polyphenols degradation. In a study performed by Liazid et al. (2007), it was found that the highest concentration of caffeic acid, *p*-coumaric acid, ferulic acid, and sinapic acid was obtained at a power of 500 W by operating at a temperature of 50 °C for 20 min. Effectively, increasing the temperature to 100 °C did not yield any significant difference in the concentration of these acids. However, when the temperature was raised from 125 °C to 175 °C, there was a significant reduction in their concentration. These findings were further supported by the research of Mena-García et al. (2020), who observed a similar trend. They found that increasing the temperature of MAE from 50 °C to 120 °C for 3 min resulted in an enhanced recovery of phenolic compounds from artichoke waste, with the best outcomes at 120 °C. Similar results were reported for the recovery of polyphenols from tomato waste (Tranfić Bakić et al., 2019) and walnut leaves (Vieira et al., 2017), for which a temperature of 90 °C for 5 min and of 107 °C for 3 min of extraction was required for extracting the overall phenolic content, respectively.

UAE is another modern green technique used to extract polyphenols. It is faster compared to traditional SLE and allows lower extraction temperature and solvent volume enhancing the extract quality. Therefore, it can be considered efficient and low cost, as expensive instruments are not required (Alirezalu et al., 2020; Belwal et al., 2018). The absence of thermal effects makes UAE particularly suitable for extracting polyphenols. However, the main drawback of this technique is the challenge of scaling up the process, limiting its industrial application (Banozic et al., 2019). The extraction process consists in mixing the sample with a solvent and subjecting it to ultrasound waves at a controlled temperature (Mosic et al., 2021). Ultrasound waves enhance the extraction mechanism by generating cavitation bubbles, which eventually reach an unstable state and collapse, resulting in localized zones of high pressure and temperature (Lefebve et al., 2021; Panja et al., 2018). The frequency range of 20-200 kHz is recommended for most bioactive compounds to maximize the permeability of cell walls and induce cavitation (Alara et al., 2021). Specifically, the lowest frequency range (20-40 kHz) generates larger cavitation bubbles in the extraction solvents, effectively disrupting the plant cell walls and enhancing tissue permeability (Dzah et al., 2020). This facilitates the penetration of the solvent into the inner part of the material and enables easier the extraction of the desired compounds (Daud et al., 2022). Other researchers investigated the mechanical effect

of ultrasounds, studying the amplitude and ultrasound intensity, expressed as ultrasound power. Alves Filho et al. (2020) investigated the water extraction of chlorogenic acids (CGAs) from potato peel, with a specific focus on the ultrasonic power density, referring to the power transmitted per liter of solvent. They conducted the extraction under three different conditions: 20, 35, and 50 W/L. The milder conditions resulted in an enhanced extraction of 3,4-dicaffeoylquinic acid (diCQA) and 3,5-diCQA, while the extraction of tri-CQAs was not significantly improved, as they partially hydrolyzed to 3,4-diCQA. However, when exposed to a power density of 50 W/L, higher amounts of 3-CQA and 3-caffeoyl-4-feruloylquinic acid were extracted, which were not obtained without sonication and when applying the lowest power density. Unfortunately, under these conditions, 3,4-diCQA underwent hydrolysis, leading to the formation of 3-CQA. These findings underline the importance of carefully selecting appropriate values for power density and pH, considering the specific waste matrix and its phenolic composition. Other parameters that should be considered and optimized to maximize the extraction yield are solvent type and concentration, solid to solvent ratio, particle size, extraction time, and temperature (Christou et al., 2020).

Another powerful and sustainable extraction method is SFE (supercritical fluids extraction), which provides the use of GRAS solvents and low extraction times. SFE is based on the utilization of supercritical fluids (SF) as solvents. They possess characteristics of both liquids and gases; in fact, their high diffusivity, low viscosity, and density are similar to that of a liquid. This unique combination allows supercritical fluids to efficiently permeate solid materials, resulting in an enhanced rate of mass transfer and solute diffusion (Al Jitan et al., 2018, Anticona et al., 2020). The most widely used SF is carbon dioxide, which have several advantages, such as good solvent power, low cost, safe handling (GRAS status), easy to be removed by decompression and recyclability (Chemat et al., 2017; Panja et al., 2018; Lin et al., 2021). Supercritical CO_2 (SC-CO_2) extraction involves the use of carbon dioxide (CO_2) at temperatures and pressures above its critical point (31 °C and 7.38 MPa, respectively) to extract bioactive compounds. These specific conditions are essential for preserving thermolabile phytochemicals, such as polyphenolic compounds (Okoile et al., 2019). Generally, low polar and small molecules are easily soluble in SC-CO_2, while large and polar molecules are extracted with the addition of a co-solvent, such as ethanol, methanol, or water, which improves the extraction yield by hydrogen bonds, dipole-dipole or dipole induced dipole interactions with the solute (Essien et al., 2020). Effectively, Caballero et al. (2020) obtained improved recovery of CGAs from olive waste with the addition of ethanol as cosolvent (1:3 w/v) when extracted at 50 °C for 60 min in the 200-300 bar pressure range. The main parameters to be considered when using SFE for polyphenolic extraction are temperature,

pressure, co-solvent concentration, extraction time, and sample particle size. Slight temperature and pressure variations cause significant changes in SFE properties, because of their direct effect on compound solubility (Alara et al., 2020, Essien et al., 2020). By increasing temperature, SC-CO_2 has low-density solvent properties and the phytocompounds volatility improves (Uwineza et al., 2020). Similarly, increasing the pressure at a specific temperature leads to an increase in solvent density, thereby enhancing the solubility of polyphenols (Essien et al., 2020; Nagavakar et al., 2019). For every temperature, an increase in pressure is directly associated with an increase in SC-CO_2 density, which directly impacts the solubility of target solutes and consequently improves the extraction yield (Pellicanò et al., 2020). Effectively, in the study of Pellicanò et al. (2020) on the recovery of polyphenols from tomato skin by-products, the analysis of the impact of varying SFE pressure on phenolic acids showed a strong correlation between extraction and applied pressure. Increasing the pressure from 350 bar to 550 bar led to a 1.56-fold increase in the extraction yield of all phenolic acids, except caffeic acid. Furthermore, a significant 1.94-fold improvement in the extraction performance was achieved by applying 550 bar compared to lower pressures for ferulic acid. A similar trend was observed for *p*-coumaric acid, highlighting the key role of this parameter in successfully extracting polyphenols (Pellicanò et al., 2020). In general, the extraction yield tends to increase as the contact time between the solvent and solutes is prolonged until reaching an optimum operating time (Tyskiewicz et al., 2018). This extended contact time allows for improved penetration of SC-CO_2 into the matrix, leading to enhanced dissolution and interaction of solutes with SC-CO_2 over time (Tyskiewicz et al., 2018, Nagavekar et al., 2019). Additionally, sample particle size plays a crucial role in optimizing SC-CO_2 extraction. Smaller particle sizes can accelerate the extraction rate of solutes by increasing the specific interfacial area and reducing the diffusion path for solutes (Nagavekar et al., 2019).

PLE is an innovative technique widely used for the extraction of phenolic compounds, in particular flavonoids and anthocyanins from different plants (Avanza et al., 2021; Frosi et al., 2021). This extraction method uses high pressure to keep the extraction solvent in liquid form below its boiling point at the designated temperature, enhancing the mass-transfer rate and improving the solubility of bioactive compounds through the reduction of viscosity and surface tension (Aamer et al., 2017). PLE offers many advantages over traditional methods, including reduced solvent consumption, shorter extraction times, simplified operating procedures, and exclusion of light and oxygen during the process. One of the most environmentally friendly variations of PLE is known as Sub-critical Water Extraction (SWE) or Pressurized Hot Water Extraction (PHWE), which employs water as the extraction solvent. When water is heated to temperatures between 200-250 °C, its dielectric constant decreases and becomes like that of

organic solvents, making it highly polar. Consequently, SWE represents an effective alternative to organic solvents in certain applications (Xu 2017). Extraction solvent, temperature and pressure, time, matrix characteristics, and number of cycles are key factor to be considered in PLE (Xu et al., 2017; Aamer et al., 2017). The solvent must be chosen in relation to the affinity with analytes to be recovered and PLE efficiently uses GRAS solvents, such as ethanol and water, under high temperature and pressure conditions, providing high extraction yields in a short time (Frosi et al., 2021). Temperature can be applied from room temperature to 200 °C and pressure from 35 bar to 200 bar (Xu et al., 2017). The use of high temperature under reduced pressure generates thermal energy which helps to overcome molecular bonding forces between plant matrix and solvent molecules, leading to desorption (Aamer et al., 2017). High temperatures also improve the extraction efficiency by reducing the solvent viscosity and surface tension, which lead to an improved penetration in the sample matrix. However, the working temperature should be carefully controlled to avoid intramolecular modification and thermal decomposition or degradation of thermolabile compounds (Battistella et al., 2019; Nastic et al., 2020). Pagano et al. (2018) developed a PHWE to recover caffeoylquinic acids and flavone glycosides from artichoke by-products. They studied and optimized the main factors influencing the process efficiency and CQAs isomerization, such as temperature, number of cycles, ethanol concentration, and extraction time, using the response surface methodology. Results support that increasing the extraction temperature enhances the efficiency of PHWE by facilitating mass transfer and extraction rates. This is achieved through the increased capacity of water to dissolve analytes, accelerating diffusion rates, and reducing solvent viscosity and surface tension. However, it should be noted that the extraction efficiency of 1,5-diCQA exhibited a different trend. Initially, it increased up to approximately 100 °C, after which it started to decline. This decrease is likely attributed to the occurrence of intramolecular trans-esterification, which is promoted by the high temperatures. The highest polyphenolic recovery was obtained at 93 °C, 10% ethanol, 5 min of static extraction time and two extraction cycles (Pagano et al., 2018).

Finally, EAE is noteworthy as a suitable technique to enhance the recovery of non-extractable polyphenols (NEPs), i.e. polymeric or low molecular weight phenolics covalently linked to plant ligno-cellulosic components (Gligor et al., 2019; Dominguez-Rodriguez et al., 2021). In fact, according to the findings of Dominguez-Rodriguez et al. (2021), EAE provided sweet cherry pomace (*Prunus avium* L.) extracts richer in NEPs compared to those obtained by using the most common alkaline and acid hydrolysis procedure. EAE is also a sustainable alternative to conventional methods because it requires no organic solvents, can be performed under mild temperatures and pressures, and has a high substrate specificity. It is based on the use of

enzymes which catalyze a hydrolytic reaction acting on the structural components of plant tissues to release phytochemicals (Qadir et al., 2019, Nadar et al., 2019). Different steps are involved in the process, among which pulverizing the raw material, regulating temperature and pH, adding enzymes and incubating, inactivating enzymes, centrifuging and/or filtering, and collecting the aqueous phase of the enzymatic extract (Pontillo et al., 2021). The extraction efficiency is affected by key factors such as the type and concentration of enzymes, pH, incubation temperature and time, solid-to-liquid ratio, and particles size (Xu et al., 2017). Cellulose, hemicellulose, and pectin are typical cell walls polysaccharides which form stable complexes with bioactive compounds through hydrogen bonds or hydrophobic interactions. The plant matrix acts as a barrier to solvent diffusion, and the strong interactions mentioned earlier are responsible for the low extraction efficiency of phytochemicals from plant sources (Habeebullah et al., 2020; Saad et al., 2019). Carbohydrases like cellulase, pectinase, hemicellulase, and protease are widely used in EAE to facilitate the release of bioactives. Enzymes can be used alone for selective hydrolysis based on the localization of target compounds, or in combination with other cell-wall degrading enzymes to exploit synergistic effects, as seen in commercially available pre-formed enzyme blends (Qadir et al., 2019). For example, Qadir et al. (2019) used different commercial enzyme mixtures to recover phenolics from *Morus alba* leaves, and Zympex-014 enzyme mixture, containing various carbohydrase, amylase, and acid protease, showed the highest release of bound phenolics and resulted in an extract with higher antioxidant activity. pH is an important factor to consider as it affects enzymatic hydrolysis by modifying the protein configuration and binding capacity to substrates, which is specific to each enzyme (Nadar et al., 2018; Gligor et al., 2019). Moreover, pH can impact the dissociation of some bioactives, such as anthocyanins from *Kokum* rinds in acidic conditions or tannins from raspberry pomace in alkaline solutions (Saad et al., 2019). Extraction time and temperature also require investigation. Enzymes require a specific time to hydrolyze the plant material and prolonged extraction times may increase the release of other cellular constituents, thereby hindering the extraction of bioactives (Nguyen et al., 2021). Furthermore, temperature increase enhances enzymatic activity and reduces the viscosity of the extraction solvent, leading to higher bioactives solubility. However, extreme temperature values can gradually reduce the enzyme activity and degrade thermolabile phytochemicals (Gligor et al., 2019). EAE has certain technical limitations that impact its industrial-scale application, such as the high cost of enzymes and the low stability of their activity, which is sensitive to temperature and nutrient availability. To overcome these challenges, EAE is increasingly used as a pretreatment in combination with conventional extraction methods or more recent techniques such as UAE, MAE, and PLE. This combination

results in enhanced extraction yields, reduced extraction times, and lower enzyme costs (Xu et al., 2017, Pontillo et al., 2020). In line with these findings, Zuorro et al. (2019) investigated the recovery of flavonoids from corn husks using a sustainable extraction process. The process involved an enzymatic pretreatment of the plant material with cellulase, followed by heat-reflux extraction with aqueous ethanol. The enzyme and ethanol concentration, incubation time, and liquid-to-solvent ratio were optimized using a Box-Behnken design. In this case as well, the recovery of flavonoids was 30% higher compared to the use of a heat-reflux method.

1.3.2 Natural carriers to stabilize polyphenols: focus on food waste-derived pectin

Despite polyphenols are promising phytochemicals with several healthy benefits, they have some limitations mainly related to their solubility and bioaccessibility under the gastrointestinal tract. To overcome these drawbacks, different technologies have been studied by many research groups. Encapsulation is one of the most common techniques used to enhance the stability and shelf life of phenolic compounds (Mouritzinos et al., 2019). The most crucial parameters to be considered in the development of a such delivery system are: 1) the loading capacity (LC), indicating the mass of encapsulated material per unit mass of the carrier; 2) the encapsulation efficiency (EE), which measures the ability to retain the encapsulated material; 3) the release rate and mechanism, describing the ability to transport the functional component to its specific site of action (Mc Clements et al., 2015).

Polysaccharides, lipids, proteins, and mixed systems are among the most used carriers for the development of delivery systems. They show different encapsulation mechanisms, i.e. lipid and protein-based carriers exhibit distinct interaction patterns with bioactives, whereas polysaccharide-based carriers can effectively entrap bioactives by forming porous and highly stable networks. Detailed information can be found in a recent review published by our research group on the use of natural carriers for food active compounds (Frosi et al., 2022).

The utilization of novel carrier polymers derived from vegetable sources, particularly agricultural and food by-products, is gaining attention in response to the need of innovative sustainable ingredients (Cohen et al., 2017). Natural polysaccharides (such as starch, cellulose, gums, pectins, inulin, and soy polysaccharides) are particularly promising for this use due to their stability under high temperatures, differently from proteins and lipids, which often undergo denaturation and melting, respectively (Fathi et al., 2014). Moreover, these macromolecules possess a huge variety of modifiable functional groups, allowing for chemical functionalization in many ways depending on the intended application.

Among them, pectin has recently generated interest as it can be extracted from agricultural wastes, meeting the principle of circular economy. Pectin is composed of α (1,4) linked D-galacturonic acid residues and various neutral sugar molecules such as D-galactose and L-arabinose. According to EU regulation No. 231/2012, pectin is classified as food grade when the galacturonic acid content is at least 65% (https://www.emergenresearch.com/industry-report/pectin-market). Currently, commercial pectin (i.e. E440a for low-methoxyl pectin and high-methoxyl pectin and E440b for amidated pectin) is predominantly extracted from citrus peels (85.5%), apple pomace (14.0%), with a minor contribution from sugar beet pulp (0.5%) (Picot-Allain et al., 2022). However, due to the increasing interest in valorizing food by-

products and the high global market demand, researchers are nowadays focused on the extraction and characterization of pectin from various agro-industrial wastes, including mango and banana peels (Rivadeneira et al., 2020; Wongkaew et al., 2021), pumpkin and melon peels (Torkova et al., 2018, Medvedkov et al., 2021), cocoa pod husk (Pryangini et al., 2018), eggplant (Kazemi et al., 2019), tomato (Ninčević Grassino et al., 2020), and potato peels (Xie et al.,2018).

The degree of esterification (DE) refers to the number of methoxy groups substituting the carboxylic acid moiety on the galacturonic acid residues and it is a crucial factor influencing the mechanical and chemical properties of pectin, and therefore its application (Noreen et al., 2017; Rehman et al., 2019; Rodríguez Robledo and Castro Vázquez, 2020). Based on the DE value, pectin can be classified into high-methoxylated (DE > 50%), characterized by a high presence of methoxylated chains interconnected through numerous hydrophobic interactions, suitable as emulsifying and stabilizing agents, and low-methoxylated (DE < 50%), which forms gels in presence of calcium ions and is less sensitive to an acidic environment, making it more proper for encapsulation (Noreen et al., 2017; Rodríguez Robledo and Castro Vázquez,2020).

Different studies have shown that low-methoxylated pectin can be used to create carrier systems for delivering nutraceuticals with high encapsulation efficiency and loading capacity (Dib et al., 2022; Padma Ishwarya et al., 2022). The great advantage of using pectin as carrier agent is its resistance to protease and amylase hydrolysis during digestion (Rodríguez Robledo and Castro Vázquez 2020). Furthermore, pectin-based encapsulation systems have demonstrated controlled release of the encapsulated compounds, improving their availability for intestinal absorption, as observed in the study by Hu et al. (2017). In their research, citrus peel pectin was used to encapsulate a citrus peel extract (CPE) in a nano-system formed through the ionic gelation technique in the presence of calcium. The release kinetics of CPE and encapsulated CPE were compared after simulated gastric digestion. The data revealed that approximately 73% of flavonoids were released from CPE during the first 2 h of gastric digestion, reaching 100% release within the subsequent 4 h. In contrast, the release rate of encapsulated CPE accelerated with increasing pH. In fact, about 28% of flavonoids were released in the simulated gastric fluid, whereas 91% of release was registered after 22 h of digestion in simulated intestinal fluids (pH 7.5–8), probably due to the polysaccharide matrix relaxation which led to the release of entrapped flavonoids (Hu et al., 2017). This trend was further confirmed by Pamunuwa et al. (2020) and Goëlo et al. (2020), who established a correlation between environmental pH and the release rate of encapsulated phytochemicals.

Another point is that pectin is resistant to the gastric environment and human digestive enzymes, but it can be fully digested by colon microflora. Thus, pectin-based formulations can be applied for colonic targeting and probiotics encapsulation, through the addition of cross-linker such as polysaccharides (i.e. chitosan (Shishir et al., 2019) or oligochitosan (Lee et al., 2020)) or proteins (i.e. zein (Liang et al., 2022)), able to protect and stabilize the formulation until the intestinal district. Lee et al. (2020) performed a study in which hydrogel beads were developed for the delivery of quercetin using de-esterified pectin from yuzu (*Citrus junos*) peel (DEYPP) with Ca^{2+} cross-linking and the addition of oligochitosan. Hydrogel beads were prepared at different concentrations of DEYPP (1%, 1.5%, and 2% *w/v* pectin) to encapsulate quercetin using the mechanism of ionic gelation. *In vitro* release studies showed that the release of quercetin from the oligochitosan-DEYPP hydrogel beads in simulated gastric intestinal fluids was below 1% for all formulations. However, the release of quercetin significantly increased when the beads were exposed to simulated colon fluid for 12 h (i.e. 99.54% from 1% *w/v* pectin beads, 98.72% from 1.5% *w/v* pectin beads, and 65.37% from 2% *w/v* pectin beads). These findings indicated that the degree of biopolymer hydrolysis and the release of the active compound were affected by the DEYPP concentration. An enzymatic method was employed to develop a hydrogel based on sugar beet pectin (SBP) and soy protein isolate (SPI) for the delivery of *Lactobacillus paracasei* LS14 using laccase. SBP and SPI are well-known for their gelling properties, and by increasing their concentration in the formulation, a highly cross-linked gel was achieved with improved hardness and reduced swelling tendency. Different formulations were tested to optimize the SBP-SPI ratio, and an encapsulation efficiency of over 90% was obtained. The encapsulation of probiotics led to the formation of an irregular structure with enhanced rheological properties. The high concentration of SPI in the hydrogel formed a rigid honeycomb structure, which protected against pepsin and acid degradation in the gastrointestinal environment. Conversely, the encapsulated probiotic bacteria were rapidly released in the intestinal environment due to the ionization of free SBP and SPI carboxyl groups induced by the basic pH. This created a large osmotic force that promoted gel swelling and facilitated pancreatin permeation, resulting in matrix erosion. The SBP-SPI-based hydrogel demonstrated great potential for probiotic delivery, as supported by storage tests (Yan et al., 2020).

Overall, pectin can be considered a promising polysaccharide for the development of innovative controlled-release and colon-targeted delivery systems.

1.4 Production of biochar for energy applications

Food wastage can also be used for energetic purposes, starting with the production of biochar. Biochar is a carbon solid produced by the thermal treatment of organic biomass in absence of air (Rawat et al., 2023; Ismal et al., 2023). The common employed thermochemical technologies include combustion, gasification, and pyrolysis. Combustion involves the burning of biomass which is correlated to the release of pollutants in the air, while gasification converts biomass into a syngas mixture of carbon monoxide, hydrogen, and other gases. Among all, pyrolysis is the most common method and implies the thermal decomposition of biomass in absence of oxygen through the application of high temperature (from 250 °C to 900 °C) (Ismal et al., 2023). During pyrolysis, the lignocellulosic components of organic waste undergo various processes such as depolymerization, decomposition, and cross-linking at specific temperatures. The reaction stages include moisture removal at 100 °C, hemicellulose degradation at 200-260 °C, cellulose decomposition at around 240-350 °C, and eventually the breakdown of lignin at a temperature of approximately 280-500 °C (Yuan et al., 2021). As a result, the entire pyrolysis process eliminates all volatile components of the syngas (CO, CO_2, CH_4, etc.), thus leaving behind a solid residue of carbon materials (biochar) with a porous network and high specific area (Wang et al., 2014). The pyrolysis process conditions can be optimized to obtain biochar products with desired yield and quality, i.e. by altering key parameters such as heating temperature, residence time, heating rate, and particle size of the waste material (Ismal et al., 2023).

Effectively, the use of biochar for energy applications requires specific properties such as high surface area, high porosity, enhanced graphitization and determinate surface chemistry. In general, the specific surface area of biochar tends to increase if high pyrolysis temperature is applied. This means that higher temperatures during the carbonization process typically led to a greater surface area available for chemical reactions and adsorption. However, it is important to note that at extremely high temperatures there is a risk of shrinkage of the biochar matrix and pores (Rawat et al., 2023). Thus, to obtain electrode materials with high capacitive value the pyrolysis alone is not sufficient, and a correct activation of the biochar is required, which is typically achieved through physical or chemical methods. The physical activation of biochar is performed by altering the atmosphere during carbonization, commonly using CO_2 or NH_3. During the process, carbon on the surface or volatile compounds trapped in the pores are removed by the reacting gases. An increase in surface area and porosity is a common trend observed with higher activation temperatures. However, extensive biochar oxidation can result in a wider pore size distribution (Tan et al., 2017). In chemical activation, biochar is mixed with acids, bases, or oxidizing agents such as KOH, NaOH,

$ZnCl_2$, H_3PO_4, HNO_3, $KMnO_4$, or H_2O_2, followed by carbonization and removal of metal residues through acid washing. In comparison to physical activation, which removes carbon atoms from the surface in a non-selective way, chemical activation selectively removes the non-graphitic part of the carbon. Additionally, achieving the number of pores enhancement in physical activation requires a relatively higher activation temperature compared to chemical methods (Cha et al., 2016). To sum up, also depending on the type of chosen activation, biochar pores properties can be modulated to obtain microporous, mesoporous or hierarchical structures and in turn create biochar with desirable characteristics for different energy storage perspectives (Rawat et al., 2023). Surely, the production of biochar from low-cost and sustainable biomass represents a promising alternative precursor to produce activated carbon.

1.4.1 Electrochemical energy storage: supercapacitors

Currently there is an increasing interest in finding new renewable sources to produce energy, such as solar, wind, hydrothermal and geothermal. However, these sources require the implementation of energy storage devices to address the issue of intermittency in electricity supply. Rechargeable batteries and supercapacitors have emerged as the leading choices for electrochemical energy storage, offering high energy and power densities, respectively. For instance, these devices contain electrodes carbon materials thanks to the electrochemical properties of the allotropes, i.e. graphite, fullerenes, carbon nanotubes and graphene (Wang et al., 2018). Since agriculture and food wastes are composed of a carbonaceous skeleton of cellulose, hemicellulose and lignin and other heteroatoms (i.e. nitrogen, phosphorous, and sulphur), they could be promising eco-friendly and low-cost materials for energy storage devices as well as for other energetic applications, such as hydrogen storage, through the conversion into biochar.

The porous structure of activated biochar can facilitate the transfer of electrolyte ions, enabling enhanced electrochemical performances in energy storage systems. This feature allows biochar to effectively store and release energy, making it a promising electrode material for the development of supercapacitors. Electrochemical capacitors (ECs), also known as "supercapacitors" or "ultracapacitors," are electrochemical energy storage devices that fill the performance gap between capacitors and batteries in terms of power and energy densities (Senthil et al., 2021). Tian et al. (2018) studied the production of activated porous carbon from wild rice stems using a hydrothermal treatment followed by an activation process. The resulting porous carbon material exhibited a surface area of 1228 $m^2\ g^{-1}$ and demonstrated a specific capacitance of 301 $F\ g^{-1}$ at 1 $A\ g^{-1}$. These findings indicate that the

material has high energy density (13.05 Wh kg^{-1}) and power density (250 kW kg^{-1}). Other studies highlight the potential of food waste-derived materials for the synthesis of porous carbon with desirable properties for supercapacitor applications. Qu et al. (2015) used corncobs to prepare porous carbon using a pre-carbonization process followed by KOH activation. The resulting porous carbon derived from corncobs exhibited a surface area of 1210 m^2 g^{-1} and demonstrated a specific capacitance of 120 F g^{-1} at a current density of 1 A g^{-1}, using a 6 M KOH electrolyte. In addition, Wu et al. (2013) reported the synthesis of porous carbon derived from watermelon biomass. The process involved a hydrothermal treatment followed by an activation process. The resulting melon-derived porous carbon displayed a specific capacitance of 358 F g^{-1} at a current density of 0.5 A g^{-1} in a KOH electrolytic system. Furthermore, Zhang et al. (2018) successfully synthesized 3D hierarchical porous carbon from garlic skins using a simple chemical activation method. The resulting carbon material derived from garlic skins exhibited a high surface area of 2818 m^2 g^{-1}, creating hierarchical porous structures consisting of macro-, meso- (2-4 nm), and micro- (0.6-1 nm) porous frameworks. When used as an electrode, the garlic skin-derived carbon demonstrated specific capacitances of 427 F g^{-1} and 315 F g^{-1} at current densities of 0.5 A g^{-1} and 50 A g^{-1}, respectively. These impressive capacitance values can be attributed to the presence of the hierarchical porous structure, which provides ideal channels for ion diffusion and reduces migration resistance. It can be concluded that the presence of hierarchical pores in these materials effectively plays a crucial role in facilitating efficient electrochemical processes. Specifically, the micropores enable the accumulation of ions, the mesopores facilitate the transport and diffusion of ions, and the macropores contribute to adsorption and storage. This hierarchical pore structure helps reduce diffusion pathways and minimize diffusion resistance, ultimately enhancing ion transport within the supercapacitor, maximizing the capacitance value. Thus, a multimodal porous structure is highly desirable to achieve superior electrochemical performance in supercapacitors and biochars. Food waste have shown to be promising low-cost and innovative carbon-based materials that can be customized in term of physical and electrochemical properties for energy storage devices purposes (Rawat et al., 2023).

1.4.2 Hydrogen storage

Worldwide energy consumption increased from 1737 TW-h to 2373 TW-h in the period 2016 to 2021, which represents a 37 % increase over a five-year period (Ritchie et al. 2023). This trend will continue to grow in the following years due to the increasing world population, improvement of their living standards, the rapid industrialization, and the development of technological innovations. By 2022 global average temperature was 1.1 °C above pre-

industrial times (Provisional State of the Global Climate in 2022). The rise in the global average temperature is largely caused by the emission of GHG (CO_2, CH_4, N_2O and fluorinated gases). By 2021 worldwide CO_2 emissions account for 89 % GHG due to the combustion of fossil fuels (Global Energy Review: CO_2 emission in 2021) To address the environmental problems related to global warming an energy transition is urgently needed and thus, meet the objectives of the Paris Agreement of limiting average global temperature increase below 2° C. In this regard, the use of hydrogen, which is the most abundant element on earth, with the highest energy per mass (120 MJ/kg) of any fuel is considered a promising clean energy source.

Currently, hydrogen is obtained from non-renewable and renewable technologies. In the first case, H_2 is produced from fossil fuels via steam reforming, partial oxidation or gasification. In the latter case, H_2 generation take place via gasification of biomass/biofuels and water splitting (Dou et al., 2017). By 2021, it was estimated that 96% of global H_2 production came from non-renewable technologies (47% natural gas, 27% coal and 22% as by-product from oil) and only 4% was obtained from renewable sources (https://www.irena.org/Energy-Transition/Technology/Hydrogen). Although, significant efforts have been conducted to boost H_2 production from renewable energies (Wang et al., 2019; Medina-Llamas et al., 2023). The implementation of a hydrogen-based economy is hampered because there aren't suitable technologies for H_2 storage that can be safe, affordable and efficient. Consequently, the development of suitable materials for hydrogen storage is a key aspect for an ecological energy transition.

A recent innovative energetic application of biochar is hydrogen storage. Hydrogen is in a gaseous state at room temperature and needs to be converted into a compressed or liquefied state for storage, bringing attention to risk and reliability issue. Various techniques have been explored for hydrogen storage, including physical sorption methods using metal-organic frameworks (Shet et al., 2021) and carbon materials, such as biochar (Mohan et al., 2019). Zeolites are challenging materials to scale up because less ordered structures or mixtures of crystalline phases are obtained (Krishna et al. 2012). On the other hand, nanoporous carbon materials exhibit interesting properties, such as chemical stability, high thermal and electrical conductivity and high strength (Ma et al., 2020). Nanoporous carbon materials, such as activated carbons (ACs), have a microporous and mesoporous structure combined with a light weight, which is essential to ensure a low energy consumption during H_2 transportation. ACs with high specific surface area (SSA) have been widely used for water and air remediation (Collivignarelli et al., 2022) gas adsorbents (Sreńscek-Nazzal et al., 2019) and catalysts (Samikannu et al., 2019). ACs can be easily produced from biochar obtained from agricultural wastes such as coffee beans, rice husk, wood, corncob, etc (Illankoon et al., 2022) The

synthesis of ACs from agricultural wastes have several advantages since their precursors are abundant, easily available and usually considered as a material with no economic value.

The hydrogen storage capacity of carbon materials depends on factors such as temperature, pressure, specific surface area, and pore volume (Rawat et al., 2023).

Biochar is produced when biomass undergoes a thermochemical conversion process under an oxygen-free atmosphere at specific temperatures and pressures. During the process, the organic matter decomposes, leaving a carbon solid residue, along with an organic liquid known as bio-oil or tar and a mixture of gases consisting of hydrogen, carbon oxides and light hydrocarbons (Wang et al., 2020). ACs are prepared by the chemical activation of biochar using compounds such as: KOH, NaOH, $ZnCl_2$, HNO_3 or H_3PO_4. Among them, KOH is widely used as an activation material due to its lower activation temperature, higher yield, well-defined micropore size distribution and high SSA values ranging from 2000 – 3000 m^2/g (Wang. Et al., 2019). In general, it is agreed that the chemical activation mechanism using KOH take place via the overall reaction (Singh et al., 2023)

$$6KOH+2C \rightarrow 2K+3H_2+2K_2CO_3 \quad (1)$$

The set of consecutive reactions taking place during the activation of biochar using KOH have been previously reported (Lozano-Castelló et al., 2007; Otowa et al., 1993).

Dogan et al. (2020) developed a biochar from tangerine peel using KOH and $ZnCl_2$ which resulted in a hydrogen capacity of 0.2 wt% (at 25 °C, 30 bar) in $ZnCl_2$-activated biochar due to its increased specific surface area. The hydrogen sorption of the biochar occurs through Van der Waals interactions and shows a completely reversible ability. Deng et al. (2023) recently developed a biochar from corn straws by KOH melting activation, obtaining a high microporous ratio, exceeding 96.46%. Under suitable activation conditions, the specific surface area of the biochar reached 2801.88 m^2/g, and it displayed an absolute hydrogen adsorption capacity of 2.53 wt% at 1 bar, which increased to 5.32 wt% at 50 bar, both at -196 °C. During the KOH activation process, circular holes with a regular pattern formed on the surface of the biochar, gradually progressing from the inside to the outside. Furthermore, the thermal stability of the biochar increased with the activation temperature but decreased with the activation ratio.

Additionally, the introduction of heteroatoms on the biochar surface has been shown to enhance the hydrogen storage capacity, as occurred for the addition of oxygen to a biochar obtained from olive stone, previously activated by KOH and subjected to ozone oxidation (Schaefer et al., 2020).

Another point is that hydrogen (H_2) storage capacity of biochar-based materials is typically lower compared to metal hydrides such as MgH_2. Nevertheless, enhanced H_2 capacity has been observed when biochar is used as an additive during the ball milling process with Mg. This improvement is attributed to biochar ability to disperse the metal particles, to promote the conversion to metal hydride and to lower the temperature at which the hydride decomposition occurs. Recently, Zhang et al. (2022) prepared a biochar from grapefruit peel combined with MgH_2. The composite material combining metal hydrides and biochar has demonstrated remarkable reversible hydrogen storage capacity. In particular, the MgH_2 biochar composite exhibited an absorption of 6.13 wt% of H_2 at 225 °C and 30 bar H_2 pressure, which is comparable to pure MgH_2. Furthermore, the composite displayed a reversible hydrogen storage capacity above 98% for up to 10 cycles. In contrast, the dehydrogenation of pure MgH_2 led to the agglomeration of Mg particles, preventing rehydrogenation. These results were supported by another study conducted by Yeborah et al. (2020) who reported that the addition of 20 wt.% palm kernel shell derived biochar during the ball milling process of magnesium enhanced the hydrogen sorption of Mg by increasing the conversion of Mg into MgH_2 to 93% compared to 75% for milled MgH_2. This incorporation also resulted in a decrease of 40 °C in the MgH_2 decomposition temperature. From these studies it can be concluded that the porous structure of biochar effectively disperses the MgH_2 matrix and provides efficient channels for hydrogen transfer in the composites. Further exploration is required to better understand the relationship between pores structure parameters and the hydrogen storage capacity of biochar. This deeper understanding is necessary to effectively regulate the activation process and enhance the pore structure, to strengthen the hydrogen storage capacity of biochar.

ACs obtained from agricultural waste have been previously used for H_2 storage. For instance, Akasaka and co-authors (Akasaka et al., 2011) reported the production of ACs using coffee beans activated with KOH, the resulting material had a SSA of 2070 m^2/g and a H_2 storage capacity of 4.0 wt. % at 77 K. A similar approach was conducted by Komatsu et al. (Komatsu et al., 2021) using rice husk and KOH, the resulting material was able to store 7.2 wt.% H_2 when the AC was subjected to a rapid cooling step, while a 5.5 wt. % was obtained with a natural cooling step. Other raw materials such as tamarind seeds and almond shells showed H_2 storage capacities of 4.73 % and 2.53 wt. %, respectively at 77 K (Bicil et al., 2021). Another study by the present authors revealed that H_2 storage in rice husk biochar pyrolyzed at 950 °C and activated with KOH at 2:1 showed 2.3 wt.% at 77K and 6 bar (Illankoon et al., 2022). The former reports demonstrate the potential to use agricultural wastes for energy storage applications.

2. AIM OF THE WORK

The aim of this project supported by Cariplo Foundation Grant is to valorize Lombard AFW for food and energy applications to develop innovative value-added ingredients suitable for food supplements and find new carbon-based materials for solid state hydrogen storage.

Cereals and vegetables by-products were collected from local organic farms and selected considering region consumption, cultivation, and seasonality. Among cereals, corn cob, rice husk and wheat processing by-products were investigated as well as asparagus bottom parts, pumpkin and melon peels among vegetables. All the organic wastes were dried and powdered to obtain new raw materials.

Concerning food topic, four different green extraction methods were investigated and applied to each organic waste to obtain extracts rich in polyphenols. A conventional extraction approach was compared to an extraction method assisted by microwaves. Moreover, the efficiency of traditional different hydroalcoholic mixtures was studied in relation to different Natural Deep Eutectic Solvent mixtures (NaDES), novel solvents that have attracted considerable interest in the industry for their chemical inertness with water, easy preparation, and low cost. For each method, the influence of various parameters on the extraction yield was investigated using different designs of experiments (DOE) to optimize the extraction conditions. The richest extracts in metabolites obtained from each AFW was then tested for antiglycative and antioxidant activities, using different model systems and assays. Among the six extracts considered, the most active was chemically characterized and investigated for its potential use as food supplement ingredient. The extract bioaccessibility was evaluated using an *in vitro* simulated digestion protocol and an intestinal-targeted formulation was optimized to improve extract stability under gastrointestinal conditions. Rice husk and wheat processing by-products are not traditionally used for food applications, thus any product intended for this use undergoes to Novel Food legislation for the commercialization. To assess the potential use of a polysaccharide carrier extracted from food waste as encapsulating agent, pumpkin peel was evaluated as source of pectin.

In the frame of energy storage, to the best of our knowledge, there are no reports on the hydrogen storage capacity using the six organic wastes we focused on during my PhD research work.

The work scheme followed in this work is below summarized (Figure 2):

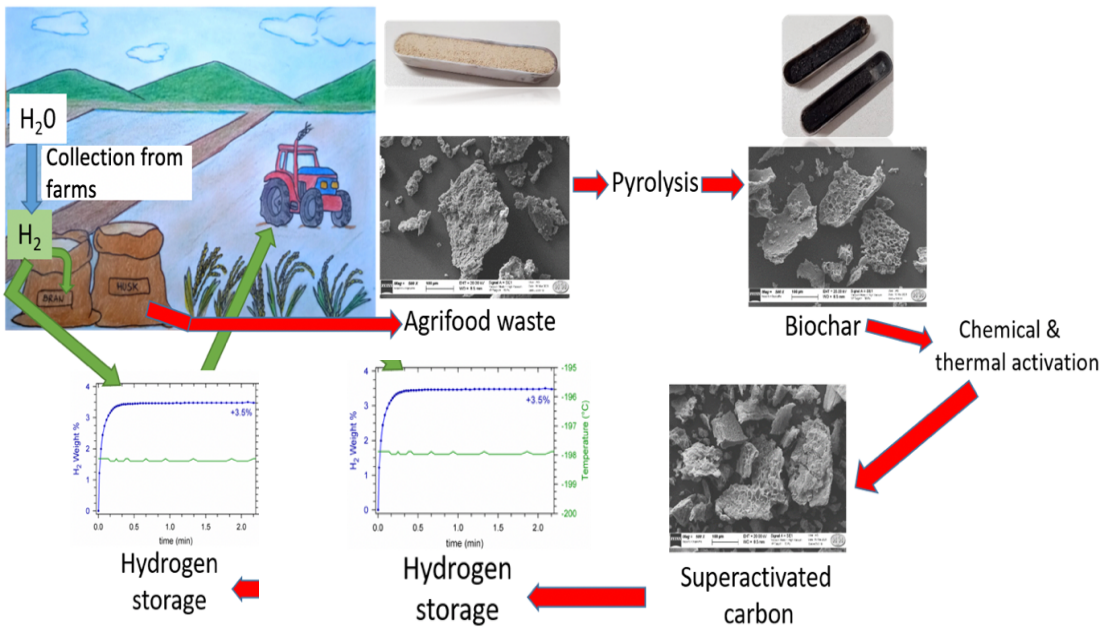

Figure 2. Working scheme from the farm to hydrogen storage.

Each AFW was submitted to pyrolysis, obtaining biochar, and subsequently converted to activated carbon (AC) through a chemical activation with potassium hydroxide (KOH). The carbon-based materials were physico-chemically characterized with different techniques before and after pyrolysis. Differential scanning calorimetry (DSC) and thermogravimetric analysis (TGA) were employed to evaluate the materials' stability at different temperatures. Additionally, Brunauer–Emmett–Teller (BET) measurements and scanning electron microscopy (SEM) imaging were used to examine the materials' porosity and morphology. Infrared spectroscopy (IR) and energy-dispersive X-ray spectroscopy (EDX) were used to investigate their chemical and elemental composition.

The effect of the weight ratio between the basis and biochar on the characteristics of the produced AC were explored concerning the hydrogen sorption performance. Finally, gravimetric and volumetric capacities and sorption kinetics were tested with the use of a manometric instrument.

3. MATERIALS AND METHODS

3.1 Chemicals

Ethanol 96% (v/v), disodium hydrogen phosphate dodecahydrate, sodium carbonate decahydrate and sodium bicarbonate were purchased from Carlo Erba (Milano, Italy). Methanol (ACS reagent, HPLC and HPLC-MS grade, purity grade ≥ 99,9%), formic acid (reagent grade, ≥ 95%, HPLC and HPLC-MS grade), choline chloride (purity grade ≥ 98%), urea (purity grade ≥ 99.5%), lactic acid (purity grade ≥ 90%), citric acid (purity grade ≥ 99.5%), glycerol (purity grade ≥ 99%), 1,2-propandiol (purity grade ≥ 99%), tartaric acid (purity grade ≥ 99.5%), acetic acid (purity grade ≥ 99.5%), D-(+)-glucose (GLU, purity grade >99.5%), 6-hydoxy-2,5,7,8-tetramethylchroman-2-carboxilic acid (Trolox C), 2,2-diphenil-1-picryzil-hydrazyl (DPPH), 2,2'-azino-bis(3-ehtylbenzothiazoline-6-sulphonic acid) diammonium salt (ABTS), nitrotetrazolium blue chloride (NBT), methylglyoxal (MGO, 40% aqueous solution), glyoxal (GO, 40% aqueous solution), 5-methylquinoxaline (5-MQ), *o*-phenylenediamine (OPD, grade purity ≥98%), *o*-phtaldialdehyde (OPA, grade purity ≥97%) bovine serum albumin (BSA, grade purity ≥98%), D(+) glucose (GLU, grade purity ≥98%,), aminoguanidine hydrochloride (AG, grade purity ≥98%), sodium hydrogen phosphate monohydrate, potassium hydrogen phosphate, sodium hydroxide pellets, sodium azide (grade purity 99.5%), sodium borate, sodium dodecyl sulphate (SDS), 2-mercaptoethanol (grade purity ≥99.0%), chlorogenic acid (CGA, grade purity ≥98%), *p*-coumaric acid (p-CA, grade purity, ≥ 98.0%), zein, type IV-porcine pancreatic α-amylase, pepsin from porcine gastric mucosa (≥ 400 U mg^{-1}), bile extract porcine, pancreatin (8 x USP) from porcine pancreas, protease from *Streptomyces griseus* type XIV (≥ 3.5 U mg^{-1}), Pectinex® Ultra SPL (aqueous solution ≥ 3800 units/mL) were provided by Merck KGaA (Darmstadt, Germany). Kaempferol-3-*O*-glucoside were purchased from Extrasynthese (Genay, Rhone, France). Genu®Pectin LM 102 AS was provided by Azelis Group NV. Pullulan GFC standard kit and Sep-Pak C18 cartridges (6 mL, 1 g sorbent) were purchased from Waters Corporation (Massachusetts, MA, USA). Water was obtained from Millipore Direct-QTM system (Merk-Millipore, Milan, Italy).

3.2 Plant materials

Corn cobs (CC), rice husks (RH), and wheat processing by-products (WPP) were obtained from local organic farms located in Pavia, Italy. To prepare the three cereals for further analysis, they were dried in an oven at 45 °C overnight until their moisture content reached approximately 1%. Subsequently, the dried cereals were ground into a fine powder, passing through a 500 µm sieve screen. CC were grated using an automatic grater (FILMAR mod.

GR12S23050M, 230V, 50Hz, 750W, Villa Verucchio, Rimini, Italy) and a coffee grinder (Moulinex coffee grinder, mod. MC300132, 220-240V, 180W). The latter was also used for powdering WP, while a chopping knife was used to grind RH. To ensure proper preservation, the samples were stored in amber glass bottles at 4-8 °C before the extraction process.

Among vegetables, melon peel (MP), pumpkin peel (PP), and asparagus bottom parts (ABP) were purchased from a local market, considering the biological origin of the wastes. They were freeze-dried and ground into powder using the coffee grinder to pass through a 500 µm sieve screen. To ensure proper preservation, also these samples were stored in amber glass bottles at 4-8 °C as for cereal by-products.

3.3 Polyphenols extraction methods

Four different extraction methods were investigated for each AFW, which procedure were reported in the sections 3.3.1 and 3.3.2. An extraction assisted by microwaves in acidic conditions was also developed and studied for the recovery of pectin from PP (see section 3.3.3).

3.3.1 Extractions with hydroalcoholic solvents

3.3.1.1 Conventional extraction (CSE-HA)

CSE was conducted using a thermostatic water bath (Memmert Dubnoff WNB 7-45/WNE) equipped with a stirring device (ENCO srl, Spinea, Venezia, Italy). Firstly, 500 mg of AFW powder was accurately weighed and placed into a flask. The extraction process followed specific operating conditions determined by experimental designs (refer to Tables 2 and 4), taking into account various parameters such as solid to solvent ratio (SSR), temperature (T), percentage of ethanol in the hydroalcoholic mixtures (EtOH %), and extraction time (t). Throughout the process, stirring was maintained at a constant speed of 80 stroke/min. Subsequently, each sample was filtered using a paper filter (Cordenons Technical Papers, 90 gsm). Ethanol was then evaporated under vacuum at 37 °C (using Buchi R-II rotary evaporator, Buchi, UK) until approximately 145 psi was achieved. The resulting aqueous suspension was freeze-dried (using Modulyo freeze-drier s/n 5101, Akribis scientific limited, Cheshire, UK) to obtain a solid product.

3.3.1.2 Microwave-Assisted Extraction (MAE-HA)

MAE process was carried out using a microwave apparatus equipped with a Teflon vessel system (Ethos LEAN, Sorisole, Italy). In the procedure, 500 mg of AFW powder was accurately weighed and placed into the extraction vessel. The extraction conditions were determined

based on experimental designs (refer to Tables 3 and 5), considering the impact of four parameters on the recovery of polyphenols from the AFW: solid to solvent ratio (SSR), temperature (T), percentage of ethanol in the hydroalcoholic mixtures (EtOH %), and irradiation time (t). The microwave power was initially set to a maximum of 800W for 5 min to reach the desired T, followed by using a maximum energy level of 500W to maintain the samples at the extraction T. After a ventilation period of 10 min, each sample was filtered using a paper filter (Cordenons Technical Papers, 90 gsm). Ethanol was then evaporated to obtain a solid product, following the same procedure applied to CSE.

3.3.2 Extractions with Natural Deep Eutectic Solvents (NaDES)

An initial screening phase was carried out by studying four different choline chloride (ChCl)-based NaDES in fixed conditions to select an effective green solvent system for the recovery of polyphenols from AFW. Lactic acid, urea, glycerol, and 1,2-propanediol were used as hydrogen bond donors (HBDs). The different NaDES were prepared as listed in Table 1, by mixing the components under magnetic stirring at 80 °C, until a transparent stable liquid was obtained (Dai et al., 2013). Distilled water (5%, p/v) was added to each mixture to facilitate the experimental operation.

Table 1. Natural Deep Eutectic mixtures (NaDES) used in the screening phase.

NaDES	Composition	Molar Ratio
NaDES-1	Choline chloride/lactic acid	1:2
NaDES-2	Choline chloride/glycerol	1:2
NaDES-3	Choline chloride/1,2-propanediol	1:2
NaDES-4	Choline chloride/urea	1:1

3.3.2.1 CSE-NaDES

CSE was performed in the same thermostatic water bath used for CSE-HA. Briefly, 500 mg AFW powder was weighed and accurately placed into a flask. The extraction was performed under operating condition determined by experimental designs (refer to Tables 2 and 4), considering the effect of different parameters: solid to solvent ratio (SSR), temperature (T), percentage of water in NaDES mixtures (WC), and extraction time (t). The stirring was kept constant at 80 stroke/min during the process. Then, each sample was filtered under vacuum and a solid phase extraction was performed to isolate the polyphenolic fraction (PF) from NaDES mixture. For this purpose, Sep-Pak C18 cartridge were used, following the procedure

defined by Kim et al. (2002), with some modifications. Firstly, the cartridge was activated by passing 10 mL of methanol through it, followed by an equilibration step using 10 mL of distilled water. Subsequently, 5 mL of the sample was loaded onto the cartridge. NaDES were eliminated by adding 10 mL of water, and the PF was collected using 10 mL of methanol. The organic solvent was then evaporated under reduced pressure at 40 °C using a Buchi R-II apparatus (Buchi, UK) and the resulting residue was used for subsequent experiments.

3.3.2.2 MAE-NaDES

500 mg of AFW powder was accurately weighed and placed into the extraction vessel of the microwave reactor. The instrumentation model and setting were the same used for MAE-HA. The extraction was performed under operating condition determined by experimental designs (refer to Tables 4 and 5), considering the influence of solid to solvent ratio (SSR), temperature (T), water content (WC) in NaDES mixture, and irradiation time (t) on the recovery of polyphenols from wastes. After a ventilation period of 10 min, each sample was filtered under vacuum and the solid phase extraction (see 1.3.3) was performed to isolate PF from NaDES mixture and the sample was treated as for CSE-NaDES.

3.3.3 Pectin MAE with acidic water (MAE-WA)

The same microwave apparatus used for MAE-HA and MAE-NaDES extractions was employed for the extraction of pectin from PP. For this procedure, 500 mg of PP powder was weighed and placed into the extraction vessel. The extraction conditions were determined based on experimental designs (refer to Tables 2 and 3), considering the influence of four different parameters on the recovery of pectin from PP: solid to solvent ratio (SSR), temperature (T), pH of acidic water, and irradiation time (t). Initially, the microwave power was set to a maximum of 500W for 5 min to achieve the desired T. Subsequently, an energy level of up to 500W was maintained to sustain the samples at the extraction T. Following a ventilation period of 10 min, each sample was filtered through two layers of gauze. The resulting extract was then subjected to centrifugation at 25 °C and 5000 rpm for 10 min. The obtained supernatant was mixed with ethanol (2:1, v/v) and kept overnight at 4 °C. In the next step, the mixture was again centrifuged at 4 °C and 5000 rpm for 20 min. The resulting precipitate was further purified by resuspending it in water and subsequently diluting it in ethanol until a white precipitate formed. The precipitate was then collected after a second centrifugation at 4 °C and 5000 rpm for 20 min. Finally, the obtained precipitate was dried in a hot air oven at 40 °C for 16 h.

3.4 Design of experiment (DOE) approach

The DOE approach was applied to optimize the extraction conditions of each AFW extraction process (see 3.3 par. Extraction methods).

3.4.1 Screening studies of process variables

Preliminary experiments were performed to determine the effect and the interactions of the operating extraction conditions in CSE and MAE processes with hydroalcoholic solvents (CSE-HA and MAE-HA, respectively) on the recovery of phenolic compounds from AFW. A 2^4 full factorial design was selected to study four independent variables, including solvent to solid ratio (X_1, SSR), temperature (X_2, T), percentage of ethanol (X_3, EtOH) in the extraction solvent, and time (X_4, t). A total of 19 experimental runs with three repetitions in the central point of experimentation were generated for both extraction systems. The considered response variable was the phenolic compounds yield, reported as total metabolite content (TMC) and expressed as the total area of the peaks registered in RP-HPLC-DAD chromatograms at 280 or 320 nm (depending on the wavelength with the highest intensity signal). The design matrix for the experiment and the regression model for the response was calculated as follows:

$$Y = \beta_0 + \sum_{i=1}^{n} \beta_i X_i + \sum_{1 \le i \le j}^{n} \beta_i X_i X_j + \varepsilon \quad (2)$$

where Y is the predicted response (yield), *n* is the number of variables, X_i and X_j the independent variables, β_0 define the fixed response at central point, β_i and β_{ij} are the linear and the interaction coefficients, and ε is a random error. Analysis of variance (ANOVA) was carried out to determine any significance differences ($p < 0.5$) among the applied extraction conditions. The general scheme of experimental model developed using Statgraphics statistical software is shown in Table 2, using +1 and -1 coded language, where +1 and -1 indicate the maximum and the minimum limits of the fixed range studied for each variable, respectively. It was applied for all the extraction methods which provided the use of hydroalcoholic solvents, except for asparagus bottom parts (ABP) and wheat processing by-products (WPP), for which an optimization phase was directly employed.

Table 2. Full Factorial Design 2^n for screening studies for the polyphenol's recovery from AFW. Coded variables.

Run (No.)	X_1	X_2	X_3	X_4
1	*-1*	*-1*	*-1*	*-1*
2	*-1*	*-1*	*-1*	*+1*
3	*-1*	*-1*	*+1*	*-1*
4	*-1*	*-1*	*+1*	*+1*
5	*-1*	*+1*	*-1*	*-1*
6	*-1*	*+1*	*-1*	*+1*
7	*-1*	*+1*	*+1*	*-1*
8	*-1*	*+1*	*+1*	*+1*
9	*+1*	*-1*	*-1*	*-1*
10	*+1*	*-1*	*-1*	*+1*
11	*+1*	*-1*	*+1*	*-1*
12	*+1*	*-1*	*+1*	*+1*
13	*+1*	*+1*	*-1*	*-1*
14	*+1*	*+1*	*-1*	*+1*
15	*+1*	*+1*	*+1*	*-1*
16	*+1*	*+1*	*+1*	*+1*
17	*0*	*0*	*0*	*0*
18	*0*	*0*	*0*	*0*
19	*0*	*0*	*0*	*0*

3.4.2 Response surface methodology

The response surface methodology (RSM) was used to optimize the extraction conditions of the extracts obtained from all the AFW studied. The most significant factors highlighted in the screening phase were considered and the response variable was maintained the polyphenolic compound yield determined by RP-HPLC-DAD analysis. The relationship among the variables is represented using a second-order polynomial model with coded independent variables (x_j, $_j$) that follows the reported equation:

$$Y = \beta_0 + \sum_{i=1}^{n} \beta_i X_i + \sum_{i=1}^{n} \beta_{ii} X_i^2 + \sum_{1 \le i \le j}^{n} \beta_{ij} X_i X_j + \varepsilon \quad (3)$$

where Y is the predicted response (yield), *n* is the number of variables, X_i and X_j are the independent variables β_0 define the fixed response at central point, β_i, β_{ii} and β_{ij} are the linear, quadratic and interaction coefficients, and ε is a random error. Analysis of variance (ANOVA) was carried out to determine any significance differences ($p < 0.5$) among the applied extraction conditions. The adequacy of the constructed quadratic model was assessed by on the coefficient of determination (R^2), adjusted (R^2_{adj}), and the prediction error sum of squares (PRESS). For all the considered RSM designs, three extra tests in duplicate were also carried out to verify the predicted data under the optimal conditions assessed by RSM-BBD.
The applied designs were different and reported below.

3.4.2.1 Box-Behnken Design

In this work the three-level Box-Behnken Design (BBD) was the most used method to optimize extraction conditions. RSM-BBD with three factors including three repetitions in the central point of experimentation generates a total of 15 experiments (Table 3).

Table 3. Box-Behnken Design with three factors for extraction of polyphenols from AFW. Coded variables.

Run (No.)	X_1	X_2	X_3
1	*-1*	*-1*	*0*
2	*+1*	*-1*	*0*
3	*-1*	*+1*	*0*
4	*+1*	*+1*	*0*
5	*-1*	*0*	*-1*
6	*+1*	*0*	*-1*
7	*-1*	*0*	*+1*
8	*+1*	*0*	*+1*
9	*0*	*-1*	*-1*
10	*0*	*+1*	*-1*
11	*0*	*-1*	*+1*
12	*0*	*+1*	*+1*
13	*0*	*0*	*0*
14	*0*	*0*	*0*
15	*0*	*0*	*0*

However, in the case of CSE-HA extraction of ABP and WPP, CSE-NaDES extraction of CC, RH, and MP, and CSE-HA of ABP and WPP was necessary to study four factors at the same time, generating a total of 27 experiments. Considering that the conventional extraction procedure involving the use of NaDES is quite laborious, it is not possible to perform all the extractions in a single day. This requires dividing the experimental design into 3 blocks of 10 extractions with two replicates at the central point for each block, a feature provided by the model to account for day-to-day variability, with a total of 30 experiments generated (Table 4).

Nevertheless, for CSE-HA of PP, ABP, and WPP some problems about the model validation arose as well as about the reproducibility of polyphenolic yields obtained from central points between different blocks for some matrices. Hence, there was a need to employ a less intricate and complex mathematical model, as could be the Draper-Lin small composite design.

Table 4. Box-Behnken Design with four factors for extraction of polyphenols from AFW. Coded variables.

Run (No.)	*blocks*	X_1	X_2	X_3	X_4
1	*1*	*-1*	*-1*	*0*	*0*
2	*1*	*+1*	*-1*	*0*	*0*
3	*1*	*-1*	*+1*	*0*	*0*
4	*1*	*+1*	*+1*	*0*	*0*
5	*1*	*0*	*0*	*-1*	*-1*
6	*1*	*0*	*0*	*+1*	*-1*
7	*1*	*0*	*0*	*-1*	*+1*
8	*1*	*0*	*0*	*+1*	*+1*
9	*1*	*0*	*0*	*0*	*0*
10	*1*	*0*	*0*	*0*	*0*
11	*2*	*+1*	*0*	*0*	*-1*
12	*2*	*-1*	*0*	*0*	*-1*
13	*2*	*+1*	*0*	*0*	*+1*
14	*2*	*-1*	*0*	*0*	*+1*
15	*2*	*0*	*+1*	*-1*	*0*
16	*2*	*0*	*-1*	*-1*	*0*
17	*2*	*0*	*+1*	*+1*	*0*
18	*2*	*0*	*-1*	*+1*	*0*
19	*2*	*0*	*0*	*0*	*0*
20	*2*	*+1*	*0*	*0*	*0*
21	*3*	*-1*	*0*	*-1*	*0*
22	*3*	*+1*	*0*	*-1*	*0*
23	*3*	*-1*	*0*	*+1*	*0*
24	*3*	*0*	*0*	*+1*	*0*
25	*3*	*0*	*-1*	*0*	*-1*
26	*3*	*0*	*+1*	*0*	*-1*
27	*3*	*0*	*-1*	*0*	*+1*
28	*3*	*0*	*+1*	*0*	*+1*
29	*3*	*0*	*0*	*0*	*0*
30	*3*	*0*	*0*	*0*	*0*

3.4.2.2 Draper-Lin small composite design

The Draper-line blocked cube star was chosen because it is a small composite design generally used to save time in long experiments and when there are unknown causes of errors. The model involves 20 experiments (Table 5), which are divided into two blocks considering the extraction procedure length. Therefore, compared to the BBD with 30 experiments, we have one fever block and 10 fever experiments. Therefore, it was then used to optimize CSE-HA of PP, ABP, and WPP.

Table 5. Draper-Lin small composite design blocked-cube stare for extraction of polyphenols from AFW. Coded variables.

Run (No.)	*Blocks*	X_1	X_2	X_3	X_4
1	*1*	*+1*	*+1*	*+1*	*-1*
2	*1*	*+1*	*+1*	*-1*	*-1*
3	*1*	*+1*	*-1*	*+1*	*+1*
4	*1*	*-1*	*+1*	*-1*	*+1*
5	*1*	*+1*	*-1*	*-1*	*+1*
6	*1*	*-1*	*-1*	*+1*	*-1*
7	*1*	*-1*	*+1*	*+1*	*+1*
8	*1*	*-1*	*-1*	*-1*	*-1*
9	*1*	*0*	*0*	*0*	*0*
10	*1*	*0*	*0*	*0*	*0*
11	*2*	*-1.68*	*+1*	*0*	*0*
12	*2*	*+1.68*	*+1*	*0*	*0*
13	*2*	*0*	*-1.68*	*0*	*0*
14	*2*	*0*	*+1.68*	*0*	*0*
15	*2*	*0*	*0*	*-1.68*	*0*
16	*2*	*0*	*0*	*+1.68*	*0*
17	*2*	*0*	*0*	*0*	*-1.68*
18	*2*	*0*	*0*	*0*	*+1.68*
19	*2*	*0*	*0*	*0*	*0*
20	*2*	*0*	*0*	*0*	*0*

3.4.2.3 Taguchi Orthogonal Array

The Taguchi Orthogonal Array was used to optimize the oral formulation to deliver the most promising extract obtained according to the results of bioactivity assays. For this purpose, a full factorial array analysis was chosen because of long time needed and because a level of precision in the result was not critically required. In this DOE (orthogonal array, commonly known as a factorial design 3*3-1) the necessary number of experiments was 9 deriving from 3 levels (L) x 3 replications (each level for each factor tested 3 times) (Cimbala, 2014). Two experiments in the central point were added, for a total of 11 runs, as shown in Table 6. It's important to note that orthogonal arrays represent the optimal and most used type of Taguchi array. It is advisable to opt for orthogonal arrays in the experiments whenever time and budget constraints allow. The selection of experimental test arrays is typically determined by striking a balance between the cost of conducting the experiments, which includes the time required to carry them out, and the precision of the results sought.

Table 6. Factorial design 3*3-1 for the optimization of the oral formulation. Coded variables.

Run (No.)	X_1	X_2	X_3
1	*-1*	*-1*	*-1*
2	*0*	*-1*	*0*
3	*+1*	*-1*	*+1*
4	*-1*	*0*	*0*
5	*0*	*0*	*+1*
6	*+1*	*0*	*-1*
7	*-1*	*+1*	*+1*
8	*0*	*+1*	*-1*
9	*+1*	*+1*	*0*
10	*0*	*0*	*0*
11	*0*	*0*	*0*

3.5 RP-HPLC-DAD analysis of polyphenolic compounds

RP-HPLC-DAD analyses were carried out to separate and identify the polyphenolic compounds in the extracts, and to perform a semi-quantitative analysis expressing the total metabolite content (TMC) as the total area of peaks recorded at three different wavelengths: 280 nm, indicative of flavonoids; 320 nm, characteristic of hydroxycinnamic acids; and 370 nm, representing hydroxybenzoic acids. The chromatograms were generated by simultaneously recording three wavelengths. However, for each AFW sample, only one reference wavelength was chosen to calculate the TMC, selecting the wavelength with the highest signal intensity absorption.

An HPLC Agilent 1200 system (Waldbronn, Germany) equipped with an online degasser for the mobile phase, a quaternary pump, a diode array detector (DAD), and a Gemini® C18 analytical column (150 x 2.0 mm i.d., 5 µm, Phenomenex, Torrance, CA, USA) was used. The system operated at a constant flow rate of 0.3 mL/min, with an injection volume of 20 µL. UV-Vis spectral data of the samples were acquired in the wavelength range 200-700 nm, and chromatograms were recorded at 280 nm, 320 nm, and 370 nm. The ChemStation software was used for data acquisition and processing.

The mobile phase consisted of two components: solvent A, composed of 0.1% formic acid in water, and solvent B, which was methanol. Different gradient methods were developed to analyze the extracts, depending on the AFW analyzed:

- CC and RH

The following gradient table was used for the separation: 0-10 min, 10-30% B; 10-20 min, 30-45% B; 20-30 min, 45-55% B; 30-35 min, 55-65% B; 35-40 min, 65-75% B; 40-45 min, 75-85% B; 45-48 min, 85% B, followed by a 12-min column reconditioning.

- MP and PP

The following gradient table was used for the separation: 0-40 min, 5-55% B; 40-50 min, 55-85% B; 50-53 min, 85% B; 53-60 min, 85-5% B, followed by a 10-min column reconditioning.

- ABP

The following gradient table was used for the separation: 0-40 min, 10-55% B; 40-50 min, 55-85% B; 50-53 min, 85% B; 53-60 min, 85-10% B, followed by a 10-min column reconditioning.

- WPB

The following gradient table was used for the separation: 0-20 min, 5-30% B; 20-30 min, 30-45% B; 30-35 min, 45-55% B; 35-40 min, 55-65% B; 40-48 min, 65-85% B; 48-55 min, 85-5% B, followed by a 5-min column reconditioning.

3.6 Antiglycative activity

3.6.1 Evaluation of Amadori products inhibition

Amadori products were quantified as fructosamine using the nitroblue-tetrazolium (NBT) salt assay, following the method described by Zhang et al. (2011) with slight modifications (Maietta et al., 2017). To prepare glycated material, bovine serum albumin (BSA) and glucose (GLU) were incubated in the presence and absence of the extract (0.5, 1 and 2.5 mg/mL) for 14 days. Subsequently, the glycated BSA (0.5 mL) was mixed with 0.3 mM NBT reagent (2.0 mL) in 100 mM sodium carbonate buffer (pH 10.35) at room temperature for 20 min. Fructosamine present in the systems can reduce NBT, leading to the formation of a tetrazolyl radical, resulting in the production of monoformazan (MF^+), a colored compound. The presence of MF^+ was then measured spectrophotometrically at 530 nm using a PerkinElmer Lambda 25 spectrophotometer. The inhibitory capacity of the extracts in generating fructosamine was calculated as follows:

$$inhibition\ \% = \left[1 - \left(\frac{Abs_{glycated\ sistem\ (BSA,GLU,extract)} - Abs_{background\ (BSA,extract)}}{Abs_{glycated\ system\ (BSA,GLU)} - Abs_{background\ (BSA)}}\right)\right] x\ 100 \quad (4)$$

The reported values are the means of three independent experiments, each performed in duplicate.

3.6.2 Evaluation of antiglycative capacities

The antiglycative capacities of extracts from AFW were assessed using the BSA-GLU system and the BSA-MGO system, following a slightly modified version of the method introduced by Mesías et al. (2013) and Maietta et al. (2017). In all experiments, aminoguanidine (AG) was used as a positive control. The freeze-dried extracts (at concentrations of 0.5, 1, and 2 mg dry matter/mL reaction mixture) were reconstituted in water. Simultaneously, BSA (35 mg/mL) and MGO (0.4 mg/mL) were dissolved in 0.1 M phosphate buffer, pH 7.4. To prevent microbial contamination, 0.02% (w/v) sodium azide was added to the buffer. Subsequently, a mixture consisting of 400 µL of BSA solution, 800 µL of the sugar or MGO solution, and 300 µL of extract solution or phosphate buffer (used as a blank) was prepared. This mixture was then subjected to incubation in a thermostatic bath at 37 °C (Memmert basic WNB, Schwabach, Germany). The time of the incubation varied based on the reactivity of GLU and MGO. For GLU systems, the incubation lasted 21 days, during which the formation of AGEs was weekly monitored. In the case of MGO systems, the incubation period was 7 days, and the measurements were

performed at 1, 4, and 7 days. At the end of each monitored incubation time, the reaction was stopped by placing the mixture in an ice bath for 15 min prior to the analysis. Samples dissolved in phosphate buffer were subjected to the same incubation periods as the reaction mixtures to determine their intrinsic fluorescence (background levels). The fluorescence intensity of mixtures without samples was used as a negative control. For GLU and MGO systems, the fluorescence of pentosidine-like AGEs (with excitation at 335 nm and emission at 440 nm) was recorded. In addition, in the case of MGO systems, the fluorescence of argpyrimidine-like AGEs (with excitation at 370 nm and emission at 440 nm) was also monitored (PerkinElmer L550B instrument). The inhibition percentage of AGEs formation was calculated at each incubation time using the following formula:

$$inhibition\ \% = \left[1 - \left(\frac{FI_{glycated\ sistem\ (BSA,GLU\ or\ MGO,extract)} - FI_{background\ (BSA,extract)}}{Fl_{glycated\ system\ (BSA,GLU\ or\ MGO)} - FI_{background\ (BSA)}}\right)\right] x\ 100 \quad (5)$$

where FI = Fluorescence intensity

The reported values are the means of three independent experiments, each performed in duplicate.

3.6.3 Evaluation of MGO and GO trapping capacity

The capacity to trap MGO and GO was assessed following a method initially proposed by Mesías et al. (2013) with slight modifications. A 100 µL sample of either 5.2 mM GO or 5.2 mM MGO (both dissolved in 100 mM phosphate buffer at pH 7.4) was combined with 50 µL of 6.1 mM 5-methylquinoxaline (5-MQ) dissolved in 50% (v/v) methanol solution, used as internal standard. Additionally, 100 µL of an aqueous solution obtained dissolving AFW dry extracts (at concentrations of 0.5, 1, and 2.5 mg dry matter/mL) or of phosphate buffer (used as a control) was added. The reaction mixture was then brought to a final volume of 1 mL by dilution with phosphate buffer. Subsequently, the mixture was incubated at 37 °C for 1, 24, and 48 h.

Following incubation, 200 µL of orthophenylene diamine (OPD) (10.8 mg/mL in phosphate buffer) was added to the mixtures which were subjected to a 30-min derivatization step at 37 °C. GO and MGO were quantified as quinoxaline and 2-methylquinoxaline, respectively, using a HPLC-DAD method. The analysis was performed using a Gemini® C18 analytical column (150 x 2.0 mm i.d., 5 µm, Phenomenex, Torrance, CA, USA) at a constant flow rate of 0.3 mL/min and an injection volume of 5 µL. Isocratic elution was performed using a solvent mixture consisting of a 50/50 v/v 0.5% acetic acid aqueous solution and methanol. Chromatograms were recorded at 315 nm.

Unreacted GO and MGO concentrations were determined from the ratio between the quinoxaline or 2-methylquinoxaline obtained through the conversion of GO and MGO, respectively, and 5-MQ, the internal standard. The percentage of MGO and GO trapped was calculated using the following formula:

$$GO\ and\ MGO\ decrease\ (\%) = \left(\frac{MGO\ or\ GO_{control\ sample} - MGO\ or\ GO_{sample}}{MGO\ or\ GO_{control\ sample}}\right) x100 \quad (6)$$

The reported values are the means of three independent experiments, each performed in duplicate.

3.6.4 Determination of free amino groups

The unreacted lysine groups in glycated materials after the sample incubation were determined using the *o*-phthaldialdehyde (OPA) assay (Fayle et al., 2011). The OPA reagent was prepared by combining 25 mL of 0.1 M sodium borate, 2.5 mL of 20% SDS, 100 µL of 2-mercaptoethanol, and 40 mg of OPA that had been previously dissolved in 1 mL of methanol. The resulting mixture was adjusted with water to reach a final volume of 50 mL. This OPA reagent was freshly prepared each day. To assess the availability of lysine, a 50 µL aliquot of the sample (containing glycated material generated in the BSA-GLU system in presence of the extract at final concentrations of 0.5, 1, and 2.5 mg/mL) was diluted at a 1:2 ratio with PBS. Subsequently, this diluted sample was added to 1 mL of OPA reagent directly in a 1 mL cuvette. The solution was mixed and then incubated for 2 min at room temperature. Following incubation, the absorbance was measured at 340 nm using a spectrophotometer, with a blank containing only the OPA reagent. Untreated BSA was used as control sample and considered to possess 100% free amino groups. Free lysine was calculated using the following equation:

$$Free\ lysine\ (\%) = \left(\frac{Abs_{control} - Abs_{sample}}{Abs_{control}}\right) x\ 100 \quad (7)$$

The reported values are the means of three independent experiments, each performed in duplicate.

3.7 Antioxidant activity

3.7.1 DPPH radical assay

The antiradical activity was assessed through the measurement of scavenging activity against the stable-colored DPPH (2,2-diphenyl-1-picrylhydrazyl) free radical (Maietta et al., 2018). One hundred µL of sample solutions at different concentrations (0.5, 1, 2.5, and 5 mg dry matter/mL) or of control solution (KH_2PO_4/NaOH buffer at pH 7.4) was combined with 3.9 mL of a DPPH radical solution in a 6 x 10^5 mol/L methanol/KH_2PO_4/NaOH buffer (50:50, v/v). The subsequent change in color of the mixture was tracked at 515 nm after 20 min of reaction using a spectrophotometer (Perkinelmer Lambda25). The degree of discoloration observed in the mixture corresponded to the scavenging activity against the DPPH radical. The antiradical activity was quantified using the following formula:

$$Anti - DPPH\ activity\ (\%) = \left(\frac{Abs_{control} - Abs_{sample}}{Abs_{control}}\right) x\ 100 \qquad (8)$$

This measurement provided insight into the ability of the samples to neutralize the DPPH radical and, thus, their potential antioxidant properties.

The reported values are the means of three independent experiments, each performed in duplicate. Methanolic solution of Trolox C in the concentration range 400-1000 µM were used for the calibration curve. Results were expressed as Trolox equivalent.

3.7.2 ABTS radical cation assay

The antiradical activity was assessed through the determination of the scavenging activity against the ABTS cation radical ($ABTS^{\bullet+}$), following a method outlined by Re et al. (1999) with slight modifications. In summary, an $ABTS^{\bullet+}$ stock solution was prepared by combining 7 mM cation radical with 2.45 mM potassium persulfate. This mixture was allowed to stand in darkness at room temperature for 16 h before being used. Subsequently, the solution was diluted using ethanol to obtain an absorbance of 0.70 ± 0.02 at 734 nm. For the experimental procedure, a 20 µL aliquot of the extract (at concentrations of 0.5, 1, 2.5, and 5 mg dry matter/mL) or ethanol (used as control sample) was added to 1 mL of the diluted $ABTS^{\bullet+}$ solution. The absorbance of the resulting reaction mixture was measured at 734 nm after a 10 min incubation period using a spectrophotometer (Perkin-Elmer Lambda 25). The capacity to scavenge the ABTS cation radical was determined by calculating the decrease in absorbance observed in the reaction mixture. This decrease in absorbance indicated the ability of the extracts to neutralize the $ABTS^{\bullet+}$ radical, thereby revealing their potential antioxidant properties. The calculation of this ability was performed using the following formula:

$$ABTS^{\bullet+} inhibition\ (\%) = \left(\frac{Abs_{control} - Abs_{sample}}{Abs_{control}}\right) x100 \quad (9)$$

The reported values are the means of three independent experiments, each performed in duplicate. Methanolic solution of Trolox C in the concentration range 300-1200 μM were used for the calibration curve. Results were expressed as Trolox equivalent.

3.8 Pumpkin Peel Pectin (PPP) characterization

3.8.1 Chemical characterization

3.8.1.1 Degree of Esterification (DE)

The determination of the degree of esterification of PPP was carried out using a titrimetric approach as detailed by Raji et al. (2017). Pectin dried sample (100 mg) was wetted with ethanol (2mL) and dissolved in 20 mL of deionized water at 40 °C. After 1 h of stirring, the pectin was completely hydrated and the solution was added of five drops of phenolphthalein indicator. Subsequently, the solution underwent titration with 0.1 M NaOH and the volume of NaOH solution required to induce a color change was recorded as the initial titer (V1). Next, 10 mL of 0.1 M NaOH was introduced and a vigorous agitation followed by a 15 min rest period was applied. Then, 10 mL of 0.1 M HCl was added and agitation continued until the disappearance of the pink color. The solution was finally titrated with 0.1 M NaOH, and the volume of NaOH solution used was noted as the saponification titer or final titer (V2). The degree of esterification (DE) was computed using the following formula:

$$DE\ (\%) = \left(\frac{V2\ (mL)}{V1\ (mL) + V2\ (mL)}\right) * 100 \quad (10)$$

3.8.1.2.1 Molecular weight (SEC-RID-HPLC analysis)

PPP average molecular weight (Mw) and polydispersity index (Pi) were assessed using size exclusion chromatography (SEC) with an Agilent 1200 chromatographic system coupled to a G7162A Refractive Index Detector (RID) from Agilent Technologies (Santa Clara, CA, USA). The mobile phase was a 0.1 M NaCl solution (w/v) containing 0.02% NaN_3 (w/v), which was filtered through a 0.45 μm Nylon membrane (Merck-Millipore, Milan, Italy). For the chromatography setup, an Ultrahydrogel™ 2000 column (12 μm, 7.8 mm × 300 mm) and an Ultrahydrogel™ 250 column (6 μm, 7.8 mm × 300 mm) from Waters Corporation (Milford, MA, USA) were connected in series and operated with a consistent flow rate of 0.8 mL/min. Both columns and

the detector were maintained at 40 °C. Calibration was performed using narrow pullulan standards in the range of 5 × 10^3 to 642 × 10^3 g/mol (Waters Corporation, Milford, MA, USA). Sample preparations involved dissolving PPP or pullulan standards in 0.1 M NaCl to achieve a final concentration of 1 mg/mL. Prior to injection, samples were filtered using a cellulose microporous membrane filter (0.45 mm, Merck-Millipore, Milan, Italy), and an injection volume of 50 µL was used.

3.8.2 Techno-functional properties

3.8.2.1 Emulsion stability

The study of emulsion stability (ES) for the pectin samples was performed in agreement with the methodology outlined by Mendez et al. (2021). Briefly, solutions of 1 and 3%, w/v, pectin samples were prepared by dissolving the powder in acidic water (pH maintained at 3). Oil-in-water emulsions were formulated by dispersing pectin aqueous solution in sunflower oil using a high-speed homogenization apparatus at 10000 rpm for 5 minutes (Ultra-turrax, IKA, Mullheim, Germany), testing two different oil concentration 35% (v/v) or 60% (v/v). The assessment of ES for the pectin samples involved the storage of the prepared emulsions at 4 °C for 1 and 6 days to test their stability. ES was subsequently calculated using the following equation:

$$ES\ (\%) = \left(\frac{Volume\ of\ remaining\ emulsion\ layer}{Initial\ volume\ of\ emulsion}\right) * 100 \qquad (11)$$

3.8.2.2 Water Holding Capacity (WHC) and Fat Binding Capacity (FBC)

The determination of water and oil (fat) holding capacities of the pectin samples was performed using a method adapted from Panwar et al. (2023) with minor adjustments. To outline the procedure, 200 mg of powdered pectin samples were combined with 2 mL of distilled water or sunflower oil, followed by vigorous vortexing for 1 min at room temperature. Subsequently, the solution underwent centrifugation at 4000 rpm for 20 min. The resulting supernatant was removed and the remaining residue was weighed. The water and oil holding capacities were quantified as the amount of water or oil retained per 1 g of pectin samples.

3.8.3 Structural features and thermal properties

3.8.3.1 Fourier transformation infrared spectroscopy (FTIR)

The Fourier-transform infrared (FTIR) spectra of pectin were acquired with a resolution of 4 cm^{-1}. The spectra were acquired using a Nicolet iS10 spectrometer (Thermo Fisher Scientific, USA) employing the KBr disk method in the range of 4000–450 cm^{-1}.

3.8.3.2 Thermal properties (TGA and DSC)

PPP thermal characteristics were analyzed through differential scanning calorimetry (DSC) and thermogravimetric analysis (TGA), adopting the methodology outlined by Panwar et al. (2023). In the DSC assessment, a small quantity of powdered sample was hermetically sealed within an aluminum pan and introduced into the analysis instrument (PerkinElmer, DSC 4000, UK). The measurements encompassed a temperature span from 0 to 300 °C.

Furthermore, the thermogravimetric analysis of the pectin samples was executed using a thermogravimetric analyzer (TGA 4000, PerkinElmer, USA) operating within a nitrogen environment. This analysis covered the temperature range of 50 - 600 °C, employing a heating rate of 10 °C per minute.

3.8.4 Rheological and mechanical properties

The rheological properties of pumpkin pectin (PP) samples were investigated using a Kinexus DSR Rheometer (Netzsch, Selb, Germany) equipped with a parallel-plate geometry (acrylic diameter 20 mm; gap 34 µm). Sample viscosity was measured using a flow step program, with increasing shear rates (0.001–1000 s^{-1}), to examine their non-Newtonian behavior and their tendency to exhibit shear-thinning.

To assess the storage (G') modulus PP, frequency sweep experiments were conducted as a function of angular frequency (0.1–100 Hz) at a fixed strain of 1%.

Each experiment was performed in triplicate, and data were processed using OriginLab software.

3.9 Rice husk extract (RHE) formulation

3.9.1 RHE chemical characterization by RP-HPLC-DAD-ESI-MS^n

Phytochemicals present in RHE were identified by LC-MS using a Thermo Finnigan Surveyor Plus High-Performance Liquid Chromatography (HPLC) apparatus from Thermo Fischer Scientific (Waltham, MA, USA). The HPLC system was equipped with a quaternary pump, a Surveyor UV-Visible photodiode-array detector, a Surveyor Plus autosampler, and a vacuum degasser. The system was connected to an LCQ Advantage Max ion trap spectrometer through an Electrospray Ionization (ESI) source. The analyses were carried out using the same column, mobile phase, and gradient used for rice husk extracts RP-HPLC-DAD analysis (see Par. 3.5). The ion trap spectrometer operated in a data-dependent mode, performing a full scan in the range of 50 to 1500 *m/z* (mass-to-charge ratio), as well as MS^n (multi-stage) scans to obtain fragment ions with a width of 35% and an isolation width of 3 *m/z*. For setting up the mass spectrometer parameters, chlorogenic acid and kaempferol-3-*O*-glucoside were used as reference compounds (100 ppm in 0.1% formic acid-methanol, 50:50, v/v) for flow injection analysis. The ionization polarity was set to both negative and positive modes. The sheath gas flow rate was adjusted to 20 arbitrary units (AU), while the auxiliary gas flow rate was set to 10 AU. The ionization voltage was maintained at 5 kilovolts (kv), and the capillary temperature was set to 300 °C. Data acquisition and processing were carried out using the Thermo Fischer Scientific Excalibur 2.1 software.

3.9.2 Polyphenols quantification in RHE by RP-HPLC-DAD analysis

The chromatographic method described in section 3.5 for RH analysis was subjected to validation following ICH guidelines for bioanalytical methods validation (ICH guidelines). Polyphenols in RH extract were quantified as *p*-coumaric acid (*p*-CA) equivalent content. Preliminary experiments were performed to investigate any potential matrix effects. To this purpose, *p*-CA calibration curves were constructed using *p*-CA dissolved in rice husk extract (RHE-2) and in an aqueous methanol solution (50:50, v/v). These two solutions were used to create two distinct five-point calibration curves in the concentration range 0.5 - 20 µg/mL; each point was analyzed in triplicate. Chromatograms were recorded at 320 nm. Injection volume: 10 µL.

Several key parameters were evaluated during the validation process:

1. **Specificity:** This was determined by comparing the chromatograms obtained for CA with those obtained for a blank solution (mobile phase).
2. **Selectivity:** The retention time of CA standard in aqueous methanol solution (50:50, v/v) was compared to the retention time of CA in RHE-2, recorded at 320 nm.

3. Linearity: Three CA calibration curves were constructed in three consecutive days within the range of 0.5-20 µg/mL. The integrated peak areas obtained at five different concentration levels (0.5 1, 5, 10, and 20 µg/mL) were plotted against the corresponding theoretical CA concentrations.
4. Intra-day Precision: This was assessed by triplicate analysis of the lowest, medium, and high CA concentrations (0.5, 5, and 20 µg/mL) for three consecutive days, with the relative standard deviation calculated for replicate analyses.
5. Accuracy: Recovery studies were conducted for CA at three different concentration levels (0.5, 5, and 20 µg/mL), each performed in triplicate.
6. Limit of Detection (LOD) and Limit of Quantification (LOQ): These parameters were estimated using a signal-to-noise ratio (S/N) of 3 and 10, respectively.

3.9.3 Preparation of RHE loaded zein-pectin hydrogel beads

Hydrogel beads composed of a pectin/zein complex were prepared using the ionic gelation technique. This involved the introduction of a pectin solution (0.5%, 1.75%, and 3%, w/v) into an ethanol solution (75%) containing zein and calcium chloride. The mixture was continuously stirred at room temperature. The concentrations of zein used in the ethanol solution were 1%, 5.5% or 10% (w/v), and the concentration of calcium chloride was 0.5%, 2.25% and 4 %(w/v). The formation of discrete pectin droplets was achieved through the utilization of a syringe. Following their production, these droplets were allowed to undergo a curing process during a 15-min period in the receiving phase. Subsequently, the droplets underwent washing steps using ethanol (96%) and milliQ water twice before being freeze-drying (Modulyo freeze-drier s/n 5101, Akribis scientific limited, Cheshire, UK). Ten different formulations were investigated using RSM (see section 3.4.2.3).

3.9.4 Determination of encapsulation efficiency

The encapsulation efficiency of the extract was assessed using the method proposed by Contado et al. (2020), with slight modifications. Briefly, 10 mg of freeze-dried beads were dissolved in 20 mL of methanol. After 10 min, 20 mL of an aqueous methanol solution (50:50, v/v) were added. The suspension was mixed using a magnetic stirrer for 4 h, followed by an additional hour at 37 °C in a thermostatic bath. The resulting solution was then centrifuged at 5000 rpm, 25 °C for 20 min and the supernatant was subjected to HPLC–UV analysis, as detailed in section 3.10.2.

The determination of the encapsulation efficiency (EE) of the extract was conducted by considering *p*-coumaric acid (*p*-CA) as the marker compound, being it the main constituent of the extract. This assessment was carried out using the following equations:

$$EE\ (\%) = \left(\frac{Actual\ amount\ of\ p{-}CA\ encapsulated\ in\ beads}{Initial\ amount\ of\ p{-}CA\ present\ in\ RHE\ encapslated} \right) * 100 \qquad (12)$$

3.10 In vitro gastrointestinal stability studies

The stability of pure and encapsulated RHE extract was evaluated using a static *in vitro* simulated digestion method. The procedure was conducted in accordance with established protocols, which were documented by Brodkorb et al. (2019) for simulated oral, gastric, and intestinal digestion, and by Zhang et al. (2011) for simulated colonic digestion.

During the simulated oral digestion phase, 2.5 mg/mL of RHE or RHE-loaded pectin/zein beads were exposed to 4 mL of simulated salivary fluid (SSF) electrolyte stock solution. The resulting mixture was diluted to 10 mL using ultra-pure water and 25 μL of $CaCl_2$ (0.3M) and stirred through a magnetic stirrer for 2 min. Following this, 8 mL of simulated gastric fluid (SGF) electrolyte stock solution, 1.25 mL of pepsin solution (80 mg/mL in chloride acid 0.1M) and 40 μL of $CaCl_2$ were added to the oral digestion mixture. The pH of the gastric digestion mixture was subsequently adjusted to 3.0±0.1 using 1 M HCl, then diluted to 20 mL with ultra-pure water. The mixture was subjected to incubation in a water bath shaker at 80 rpm, 37 °C for 2 h to simulate gastric digestion. Continuing the process, the gastric digestion mixture was supplemented with 16 mL of simulated intestinal fluid (SIF) electrolyte stock solution added with 100 mg of porcine bile, 1.25 mL of pancreatin solution (32 mg/mL in water) and 5 μL of $CaCl_2$. This mixture for intestinal digestion was diluted to 40 mL using ultra-pure water. The pH was adjusted to 7.0±0.1 using 1 M NaOH and 1 M HCl, and the mixture was incubated in a water bath shaker at 80 rpm, 37 °C for 2 h to simulate intestinal digestion. For the simulation of the colonic digestion phase, the intestinal digestion mixture was combined with 2.5 mL of protease (1mg/mL) and incubated for 1 h in the water shaker bath at 30 rpm. After that 3 mL/L of Pectinex Ultra SP-L (a blend of pectinases, hemicellulases, and beta-glucanases) was added and the mixture was then subjected to incubation in a water bath shaker at 30 rpm, 37 °C for 16 h.

At the end of each phase, the sample was heated in a water bath at 90 °C for 5 min in order to inactivate the enzymes. Then, they were centrifugated at 5000 rpm, 25 °C for 10 min and

the supernatants were freeze-dried, thus obtaining a ready-to-use powder for bioaccessibility studies.

3.11 Bioaccessibility evaluation

The amount of soluble polyphenols in each collected fraction deriving from both RHE and encapsulated RHE digestion was indicative of the sample portion potentially available for absorption. To assess bioaccessibility, the freeze-dried samples obtained after the digestion process (see section 3.11) were reconstituted using an appropriate volume of 0.1% formic acid and methanol, 50:50, v/v (used as mobile phase in the chromatographic analyses). Subsequently, the mixture was filtered through 0.45 mm RC syringe filters (Phenomenex, Torrance, CA, USA) before RP-HPLC analysis (following the validated method described in section 3.10.2). The determination of the bioaccessibility index (BI) was based on the measure of the peak areas corresponding to *p*-CA. The results were calculated as follow:

$$BI\ (\%) = \left(\frac{Amount\ of\ p{-}CA\ solubilized\ after\ each\ digestion\ step}{Initial\ amount\ of\ p{-}CA\ present\ in\ RHE\ before\ digestion} \right) * 100 \qquad (13)$$

3.12 Characterization and production of biochar

3.12.1 Activation with KOH

The different organic wastes were pyrolyzed in a tubular furnace under N_2 flux (50 mL/min). Two pyrolysis conditions were tested: 10 °C/min up to 650 °C or up to 950 °C with an isothermal step of 12 h, followed by a cooling step at 10 °C/min until room temperature.

Pyrolyzed samples were mixed with KOH at different weight ratios KOH: Biochar (6:1 and 2:1). The mixture was subjected to a two-step thermal treatment using a tubular furnace under N_2 flux. The first step was 350°C at 3 °C/min and 1 h dwell. In the second step the temperature was increased up to 650°C at 5 °C/min and kept 2 h dwell. The cooling step took place at a rate of 10 °C/min until room temperature.

Through the activation process, the decomposition of KOH and the removal of C, Si and other elements take place simultaneously.

$4KOH + C \rightarrow K_2CO_3 + K_2O + 2H_2$ (14)

$2KOH \rightarrow K_2O + H_2O$ (15)

$C + H_2O \rightarrow H_2 + CO$ (16)

$CO + H_2O \rightarrow H_2 + CO_2$ (17)

$K_2O + CO_2 \rightarrow K_2CO_3$ (18)

$H_2O + H_2 \rightarrow 2K + H_2O$ (19)

$K_2O + C \rightarrow 2K + CO$ (20)

$K_2CO_3 + 2C \rightarrow 2K + 3CO$ (21)

$K_2O + SiO_2 \rightarrow K_2SiO_3$ (22)

From equations (14) - (22) described above, the biochar generates several intermediates by the reactions between C and KOH, which further decompose at higher temperatures and are released as various by-products gases (Otowa et al., 1997; Senthil et al., 2021).

The gas emitted by the by-products contributes to the formation of a porous structure and a high surface area for the biochar. The obtained material was washed with 100 mL 0.5 M HCl solution under magnetic agitation for 1 h. Next, the materials were filtrated and rinsed with distilled water until its pH was close to 7. The samples were dried in an oven at 80 °C for 24 h.

3.12.2 TGA, DSC and IR

Thermogravimetric analysis (TGA) was conducted to determine the pyrolysis temperature of the wastes, coincident with the temperature at which all the organic compounds are decomposed (TGA Q5000, TA Instruments Inc., USA). The experimental conditions were from

45 °C to 1000 °C at 10 °C/min under N_2 flux (10 ml/min). Differential scanning calorimetry (DSC) was performed to study the evolution of the decomposition by a Q2000 apparatus (TA Instruments, New Castle, DE, USA) interfaced with a TA5000 data station under nitrogen flux (10 mL min–1) in an aluminum pan by heating about 3 mg of sample from -80 °C up to 350 °C (heating rate 10K min–1), cooling down to -80 °C and heating to 25 °C. The onset temperatures were defined by the Data Analysis software by TA Instruments. FTIR analyses were conducted by a Nicolet FTIR iS10 spectrometer (Nicolet, Madison, WI, USA) equipped with Smart iTR with diamond plate. The analyses were performed by collecting 32 scans from 4000 to 600 cm^{-1} and 4 cm^{-1} of resolution.

3.12.3 EDX, SEM and BET

Surface morphology was analyzed using a scanning electron microscope (Zeiss EvoMA 10 SEM) with an acceleration voltage of 20 kV and 8.5 mm working distance. Prior the analysis the samples were sputtered with gold. As well, energy dispersive X-ray spectroscopy (EDX, Oxford) was used for identifying the elemental composition of the samples. Porosimeter analyses were conducted by BET measurements via a Sorptomatic 1990 Instrument, ThermoFisher Scientific. The total pore volume was analyzed by the amount of N_2 adsorbed at relative pressure (P/P_0 = 0.99).

3.13 Manometric analysis

The hydrogen storage capacity of the samples was evaluated via a PCTPro2000 manometric instrument by Setaram (France). The experiments were carried on about 500 mg of sample at – 196 °C in a pressure range 0 - 20 bar. As a pre-treatment step, the samples were heated up to 120 °C under vacuum. For the kinetic measurements, H_2 was injected until the pressure reached 6 bar. For the pressure composition isothermal measurements, the hydrogen pressure increased by small aliquots from 0 to 20 bar. High purity H_2 (99.9999 %) was used to minimize the effect of moisture or other contaminants. All data were collected in an automatic mode to ensure reproducibility. Blank experiments were performed to identify leaks in the system. For the analysis it is assumed that the amount of H_2 stored in the sample at the beginning of the experiment is zero.

4. RESULTS AND DISCUSSION

SECTION I: FOOD

4.1. Optimization of corn cob extract (CBE)

Table 7 presents the outcomes of the screening phase for the conventional extraction method with hydroalcoholic solvents (CSE-HA). The considered experimental ranges (-1; +1) were: EtOH 20-80%, T 30-60 °C, t 10-60 min, SSR 15-30 mL/g. The results are expressed as the total metabolite content (TMC) yield values. 320 nm was chosen as wavelength to calculate the TMC, considering the higher intensity signal compared to the others.

Table 7. Full Factorial Design 2^n for CSE-HA extraction of polyphenols from corn cob. Actual variables.

Run (No.)	EtOH (%)	T (°C)	t (min)	SSR (mL/g)	TMC (mAu*s) (at 320 nm)
1	20	30	10	15	27097.5
2	20	30	10	30	47399.7
3	20	30	60	15	35029.3
4	20	30	60	30	58508.5
5	20	60	10	15	37337.3
6	20	60	10	30	58821.6
7	20	60	60	15	30898.2
8	20	60	60	30	91797.2
9	80	30	10	15	95120.2
10	80	30	10	30	12305.8
11	80	30	60	15	85018.0
12	80	30	60	30	161756.5
13	80	60	10	15	100746.0
14	80	60	10	30	151033.5
15	80	60	60	15	107818.9
16	80	60	60	30	220140.2
17	50	45	35	22.5	133278.9
18	50	45	35	22.5	133469.9
19	50	45	35	22.5	133365.4

TMC ranged between 27097.5 and 220140.2 mAu*s. The lowest values were obtained for run #1, characterized by lowest ethanol concentration (20%), T (30°C), t (10 min), and SSR (15

mL/g); conversely, the highest values were obtained for run #16, characterized by highest EtOH concentration (80%), T (60 °C), t (60 min), and SSR (30 mL/g). To understand the significance and statistical relevance of the factors examined in the model, including linear, quadratic and interactive impacts, a standardized Pareto Chart diagram (Figure 3) has been used. This diagram visually portrays the relative contributions of all the considered variables.

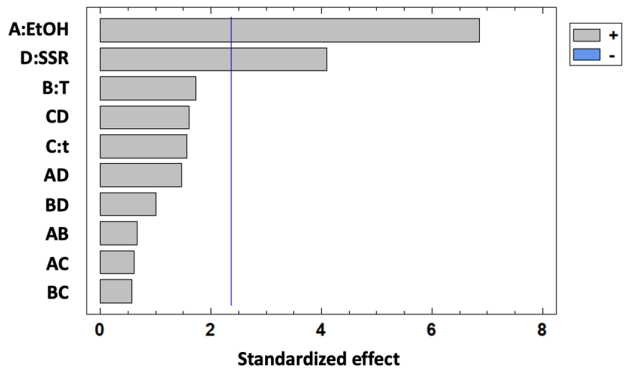

Figure 3. Standardized Pareto Chart constructed for TMC yield in CSE-HA screening phase. The positive and negative effect of the factors (reported as horizontal bars) on the response variable (TMC) is represented in grey and blue, respectively. The blue vertical line tests the significance of the effect at the 95% confidence level.

All the considered variables had a positive effect on the response, as evidenced by the grey horizontal bars in the chart. However, among these variables, only the EtOH percentage (A: EtOH) in the extraction mixture and SSR (D:SSR) had a significant effect on the yield. Conversely, alterations in T and t did not bring about a substantial variation in the extraction yield, despite their positive impact. Previous studies, such as those conducted by Lao et al. (2018) on pigmented corn cob and Das and Dewanjee (2018) on rice bran, reported similar extraction performances. In fact, these studies indicated that higher polyphenolic recoveries were achieved with increasing EtOH concentration in the hydroalcoholic solvent, up to a certain threshold. EtOH helps in the release of bioactives by disrupting bonds between solutes and plant matrix, while the presence of water in the extraction mixture promotes swelling of the plant matrix (Das and Dewanjee, 2018; Lao et al., 2018; Frosi et al., 2021). In contrast, SSR is responsible for generating a mass transfer gradient that facilitates the release of polyphenols. This step plays a key role in this type of extraction process.

The positive effect of T can be explained as it promotes the vegetable tissue relaxing, thereby weakening interaction between polyphenols and protein/polysaccharides. This could facilitate the diffusion of polyphenols into the solvent, as explained by Das and Dewanjee, 2018. Nonetheless, it is important to note that polyphenols are susceptible to thermal degradation

when exposed to temperatures above 70 °C during conventional extractions (Rodríguez Amado et al., 2014; Das and Dewanjee, 2018). Given the temperature values considered and the subsequent lack of significance, a decision was made to maintain a constant temperature of 60 °C in the subsequent optimization phase to prevent thermal degradation of compounds. To optimize the conventional extraction of phenolic compounds from corn cob, a Box-Behnken design (BBD) approach was used. The experimental design and corresponding extraction yield values are outlined in Table 8. The experimental ranges (-1; +1) considered were: EtOH 50-80%, t 30-90 min, SSR 20-40 mL/g. T was fixed at 60 °C.

Table 8. Box-Behnken Design for CSE-HA extraction of polyphenols from corn cob. Actual variables.

Run No.	EtOH (%)	t (min)	SSR (mL/g)	TMC (mAU*s) (at 320 nm)
1	65	30	20	183809.6
2	65	30	40	191190.1
3	65	90	20	200605.9
4	65	90	40	221745.7
5	50	60	20	211329.3
6	50	60	40	191738.9
7	80	60	20	222158.3
8	80	60	40	198938.4
9	50	30	30	202580.1
10	50	90	30	244134.4
11	80	30	30	214432.3
12	80	90	30	237772.6
13	65	60	30	215549.9
14	65	60	30	217807.0
15	65	60	30	213203.0

The mathematical expression of the second-order polynomial equation for the response surface obtained is presented below:

$$Y = -76305.4 + 18780.9*SSR + 6671.89*t - 1962.12*EtOH - 223.434*SSR2 - 138.589*SSR*t - 125.381*SSR*EtOH - 59.4422*t2 - 10.1189*t*EtOH2 + 34.9344*EtOH2 - 1.46189*SSR2*t + 2.08968*SSR2*EtOH + 1.98141*SSR*t2 \quad (23)$$

ANOVA results indicated that both t and EtOH significantly affected the yield as well as the interaction between these two factors ($p < 0.05$). R^2 and R^2_{adj} values were 99.50% and 98.26%, respectively, and indicated a close agreement between experimental and predictive values (Table 9).

Table 9. Variance analysis of the Box-Behnken model for polyphenolic compounds extraction yield obtained with CSE-HA.

Source	Sum of squares	df	Mean square	F ratio	*p* value
A: SSR	4.58E8	1	4.58E8	93.07	0.0006
B: time	1.05E9	1	1.05E9	213.86	0.0001
C: EtOH	7.54E6	1	7.54E6	1.53	0.2837
AA	1.14E9	1	1.14E9	231.90	0.0001
AB	4.73E7	1	4.73E7	9.61	0.0362
BC	8.29E7	1	8.29E7	16.85	0.0148
CC	2.29E8	1	2.29E8	46.61	0.0024
AAB	3.85E7	1	3.85E7	7.81	0.0490
AAC	1.96E7	1	1.96E7	3.99	0.1164
ABB	6.36E8	1	6.36E8	129.19	0.0003
PRESS	8.74E8				

By analyzing the surface plots obtained for TMC yield as a function of SSR and time, the optimum values for the two parameters resulting in the highest extraction yield could be found near the higher-level values in the experimental domain (Figure 4). In fact, using the statistical software, the optimal conditions for maximizing the extraction yield have been determined. These conditions include EtOH percentage of 50.3%, SSR of 32.7 mL/g, and extraction time of 89.9 min. These settings have been identified to give the maximum extraction yield, calculated to result in a total peaks area of 244226.0 mAu*s. The confidence intervals for the mean value of the extraction yield ranged from 238489.0 mAu*s (lower bound) to 249963.0 mAu*s (upper bound) at a 95% confidence level. It is important to emphasize that the experimental value should fall within this range. In this context, these optimal conditions are expected to offer the most efficient extraction process, leading to a substantial enhancement in the extraction yield of the targeted compounds.

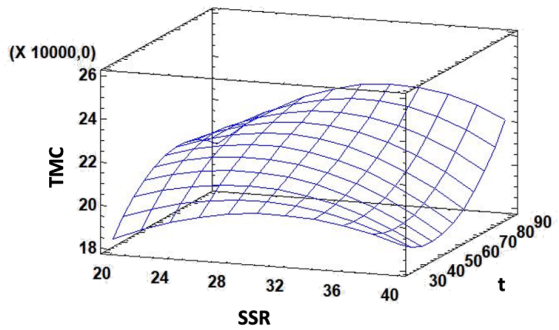

Figure 4. Total metabolite content (TMC, expressed as sum of all peaks area, mAu*s) response surface showing the effect of solvent to solid ratio (SSR) and time (t) at 65% of ethanol (EtOH).

To validate the adequacy of the second-order polynomial equation model, a verification experiment was carried out. Three additional extractions were performed under optimal predicted conditions: 50.3% EtOH, 60 °C, 89.9 min, and 32.7 mL/g SSR. The obtained extracts were analyzed by RP-HPLC-DAD and the mean total area of the peaks recorded in the chromatographic profiles at 320 nm was 242965.2 ± 3411,5 mAu*s, confirming the adequacy of the fitted model. Therefore, corn cob extract 1 (CBE-1) was obtained using the above reported experimental conditions.

Considering the microwave assisted-extraction with hydroalcoholic solvents (MAE-HA), the results of the screening phase are reported in Table 3. The considered experimental ranges (-1; +1) were: EtOH 30-70%, T 40-70 °C, t 3-30 min, SSR 15-30 mL/g. The generated experimental design is reported in Table 10.

The minimum value of TMC was obtained for run#1 (EtOH=30%; T=40 °C; t=5min; SSR=15mL/g), while the maximum TMC for run#16 (EtOH=70%; T=70 °C; t=30min; SSR=35mL/g). The Pareto plot (Figure 5) showed that the main factors significantly affecting the process were EtOH concentration (positive effect, *p*-value=0.0002), SSR (positive effect, *p*-value=0.0076), and T (positive effect, *p*-value=0.0282).

Table 10. Full Factorial Design 2^n for MAE-HA extraction of polyphenols from corn cob. Actual variables.

Run No.	EtOH (%)	T (°C)	t (min)	SSR (mL/g)	TMC (mAu*s) (at 320 nm)
1	30	40	5	15	83834.9
2	70	40	5	15	146196.0
3	30	40	5	35	107713.8
4	70	40	5	35	195188.0
5	30	70	5	15	115964.5
6	70	70	5	15	156322.0
7	30	70	5	35	133132.8
8	70	70	5	35	214639.6
9	30	40	30	15	85099.9
10	70	40	30	15	171865.8
11	30	40	30	35	119685.7
12	70	40	30	35	200423.9
13	30	70	30	15	115865.3
14	70	70	30	15	191685.4
15	30	70	30	35	159804.9
16	70	70	30	35	274147.2
17	50	55	17.5	25	181325.2
18	50	55	17.5	25	194617.9
19	50	55	17.5	25	195129.9

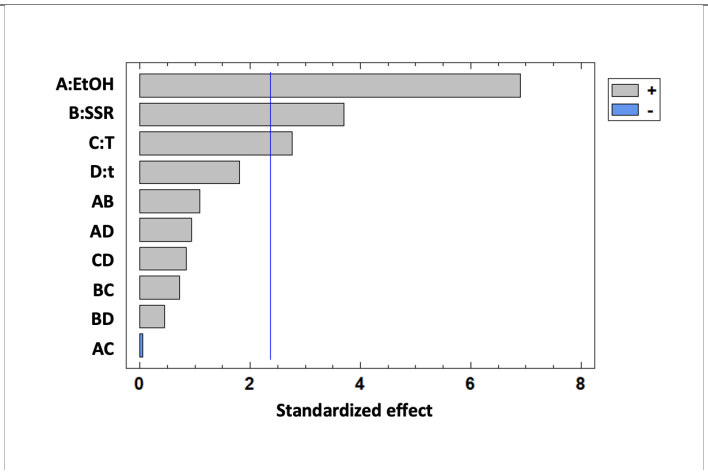

Figure 5. Standardized Pareto Chart constructed for TMC yield in MAE-HA screening phase. The positive and negative effect of the factors (reported as horizontal bars) on the response variable (TMC) is represented in grey and blue, respectively. The blue vertical line tests the significance of the effect at the 95% confidence level.

Although time also demonstrated a positive effect, its impact was not statistically significant (*p*-value=0.1125) within the examined range (5-30 min) for polyphenol recovery. Consequently, time was held constant at 5 min in the following optimization experiments. This decision was influenced by the common observation that MAE generally achieves the highest extraction yields within a few minutes (Tranfić Bakić et al., 2019; Mena-García et al., 2020), aiming to reduce the processing time, differently from the previously investigated conventional solid-liquid extraction (CSE-HA) method.

Results indicated that the use of 70% EtOH as extraction solvent provide the best yields, especially with high SSR values. Effectively, MAE hydroalcoholic solvent mixtures containing high EtOH percentage usually provide the best polyphenolic recoveries, due to the dielectric properties of ethanol, allowing it to absorb more energy compared to water (Galan et al., 2017; Frosi et al., 2021). Despite the thermolabile nature of polyphenols, literature studies highlighted increased stability with MAE (Pimentel-Moral et al., 2018) even at temperatures up to 100 °C for 20 min at 500W (Liazid et al., 2007). Hence, we selected a T range of 60-90 °C for further experiments, maintaining the non-significant factors constant, based on the outcomes of the preliminary screening phase. Furthermore, for MAE-HA we applied a Box-Behnken design (BBD) approach to optimize the extraction of phenolic compounds from CC using microwaves. The complete experimental design, along with the observed and predicted extraction yields, is detailed in Table 11. The considered experimental ranges (-1; +1) were: EtOH 50-80%, T 60-90 °C, SSR 25-45 mL/g. Extraction time was set at 5 min.

The derived second-order polynomial equation for the response surface is as follows:

$$Y= 381282.0 - 29696.1*SSR + 4033.25*T + 3652.02*EtOH + 561.612*SSR2 + 52.5278*SSR*T + 441.724*SSR*EtOH - 63.3073*T2 + 50.5599*T*EtOH - 73.2862*EtOH2 + 1.16415E\text{-}10*SSR3 - 4.34403*SSR2*T - 5.5825*SSR2*EtOH + 1.43356*SSR*T2 - 2.61934E - 10*SSR*T*EtOH - 2.03727E\text{-}10*SSR*EtOH2 + 1.45519E\text{-}10*T2*EtOH - 1.01863E\text{-}10*EtOH3 \quad (24)$$

According to the ANOVA results presented in Table 12, SSR, T, and EtOH significantly affected the yield ($p < 0.05$) with a close agreement between experimental and predictive results (R^2: 99.94%; R^2_{adj} 90.61%).

Table 11. Box-Behnken Design for MAE-HA extraction of polyphenols from corn cob. Actual variables.

Run No.	EtOH (%)	T (°C)	SSR (mL/g)	TMC (mAU*s) (at 320 nm)
1	65	60	25	190067.8
2	65	60	45	249988.1
3	65	90	25	243994.5
4	65	90	45	282002.1
5	50	75	25	234220.0
6	50	75	45	261448.2
7	80	75	25	179224.3
8	80	75	45	237021.7
9	50	60	35	232585.5
10	50	90	35	265836.0
11	80	60	35	186870.1
12	80	90	35	265623.5
13	65	75	35	258155.4
14	65	75	35	254921.5
15	65	75	35	258442.0

Table 12. The analysis of variance of the Box-Behnken model for polyphenolic compounds extraction with MAE and hydroalcoholic solvents (MAE-HA).

Source	Sum of squares	df	Mean square	F ratio	*P* value
A: SSR	1.80E9	1	1.80E9	473.03	0.0021
B: T	3.14E9	1	3.14E9	820.82	0.0012
C: EtOH	5.27E8	1	5.27E8	138.02	0.0072
AA	5.96E8	1	5.96E8	115.99	0.0063
AB	1.20E8	1	1.20E8	31.42	0.0304
AC	2.34E8	1	2.34E8	61.15	0.0160
BB	3.22E7	1	3.22E7	8.44	0.1009
BC	5.17E8	1	5.17E8	135.48	0.0073
CC	1.00E9	1	1.00E9	262.75	0.0038
AAB	8.49E7	1	8.49E7	22.22	0.0422
AAC	1.40E8	1	1.40E8	36.70	0.0262

ABB	2.08E7	1	2.08E7	5.44	0.1448
PRESS	1.72E7				

In Figure 6 the surface plots obtained for TMC yield as a function of T and SSR is reported: 88.06 °C and 42.8 mL/g of SSR were defined to maximize the extraction yield, calculated for a total area of the peaks of 282495.0 mAu*s with an inferior and superior 95% confidence level for the mean value of 276718.0 mAu*s and of 288272.0 mAu*s, respectively. Also, for this extraction approach, the experimental value yield is included in the calculated range.

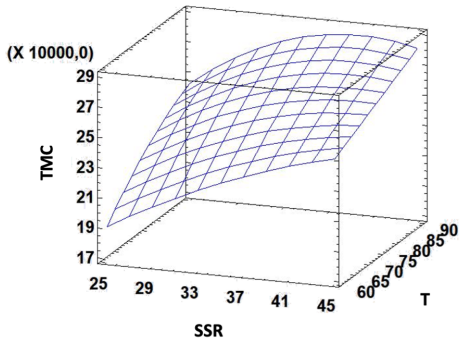

Figure 6. Response surface plot showing the effect of temperature (T) and solvent to solid ratio (SSR) on polyphenolic yield, as total metabolite content (TMC).

Validation of the second-order polynomial equation model was achieved through an additional set of experiments performed under the optimal predicted conditions (62.4% EtOH, 88 °C, 5 min, and 42.8 mL/g SSR). The obtained extract was analyzed by RP-HPLC-DAD and the mean of the total area values of the chromatographic peaks recorded at 320 nm (285345.0 ± 3737.67 mAu*s) confirmed the robustness of the model. The optimized corn cob extract, namely CBE-2, was obtained using the above reported experimental conditions.

During the initial screening phase of the MAE-NaDES approach, the efficacy of different NaDES mixtures was assessed by comparing TMC, as reported in section 3.3.2. The best results were achieved with NaDES-1 ($ChCl_2$-lactic acid, TMC=86047.5 mAu*s) and NaDES-2 ($ChCl_2$- glycerol, TMC=71376.6 maU*s), followed by NaDES-3 ($ChCl_2$-1,2-propanediol, TMC=46135,6 mAu*s) and NaDES-4 ($ChCl_2$-Urea = 55753,3 mAu*s). Even if NaDES-1 displayed the highest overall peak area, NaDES-2 was selected for further optimization because it contained the highest number of different polyphenolic compounds, as evident in the chromatographic profile (specific data not shown). Applying the Box-Behnken design (BBD) methodology, we subsequently improved the extraction process using NaDES-2 as the solvent. The comprehensive experimental design, inclusive of observed and predicted extraction yield

values, is outlined in Table 13. The considered experimental ranges (-1; +1) were: water content (WC) in NaDES mixture 20-50%, T 50-90 °C, SSR 20-40 mL/g, while time was maintained fixed at 5 min.

Table 13. Box-Behnken Design for MAE-NaDES extraction of polyphenols from corn cob. Actual variables.

Run No.	WC (%)	T (°C)	SSR (mL/g)	TMC (mAU*s)
1	20	50	30	45165.6
2	50	50	30	26935.6
3	20	90	30	71075.0
4	50	90	30	46273.6
5	20	70	20	68629.0
6	50	70	20	46777.5
7	20	70	40	38476.5
8	50	70	40	29770.7
9	35	50	20	45866.1
10	35	90	20	84083.3
11	35	50	40	30385.8
12	35	90	40	53048.5
13	35	70	30	51857.4
14	35	70	30	41357.5
15	35	70	30	43779.7

The mathematical formula of the second-order polynomial equation deriving from the response surface is as follows:

$$Y= 248458.0 – 6843.77*WC – 3672.48*T – 2525.98*SSR + 50,1961*WC2 + 128.082*WC*T + 26.9199*WC*SSR + 29.604*T2 – 19.4431*T*SSR + 31.160*SSR2 – 0.868472*WC2*T – 0.0715778*WC2*SSR – 0.519754*WC*T2 + 1.9645E- 10*WC*T*SSR \quad (25)$$

T and WC significantly affected the extraction yield ($p < 0.05$), as evidenced by ANOVA results presented in Table 14. There was a strong accordance between the outcomes of experimental trials and the predicted values, denoted by the high coefficients of determination (R^2: 98.23%;

R^2_{adj}: 88.09%). These two factors are effectively reported also by other authors as crucial factors influencing the NaDES mixture properties and consequently their extraction capacities (Xia et al., 2015; Huang et al., 2017; Ivanović et al., 2020). In fact, high temperature and small water content in the solvent contribute to decrease NaDES mixtures viscosity, make them easier to handle and use, as it is confirmed by the positive influence of temperature and negative influence of water content showed by the statistical model.

Table 14. The analysis of variance of the Box-Behnken model for polyphenolic compounds extraction yield for MAE-NaDES process.

Source	Sum of squares	df	Mean square	F ratio	*P* value
A: WC	2.33E8	1	2.33E8	7.72	0.1088
B: T	9.26E8	1	9.26E8	30.65	0.0311
C: SSR	5.41E8	1	5.41E8	17.89	0.0516
AA	3.03E7	1	3.03E7	1.00	0.4218
AB	1.08E7	1	1.08E7	0.36	0.6107
AC	4.32E7	1	4.32E7	1.43	0.3544
BB	7.69E7	1	7.69E7	2.55	0.2517
BC	6.04E7	1	6.04E7	2.00	0.2928
CC	3.58E7	1	3.58E7	1.19	0.3899
AAB	3.05E7	1	3.05E7	1.01	0.4206
AAC	51874.2	1	51874.2	0.00	0.9707
ABB	1.94E7	1	1.94E7	0.64	0.5066
PRESS	1.36E8				

The surface plots obtained for TMC yield as a function of T and WC is reported in Figure 7.

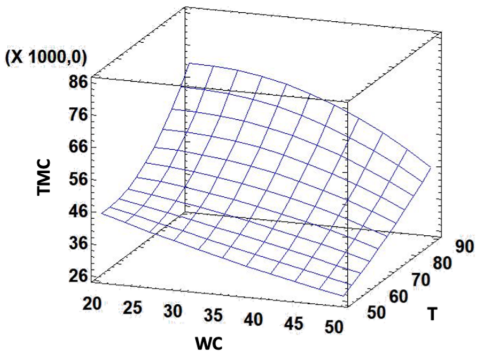

Figure 7. Response surface plot showing the effect of water content (WC) and temperature (T) on polyphenolic yield, expressed as total metabolite content (TMC).

The optimal conditions to maximize the extraction yield were 90 °C and 20% of water content. Under these conditions, the total area of the peaks was 93155.9 mAu*s, with a 95% confidence interval for the mean value ranging from 61676.6 mAu*s to 124635.0 mAu*s.The approach applied to validate the equation models for the previously described extraction methods was likewise used to validate the second-order polynomial equation derived for the NaDES extraction. Analyzing the outcomes of the three additional experiments performed under the optimal predicted conditions (20% water content, 90 °C, 5 min, and 20 mL/g SSR, the mean total area values of the peaks recorded at 320 nm were 108000.2 ± 4530.03 mAu*s. This result confirmed the accuracy of the fitted model. The resultant extract obtained under the mentioned experimental conditions was designated as CBE-3 (Corn Cob Extract 3).

Considering the use of NaDES with CSE, the initial screening of the different NaDES mixtures highlighted NaDES-4 ($ChCl_2$-Urea, TMC=76794.9 mAu*s) as the most promising, followed by NaDES-1 ($ChCl_2$- lactic acid, TMC=66624.8 maU*s), NaDES-2 (ChCl2-glycerol, TMC=61375.6 mAu*s) and NaDES-3 ($ChCl_2$-1,2-propanediol = 31024.2 mAu*s). The Box-Behnken design (BBD) was subsequently used to optimize the extraction process using NaDES-4 as the solvent. The considered experimental ranges (-1; +1) were the same used for MAE-NaDES, except for time which was investigated in the range 30-90 minutes. The comprehensive experimental design with four factors, inclusive of observed and predicted extraction yield values, is outlined in Table 15.

Table 15. Box-Behnken Design for CSE-NaDES extraction of polyphenols from corn cob. Actual variables.

Run No.	WC (%)	T (°C)	t (min)	SSR (mL/g)	TMC (mAu*s) (at 320 nm)
1	30	50	90	10	57941.9
2	30	50	30	10	40848.8
3	40	60	60	30	60877.3
4	20	60	60	30	107885
5	30	50	30	50	56088
6	20	40	60	30	78600.1
7	30	50	90	50	64007.4
8	40	40	60	30	49122.8
9	30	50	60	30	77406.3
10	30	50	60	30	67838.5
11	20	50	60	10	71793.7
12	20	50	60	50	82654
13	30	40	90	30	67438.9
14	30	60	90	30	96702.2
15	30	60	30	30	76931.2
16	30	40	30	30	58918.8
17	40	50	60	50	55912.2
18	40	50	60	10	37635.2
19	30	50	60	30	71133.7
20	30	50	60	30	67036.6
21	40	50	90	30	58290.8
22	30	40	60	50	49910.8
23	20	50	90	30	103740.8
24	20	50	30	30	87774.1
25	30	60	60	10	68348.2
26	30	60	60	50	76186.5
27	40	50	30	30	49633.7
28	30	40	60	10	44153.9
29	30	50	60	30	61910.6
30	30	50	60	30	65495.2

The mathematical formulation of the second-order polynomial equation derived from the response surface is as follows:

$$Y = 579269, - 19398,6*SSR - 16870,2*T - 2287,73*t + 475,613*WC + 135,754*SSR^2 + 487,25*SSR*T + 71,4858*SSR*t - 49,4736*SSR*WC + 163,648*T^2 - 7,29825*T*t + 98,9705*T*WC + 24,8223*t^2 - 3,82237*t*WC - 31,9371*WC^2 - 2,35765*SSR^2*T - 0,0323917*SSR^2*t + 0,979075*SSR^2*WC - 3,89618*SSR*T^2 + 5,82077E-10*SSR*T*t - 8,73115E-10*SSR*T*WC - 0,630281*SSR*t^2 - 6,40284E-10*SSR*t*WC - 1,16415E-10*SSR*WC^2 + 0,273217*T^2*t - 0,963688*T^2*WC - 0,0887306*T*t^2 - 3,20142E-10*T*t*WC + 1,16415E-10*T*WC^2 + 1,16415E-10*t*WC^2 \quad (26)$$

SSR and T were the significant factors on the extraction yield ($p < 0.05$), as evidenced by ANOVA results presented in Table 16. There was a strong correlation between the experimental and the predicted values, denoted by the high coefficient of determination values (R^2: 97.97%; R^2_{adj}: 88.20%).

The surface plots obtained for TMC yield as a function of temperature and water content is reported in Figure 8.

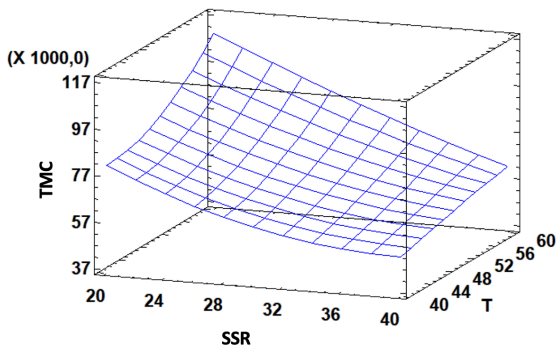

Figure 8. Response surface plot showing the effect of SSR and T on polyphenolic yield, expressed as total metabolite content (TMC) at 30 mL/g of WC and 60 min.

Table 16. The analysis of variance of the Box-Behnken model for polyphenolic compounds extraction yield for CSE-NaDES process.

Source	Sum of squares	df	Mean square	F ratio	*P* value
A:SSR	9.27E8	1	9.27E8	26.60	0.0036
B:T	6.37E8	1	6.37E8	18.27	0.0079
C:t	1.56E8	1	1.56E8	4.49	0.0877
D:WC	1.13E8	1	1.13E8	3.25	0.1311
AA	1.41E8	1	1.41E8	4.04	0.1008
AB	7.68E7	1	7.68E7	2.20	0.1978
AC	1.34E7	1	1.34E7	0.38	0.563
AD	1.38E7	1	1.38E7	0.39	0.5575
BB	8.04E7	1	8.04E7	2.31	0.1893
BC	3.16E7	1	3.16E7	0.91	0.3845
BD	1.08E6	1	1.08E6	0.03	0.867
CC	1.21E7	1	1.21E7	0.35	0.581
CD	2.10E7	1	2.10E7	0.60	0.4724
DD	1.12E9	1	1.12E9	32.1	0.0024
AAB	1.11E7	1	1.11E7	0.32	0.5967
AAC	18886	1	18886	0	0.9823
AAD	7.67E6	1	7.67E6	0.22	0.6588
ABB	3.04E7	1	3.04E7	0.87	0.3936
ACC	6.44E7	1	6.44E7	1.85	0.2323
BBC	1.34E6	1	1.34E6	0.04	0.8521
BBD	7.43E6	1	7.43E6	0.21	0.6637
BCC	1.28E6	1	1.28E6	0.04	0.8558
Total error	1.74E8	5	3.49E7		

The optimal conditions to maximize the extraction yield were 59.7 °C, 78.2 min, 24.4% of WC and 20 mL/g SSR. Under these conditions, the total area of the peaks was 117070.0 mAu*s, with a 95% confidence interval for the mean value ranging from 99349.1 mAu*s to 134791.0 mAu*s. Analyzing the outcomes of the three additional experiments performed under the optimal predicted conditions, the mean total area values of the peaks recorded at 320 nm were 102634.2 ± 3364.56 mAu*s. This outcome confirmed the accuracy of the fitted model. The resultant extract obtained under the mentioned experimental conditions was designated as CBE-4 (Corn Cob Extract 4).

To sum up, the chromatographic profiles of CBE-1, CBE-2, CBE-3, and CBE-4 registered at 320 nm are reported in Figure 9. CBE-2 (obtained with MAE-HA) shows peaks with the highest areas, which is directly correlated to the higher concentration of the analytes, followed by CBE-1 (obtained with CSE-HA). No significant difference was registered for CBE-3 and CBE-4 (Figure 9) (obtained with NaDES mixtures). It is evident that the hydroalcoholic solvents are more efficient than the NaDES tested mixture in extracting polyphenols. Therefore, CBE-2 was selected for bioactivity assays.

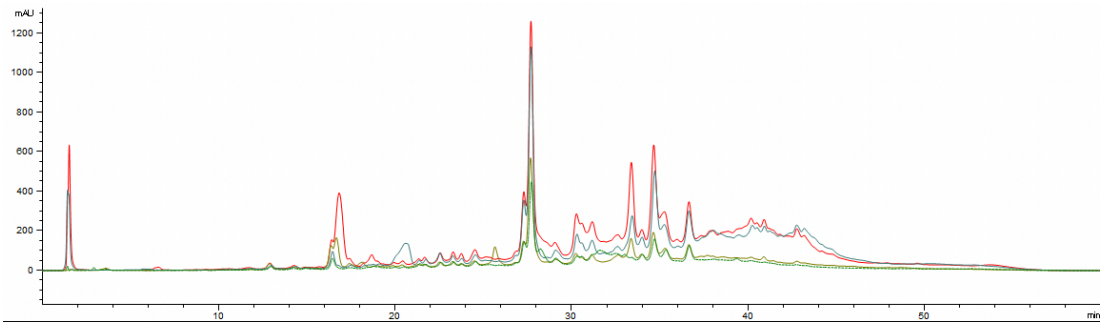

Figure 8. Overlay of the chromatographic profiles of the optimized extracts obtained from corn cob by applying CSE-HA (CBE-1, light blue line), MAE-HA (CBE-2, red line), MAE-NaDES (CBE-3, green line) and CSE-NaDES approaches (CBE-4, dark green).

4.2 Optimization of Rice Husk extract (RHE)

The same approach was used to find the optimal extraction conditions to recover polyphenols from rice husk (RH). Starting from CSE-HA, the considered experimental ranges (-1; +1) to study the impact of the factors affecting the yield in the screening phase were the same for CC (see Table 7): EtOH 20-80%, T 30-60 °C, t 10-60 min, SSR 15-30 mL/g. Table 17 shows the results in terms of total phenolic yield content (TMC, generated from the application of the experimental design. In this case, TMC ranged between 34221.8 and 180056.1 mAu*s, forming a narrower range in comparison to corn cob extracts. However, the minimum and maximum values were again achieved under identical extraction conditions: run #1 and run #16, respectively. A standardized Pareto Chart diagram (Figure 10) illustrated the significance and statistical relevance of the factor examined in the model.

Table 17. Full Factorial Design 2^n for CSE-HA extraction of polyphenols from rice husk. Actual variables.

Run (No.)	EtOH (%)	T (°C)	t (min)	SSR (mL/g)	TMC (mAu*s) (at 320 nm)
1	20	30	10	15	34221.8
2	20	30	10	30	78930
3	20	30	60	15	69880.5
4	20	30	60	30	99928.1
5	20	60	10	15	43016
6	20	60	10	30	84797.3
7	20	60	60	15	59856.3
8	20	60	60	30	129245.4
9	80	30	10	15	40239.3
10	80	30	10	30	86946
11	80	30	60	15	138294.8
12	80	30	60	30	86686.3
13	80	60	10	15	67553.4
14	80	60	10	30	126531.4
15	80	60	60	15	105380.4
16	80	60	60	30	180056.1
17	50	45	35	22.5	124733.2
18	50	45	35	22.5	125128.4
19	50	45	35	22.5	124507.5

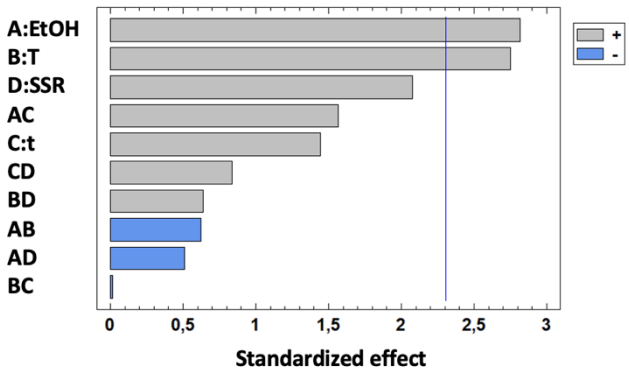

Figure 10. Standardized Pareto Chart effect for total metabolite content (TMC) yield of rice husk in CSE-HA screening phase. The positive and negative effect of the factors (reported as horizontal bars) on the response variable (TMC) is represented with grey and blue colors, respectively. The vertical line tests the significance of the effect at the 95% confidence level.

Only EtOH percentage in the extraction mixture and T had a noticeable impact on the extraction yield, while changes in SSR and extraction time did not lead to significant differences in the number of extracted compounds, despite showing some positive effects. These results confirmed the crucial role of EtOH in the extraction process, as we observed for corn cob extracts.

Considering that T had a significant positive effect on the polyphenol's extraction, we decided to focus on this factor for further optimization. Because polyphenols are sensitive to heat and could degrade with prolonged exposure especially beyond 70 °C, we also made sure not to explore temperatures over 60 °C in optimization studies. The Box-Behnken design (BBD) approach used and the corresponding extraction yield values are reported in Table 18. The experimental ranges (-1; +1) considered were: EtOH 50-80%, T 40-60 min, SSR 20-40 mL/g. The extraction time was maintained fixed at 60 min.

Table 18. Box-Behnken Design for CSE-HA extraction of polyphenols from rice husk. Actual variables.

Run No.	EtOH (%)	T (°C)	SSR (mL/g)	TMC (mAU*s) (at 320 nm)
1	50	40	30	79201.0
2	80	40	30	93511.3
3	50	60	30	103666.0
4	80	60	30	133523.6
5	50	50	20	81793.8
6	80	50	20	101485.5
7	50	50	40	81263.6
8	80	50	40	101868.4
9	65	40	20	82790.4
10	65	60	20	113928.9
11	65	40	40	87710.1
12	65	60	40	113092.4
13	65	50	30	103667.3
14	65	50	30	102897.8
15	65	50	30	108707.6

The mathematical expression of the second-order polynomial equation for the response surface obtained is presented below:

$$Y= 10383,3 - 439,013*EtOH - 663,72*T + 362,374*SSR + 20,2561*EtOH^2 + 34,8252*EtOH*T + 57,4421*EtOH*SSR - 20,0194*T^2 + 38,8682*T*SSR - 51,9652*SSR^2 - 0,884056*EtOH^2*T - 0,430156*EtOH^2*SSR + 0,705083*EtOH*T^2 \quad (27)$$

T and SSR were the significant factors ($p < 0.05$), as evidenced by ANOVA results presented in Table 19. EtOH, on the other hand, is not a statistically significant factor (p-value = 0.5430) affecting the extraction yield, but a positive influence on it was confirmed. There was also a strong accordance between the outcomes of experimental trials and the predicted values, denoted by the high coefficients of determination (R^2: 99.37%; R^2_{adj}: 95.65%).

Table 19. The analysis of variance of the Box-Behnken model for polyphenolic compounds extraction yield for MAE-NaDES process.

Source	Sum of squares	df	Mean square	F ratio	*P* value
A:EtOH	5424.32	1	5424.32	0	0.9835
B:T	1.04E9	1	1.04E9	104.37	0.0094
C:SSR	4.88E8	1	4.88E8	48.97	0.0198
AA	2.54E8	1	2.54E8	25.49	0.0371
AB	8.28E6	1	8.28E6	0.83	0.4580
AC	208438	1	208438	0.02	0.8982
BB	2.46E7	1	2.46E7	2.47	0.2566
BC	6.04E7	1	6.04E7	6.07	0.1328
CC	9.97E7	1	9.97E7	10.01	0.0870
AAB	7.91E6	1	7.91E6	0.79	0.4668
AAC	1.87E6	1	1.87E6	0.19	0.7068
ABB	2.24E6	1	2.24E6	0.22	0.6822
Total error	1.99E7	2	9.96E6		

The surface plots obtained for TMC yield as a function of EtOH and T is reported in Figure 11.

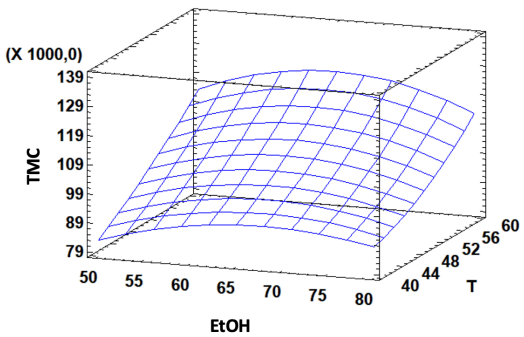

Figure 11. Response surface plot showing the effect of EtOH and T on polyphenolic yield, expressed as total metabolite content (TMC) at 30 mL/g of WC and 60 min.

The optimal conditions to obtain the best extraction yield were 60 °C, 64.1% of EtOH, 40 mL/g SSR, and 60 min of extraction. Under these conditions, the total area of the peaks was 133067.0 mAu*s, with a 95% confidence interval for the mean value ranging from 127937.0 mAu*s to 138196.0 mAu*s.

Analyzing the results of the three additional experiments performed under the optimal predicted conditions, the mean total area values of the peaks recorded at 320 nm were 130154.3 ± 3270.4 mAu*s. This result confirmed the accuracy of the fitted model and the resultant extract obtained under the mentioned experimental conditions was named RHE-1 (Rice Husk extract 1).

Considering MAE-HA, in Table 20 are reported the experimental TMC values obtained in the screening phase. The considered experimental ranges (-1; +1) were: EtOH 30-70%, T 40-60 °C, t 5-35 min, SSR 15-30 mL/g.

Table 20. Full Factorial Design 2^n for MAE-HA extraction of polyphenols from rice husk. Actual variables.

Run No.	EtOH (%)	T (°C)	t (min)	SSR (mL/g)	TMC (mAu*s) (at 320 nm)
1	30	40	5	15	44026.1
2	30	40	5	35	53250.2
3	30	80	5	15	73121.4
4	30	80	35	35	67167.3
5	30	40	35	15	46771.2
6	30	40	35	35	60918.1
7	30	80	35	15	107120.0
8	30	80	5	35	69380.9
9	70	40	5	15	62104.9
10	70	40	5	35	79735.8
11	70	80	5	15	93851.4
12	70	80	5	35	108931.0
13	70	40	35	15	71067.7
14	70	40	35	35	84906.3
15	70	80	35	15	111471.3
16	70	80	35	35	128500.3
17	50	60	20	25	94467.9
18	50	60	20	25	97625.2
19	50	60	20	25	98631.8

The minimum value of TMC was obtained for run#1 (EtOH=30%; T=40 °C; t=5min; SSR=15mL/g), while the maximum TMC for run#16 (EtOH=70%; T=80 °C; t=35min; SSR=35mL/g). The Pareto plot (Figure 12) showed that the main factors significantly affecting the process were T (positive effect) and EtOH concentration (positive effect), even if all the factors considered had a positive impact on the yield.

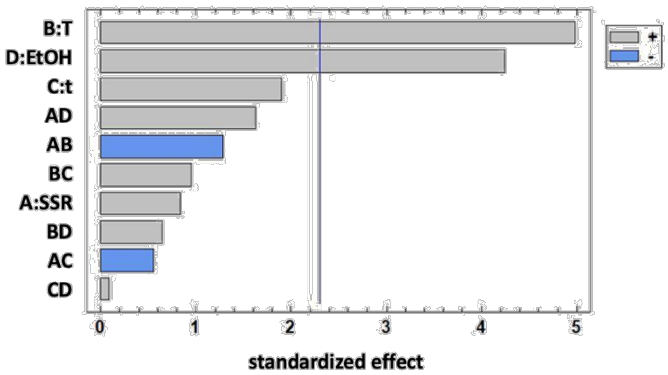

Figure 12. Standardized Pareto Chart effect for total metabolite content (TMC) yield in MAE-HA screening phase. The positive and negative effect of the factors (reported as horizontal bars) on the response variable (TMC) is represented with grey and blue colors, respectively. The vertical line tests the significance of the effect at the 95% confidence level.

Based on the obtained results, a fixed time of 5 min was selected for further optimization. This decision is in accordance with the observation that MAE typically yields the highest extraction efficiency within a short time (Mena Garcia et al., 2020; Tranfić Bakić et al., 2019). Additionally, SSR was set at the highest level tested (35 mL/g) due to its positive correlation with the EtOH percentage (see the interaction AD in the Pareto Plot, Figure 12).

A Box-Behnken design (BBD) approach was also used for MAE-HA to optimize the extraction process. The complete experimental design, along with the observed and predicted extraction yields, is detailed in Table 21. The considered experimental ranges (-1; +1) were: EtOH 50-80% and T 60-90 °C.

Table 21. Box-Behnken Design for MAE-HA extraction of polyphenols from rice husk. Actual variables.

Sample	EtOH (%)	T (°C)	TMC (mAU*s) (at 320 nm)
1	60	60	102564.9
2	80	60	96972.2
3	60	90	120588.4
4	80	90	136819.6
5	60	75	98178.2
6	80	75	112884.1
7	70	60	90576.6
8	70	90	113531.8
9	70	75	89423.5
10	70	75	91898.6

The second-order polynomial equation representing the response surface was as follows:

$$Y = 1.08526E6 - 20973.3\ EtOH - 8219.48\ T + 133.341\ EtOH^2 + 36.3732\ EtOH\ T + 43.8095\ T^2 \quad (28)$$

ANOVA results indicated both T and EtOH concentration as significant factors affecting the yield, as well as the interaction between these two factors ($p < 0.05$). The R^2 and R^2_{adj} values were 97.72% and 94.87%, respectively, highlighting a strong agreement between experimental and predicted outcomes (refer to Table 22).

Table 22. The analysis of variance of the Box-Behnken Design model for polyphenolic compounds extraction yield for MAE-HA process.

Source	Sum of squares	df	Mean square	F ratio	P value
A:EtOH	1.07E8	1	1.07E8	8.83	0.0411
B:T	1.09E9	1	1.09E9	89.83	0.0007
AA	4.15E8	1	4.15E8	34.23	0.0043
AB	1.19E8	1	1.19E8	9.82	0.0350
BB	2.27E8	1	2.27E8	18.70	0.0124
Total error	4.85E7	4	4.85E7		

Upon analyzing the surface plots generated for TMC yield in relation to T and EtOH percentage, optimal parameter values that yielded the highest extraction efficiency were identified near the upper range values within the experimental domain (as illustrated in Figure 13).

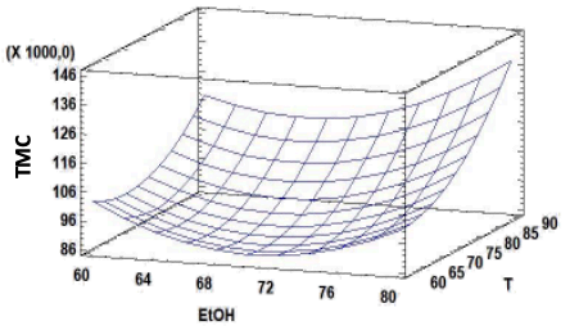

Figure 13. Response surface plot showing the effect of ethanol content (EtOH) and temperature (T) on polyphenolic yield, expressed as total metabolite content (TMC).

Notably, the statistical software determined that setting the temperature at 90 °C and using 80% EtOH the extraction yield should be the best. This configuration yielded a calculated total peak area of 137771 mAu*s. The 95% confidence interval for the mean extraction yield value ranged from 129139 mAu*s to 146404 mAu*s, within which the experimental value is expected to fall. The appropriateness of the second-order polynomial equation model was then verified performing an additional set of three experiments under the optimal predicted conditions: 80% EtOH, 90 °C T, 5 min, and 35 mL/g SSR. The resultant extracts were subjected to analysis using RP-HPLC-DAD, and the mean total area of peaks recorded in the

chromatographic profiles at 320 nm was 135852.3 ± 1989.8 mAu*s. This finding further validates the accuracy of the model. The extract obtained was indicated as RHE-2.

The same extraction method was also studied with NaDES mixtures. Different NaDES mixture were tested in fixed conditions to find the most efficient for optimization. The best results were achieved with NaDES-1 ($ChCl_2$-Lactic acid, TMC=32489.1 mAu*s) and NaDES-3 ($ChCl_2$-1,2-propanediol, TMC=26178.4 maU*s), followed by NaDES-2 (ChCl2-Glycerol, TMC=21829,5 mAu*s) and NaDES-4 ($ChCl_2$-Urea = 20711.0 mAu*s). Then, the extraction process was optimized using NaDES-1 as the solvent. The comprehensive BBD employed, inclusive of observed extraction yield values, is outlined in Table 23. The considered experimental ranges (-1; +1) were: water content (WC) in NaDES mixture 20-50%, T 50-90 °C, SSR 20-40 mL/g, while time was maintained fixed at 5 min.

Table 23. Box-Behnken Design for MAE-NaDES extraction of polyphenols from rice husk. Actual variables.

Run No.	WC (%)	T (°C)	SSR (mL/g)	TMC (mAU*s) (at 320 nm)
1	20	50	30	28635.0
2	50	50	30	20450.8
3	20	90	30	27221.5
4	50	90	30	35865.0
5	20	70	20	35056.1
6	50	70	20	35727.7
7	20	70	40	12539.0
8	50	70	40	18949.7
9	35	50	20	25178.0
10	35	90	20	50758.0
11	35	50	40	15343.7
12	35	90	40	22289.0
13	35	70	30	19041.0
14	35	70	30	20704.7
15	35	70	30	22997.4

The mathematical formulation of the second-order polynomial equation derived from the response surface is as follows:

$$Y = 247352, - 8446,57*WC - 3740,07*T - 1297,68*SSR + 84,912*WC^2 + 124,697*WC*T + 17,2792*WC*SSR + 22,0995*T^2 - 23,2934*T*SSR + 25,0143*SSR^2 - 1,02914*WC^2*T - 0,1102*WC^2*SSR - 0,275958*WC*T^2 + 1,38243E-10*WC*T*SSR- 1,01863E-10*T*SSR^2 \quad (29)$$

T (*p*-value= 0.0146) and SSR (*p*-value= 0.0106) were the significant factors of the extraction yield, as evidenced by ANOVA results presented in Table 24. Once again, T was as a crucial factor affecting the NaDES efficiency, as previously discussed for CC. There was a strong accordance between the outcomes of experimental trials and the predicted values, denoted by the high coefficient of determination values (R^2: 99.42%; R^2_{adj}: 95.96%).

Table 24. The analysis of variance of the Box-Behnken model for polyphenolic compounds extraction yield for MAE-NaDES process.

Source	Sum of squares	df	Mean square	F ratio	P value
A:WC	1.25E7	1	1.25E7	3.18	0.2166
B:T	2.64E8	1	2.64E8	67.02	0.0146
C:SSR	3.67E8	1	3.67E8	92.95	0.0106
AA	1.71E7	1	1.71E7	4.33	0.1728
AB	7.08E7	1	7.08E7	17.94	0.0515
AC	8.23E6	1	8.23E6	2.09	0.2854
BB	9.14E7	1	9.14E7	23.17	0.0406
BC	8.68E7	1	8.68E7	22	0.0426
CC	2.31E7	1	2.31E7	5.85	0.1367
AAB	4.29E7	1	4.29E7	10.87	0.0810
AAC	122958	1	122958	0.03	0.8761
ABB	5.48E6	1	5.48E6	1.39	0.3597
Total error	7.89E6	2	3.95E6		

The surface plots obtained for TMC yield as a function of WC and T is reported in Figure 14.

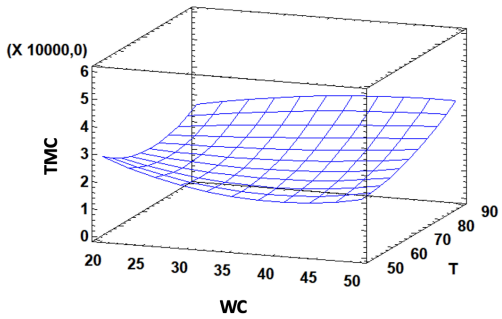

Figure 14. Response surface plot showing the effect of water content (WC) and temperature (T) on polyphenolic yield, expressed as total metabolite content (TMC).

The optimal extraction conditions were 89.9 °C, 45.3 % WC and 20 mL/g SSR. Under these conditions, the total area of the peaks was 51561.3 mAu*s, with a 95% confidence interval for the mean value ranging from 42863.8 mAu*s to 60258.8 mAu*s.

Analyzing the outcomes of the three additional experiments performed under the optimal predicted conditions, the mean total area values of the peaks recorded at 320 nm were 55684.85 ± 4491.52 mAu*s. This result confirmed the accuracy of the fitted model. The resultant extract obtained under the mentioned experimental conditions was named RHE-3 (Rice Husk Extract 3).

Considering the use of NaDES with CSE, the initial screening of the different NaDES mixtures highlighted NaDES-4 ($ChCl_2$-Urea, TMC=31649.9 mAu*s) as the most promising to be used for the BBD (NaDES-1: $ChCl_2$- lactic acid, TMC=19575.4 maU*s; NaDES-2: $ChCl_2$-glycerol, TMC=16775.5 mAu*s; NaDES-3: $ChCl_2$-1,2-propanediol, TMC=10449.6 mAu*s). The considered experimental ranges (-1; +1) were WC in NaDES mixture 10-50%, T 40-60 °C, SSR 20-40 mL/g, t 30-90 min. The comprehensive experimental design with four factors, inclusive of observed and predicted extraction yield values, is reported in Table 25.

The mathematical formulation of the second-order polynomial equation derived from the response surface is as follows:

$$Y = 43542,8 + 326,022*WC + 158,59*T - 557,546*t - 2146,61*SSR + 107,588*WC^2 - 133,261*WC*T - 2,10017*W*t + 29,0108*WC*SSR - 5,77608*T^2 + 21,8281*T*t + 53,3233*T*SSR + 5,50442*t^2 - 4,11833*t*SSR + 11,953*SSR^2 - 1,75111*WC^2*T - 0,0244083*WC^2*t - 0,529138*WC^2*SSR + 2,19012*WC*T^2 + 0,0102944*WC*t^2 - 0,064125*T^2*t - 0,752925*T^2*SSR - 0,127794*T*t^2 \quad (30)$$

Table 25. Box-Behnken Design for CSE-NaDES extraction of polyphenols from rice husk. Actual variables.

Run No.	WC (%)	T (°C)	t (min)	SSR (mL/g)	TMC (mAu*s) (at 320 nm)
1	10	40	60	30	19573.4
2	50	40	60	30	39311.4
3	10	60	60	30	20957.0
4	50	60	60	30	25242.8
5	30	50	30	20	23395.6
6	30	50	90	20	31617.4
7	30	50	30	40	15895.1
8	30	50	90	40	19174.9
9	30	50	60	30	19326.2
10	30	50	60	30	18378.8
11	10	50	60	20	24303.6
12	50	50	60	20	28650.0
13	10	50	60	40	11194.0
14	50	50	60	40	13350.4
15	30	40	30	30	14590.0
16	30	60	30	30	19907.9
17	30	40	90	30	19907.9
18	30	60	90	30	25322.1
19	30	50	60	30	19545.7
20	30	50	60	30	17512.8
21	10	50	30	30	12022.9
22	50	50	30	30	18440.1
23	10	50	90	30	19983.1
24	50	50	90	30	20809.9
25	30	40	60	20	21508.3
26	30	60	60	20	33568.5
27	30	40	60	40	14424.8
28	30	60	60	40	17697.3
29	30	50	60	30	18415.3
30	30	50	60	30	19223.2

Among the studied parameters, SSR, T, and t were significant factors affecting the extraction yield ($p < 0.05$). SSR had a negative impact, while T had a positive effect, as supported by the ANOVA results presented in Table 26. Although changes in WC appeared to increase the extraction yield, these effects did not reach statistical significance. There was an accordance between the outcomes of experimental trials and the predicted values, denoted by the high coefficient of determination values (R^2: 97.83%; R^2_{adj}: 87.42%).

Table 26. The analysis of variance of the Box-Behnken model for polyphenolic compounds extraction yield for CSE-NaDES process.

Source	Sum of squares	df	Mean square	F ratio	P value
A:WC	1.06E7	1	1.06E7	2.17	0.2006
B:T	5.88E7	1	5.88E7	12.07	0.0178
C:t	3.31E7	1	3.31E7	6.79	0.0479
D:SSR	9.94E7	1	9.94E7	20.43	0.0063
AA	7.96E6	1	7.96E6	1.64	0.2570
AB	5.97E7	1	5.97E7	12.26	0.0172
AC	7.81E6	1	7.81E6	1.61	0.2610
AD	1.20E6	1	1.20E6	0.25	0.6407
BB	7.69E7	1	7.69E7	15.8	0.0106
BC	2318.42	1	2318.42	0	0.9834
BD	1.93E7	1	1.93E7	3.97	0.1030
CC	1.85E6	1	1.85E6	0.38	0.5650
CD	6.11E6	1	6.11E6	1.25	0.3136
DD	9.80E6	1	9.80E6	2.01	0.2152
AAB	9.81E7	1	9.81E7	20.16	0.0065
AAC	171581	1	171581	0.04	0.8585
AAD	8.96E6	1	8.96E6	1.84	0.2329
ABB	3.84E7	1	3.84E7	7.88	0.0376
ACC	68672.2	1	68672.2	0.01	0.9101
BBC	74016.3	1	74016.3	0.02	0.9067
BBD	1.13E6	1	1.13E6	0.23	0.6498
BCC	2.65E6	1	2.65E6	0.54	0.4941
Total error	2.43E7	5	4.87E6		

The surface plots obtained for TMC yield as a function of WC and T is reported in Figure 15.

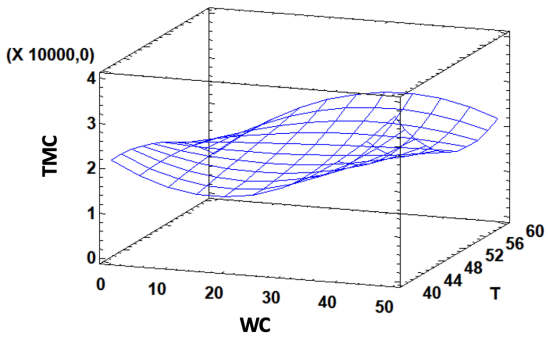

Figure 15. Response surface plot showing the effect of water content (WC) and temperature (T) on polyphenolic yield, expressed as total metabolite content (TMC).

In this case, the optimal conditions were 40 °C, 90 min, 50% of WC and 20 mL/g SSR. Under these conditions, the total area of the peaks was 46437.1 mAu*s, with a 95% confidence interval for the mean value ranging from 32630.0 mAu*s to 60064.2 mAu*s. The mean total area values of the peaks recorded at 320 nm for the three additional experiments were 30617.65 ± 444.7 mAu*s. This value did not confirm the accuracy of the fitted model. Therefore, we decided to not perform any additional study, as this extraction method yielded the lowest results among all the methods we investigated. The resultant extract obtained under the mentioned experimental conditions was named RHE-4 (Rice husk extract 4).

To sum up, the chromatographic profiles of RHE-1, RHE-2, RHE-3 and RHE-4 registered at 320 nm are reported in Figure 16. RHE-2 showed peaks with the highest areas, which is directly correlated to the higher concentration of the analytes, followed by RHE-1, RHE-3, and RHE-4 (Figure 16). These results confirmed the extraction efficiency of MAE-HA process, already found for the corn cob matrix.

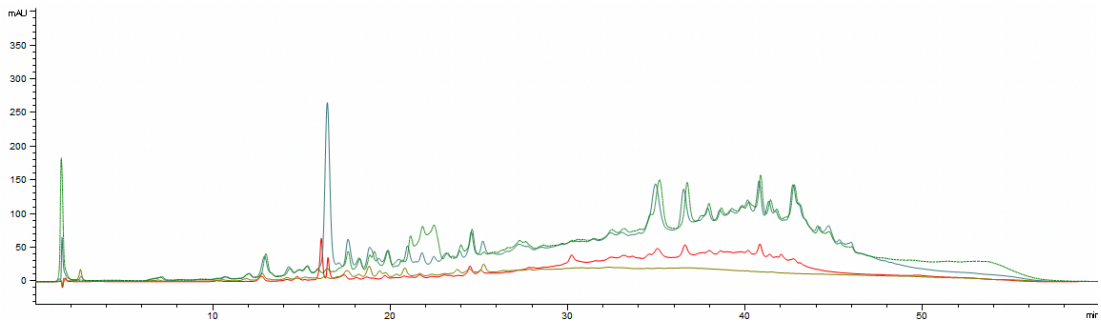

Figure 16. Overlay of the chromatographic profiles of the optimized extracts obtained by applying CSE-HA (RHE-1, dark green), MAE-HA (RHE-2, light blue), MAE-NaDES (RHE-3, red line), and CSE-NaDES (RHE-4, green).

4.3 Optimization of Melon Peel extract (MPE)

The considered experimental ranges (-1; +1) to study the impact of the studied factors on the polyphenols extraction yield in the screening phase for CSE-HA were: EtOH 25-95%, T 30-60 °C, t 30-90 min, SSR 20-50 mL/g. Based on literature data according which hydroalcoholic extracts containing 95% EtOH were the most promising for antioxidant activity and phenolic content (Vella et al., 2019; Mallek-Ayadi et al., 2017), we investigated EtOH percentage in the extraction mixture even higher than those typically studied in cereals.

Table 27 shows the results in terms of total polyphenolic yield content, always expressed as TMC, obtained from the application of the experimental design. For this AFW, 280nm resulted to be the wavelength with the highest signal intensity and thus selected as reference.

Table 27. Full Factorial Design 2^n for CSE-HA extraction of polyphenols from rice husk. Actual variables.

Run (No.)	EtOH (%)	T (°C)	t (min)	SSR (mL/g)	TMC (mAu*s) (at 280 nm)
1	25	30	30	20	117619.0
2	95	30	30	20	45171.3
3	25	60	30	20	106581.8
4	95	60	30	20	59218.4
5	25	30	90	20	115021.5
6	95	30	90	20	43871.9
7	25	60	90	20	111410.7
8	95	60	90	20	60947.1
9	25	30	30	50	146562.5
10	95	30	30	50	53794.4
11	25	60	30	50	146088.2
12	95	60	30	50	67719.7
13	25	30	90	50	149233.0
14	95	30	90	50	57263.5
15	25	60	90	50	145772.0
16	95	60	90	50	76011.8
17	60	45	60	35	92634.5
18	60	45	60	35	91961.5
19	60	45	60	35	92295.6

In this case, TMC ranged between 43871.9 and 149233 mAu*s. The lowest value was obtained for run #6, characterized by the highest EtOH concentration (95%), 30 °C, 90 min, and SSR of 20 mL/g; conversely, the highest value was obtained for run #13, characterized by the lowest EtOH concentration (25%), 30 °C, 90 min, and SSR of 50 mL/g. The Pareto Chart diagram (Figure 17) indicated that the EtOH content in the extraction mixture, SSR, and T significantly impacted the extraction yield. Moreover, unlike what is expected EtOH exhibited a negative influence on the polyphenolic yield, whereas both SSR and T exerted a positive effect.

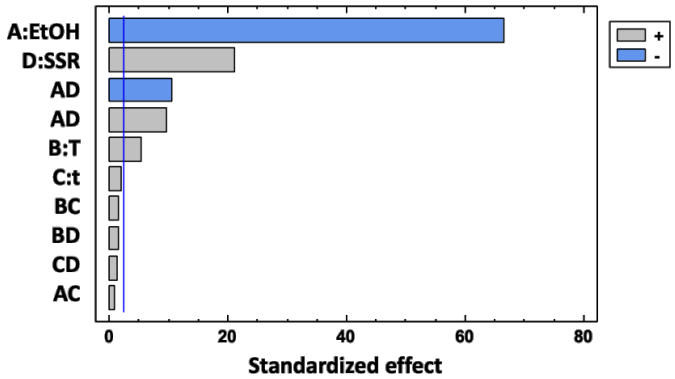

Figure 17. Standardized Pareto Chart effect for total metabolite content (TMC) yield in CSE-HA screening phase for MP. The positive and negative effect of the factors (reported as horizontal bars) on the response variable (TMC) is represented with grey and blue colors, respectively. The vertical line tests the significance of the effect at the 95% confidence level.

These findings reiterated the key role of EtOH content in the solvent mixture, as we observed in the same extraction approach with cereal matrices, once again underscoring that the main driving force for extraction efficiency in CSE is the solvent strength. Conversely, variations in extraction time did not bring about changes in TMC, despite displaying a positive trend. Thus, aiming to establish an eco-friendly and rapid extraction processes, a fixed time parameter of 30 min was selected for the further optimization step. The adopted Box-Behnken design (BBD) methodology and the corresponding extraction yield values are reported in Table 28. The explored ranges (-1 to +1) were: EtOH 50-80%, T 40-60 °C, and SSR 20-40 mL/g. The extraction time remained fixed at 30 min, as indicated before.

Table 28. Box-Behnken Design for CSE-HA extraction of polyphenols from melon peel. Actual variables.

Run No.	EtOH (%)	T (°C)	SSR (mL/g)	TMC (mAU*s) (at 280 nm)
1	20	40	50	194689.4
2	50	40	50	160993.0
3	20	60	50	209737.0
4	50	60	50	174980.7
5	20	50	40	202741.5
6	50	50	40	155824.5
7	20	50	60	211295.0
8	50	50	60	142917.9
9	35	40	40	178842.9
10	35	60	40	185833.5
11	35	40	60	180241.9
12	35	60	60	151709.9
13	35	50	50	180142.8
14	35	50	50	183782.6
15	35	50	50	185561.5

The mathematical expression of the second-order polynomial equation for the response surface obtained is presented below:

$$Yield = -1{,}3987E6 + 49244{,}9*EtOH + 39221{,}8*T + 16691{,}0*SSR - 425{,}322*EtOH^2 - 1175{,}83*EtOH*T - 256{,}434*EtOH*SSR - 283{,}741*T^2 - 88{,}8065*T*SSR - 79{,}5527*SSR^2 + 1{,}74623E\text{-}10*EtOH^3 + 5{,}61963*EtOH^2*T + 3{,}15239*EtOH^2*SSR + 7{,}8069*EtOH*T^2 + 1{,}01863E\text{-}9*EtOH*T*SSR - 2{,}32831E\text{-}10*EtOH*SSR^2 - 1{,}16415E\text{-}10*T^3 + 8{,}14907E\text{-}10*T^2*SSR \quad (31)$$

EtOH and SSR were significant factors ($p < 0.05$), as evidenced by ANOVA results presented in Table 29. T, on the other hand, is not statistically significant (p-value = 0.0599), but a negative effect on the yield is highlighted. There was also a strong accordance between the outcomes of experimental trials and the predicted values, denoted by the high coefficient of determination values (R^2: 99.74%; R^2_{adj}: 98.16%).

Table 29. The analysis of variance of the Box-Behnken model for polyphenolic compounds extraction yield for CSE-HA process.

Source	Sum of squares	df	Mean square	F ratio	P value
A:EtOH	3.32E9	1	3.32E9	435.59	0.0023
B:T	1.16E8	1	1.16E8	15.21	0.0599
C:SSR	2.68E8	1	2.68E8	35.09	0.0273
AA	3.30E7	1	3.30E7	4.32	0.1732
AB	280847	1	280847	0.04	0.8656
AC	1.15E8	1	1.15E8	15.09	0.0603
BB	4.07E6	1	4.07E6	0.53	0.5411
BC	3.15E8	1	3.15E8	41.35	0.0233
CC	2.34E8	1	2.34E8	30.63	0.0311
AAB	3.20E8	1	3.20E8	41.91	0.0230
AAC	1.01E8	1	1.01E8	13.19	0.0682
ABB	2.74E8	1	2.74E8	35.95	0.0267
Total error	1.53E7	2	7.63E6		

The surface plots obtained for TMC yield as a function of EtOH and T is reported in Figure 18.

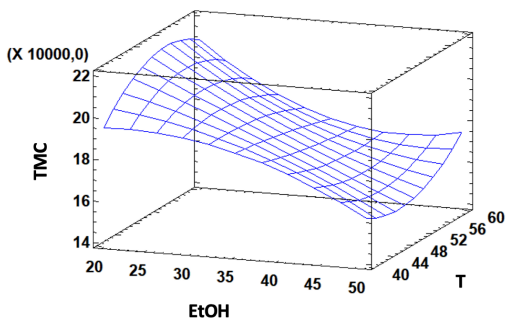

Figure 18. Response surface plot showing the effect of ethanol content (EtOH) and temperature (T) on polyphenolic yield, expressed as total metabolite content (TMC).

The optimal conditions to maximize the extraction yield were 20.3% of EtOH, 52.97 °C, and 51.5 mL/g SSR for 30 min of extraction. Under these conditions, the total area of the peaks was 212502 mAu*s, with a 95% confidence interval for the mean value ranging from 204663 mAu*s to 220314.0 mAu*s.

The mean total area value of the peaks recorded at 280 nm for the three additional experiments performed under the optimal predicted conditions was 206531.8±6044.7 mAu*s, thus confirming the accuracy of the fitted model and the resultant extract obtained under the mentioned experimental conditions was designated as MPE-1 (Melon Peel Extract 1).

Considering MAE-HA, in Table 30 are reported TMC yield values (expressed as total area of peaks registered at 280 nm) obtained in the screening phase. The considered experimental ranges (-1; +1) were: EtOH 25-95%, T 40-80 °C, t 5-15 min, SSR 20-40 mL/g.

The minimum and maximum value of TMC was obtained for run#10 (EtOH=95%; T=40 °C; t=5min; SSR=40mL/g) and for run#15 (EtOH=25%; T=80 °C; t=15min; SSR=40mL/g), respectively. The Pareto plot (Figure 19) gave analogous results as for the screening of CSE-HA.

Table 30. Full Factorial Design 2^n for MAE-HA extraction of polyphenols from melon peel. Actual variables.

Run No.	EtOH (%)	T (°C)	t (min)	SSR (mL/g)	TMC (mAu*s) (at 280 nm)
1	25	40	5	20	94324.7
2	95	40	5	20	63976.3
3	25	80	5	20	127081.9
4	95	80	5	20	96025.6
5	25	40	15	20	117681.1
6	95	40	15	20	74389.6
7	25	80	15	20	129573.1
8	95	80	15	20	97223.9
9	25	40	5	40	161364.2
10	95	40	5	40	59003.2
11	25	80	5	40	143915.7
12	95	80	5	40	118249.3
13	25	40	15	40	158982.4
14	95	40	15	40	72423.1
15	25	80	15	40	179015.7
16	95	80	15	40	114152.1
17	60	60	10	30	144433.3
18	60	60	10	30	143924.3
19	60	60	10	30	145295.1

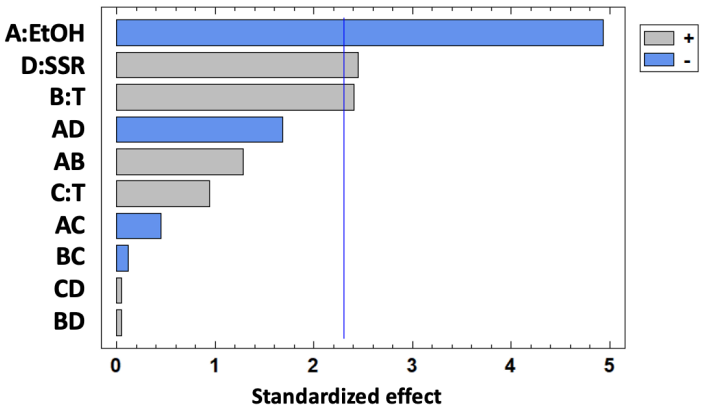

Figure 19. Standardized Pareto Chart effect for total metabolite content (TMC) yield in MAE-HA screening phase for MP. The positive and negative effect of the factors (reported as horizontal bars) on the response variable (TMC) is represented with grey and blue colors, respectively. The vertical line tests the significance of the effect at the 95% confidence level.

Therefore, EtOH content is the most significative variable, with a confirmed negative effect on the yield, followed by SSR and T with a positive influence. Conversely, time had not again a significative effect and for this reason a fixed time of 5 min was selected for further optimization. This is in accordance with what is reported in literature about the need to not prolong the extraction time in MAE (Mena Garcia et al., 2020; Tranfić Bakić et al., 2019), as discussed for RH and CC. A BBD approach was employed to optimize the extraction of polyphenolic compounds from MP using microwaves. The complete experimental design, along with the observed and predicted extraction yields, is detailed in Table 31. The considered experimental ranges (-1; +1) were: EtOH 20-60%, T 60-90 °C, SSR 30-50 mL/g. Extraction time was set at 5 min.

The second-order polynomial equation representing the response surface was as follows:

$$Y = 226220 - 15053.8*EtOH - 10445.6*T + 12352.2*SSR - 65.2782*EtOH^2 + 536.979*EtOH*T - 106.119*EtOH*SSR + 77.4617*T^2 - 34.7573*T*SSR - 80.7499*SSR^2 - 0.350783*EtOH^2*T + 1.64156*EtOH^2*SSR - 3.45042*EtOH*T^2 + 1.63709E\text{-}10*EtOH*T*SSR + 1.16415E\text{-}10*T^2*SSR \quad (32$$

Table 31. Box-Behnken Design for MAE-HA extraction of polyphenols from melon peel. Actual variables.

Run No.	EtOH (%)	T (°C)	SSR (mL/g)	TMC (mAU*s) (at 280 nm)
1	20	60	40	161525.5
2	60	60	40	115351.0
3	20	90	40	162466.1
4	60	90	40	105916.0
5	20	75	30	133821.8
6	60	75	30	103430.9
7	20	75	50	170215.8
8	60	75	50	159989.6
9	40	60	30	116742.9
10	40	90	30	127132.3
11	40	60	50	160514.0
12	40	90	50	150049.0
13	40	75	40	161923.1
14	40	75	40	158819.2
15	40	75	40	160185.9

Table 32. The analysis of variance of the Box-Behnken Design model applied to polyphenolic compounds extraction yield using MAE-HA process.

Source	Sum of squares	Df	Mean square	F ratio	*P* value
A:EtOH	4.12E8	1	4.12E8	170.43	0.0058
B:T	1428.84	1	1428.84	0	0.9828
C:SSR	1.11E9	1	1.11E9	459.43	0.0022
AA	3.97E8	1	3.97E8	164.07	0.0060
AB	2.69E7	1	2.69E7	11.12	0.0794
AC	1.02E8	1	1.02E8	42.01	0.0230
BB	6.85E8	1	6.85E8	283.24	0.0035
BC	1.09E8	1	1.09E8	44.93	0.0215
CC	2.41E8	1	2.41E8	99.49	0.0099
AAB	8.86E6	1	8.86E6	3.66	0.1958
AAC	8.62E7	1	8.62E7	35.63	0.0269
ABB	4.82E8	1	4.82E8	199.24	0.0050
Total error	4.84E6	2	2.42E+06		

The analysis of the surface plots generated for TMC yield in relation to EtOH percentage in solvent mixtures and T, the optimal parameter values that yielded the highest extraction efficiency were identified near the upper range values within the experimental domain (as illustrated in Figure 20).

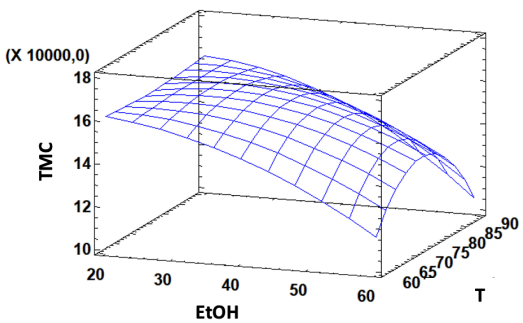

Figure 20. Response surface plot showing the effect of ethanol content (EtOH) and temperature (T) on polyphenolic yield, expressed as total metabolite content (TMC).

The statistical software determined that setting the temperature at 60 °C, using 20% EtOH and 50 mL/g SSR it could be possible to maximize the extraction yield. This configuration yielded a calculated total peak area of 176861 mAu*s. The 95% confidence interval for the mean extraction yield value ranged from 167954 mAu*s to 185768 mAu*s, within which the experimental value is expected to fall. The appropriateness of the second-order polynomial equation model was then verified performing an additional set of three experiments under the optimal predicted conditions. The resultant extracts were subjected to analysis using RP-HPLC-DAD, and the mean total area of peaks recorded in the chromatographic profiles at 320 nm was determined to be 179916.8 ± 2004.2 mAu*s. This finding further validated the accuracy of the model. The extract thus obtained was named MPE-2.

The same extraction method was also investigated when NaDES mixtures have been used. Regarding the screening phase with the use of different NaDES mixture in fixed conditions, the best results were achieved with NaDES-4 ($ChCl_2$-Urea, TMC=18270.8 mAu*s) and NaDES-2 ($ChCl_2$-Glycerol, TMC=15670.1 mAu*s), followed by NaDES-3 ($ChCl_2$-1,2-propanediol, TMC=21829,5 mAu*s). NaDES-1 (containing lactic acid as HBD) let to filtration problems that made it impossible to recover the sample.

Thus, the extraction process was optimized using NaDES-2. The comprehensive BBD used, inclusive of observed extraction yield values, is reported in Table 33. The considered experimental ranges (-1; +1) were: EtOH 20-50%, T 50-90 °C, SSR 30-50 mL/g. Extraction time was set at 5 min.

Table 33. Box-Behnken Design for MAE-NaDES extraction of polyphenols from melon peel. Actual variables.

Run No.	WC (%)	T (°C)	SSR (mL/g)	TMC (mAU*s) (at 280 nm)
1	20	50	40	15016.3
2	50	50	40	31366.4
3	20	90	40	22116.7
4	50	90	40	29308.9
5	20	70	30	18517.0
6	50	70	30	39337.3
7	20	70	50	12435.1
8	50	70	50	16083.1
9	35	50	30	55993.4
10	35	90	30	42443.0
11	35	50	50	20067.6
12	35	90	50	21426.1
13	35	70	40	30193.6
14	35	70	40	26670.6
15	35	70	40	23147.6

The mathematical formula of the second-order polynomial equation derived from the response surface is as follows:

$$Y = -82810{,}0 + 17606{,}1*WC - 1601{,}78*T - 150{,}004*SSR - 224{,}405*WC^2 - 69{,}2541*WC*T - 243{,}338*WC*SSR + 15{,}314*T^2 + 18{,}6361*T*SSR + 27{,}2649*SSR^2 + 0{,}957489*WC^2*T + 3{,}0674*WC^2*SSR - 0{,}0385833*WC*T^2 \quad (33)$$

SSR was the only significant factor ($p < 0.05$), as evident by ANOVA results presented in Table 34. There was a strong correlation between the outcomes of experimental trials and the predicted values, denoted by the high coefficient of determination values (R^2: 98.71%; R^2_{adj}: 90.9%). The study indicated that WC and T had no significant effect on the yield for this type of waste, while SSR was the predominant factor influencing the polyphenolic extraction yield.

Table 34. The analysis of variance of the Box-Behnken model for polyphenolic compounds extraction yield for MAE-NaDES process.

Source	Sum of squares	Df	Mean square	F ratio	P value
A:WC	1.50E8	1	1.50E8	12.06	0.0739
B:T	3.72E7	1	3.72E7	2.99	0.2257
C:SSR	8.11E8	1	8.11E8	65.31	0.0150
AA	2.25E8	1	2.25E8	18.12	0.0510
AB	2.10E7	1	2.10E7	1.69	0.3233
AC	7.37E7	1	7.37E7	5.94	0.1351
BB	1.15E8	1	1.15E8	9.28	0.0930
BC	5.56E7	1	5.56E7	4.48	0.1686
CC	2.74E7	1	2.74E7	2.21	0.2754
AAB	3.71E7	1	3.71E7	2.99	0.2258
AAC	9.53E7	1	9.53E7	7.68	0.1093
ABB	107185	1	107185	0.01	0.9344
Total error	2.48E7	2	1.24E7		

The surface plots obtained for TMC yield as a function of WC and T is reported in Figure 21. The optimal conditions were 50 °C, 41% WC, and 30.6 mL/g SSR. Under these conditions, the total area of the peaks was 56261 mAu*s, with a 95% confidence interval for the mean value ranging from 42238.5 mAu*s to 70283.5 mAu*s.

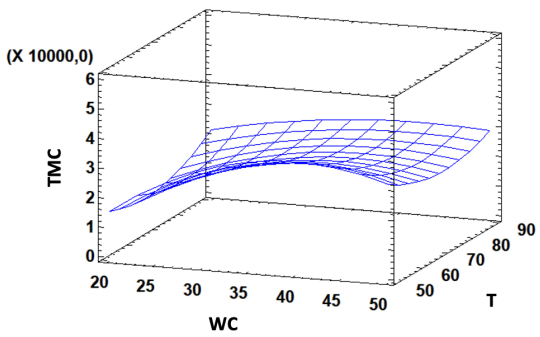

Figure 21. Response surface plot showing the effect of water content (WC) and temperature (T) on polyphenolic yield, expressed as total metabolite content (TMC).

The mean total area values of the peaks recorded at 280 nm in the three additional experiments conducted under the optimal predicted conditions were calculated to be 33853.6 ± 4203.6 mAu*s, thus confirming the accuracy of the fitted model. The resultant extract

obtained under the mentioned experimental conditions was designated as MPE-3 (Melon Peel Extract 3).

Considering the use of NaDES with CSE, the initial screening of the different NaDES mixtures highlighted NaDES-4 ($ChCl_2$-Urea, TMC=47772 mAu*s) as the most promising to be used for BBD (NaDES-1: $ChCl_2$- lactic acid, TMC=44540 maU*s; NaDES-2: $ChCl_2$-glycerol, TMC=36828.9 mAu*s; NaDES-3: $ChCl_2$-1,2-propanediol, TMC=11515.4 mAu*s). The considered experimental ranges (-1; +1) were water content (WC) in NaDES mixture 20-50%, T 40-60 °C, SSR 30-50 mL/g, t 30-90 min. The comprehensive experimental design with four factors, inclusive of observed and predicted extraction yield values, is reported in Table 35.

The mathematical formula of the second-order polynomial equation derived from the response surface is as follows:

$$Y = 252443 + 7571.34*WC - 14771.0*T + 562.051*t - 4383.17*SSR - 131.528*WC^2 + 28.3069*WC*T - 3.02383*WC*t - 158.054*WC*SSR + 159.158*T^2 + 18.6864*T*t + 288.133*T*SSR - 19.4204*t^2 + 2.17692*t*SSR - 14.8245*SSR^2 + 1.34426*WC^2*T - 0.422467*WC^2*t + 2.16356*WC^2*SSR- 1.1635*WC*T^2 + 2.18279E-10*WC*T*t + 1.89175E-10*WC*T*SSR + 0.296341*WC*t^2 - 0.4533*T^2*t - 2.66552*T^2*SSR + 0.222308*T*t^2 + 1.81899E-10*T*t*SSR \quad (34)$$

As demonstrated by the ANOVA results detailed in Table 36, both WC (*p*-value= 0.047) and SSR (*p*-value= 0.0069) were identified as significant factors affecting the extraction yield. Specifically, WC exhibited a negative impact, whereas SSR had a positive influence. Conversely, variations in T and extraction time also showed an increasing in the extraction yield, but these effects did not reach statistical significance. There was a strong correlation between the values experimentally obtained and the predicted values, denoted by the high coefficients of determination (R^2: 98.45%; R^2_{adj}: 91.01%).

Table 35. Box-Behnken Design for CSE-NaDES extraction of polyphenols from melon peel. Actual variables.

Run No.	WC (%)	T (°C)	t (min)	SSR (mL/g)	TMC (mAu*s) (at 280 nm)
1	20	40	60	40	28333.0
2	50	40	60	40	35705.8
3	20	60	60	40	28064.9
4	50	60	60	40	39070.6
5	35	50	30	30	39590.8
6	35	50	90	30	42777.3
7	35	50	30	50	26740.6
8	35	50	90	50	32539.4
9	35	50	60	40	35176.8
10	35	50	60	40	34726.6
11	20	50	60	30	24598.7
12	50	50	60	30	39260.1
13	20	50	60	50	24772.3
14	50	50	60	50	35470.4
15	35	40	30	40	32905.3
16	35	60	30	40	32386.0
17	35	40	90	40	34658.1
18	35	60	90	40	34178.9
19	35	50	60	40	35786.3
20	35	50	60	40	34084.4
21	20	50	30	40	39076.9
22	50	50	30	40	57089.9
23	20	50	90	40	35198.3
24	50	50	90	40	58547.2
25	35	40	60	30	56145.4
26	35	60	60	30	47328.4
27	35	40	60	50	34954.1
28	35	60	60	50	34769.5
29	35	50	60	40	41251.6
30	35	50	60	40	48103.3

Table 36. The analysis of variance of the Box-Behnken model for polyphenolic compounds extraction yield for CSE-NaDES process.

Source	Sum of squares	df	Mean square	F ratio	*P* value
A:WC	1.61E8	1	1.61E8	23.57	0.0047
B:T	2.03E7	1	2.03E7	2.97	0.1455
C:t	2.02E7	1	2.02E7	2.96	0.1461
D:SSR	1.33E8	1	1.33E8	19.53	0.0069
AA	3.38E6	1	3.38E6	0.5	0.5128
AB	3.30E6	1	3.30E6	0.48	0.5178
AC	7.12E6	1	7.12E6	1.04	0.3539
AD	3.93E6	1	3.93E6	0.58	0.4823
BB	1.62E7	1	1.62E7	2.38	0.1837
BC	402.002	1	402.002	0	0.9942
BD	1.86E7	1	1.86E7	2.73	0.1594
CC	2.37E7	1	2.37E7	3.48	0.1212
CD	1.71E6	1	1.71E6	0.25	0.6383
DD	1.51E7	1	1.51E7	2.21	01974
AAB	1.83E7	1	1.83E7	2.68	0.1624
AAC	1.63E7	1	1.63E7	2.38	0.1833
AAD	4.74E7	1	4.74E7	6.95	0.0462
ABB	6.09E6	1	6.09E6	0.89	0.3881
ACC	3.20E7	1	3.20E7	4.69	0.0826
BBC	3.70E6	1	3.70E6	0.54	0.4946
BBD	1.42E7	1	1.42E7	2.08	0.2086
BCC	8.01E6	1	8.01E6	1.17	0.3281
Total error	3.41E7	5	6.82E6		

The surface plots obtained for TMC yield as a function of WC and T is reported in Figure 22.

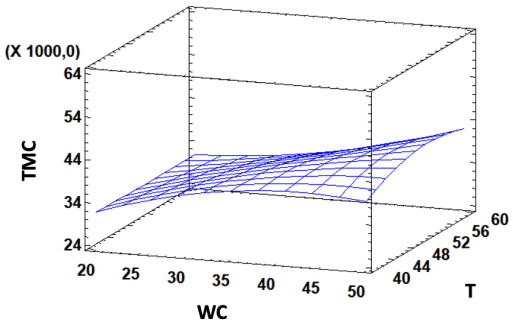

Figure 22. Response surface plot showing the effect of water content (WC) and temperature (T) on polyphenolic yield, expressed as total metabolite content (TMC).

The optimal conditions to be set to maximize the extraction yield were 60 °C, 40 min, 50% of WC, and 30 mL/g SSR. Under these conditions, the total peaks area was 53380.3 mAu*s, with a 95% confidence interval for the mean value ranging from 37518 mAu*s to 67041.8 mAu*s. Analyzing the outcomes of the mean total area values of the peaks recorded at 280 nm calculated for the three additional experiments performed under the optimal predicted conditions were 41098.1 ± 1932.6 mAu*s. This confirmed the accuracy of the fitted model. The resultant extract obtained under the mentioned experimental conditions was named MPE-4 (Melon Peel Extract 4).

To sum up, the chromatographic profiles of MPE-1, MPE-2, MPE-3, and MPE-4 registered at 280 nm are reported in Figure 23. MPE-1 showed peaks with the highest areas, followed by MPE-2, MPE-4, and MPE-3 (Figure 23). These results indicated that CSE-HA method represented the best extraction approach to recover phenolic compounds from melon peel, independently from the extraction solvent used. Among the various solvents tested, hydroalcoholic solvents proved to be particularly effective in enhancing the extraction yield.

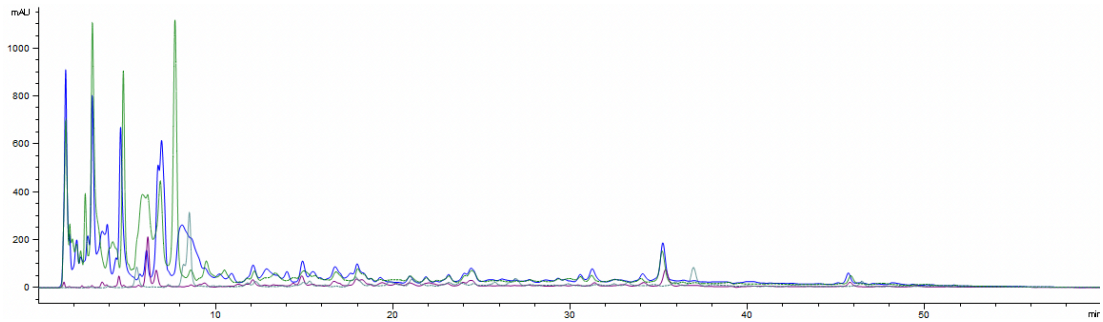

Figure 23. Overlay of the chromatographic profiles of the optimized extracts obtained by applying CSE-HA (MPE-1, green line), MAE-HA (MPE-2, blue line), MAE- NaDES (MPE-3, violet line) and CSE-NaDES (MPE-4, light blue line).

4.4 Optimization of pumpkin peel extract (PPE)

Considering that melon peel belongs to the same botanical family as pumpkin peel (Cucurbitaceae), the considered experimental ranges (-1 to +1) for studying the impact of the factors on yield during the screening phase for CSE-HA were initially the same: EtOH 25-95%, T 30-60 °C, t 30-90 min, SSR 20-50 mL/g. Table 37 shows the results in terms of total phenolic yield content, always expressed as TMC yield values registered at 280 nm (wavelength with the higher signal intensity for PPE), generated from the application of the experimental design.

Table 37. Full Factorial Design 2^n for CSE-HA extraction of polyphenols from pumpkin peel. Actual variables.

Run (No.)	EtOH (%)	T (°C)	t (min)	SSR (mL/g)	TMC (mAu*s) (at 280 nm)
1	25	30	30	20	117619.0
2	95	30	30	20	45171.3
3	25	60	30	20	106581
4	95	60	30	20	59218.4
5	25	30	90	20	115021.5
6	95	30	90	20	43871.9
7	25	60	90	20	111410.7
8	95	60	90	20	60947.1
9	25	30	30	50	146562.5
10	95	30	30	50	53794.4
11	25	60	30	50	146088.5
12	95	60	30	50	67719.7
13	25	30	90	50	149233.0
14	95	30	90	50	57263.5
15	25	60	90	50	145772.0
16	95	60	90	50	76011.8
17	60	45	60	35	92634.5
18	60	45	60	35	91961.1
19	60	45	60	35	103368.2

In this case, TMC ranged between 43871.9 and 149233 mAu*s. However, the minimal and maximal values were achieved under identical extraction conditions as for melon peel: run #6

and run #13, respectively. A standardized Pareto Chart diagram (Figure 24) illustrated the significance and statistical relevance of the factor examined in the model.

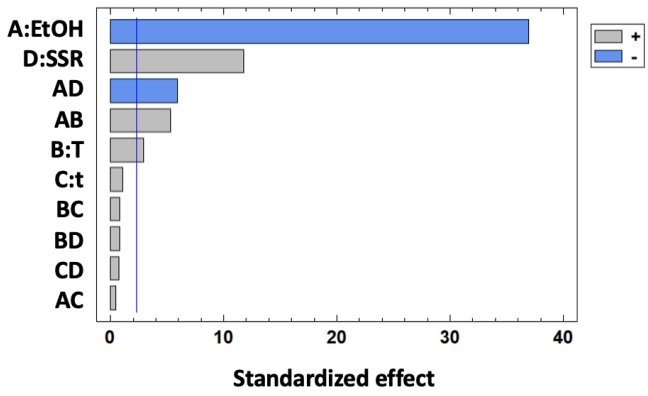

Figure 24. Standardized Pareto Chart effect for total metabolite content (TMC) yield in CSE-HA screening phase for PP. The positive and negative effect of the factors (reported as horizontal bars) on the response variable (TMC) is represented with grey and blue colors, respectively. The vertical line tests the significance of the effect at the 95% confidence level.

The results were analogous to those found for melon peels, where EtOH was the main factor affecting the yield with a negative impact, followed by SSR and T showing a positive effect on the response. On the other hand, extraction time did not lead to significant differences in the number of extracted compounds, despite showing some positive effects.

Considering the high TMC content found for melon peel extract with low EtOH content, we decided to select an experimental range of EtOH percentage in the range, 0-30%, maintaining the same ranges used for PP for the other two factors (T 40-60 °C, SSR 40-60 mL/g). The BBD thus generated is reported in Table 38. The extraction time was maintained fixed at 30 min, trying to optimize a rapid process.

The mathematical expression of the second-order polynomial equation for the response surface obtained is presented below:

$$Y = -173190 + 133.86*EtOH + 36934.2*T - 23865.2*SSR + 4.80511*EtOH^2 - 197.45*EtOH*T + 143.487*EtOH*SSR - 298.623*T^2 - 36.729*T*SSR + 231.884*SSR^2 \quad (35)$$

EtOH content and T were the significant factors affecting the extraction yield ($p < 0.05$), as evident by ANOVA results presented in Table 39. SSR, on the other hand, was not statistically significant (p-value = 0.6266). There was also a strong correlation between the experimental

data and the predicted values, denoted by the high coefficients of determination (R^2: 99.95%; R^2_{adj}: 99.71%).

Table 38. Box-Behnken Design for CSE-HA extraction of polyphenols from PP. Actual variables.

Run No.	EtOH (%)	T (°C)	SSR (mL/g)	TMC (mAU*s) (at 280 nm)
1	0	40	50	128405.8
2	30	40	50	140133.2
3	0	60	50	229949.5
4	30	60	50	123207.2
5	0	50	40	291493.0
6	30	50	40	150748.1
7	0	50	60	223155.0
8	30	50	60	168502.4
9	15	40	40	144112.7
10	15	60	40	200098.3
11	15	40	60	162309.8
12	15	60	60	203603.8
13	15	50	50	182218.7
14	15	50	50	186822.0
15	15	50	50	183574.6

Table 39. The analysis of variance of the Box-Behnken model for polyphenolic compounds extraction yield for CSE-HA process.

Source	Sum of squares	df	Mean square	F ratio	P value
A:EtOH	1.05E10	1	1.05E10	27.12	0.0034
B:T	4.13E9	1	4.13E9	10.64	0.0224
C:SSR	1.04E8	1	1.04E8	0.27	0.6266
AA	4.31E6	1	4.31E6	0.01	0.2902
AB	3.51E9	1	3.51E9	9.02	0.0300
AC	1.85E9	1	1.85E9	4.77	0.0808
BB	3.29E9	1	3.29E9	8.47	0.0334
BC	5.39E7	1	5.39E7	0.14	0.7248
CC	1.98E9	1	1.98E9	5.11	0.0734
Total error	1.94E9	5	3.89E8		

The surface plots obtained for TMC yield as a function of EtOH and T is reported in Figure 25.

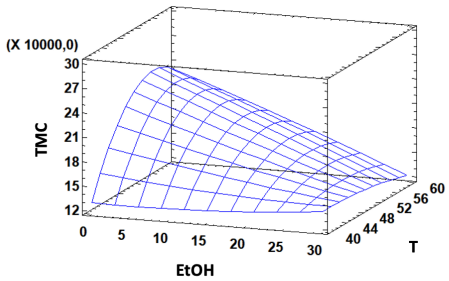

Figure 25. Response surface plot showing the effect of EtOH and T on polyphenolic yield, expressed as total metabolite content (TMC).

The optimal extraction conditions were 59.9 °C, 0% of EtOH, 40 mL/g SSR for 30 min. Under these conditions, the total peaks area was 296085.0 mAu*s, with a 95% confidence interval for the mean value ranging from 236543.0 mAu*s to 355626.0 mAu*s.

Analyzing the results of the three additional experiments performed under the optimal predicted conditions, the mean total area values of the peaks recorded at 280 nm were 239402.6 ± 3521.9 mAu*s. This result confirmed the accuracy of the fitted model and the resultant extract obtained under the mentioned experimental conditions was designated as PPE-1 (Pumpkin Peel Extract 1).

Table 40 showed the experimental total metabolite content (TMC) yield values (expressed as total area of peaks registered at 280 nm) obtained in the screening phase of MAE-HA process.

The considered experimental ranges (-1; +1) were the same considered for CSE-HA, except for time, studied for 5-15 min.

The lowest TMC value was achieved in run #6, while the highest TMC value was recorded in run #15 (EtOH=25%; T=80°C; t=15min; SSR=40mL/g), which interestingly mirrors the conditions that yielded the most effective extract from melon peel. The Pareto plot (Figure 26) showed that the main factors significantly affecting the process were the same found for CSE-HA.

Table 40. Full Factorial Design 2^n for MAE-HA extraction of polyphenols from PP. Actual variables.

Run No.	EtOH (%)	T (°C)	t (min)	SSR (mL/g)	TMC (mAu*s) (at 280 nm)
1	25	40	5	20	101269.2
2	95	40	5	20	39500.0
3	25	80	5	20	96381.4
4	95	80	5	20	54318.1
5	25	40	15	20	104687.2
6	95	40	15	20	36749.5
7	25	80	15	20	116901.3
8	95	80	15	20	67255.7
9	25	40	5	40	119466.7
10	95	40	5	40	43339.9
11	25	80	5	40	133057.7
12	95	80	5	40	64909.2
13	25	40	15	40	119707.2
14	95	40	15	40	46349.1
15	25	80	15	40	145917.4
16	95	80	15	40	62301.8
17	60	60	10	30	88858.2
18	60	60	10	30	83530.8
19	60	60	10	30	103381.0

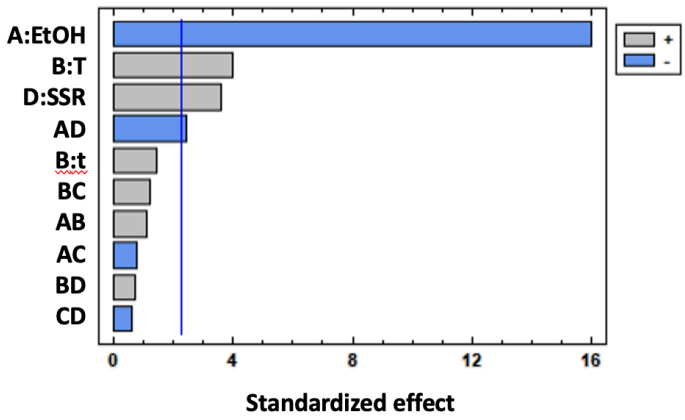

Figure 26. Standardized Pareto Chart effect for total metabolite content (TMC) yield in MAE-HA screening phase for PP. The positive and negative effect of the factors (reported as horizontal bars) on the response variable (TMC) is represented with grey and blue colors, respectively. The vertical line tests the significance of the effect at the 95% confidence level.

EtOH percentage, T, and SSR demonstrated a notable effect on the recovery of polyphenols, thus requiring further investigation during the optimization phase. A standardized extraction time of 5 min was selected for deeper exploration, aligning with the optimization employed in the study of MAE-HA of other agricultural waste materials. The complete BBD, along with the observed extraction yields, used in the optimization step is detailed in Table 41. The considered experimental ranges (-1; +1) were: EtOH 0-30%, T 60-90°C, SSR 30-50 mL/g.

Table 41. Box-Behnken Design for MAE-HA extraction of polyphenols from PP. Actual variables.

Run No.	EtOH (%)	T (°C)	SSR (mL/g)	TMC (mAU*s) (at 280 nm)
1	0	60	40	195303.9
2	30	60	40	118714.8
3	0	90	40	184365.4
4	30	90	40	117796.6
5	0	75	30	200007.1
6	30	75	30	125091.6
7	0	75	50	205781.9
8	30	75	50	126818.6
9	15	60	30	165861.9
10	15	90	30	138822.2
11	15	60	50	185487.2
12	15	90	50	142512.8
13	15	75	40	126146.1
14	15	75	40	134160.4
15	15	75	40	131153.2

The second-order polynomial equation representing the response surface was as follows:

$$Y = 580469, + 6911,86*EtOH - 3394,87*T - 13078,4*SSR - 185,821*EtOH^2 - 237,226*EtOH*T + 45,9673*EtOH*SSR + 27,2838*T^2 - 26,5578*T*SSR + 191,987*SSR^2 + 4,30796*EtOH^2*T - 1,75712*EtOH^2*SSR + 0,794141*EtOH*T^2 + 9,74978E\text{-}10*EtOH*T*SSR + 1,30967E\text{-}10*T^3 + 1,74623E\text{-}10*T^2*SSR - 2,32831E\text{-}10*T*SSR^2 \quad (36)$$

ANOVA results indicated that only EtOH content significantly affect the yield ($p < 0.05$), with a negative impact. The R^2 and R^2_{adj} values were 99.78% and 97.06%, respectively, highlighting a strong agreement between experimental and predicted values (refer to Table 42).

Table 42. The analysis of variance of the Box-Behnken Design model for polyphenolic compounds extraction yield for MAE-HA process.

Source	Sum of squares	Df	Mean square	F ratio	*P* value
A:EtOH	5.92E9	1	5.92E9	184.33	0.0468
B:T	1.23E9	1	1.23E9	38.16	0.1022
C:SSR	1.36E8	1	1.36E8	4.23	0.2881
AA	7.27E8	1	7.27E8	22.64	0.1319
AB	2.51E7	1	2.51E7	0.78	0.5391
AC	4.10E6	1	4.10E6	0.13	0.7816
BB	2.49E8	1	2.49E8	7.75	0.2195
BC	6.35E7	1	6.35E7	1.98	0.3936
CC	1.18E9	1	1.18E9	36.73	0.1041
AAB	4.23E8	1	4.23E8	13.16	0.1712
AAC	3.13E7	1	3.13E7	0.97	0.5043
ABB	1.44E7	1	1.44E7	0.45	0.6247
Total error	3.21E7	1	3.21E7		

The analysis of the surface plots generated for TMC yield in relation to EtOH concentration and T, indicated that the optimal parameter values that yielded the highest extraction efficiency were identified near the upper range values within the experimental domain (as illustrated in Figure 27).

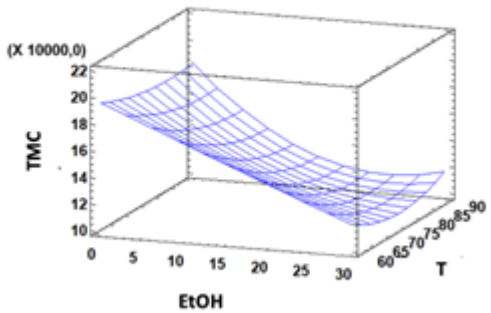

Figure 27. Response surface plot showing the effect of ethanol content (EtOH) and temperature (T) on polyphenolic yield, expressed as total metabolite content (TMC).

The optimal conditions predicted by the statistical software were: 0% EtOH, 60 °C, 5 min, and 50 mL/g SSR. This configuration yielded a calculated total peak area of 221374 mAu*s. The 95% confidence interval for the mean extraction yield value ranged from 124433 mAu*s to 318314 mAu*s, within which the experimental value is expected to fall. The appropriateness of the second-order polynomial equation model was then verified performing an additional set of three experiments under the optimal predicted conditions. The resultant extracts were subjected to RP-HPLC-DAD analysis, and the mean total area of peaks recorded in the chromatographic profiles at 280 nm was 238409.9 ± 5413.5 mAu*s. This finding further validated the accuracy of the model. The extract obtained thus obtained was named PPE-2.

The same extraction method was also investigated using NaDES mixtures. NaDES-4 ($ChCl_2$-Urea, TMC=25490.8 mAu*s) allowed to obtain the best recoveries, followed by NaDES-2 ($ChCl_2$- Glycerol, TMC=22424.3 maU*s), NaDES-1 ($ChCl_2$-Lactic acid = 15270.7 mAu*s), and NaDES-3 ($ChCl_2$-1,2-propanediol, TMC=6559.0 mAu*s).

The comprehensive BBD using NaDES, inclusive of observed extraction yield values, is outlined in Table 43. The considered experimental ranges (-1; +1) were: WC in NaDES mixture 20-50%, T 50-90 °C, SSR 20-40 mL/g, while time was maintained fixed at 5 min.

The mathematical formula of the second-order polynomial equation derived from the response surface is as follows:

$$Y = - 49671{,}8 - 3407{,}65*WC + 2039{,}1*T + 481{,}709*SSR + 53{,}4386*WC^2 + 65{,}6274*WC*T + 47{,}4672*WC*SSR - 3{,}88708*T^2 - 34{,}9645*T*SSR + 7{,}53175*SSR^2 - 0{,}382044*WC^2*T - 0{,}933022*WC^2*SSR - 0{,}487333*WC*T^2 \quad (37)$$

Table 43. Box-Behnken Design for MAE-NaDES extraction of polyphenols from PP. Actual variables

.

Run No.	WC (%)	T (°C)	SSR (mL/g)	TMC (mAU*s) (at 280 nm)
1	20	40	40	8111.2
2	50	40	40	19958.6
3	20	60	40	16848.7
4	50	60	40	22786.7
5	20	50	30	15474.9
6	50	50	30	31182.9
7	20	50	50	13718.1
8	50	50	50	18719.5
9	35	40	30	12559.3
10	35	60	30	27054.2
11	35	40	50	16640.7
12	35	60	50	17149.8
13	35	50	40	18542.0
14	35	50	40	20812.9
15	35	50	40	19721.7

WC and T were significant factors affecting the extraction yield ($p < 0.05$), as evidenced by ANOVA results presented in Table 44. There was a strong correlation between the results obtained from the experimental trials and the predicted values, as denoted by the high coefficients of determination (R2: 99.42%; R2adj: 95.94%).

Table 44. The analysis of variance of the Box-Behnken model for polyphenolic compounds extraction yield for MAE-NaDES process.

Source	Sum of squares	df	Mean square	F ratio	*P* value
A:WC	1.07E8	1	1.07E8	83.12	0.0118
B:T	5.63E7	1	5.63E7	43.63	0.0222
C:SSR	8.48E6	1	8.48E6	6.57	0.1244
AA	1.67E6	1	1.67E6	1.29	0.3737
AB	8.73E6	1	8.73E6	6.77	0.1214
AC	2.87E7	1	2.87E7	22.22	0.0422
BB	1.62E7	1	1.62E7	12.56	0.0712
BC	4.89E7	1	4.89E7	37.91	0.0254
CC	2.09E6	1	2.09E6	1.62	0.3306
AAB	1.48E6	1	1.48E6	1.15	0.3965
AAC	8.81E6	1	8.81E6	683	0.1205
ABB	1.07E6	1	1.07E6	0.83	0.4588
Total error	2.58E6	2	1.29E6		

The surface plots obtained for TMC yield as a function of WC and T is reported in Figure 28.

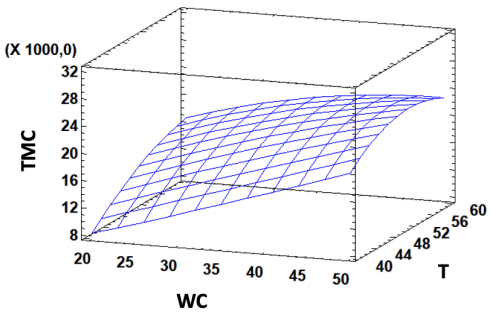

Figure 28. Response surface plot showing the effect of water content (WC) and temperature (T) on polyphenolic yield, expressed as total metabolite content (TMC).

The optimal conditions were 58.6 °C, 50% WC, and 30mL/g SSR. Under these conditions, the total area of the peaks was 33306.5 mAu*s, with a 95% confidence interval for the mean value ranging from 27459.7 mAu*s to 39153.4 mAu*s. Three additional experiments were performed under the optimal predicted conditions and the mean total area values of the peaks recorded at 280 nm were 27805.0 ± 577.0 mAu*s, confirming the accuracy of the fitted

model. The resultant extract obtained under the mentioned experimental conditions was designated as PPE-3 (Pumpkin Peel Extract 3).

Considering the use of NaDES with CSE, the initial screening of the different NaDES mixtures highlighted NaDES-4 ($ChCl_2$-Urea, TMC=22873.2 mAu*s) as the most promising to use for the BBD (NaDES-1: $ChCl_2$- lactic acid, TMC=59001.6 maU*s; NaDES-2: $ChCl_2$-glycerol, TMC=18960.2 mAu*s; NaDES-3: $ChCl_2$-1,2-propanediol, TMC=14289.8 mAu*s). For the optimization of this extraction process, we used the Draper-Lin small composite Design (see section 3.4.2.2) to reduce the number of experiments to be performed. The considered experimental ranges (-1; +1) were WC in NaDES mixture 5-65%, T 30-70 °C, SSR 20-60 mL/g, t 5-125 min. The comprehensive experimental design with four factors, inclusive of observed and predicted extraction yield values, is outlined in Table 45.

The mathematical formula of the second-order polynomial equation derived from the response surface is as follows:

$$Y = 92741{,}6 - 2566{,}97*WC - 131{,}829*T - 141{,}443*t - 3461{,}58*SSR + 15{,}48*WC^2 + 31{,}0133*WC*T + 11{,}818*WC*t + 59{,}4833*H2O*SSR - 6{,}1095*T^2 - 1{,}30608*T*t + 33{,}7999*T*SSR - 0{,}752806*t^2 + 3{,}86908*t*SSR + 13{,}054*SSR^2 - 0{,}178515*WC^2*t - 1{,}15223*WC*T*SSR - 1{,}23691E\text{-}10*WC*t*SSR - 1{,}01863E\text{-}10*T*t*SSR \quad (38)$$

SSR impacted the extraction yield ($p < 0.05$), with a negative effect (as indicated by the ANOVA results outlined in Table 46). Modifications in time, WC, and T contributed to an increase in the extraction yield, even if they were not found to be statistically significant. There was a strong concordance between the experimental results and the predicted values, denoted by the high coefficients of determination value (R^2: 97.52%; R^2_{adj}: 76.45%).

Table 45. Draper-Lin small composite design for CSE-NaDES extraction of polyphenols from PP. Actual variables.

Run No.	WC (%)	T (°C)	t (min)	SSR (mL/g)	TMC (mAu*s) (at 280 nm)
1	50	60	95	30	16012.3
2	50	60	35	30	19431.4
3	50	40	95	50	16063.2
4	20	60	35	50	8568.7
5	50	40	35	50	13272.1
6	20	40	95	30	13785.8
7	20	60	95	50	11012.9
8	20	40	35	30	14417.2
9	35	50	65	40	13613.8
10	35	50	65	40	9292.1
11	5	50	65	40	15142.4
12	65	50	65	40	21028.3
13	35	30	65	40	12219.4
14	35	70	65	40	12085.9
15	35	50	5	40	9180.2
16	35	50	125	40	14592.5
17	35	50	65	20	28023.3
18	35	50	65	60	11612.8
19	35	50	65	40	14397.7
20	35	50	65	40	14795.2

Table 46. The analysis of variance of the Box-Behnken model for polyphenolic compounds extraction yield for MAE-NaDES process.

Source	Sum of squares	Df	Mean square	F ratio	*P* value
A:WC	1.73E7	1	1.73E7	3.68	0.1951
B:T	8911.13	1	8911.13	0	0.9693
C:t	1.46E7	1	1.46E7	3.11	0.2198
D:SSR	1.35E8	1	1.35E8	28.6	0.0332
AA	1.22E7	1	1.22E7	2.59	0.2491
AB	2.05E7	1	2.05E7	4.34	0.1725
AC	744688	1	744688	0.16	0.7293
AD	315282	1	315282	0.07	0.8200
BB	5.97E6	1	5.97E6	1.27	0.3771
BC	1.23E6	1	1.23E6	0.26	0.6603
BD	1.70E6	1	1.70E6	0.36	0.6085
CC	7.34E6	1	7.34E6	1.56	0.3381
CD	1.08E7	1	1.08E7	2.29	0.2695
DD	2.73E7	1	2.73E7	5.79	0.1379
AAC	5.81E6	1	5.81E6	1.23	0.3824
Total error	9.42E6	2	4.71E6		

The surface plots obtained for TMC yield as a function of WC and T is reported in Figure 29.

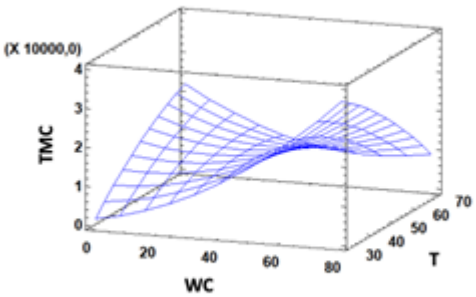

Figure 29. Response surface plot showing the effect of water content (WC) and temperature (T) on polyphenolic yield, expressed as total metabolite content (TMC).

The optimal conditions to maximize the extraction yield were 51.1 °C, 68.9 min, 48.6% of WC, and 20 mL/g SSR. Under these conditions, the total area of the peaks was 28027.1 mAu*s,

with a 95% confidence interval for the mean value ranging from 14855.5 mAu*s to 41198.7 mAu*s. Analyzing the results obtained from the three additional experiments performed under the optimal predicted conditions, the mean total area values of the peaks recorded at 280 nm were 35532.12 ± 2208.1 mAu*s. This confirmed the accuracy of the fitted model. The resultant extract obtained under the mentioned experimental conditions was designated as PPE-4 (Pumpkin Peel Extract 4).

In summary, Figure 30 presents the chromatographic profiles of PPE-1, PPE-2, PPE-3, and PPE-4, recorded at 280 nm. Although PPE-1 exhibited peaks with seemingly high areas, the mean values of the recorded areas were not statistically different from those obtained with PPE-2. In contrast, PPE-3 and PPE-4 displayed lower signal intensities and peak values. As a result, PPE-2 was selected for further bioactivity assays.

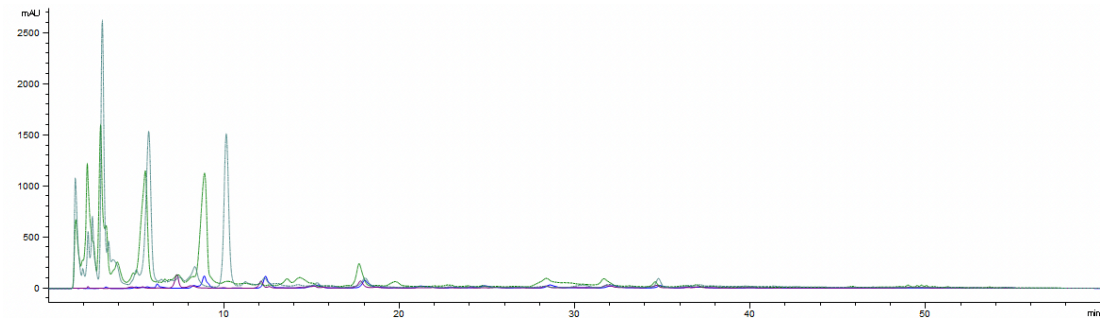

Figure 30. Overlay of the chromatographic profiles of the optimized extracts obtained by applying CSE-HA (PPE-1, light blue line), MAE-HA (PPE-2, green line), MAE- NaDES (PPE-3, violet line) and CSE-NaDES (PPE-4, blue line).

4.5 Optimization of Asparagus bottom part extract (ABE)

In order to accelerate the experimental process, we directly selected the response surface methodology for investigating and optimizing the extraction of CSE-HA and MAE-HA from asparagus bottom parts. Starting with the conventional approach, the considered experimental ranges (-1 to +1) for the BBD were: EtOH 10-90%, T 40-70 °C, t 30-90 min, SSR 20-50 mL/g. Table 47 shows the generated experimental design with four factors together with the results in terms of TMC. Prior to HPLC analysis, the samples were subjected to a 10-fold dilution.

The mathematical expression of the second-order polynomial equation for the response surface obtained is presented below:

$$Y = -6651{,}37 - 306{,}418*EtOH + 586{,}997*T + 167{,}235*t + 1805{,}15*SSR - 2{,}47401*EtOH^2 + 8{,}07433*EtOH*T + 1{,}0121*EtOH*t - 4{,}42304*EtOH*SSR - 9{,}66554*T^2 - 0{,}0520556*T^2*t + 1{,}91467*T*SSR - 2{,}12122*t^2 + 1{,}31939*t*SSR - 16{,}6933*SSR^2 \quad (39)$$

SSR and EtOH content were significant factors affecting the extraction yield ($p < 0.05$), as evidenced by ANOVA results presented in Table 48. Time and temperature, on the other hand, were not statistically significant (p-value = 0.5430), but had a positive influence and negative one, respectively. There was also a strong correlation between the outcomes of experimental trials and the predicted values, denoted by the high coefficients of determination (R^2: 95.56%; R^2_{adj}: 90.39%).

Table 47. Box-Behnken Design for CSE-HA extraction of polyphenols from AB. Actual variables.

Run (No.)	EtOH (%)	T (°C)	t (min)	SSR (mL/g)	TMC (mAu*s) (at 280 nm)
1	10	40	60	35	49063.2
2	90	40	60	35	20937.2
3	10	70	60	35	40442.1
4	90	70	60	35	31694.5
5	50	55	30	20	27556.9
6	50	55	90	20	25683.8
7	50	55	30	50	45133.4
8	50	55	90	50	45635.2
9	10	55	60	20	31707.5
10	90	55	60	20	23515.3
11	10	55	60	50	54067.9
12	90	55	60	50	35260.4
13	50	40	30	35	39955.0
14	50	70	30	35	39308.6
15	50	40	90	35	40274.9
16	50	70	90	35	39534.8
17	10	55	30	35	489248
18	90	55	30	35	29518.0
19	10	55	90	35	48098.0
20	90	55	90	35	33549.3
21	50	40	60	20	31875.7
22	50	70	60	20	29864.8
23	50	40	60	50	49192.2
24	50	70	60	50	48904.5
25	50	55	60	35	42542.7
26	50	55	60	35	44757.8
27	50	55	60	35	44109.1

Table 48. The analysis of variance of the Box-Behnken model for polyphenolic compounds extraction yield for CSE-HA process.

Source	Sum of squares	df	Mean square	F ratio	*P* value
A:EtOH	7.98E8	1	7.98E8	102.13	0
B:T	199924	1	199924	0.03	0.8755
C:t	471756	1	471756	0.06	0.8100
D:SSR	9.72E8	1	9.72E8	124.45	0
AA	8.36E7	1	8.36E7	10.7	0.0067
AB	9.39E7	1	9.39E7	12.02	0.0047
AC	5.90E6	1	5.90E6	0.76	0.4018
AD	2.82E7	1	2.82E7	3.61	0.0818
BB	2.52E7	1	2.52E7	3.23	0.0975
BC	2194.92	1	2194.92	0	0.9869
BD	742355	1	742355	0.1	0.7631
CC	1.94E7	1	1.94E7	2.49	0.1406
CD	1.41E6	1	1.41E6	0.18	0.6784
DD	7.52E7	1	7.52E7	9.64	0.0091
Total error	9.37E7	12	7.81E6		

The surface plots obtained for TMC yield as a function of EtOH content and T is reported in Figure 31.

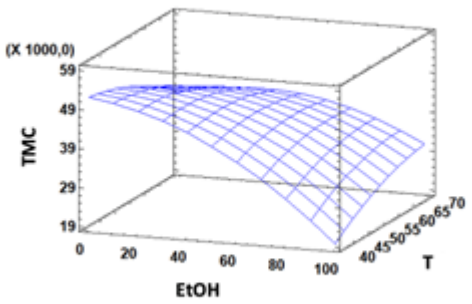

Figure 31. Response surface plot showing the effect of ethanol content (EtOH) and temperature (T) on polyphenolic yield, expressed as total metabolite content (TMC).

The optimal conditions were 45 °C T, 12% of EtOH, 50 mL/g SSR for 41 min. Under these conditions, the total area of the peaks was calculated to be 56878.6 mAu*s, with a 95% confidence interval for the mean value ranging from 50974.6 mAu*s to 62782.6 mAu*s.

Analyzing the results of the three additional experiments conducted under the optimal predicted conditions, the mean total area values of the peaks recorded at 280 nm were 52976.1 ± 1149.7 mAu*s confirming the accuracy of the fitted model and the resultant extract obtained under the mentioned experimental conditions was designated as ABE-1 (Asparagus bottom parts Extract 1).

The same experimental design was used to study and optimize MAE-HA process. Table 49 reported the BBD with four factors generated by the statistical software and TMC values obtained. The considered experimental ranges (-1; +1) were the same considered for CSE-HA, except for time, studied for 2-10 min to optimize a fast process. Once again, the extract was diluted 10-fold before chromatographic analysis.

The second-order polynomial equation representing the response surface was as follows:

$$Y = 26381{,}6 - 161{,}509*EtOH - 13{,}8235*T + 553{,}166*t + 738{,}052*SSR - 0{,}348271*EtOH^2 + 3{,}48738*EtOH*T + 3{,}89859*EtOH*t - 6{,}50008*EtOH*SSR - 0{,}665413*T^2 + 1{,}42175*T*t - 2{,}7568*T*SSR - 9{,}56536*t^2 - 11{,}3021*t*SSR + 0{,}65613*SSR^2 \quad (40)$$

ANOVA results indicated significant effects of EtOH percentage and SSR, as well as the interaction between these two factors ($p < 0.05$). The R^2 and R^2_{adj} values were 90.85% and 80.18%, respectively, highlighting a strong agreement between experimental and predicted outcomes (refer to Table 50).

Table 49. Box-Behnken Design for MAE-HA extraction of polyphenols from asparagus bottom parts. Actual variables.

Run (No.)	EtOH (%)	T (°C)	t (min)	SSR (mL/g)	TMC (mAu*s) (at 280 nm)
1	10	40	6	35	47205.9
2	90	40	6	35	25238.5
3	10	90	6	35	37013.0
4	90	90	6	35	28995.1
5	50	65	2	20	32292.9
6	50	65	10	20	35867.4
7	50	65	2	50	36650.5
8	50	65	10	50	37512.5
9	10	65	6	20	32786.0
10	90	65	6	20	31524.7
11	10	65	6	50	49547.9
12	90	65	6	50	32686.4
13	50	40	2	35	34970.5
14	50	90	2	35	35536.2
15	50	40	10	35	37133.3
16	50	90	10	35	38267.7
17	10	65	2	35	43598.1
18	90	65	2	35	24700.3
19	10	65	10	35	45608.8
20	90	65	10	35	29206.1
21	50	40	6	20	31489.0
22	50	90	6	20	33837.3
23	50	40	6	50	40671.0
24	50	90	6	50	38884.1
25	50	65	6	35	38447.8
26	50	65	6	35	36386.7
27	50	65	6	35	34286.2

Table 50. The analysis of variance of the Box-Behnken Design model for polyphenolic compounds extraction yield for MAE-HA process.

Source	Sum of squares	df	Mean square	F ratio	*P* value
A:EtOH	5.80E8	1	5.80E8	81.91	0
B:T	1.45E6	1	1.45E6	0.21	0.6586
C:t	2.09E7	1	2.09E7	2.96	0.1112
D:SSR	1.21E8	1	1.21E8	17.14	0.0014
AA	1.66E6	1	1.66E6	0.23	0.6373
AB	4.86E7	1	4.86E7	6.87	0.0223
AC	1.56E6	1	1.56E6	0.22	0.6475
AD	6.08E7	1	6.08E7	8.6	0.0126
BB	922448	1	922448	0.13	0.7244
BC	80854.9	1	80854.9	0.01	0.9166
BD	4.27E6	1	4.27E6	0.6	0.4521
CC	124923	1	124923	0.02	0.8965
CD	1.84E6	1	1.84E6	0.26	
DD	116237	1	116237	0.02	
Total error	8.49E7	12	7.08E6		

Surface plots generated for TMC yield in relation to EtOH percentage and T, indicated near the upper range values within the experimental domain as the best parameter values that yielded the highest extraction efficiency (as illustrated in Figure 32).

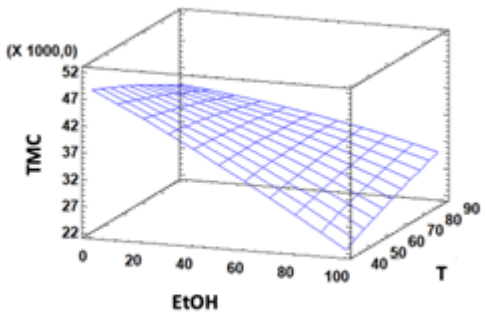

Figure 32. Response surface plot showing the effect of ethanol content (EtOH) and temperature (T) on polyphenolic yield, expressed as total metabolite content (TMC).

The optimal conditions predicted by the statistical software were: 10% EtOH, 40 °C, 5 min, and 50 mL/g SSR. This configuration yielded a calculated total peak area of 54435.9 mAu*s. The

95% confidence interval for the mean extraction yield value ranged from 47831.7 mAu*s to 61040.1 mAu*s, within which the experimental value is expected to fall. The resultant extracts obtained in the set of three experiments under the optimal predicted conditions were subjected to analysis using RP-HPLC-DAD, and the mean total area of peaks recorded in the chromatographic profiles at 280 nm was 520668.0 ± 1337.3 mAu*s. This finding further validates the accuracy of the model. The extract thus obtained was named ABE-2.

Considering MAE-NaDES, the screening phase indicated NaDES-2 ($ChCl_2$-Glycerol, TMC=6559.0 mAu*s) as the most efficient (NaDES-3, $ChCl_2$- 1,2-propanediol, TMC=38553.8 maU*s; NaDES-1, $ChCl_2$-Lactic acid, TMC=34131.2 mAu*s; NaDES-4, ChCl2-Urea = 6486.2 mAu*s).

The comprehensive BBD used for NaDES-2, inclusive of observed extraction yield values, is outlined in Table 51. The considered experimental ranges (-1; +1) were: water content (WC) in NaDES mixture 20-50%, T 40-90 °C, SSR 20-40 mL/g, while time was maintained fixed at 5 min.

Table 51. Box-Behnken Design for MAE-NaDES extraction of polyphenols from asparagus bottom parts. Actual variables.

Run No.	WC (%)	T (°C)	SSR (mL/g)	TMC (mAU*s) (at 280 nm)
1	40	20	35	15823.7
2	90	20	35	27514.3
3	40	50	35	32170.5
4	90	50	35	33930.0
5	40	35	20	39151.1
6	90	35	20	48900.8
7	40	35	50	19622.8
8	90	35	50	17518.8
9	65	20	20	22762.8
10	65	50	20	33025.1
11	65	20	50	14579.1
12	65	50	50	24910.0
13	65	35	35	19351.3
14	65	35	35	25741.7
15	65	35	35	18422.0

The mathematical formulation of the second-order polynomial equation derived from the response surface is as follows:

$$Y= 48935,2 - 807,586*T + 989,826*WC - 1073,62*SSR + 10,9337*T^2 - 6,62073*T*WC - 7,90247*T*SSR - 2,86926*WC^2 + 0,0762222*WC*SSR + 14,6363*SSR^2 \quad (41)$$

SSR emerged as significant factor on the extraction yield ($p < 0.05$), as evidenced by ANOVA results presented in Table 52, while the positive impact of WC and T were not statistically significant on the yield. There was a good concordance between the outcomes of experimental trials and the predicted values, denoted by the high coefficients of determination (R^2: 85.7%; R^2_{adj}: 60.15%).

Table 52. The analysis of variance of the Box-Behnken model for polyphenolic compounds extraction yield for MAE-NaDES process.

Source	Sum of squares	df	Mean square	F ratio	*P* value
A:T	5.56E7	1	5.56E7	1.49	0.2762
B:WC	2.35E8	1	2.35E8	6.31	0.0538
C:SSR	5.65E8	1	5.65E8	15.15	0.0115
AA	1.72E8	1	1.72E8	4.63	0.0841
AB	2.47E7	1	2.47E7	0.66	0.4529
AC	3.51E7	1	3.51E7	0.94	0.3762
BB	1.54E6	1	1.54E6	0.04	0.8470
BC	1176.49	1	1176.49	0	0.9957
CC	4.00E7	1	4.00E7	1.07	0.3474
Total error	1.86E8	5	3.73E7		

The surface plots obtained for TMC yield as a function of T and WC is reported in Figure 33.

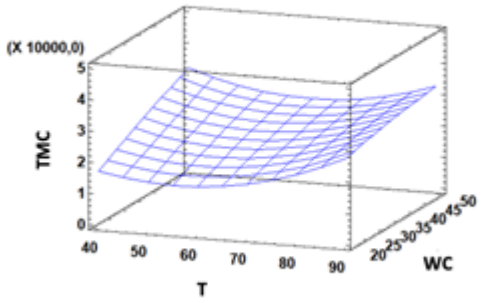

Figure 33. Response surface plot showing the effect of temperature (T) and water content (WC) on polyphenolic yield, expressed as total metabolite content (TMC).

The optimal conditions were 90 °C, 50% WC and 20mL/g SSR. Under these conditions, the total area of the peaks was 47573.9 mAu*s, with a 95% confidence interval for the mean value ranging from 29035.3 mAu*s to 66112.4 mAu*s. Analyzing the outcomes of the three additional experiments conducted under the optimal predicted conditions, the mean total area values of the peaks recorded at 280 nm were calculated to be 52812.5 ± 1453.9 mAu*s. This outcome serves to confirm the accuracy of the fitted model. The resultant extract obtained under the mentioned experimental conditions was designated as ABE-3 (Asparagus bottom parts Extract 3).

The initial screening of the different NaDES mixtures for CSE-NaDES highlighted the same solvent mixture resulted for MAE: NaDES-2 ($ChCl_2$-glycerol, TMC=28444.0 mAu*s). The others gave lower recoveries (NaDES-1: $ChCl_2$- lactic acid, TMC=23188.5 maU*s; NaDES-4, $ChCl_2$-Urea, TMC=18914.6 mAu*s; NaDES-3, $ChCl_2$-1,2-propanediol, TMC=15637.3 mAu*s) and were discarded for the optimization phase. The Draper-Lin small composite Design was used and the considered experimental ranges (-1; +1) were water content (WC) in NaDES mixture 5-65%, T 30-70 °C, SSR 20-60 mL/g, t 5-125 min. The comprehensive experimental design with four factors, inclusive of observed and predicted extraction yield values, is outlined in Table 53.

Table 53. Draper-Lin Small Composite Design for CSE-NaDES extraction of polyphenols from AB. Actual variables.

Run No.	WC (%)	T (°C)	t (min)	SSR (mL/g)	TMC (mAu*s) (at 280 nm)
1	50	60	95	30	42254.1
2	50	60	35	30	30779.5
3	50	40	95	50	28953.5
4	20	60	35	50	20460.2
5	50	40	35	50	20795.8
6	20	40	95	30	25718.5
7	20	60	95	50	21268.6
8	20	40	35	30	22064.4
9	35	50	65	40	28273.0
10	35	50	65	40	22809.5
11	5	50	65	40	18459.9
12	65	50	65	40	32860.2
13	35	30	65	40	26583.6
14	35	70	65	40	31103.9
15	35	50	5	40	23831.2
16	35	50	125	40	33450.8
17	35	50	65	20	35930.4
18	35	50	65	60	23895.7
19	35	50	65	40	28304.6
20	35	50	65	40	22610.5

The mathematical formula of the second-order polynomial equation derived from the response surface is as follows:

$$Y = 39535,5 + 74,2417*WC - 450,036*T - 46,5649*t - 325,654*SSR - 0,781299*WC^2 + 4,39083*WC*T + 4,21383*WC*t - 6,82467*WC*SSR + 6,20133*T^2 + 0,196333*T*t - 5,58825*T*SSR + 0,632717*t^2 - 2,56775*t*SSR + 8,87458*SSR^2 \quad (42)$$

Extraction time, WC and SSR were identified as influential factors affecting the extraction yield ($p < 0.05$), whereas temperature (T) did not have a significant impact on the yield, as indicated

by the ANOVA results presented in Table 54. There was a strong concordance between the outcomes of experimental trials and the predicted values, denoted by the high coefficients of determination (R^2: 94.94%; R^2_{adj}: 75.97%).

Table 54. The analysis of variance of the Box-Behnken model for polyphenolic compounds extraction yield from AB for CSE-NaDES process.

Source	Sum of squares	Df	Mean square	F ratio	*P* value
A:WC	1.04E8	1	1.04E8	11.77	0.0265
B:T	1.02E7	1	1.02E7	1.16	0.3421
C:t	1.17E8	1	1.17E8	13.32	0.0218
D:SSR	7.24E7	1	7.24E7	8.22	0.0456
AA	719195	1	719195	0.08	0.7893
AB	1.74E6	1	1.74E6	0.2	0.6801
AC	2.88E7	1	2.88E7	3.27	0.1450
AD	4.19E6	1	4.19E6	0.48	0.5282
BB	8.95E6	1	8.95E6	1.02	0.3705
BC	27753.7	1	27753.7	0	0.9579
BD	1.25E6	1	1.25E6	0.14	0.7256
CC	7.55E6	1	7.55E6	0.86	0.4070
CD	4.75E6	1	4.75E6	0.54	0.5036
DD	1.83E7	1	1.83E7	2.08	0.2226
Total error	3.52E7	4	8.81E6		

The surface plots obtained for TMC yield as a function of WC and T is reported in Figure 34.

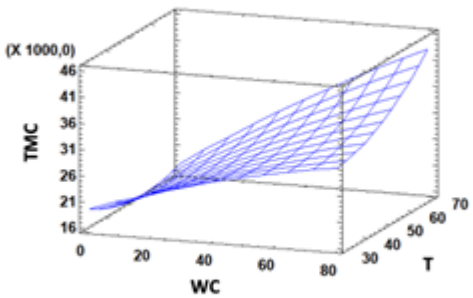

Figure 34. Response surface plot showing the effect of water content (WC) and temperature (T) on polyphenolic yield, expressed as total metabolite content (TMC).

The optimal conditions to improve the extraction yield were 50 °C, 88 min, 51.5% of WC, and 21 mL/g SSR. Under these conditions, the total area of the peaks was 45429.9 mAu*s, with a 95% confidence interval for the mean value ranging from 32539.6 mAu*s to 58320.2 mAu*s. Analyzing the results of the three additional experiments performed under the optimal predicted conditions, the mean total area values of the peaks recorded at 280 nm were calculated to be 56601.4 ± 1774.3 mAu*s. This outcome confirmed the accuracy of the fitted model. The resultant extract obtained under the mentioned experimental conditions was named as ABE-4 (Asparagus bottom part Extract 4).

To sum up, the chromatographic profiles of ABE-1, ABE-2, ABE-3 and ABE-4 registered at 280 nm are reported in Figure 34. ABE-2 shows peaks with the highest areas, which is directly correlated to the higher concentration of the analytes, followed by ABE-1, ABE-4 and ABE-3 (Figure 35).

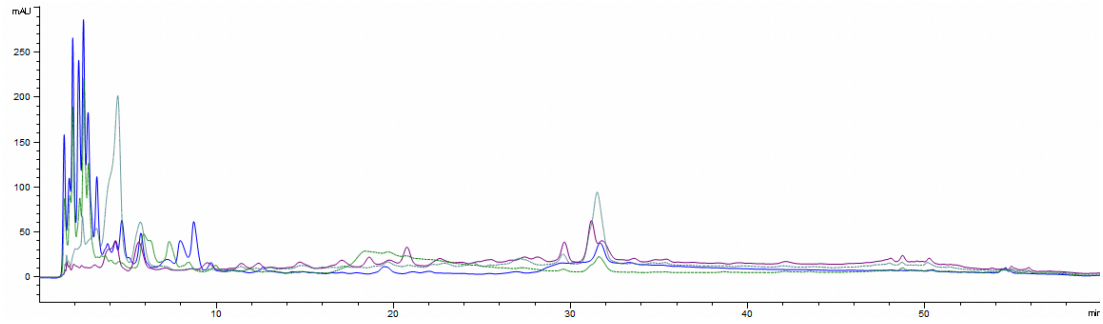

Figure 35. Overlay of the chromatographic profiles of the optimized extracts obtained by applying CSE-HA (ABE-1, green line), MAE-HA (ABE-2, blue line), MAE-NaDES (ABE-3, violet line) and CSE-NaDES (ABE-4, light blue line).

4.6 Optimization of Wheat processing by-products extracts (WPE)

As for asparagus extract, we decided to directly employ the Response Surface Methodology for investigating and optimizing the extraction of polyphenols from wheat processing by-products (WP) using CSE-HA and MAE-HA. Based on the research of Carciochi et al. (2018), we started with the study of CSE-HA, adopting the following experimental ranges (-1 to +1) for the used BBD: EtOH 40-80%, T 40-80 °C, t 30-90 min, and SSR 20-50 mL/g. Table 55 shows the generated experimental design with four factors together with the results expressed as TMC, reported at 280 nm.

The mathematical expression of the second-order polynomial equation for the response surface obtained is presented below:

$$\text{Yield} = -41023{,}4 + 2754{,}15*\text{EtOH}\ \ 1146{,}62*T + 1149{,}25*t + 1079{,}69*\text{SSR} - 24{,}1572*\text{EtOH}^2 + 6{,}83544*\text{EtOH}*T - 29{,}6809*\text{EtOH}*t - 64{,}1413*\text{EtOH}*\text{SSR} + 4{,}48774*T^2 - 13{,}6901*T*t + 65{,}5491*T*\text{SSR} + 4{,}56771*t^2 - 4{,}76711*t*\text{SSR} - 14{,}381*\text{SSR}^2 - 0{,}0875125*\text{EtOH}^2*T + 0{,}211648*\text{EtOH}^2*t + 0{,}5481*\text{EtOH}^2*\text{SSR} + 0{,}0485781*\text{EtOH}*T^2 + 0{,}0500042*\text{EtOH}*t^2 + 0{,}191142*T^2*t - 0{,}514496*T^2*\text{SSR} - 0{,}105071*T*t^2 \quad (43)$$

EtOH had a significant impact on the extraction yield ($p < 0.05$), as evidenced by ANOVA results presented in Table 56. Conversely, T, t, and SSR were not statistically significant. There was also a strong accordance between the outcomes of experimental trials and the predicted values, denoted by the high coefficient of determination values (R^2: 96.10%; R^2_{adj}: 74.70%).

Table 55. BBD for CSE-HA extraction of polyphenols from WP. Actual variables.

Run (No.)	EtOH (%)	T (°C)	t (min)	SSR (mL/g)	TMC (mAu*s) (at 280 nm)
1	40	40	60	35	25492.4
2	80	40	60	35	16150.9
3	40	80	60	35	28227.5
4	80	80	60	35	22347.3
5	60	60	30	20	18134.4
6	60	60	90	20	21334.5
7	60	60	30	50	22197.8
8	60	60	90	50	16817.1
9	40	60	60	20	22984.7
10	80	60	60	20	13618.2
11	40	60	60	50	28356.5
12	80	60	60	50	20946.8
13	60	40	30	35	20398.1
14	60	80	30	35	26515.4
15	60	40	90	35	27929.1
16	60	80	90	35	25978.6
17	40	60	30	35	26632.1
18	80	60	30	35	17983.3
19	40	60	90	35	28560.5
20	80	60	90	35	24033.4
21	60	40	60	20	20695.3
22	60	80	60	20	24275.5
23	60	40	60	50	12008.6
24	60	80	60	50	20160.3
25	60	60	60	35	21716.8
26	60	60	60	35	23738.6
27	60	60	60	35	22161.7

Table 56. The analysis of variance of the Box-Behnken model for polyphenolic compounds extraction yield for CSE-HA process.

Source	Sum of squares	df	Mean square	F ratio	*P* value
A:EtOH	7.04E7	1	7.04E7	14.15	0.0198
B:T	3.44E7	1	3.44E7	6.92	0.0582
C:t	1.19E6	1	1.19E6	0.24	0.6505
D:SSR	51529	1	51529	0.01	0.9238
AA	5.22E6	1	5.22E6	1.05	0.3634
AB	3.00E6	1	3.00E6	0.6	0.4811
AC	4.25E6	1	4.25E6	0.85	0.4078
AD	957267	1	957267	0.19	0.6835
BB	636380	1	636380	0.13	0.7387
BC	1.63E7	1	1.63E7	3.27	0.1448
BD	5.22E6	1	5.22E6	1.05	0.3634
CC	6.90E6	1	6.90E6	1.39	0.3042
CD	1.84E7	1	1.84E7	3.7	0.1267
DD	5.58E7	1	5.58E7	11.23	0.0286
AAB	980280	1	980280	0.2	0.6801
AAC	1.29E7	1	1.29E7	2.59	0.1826
AAD	2.16E7	1	2.16E7	4.35	0.1054
ABB	302059	1	302059	0.06	0.8175
ACC	1.62E6	1	1.62E6	0.33	0.5987
BBC	1.05E7	1	1.05E7	2.12	0.2195
BBD	1.91E7	1	1.91E7	3.83	0.1219
BCC	7.15E6	1	7.15E6	1.44	
Total error	1.99E7	4	4.97E6		

The surface plots obtained for TMC yield as a function of EtOH content and T is reported in Figure 36.

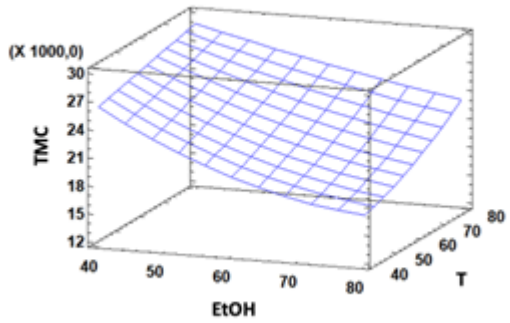

Figure 36. Response surface plot showing the effect of ethanol content (EtOH) and temperature (T) on polyphenolic yield, expressed as total metabolite content (TMC).

The identified optimal conditions were 40 °C, 41% of EtOH, 26 mL/g SSR for 90 min of extraction. Under these conditions, the total area of the peaks was 34182.2 mAu*s, with a 95% confidence interval for the mean value ranging from 23027.9 mAu*s to 45336.6 mAu*s. The analysis of the three additional experiments performed under the optimal predicted conditions indicated a mean total area value of the peaks recorded at 280 nm of 23560.5±236.7 mAu*s, thus confirming the accuracy of the fitted model. The extract obtained under the mentioned experimental conditions was named as WPE-1 (Wheat Processing By-product Extract 1).

Only one experimental design was used to study and optimize MAE-HA process. Table 57 reported the BBD with four factors generated by the statistical software and TMC obtained. The considered experimental ranges (-1; +1) were: EtOH 10-90%, T 40-90 °C, SSR 20-50 mL/g, and time fixed at 5 min.

The second-order polynomial equation representing the response surface was as follows:

$$Y = 29834{,}8 + 90{,}3499*EtOH - 218{,}909*T - 42{,}6863*SSR - 3{,}64154*EtOH^2 + 1{,}40082*EtOH*T + 1{,}093*EtOH*SSR + 0{,}545007*T^2 + 2{,}46*T*SSR - 1{,}66931*SSR^2 \quad (44)$$

ANOVA results indicated significant effects of EtOH ($p < 0.05$). SSR and T were not significant on the yield, although they displayed a positive impact. The R^2 and R^2_{adj} values were 93.43% and 81.59%, respectively, highlighting a strong agreement between experimental and predicted outcomes (refer to Table 58).

Table 57. Box-Behnken Design for MAE-HA extraction of polyphenols from WP. Actual variables.

Run No.	EtOH (%)	T (°C)	SSR (mL/g)	TMC (mAU*s) (at 280 nm)
1	10	40	35	25365.1
2	90	40	35	9212.1
3	10	90	35	20704.7
4	90	90	35	10155.0
5	10	65	20	21538.6
6	90	65	20	10459.0
7	10	65	50	19515.4
8	90	65	50	11059.0
9	50	40	20	19392.9
10	50	90	20	20215.0
11	50	40	50	21560.2
12	50	90	50	26072.3
13	50	65	35	22740.0
14	50	65	35	21590.9
15	50	65	35	21204.3

Table 58. The analysis of variance of the BBD model for polyphenolic compounds extraction yield for MAE-HA process.

Source	Sum of squares	df	Mean square	F ratio	*P* value
A:EtOH	2.67E8	1	2.67E8	45.93	0.0011
B:T	326715	1	326715	0.06	0.8221
C:SSR	5.45E6	1	5.45E6	0.94	0.3777
AA	1.25E8	1	1.25E8	21.54	0.0056
AB	7.85E6	1	7.85E6	1.35	0.2979
AC	1.72E6	1	1.72E6	0.3	0.6100
BB	428412	1	428412	0.07	0.7970
BC	3.40E6	1	3.40E6	0.58	0.4789
CC	520882	1	520882	0.09	0.7768
Total error	2.91E7	5	2.91E7		

The analysis of the surface plots generated for TMC yield in relation to EtOH content and T indicated that the optimal parameter values that yielded the highest extraction efficiency were near the upper range values within the experimental domain (as illustrated in Figure 37).

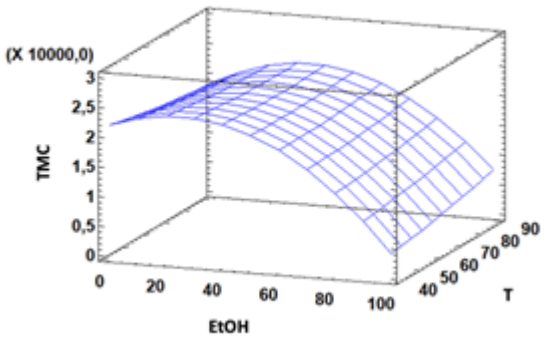

Figure 37. Response surface plot showing the effect of ethanol content (EtOH) and temperature (T) on polyphenolic yield, expressed as total metabolite content (TMC).

The optimal conditions predicted by the statistical software were: 23.8% EtOH, 40 °C, 5 min, and 24.5 mL/g SSR. This configuration yielded a calculated total peak area of 24372.0 mAu*s. The 95% confidence interval for the mean extraction yield value ranged from 19373.6 mAu*s to 29370.4 mAu*s, within which the experimental value is expected to fall. The resultant extracts conducting by additional set of three experiments under the optimal predicted conditions were subjected to analysis using RP-HPLC-DAD, and the mean total area of peaks recorded in the chromatographic profiles at 280 nm was determined to be 22129.3 ± 394.9 mAu*s. This finding further validates the accuracy of the model. The extract obtained was named WPE-2.

Considering MAE-NaDES, the screening phase among different solvent mixtures pointed out NaDES-1 ($ChCl_2$-lactic acid, TMC= 9568.4 mAu*s) as the most efficient (NaDES-2, $ChCl_2$-glycerol, TMC=7715.9 mAu*s; NaDES-4, $ChCl_2$-Urea = 6385.4 mAu*s; NaDES-3, $ChCl_2$- 1,2-propanediol, TMC=6384.4 maU*s). The comprehensive BBD applied using NaDES-1, inclusive of observed extraction yield values, is outlined in Table 59. The considered experimental ranges (-1; +1) were: WC in NaDES mixture 20-50%, T 40-90 °C, SSR 20-40 mL/g, while time was maintained fixed at 5 min.

Table 59. Box-Behnken Design for MAE-NaDES extraction of polyphenols from WP. Actual variables.

Run No.	WC (%)	T (°C)	SSR (mL/g)	TMC (mAU*s) (at 280 nm)
1	40	20	35	6647.7
2	90	20	35	6509.1
3	40	50	35	7060.0
4	90	50	35	5982.7
5	40	35	20	6341.2
6	90	35	20	6392.6
7	40	35	50	5443.9
8	90	35	50	5632.0
9	65	20	20	5956.0
10	65	50	20	7168.3
11	65	20	50	5258.4
12	65	50	50	5729.5
13	65	35	35	6005.9
14	65	35	35	6077.8
15	65	35	35	6181.9

The mathematical formulation of the second-order polynomial equation derived from the response surface is as follows:

$$Y = 5804.02 - 26.2832*T - 0.9492904*WC + 93.6268*SSR + 0.308573*T^2 - 0.6258*T*WC + 0.0911333*T*SSR + 1.19326*WC^2 - 823556*WC*SSR - 1.46207*SSR^2 \quad (45)$$

SSR (negative effect) and WC (positive effect) were significantly affected the extraction yield ($p < 0.05$), as evidenced by ANOVA results presented in Table 60. Conversely, the positive impact of T seemed to not statistically affect the yield. There was accordance between the outcomes of experimental trials and the predicted values, denoted by the coefficients of determination (R^2: 82.89%; R^2_{adj}: 52.09%).

Table 60. The analysis of variance of the Box-Behnken model for polyphenolic compounds extraction yield for MAE-NaDES process.

Source	Sum of squares	Df	Mean square	F ratio	*P* value
A:T	119170	1	119170	0.84	0.4025
B:WC	307838	1	307838	2.16	0.2017
C:SSR	1.79959E6	1	1.79959E6	12.62	0.0163
AA	137333	1	137333	0.96	0.3715
AB	220289	1	220289	1.54	0.2690
AC	4671.72	1	4671.72	0.03	0.8635
BB	266154	1	266154	1.87	0.2301
BC	137344	1	137344	0.96	0.3714
CC	399578	1	399578	2.80	0.1550
Total error	712931	5	142586		

The surface plots obtained for TMC yield as a function of T and WC is reported in Figure 38. The optimal conditions which let the highest extraction yield were 40 °C, 50% WC, and 21mL/g SSR. Under these conditions, the total area of the peaks was calculated to be 7467.6 mAu*s, with a 95% confidence interval for the mean value ranging from 6320.8 mAu*s to 8614.3 mAu*s.

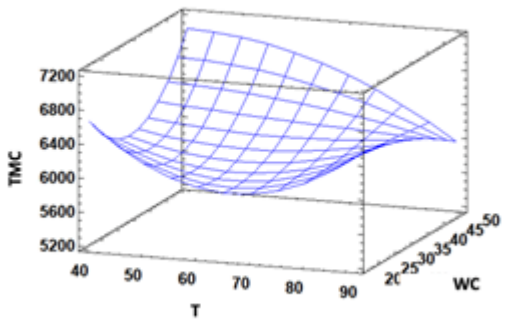

Figure 38. Response surface plot showing the effect of water content (WC) and temperature (T) on polyphenolic yield, expressed as total metabolite content (TMC).

The mean total area values of the peaks recorded at 280 nm for the three additional experiments performed under the optimal predicted conditions were 6516.4 ± 193.2 mAu*s. This result confirmed the accuracy of the fitted model. The resultant extract obtained under

the mentioned experimental conditions was named WPE-3 (Wheat processing by-product Extract 3).

The initial screening of the different NaDES mixtures for CSE-NaDES indicated that the best solvent was the same solvent mixture that gave the highest yield using MAE: NaDES-1 ($ChCl_2$-lactic acid, TMC=10766.2 maU*s). The other mixtures let to lower recoveries (NaDES-2, $ChCl_2$-glycerol, TMC=8149.6 mAu*s; NaDES-3, $ChCl_2$-1,2-propanediol, TMC=7687.4 mAu*s; NaDES-4, $ChCl_2$-Urea, TMC=6040.4 mAu*s) and were discarded in the optimization phase. The Draper-Lin small composite Design was used and the considered experimental ranges (-1; +1) were WC in NaDES mixture 5-65%, T 30-70 °C, SSR 20-60 mL/g, t 5-125 min. The comprehensive experimental design with four factors, inclusive of observed and predicted extraction yield values, is outlined in Table 61.

The mathematical formula of the second-order polynomial equation derived from the response surface is as follows:

$$Y = 9566{,}13 - 141{,}877*WC - 36{,}1204*T - 29{,}5133*t - 120{,}128*SSR + 1{,}08046*WC^2 + 2{,}105*WC*T + 1{,}75637*WC*t + 1{,}15642*WC*SSR - 0{,}361*T^2 + 0{,}197083*T*t + 1{,}31388*T*SSR - 0{,}0762361*t^2 - 0{,}03275*t*SSR + 0{,}91*SSR^2 - 0{,}0209148*WC^2*t - 0{,}043375*WC*T*SSR \quad (46)$$

Both WC and SSR appeared the most impacting factors on the extraction yield ($p < 0.05$), with WC exhibiting a positive effect and SSR exerting a positive influence (as indicated by the ANOVA results outlined in Table 62). Differently, changes in t and T seemed to increase the extraction yield, even if these effects were not statiscally significant. There was a strong correlation between the experimental results and the predicted values, denoted by the high coefficient of determination values (R^2: 99.40%; R^2_{adj}: 94.32%).

Table 61. Draper-Lin Small Composite Design for CSE-NaDES extraction of polyphenols from wheat processing by-products. Actual variables.

Run No.	WC (%)	T (°C)	t (min)	SSR (mL/g)	TMC (mAu*s) (at 280 nm)
1	50	60	95	30	6297.5
2	50	60	35	30	5880.5
3	50	40	95	50	5239.1
4	20	60	35	50	5102.1
5	50	40	35	50	5097.9
6	20	40	95	30	4924.3
7	20	60	95	50	4953.6
8	20	40	35	30	5270.0
9	35	50	65	40	5354.6
10	35	50	65	40	5359.5
11	5	50	65	40	4678.2
12	65	50	65	40	5729.0
13	35	30	65	40	5188.4
14	35	70	65	40	5432.2
15	35	50	5	40	4881.9
16	35	50	125	40	5478.6
17	35	50	65	20	6202.6
18	35	50	65	60	5434.8
19	35	50	65	40	5553.9
20	35	50	65	40	5355.5

Table 62. The analysis of variance of the Draper-Lin Small Composite Design model for polyphenolic compounds extraction yield for CSE-NaDES process.

Source	Sum of squares	df	Mean square	F ratio	P value
A:WC	552090	1	552090	56.07	0.0174
B:T	29719.2	1	29719.2	3.02	0.2245
C:t	178025	1	178025	18.08	0.0511
D:SSR	294758	1	294758	29.93	0.0318
AA	63051.2	1	63051.2	6.40	0.1271
AB	12321	1	12321	1.25	0.3796
AC	138443	1	138443	14.06	0.0643
AD	92233.7	1	92233.7	9.37	0.0922
BB	20851.4	1	20851.4	2.12	0.2829
BC	27966.1	1	27966.1	2.84	0.2340
BD	1668.72	1	1668.72	0.17	0.7205
CC	75322.8	1	75322.8	7.65	0.1096
CD	772.245	1	772.245	0.08	0.8057
DD	132496	1	132496	13.46	0.0669
AAC	79721.5	1	79721.5	8.10	0.1045
Total error	19693.3	2	9846.64		

The surface plots obtained for TMC yield as a function of WC and T is reported in Figure 39.

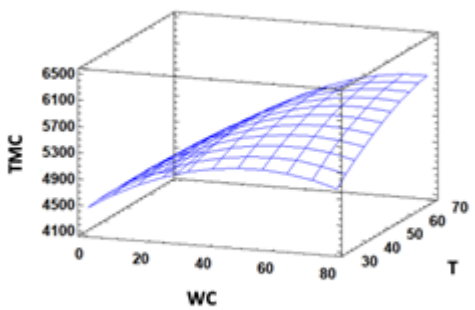

Figure 39. Response surface plot showing the effect of water content (WC) and temperature (T) on polyphenolic yield, expressed as total metabolite content (TMC).

In this case, the optimal conditions were 51 °C, 80 min, 51% of WC, and 24mL/g SSR. Under these conditions, the total area of the peaks was 6468.4 mAu*s, with a 95% confidence interval for the mean value ranging from 5963.3 mAu*s to 6973.5 mAu*s. The mean total area values of the peaks recorded at 280 nm for the three additional experiments conducted under the optimal predicted conditions were 6547.1 ± 75.14 mAu*s. This outcome confirmed the accuracy of the fitted model. The resultant extract obtained under the mentioned experimental conditions was named WPE-4 (Wheat Processing by-product Extract 4).

To sum up, the chromatographic profiles of WPE-1, WPE-2, WPE-3 and WPE-4 registered at 280 nm are reported in Figure 40. The profile registered for WPE-2 showed peaks with the highest areas, which are directly correlated to the higher concentration of the analytes, followed by WPE-1, WPE-4, and WPE-3 (Figure 40).

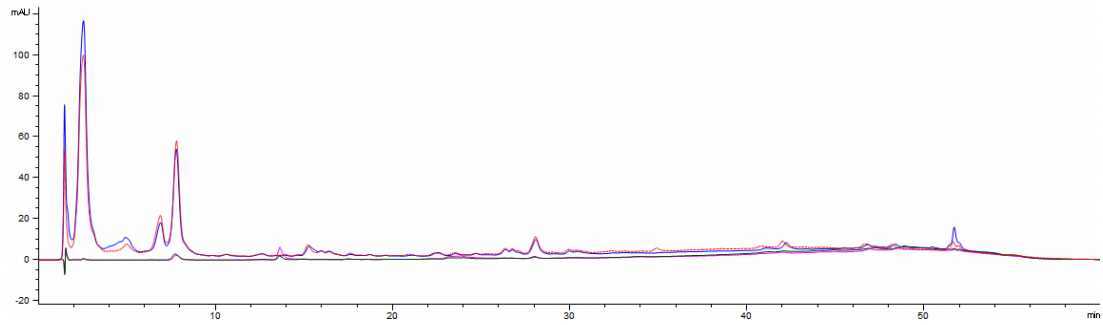

Figure 40. Overlay of the chromatographic profiles of the optimized extracts obtained by applying CSE-HA (WPE-1, red line), MAE-HA (WPE-2, blue line), MAE-NaDES (WPE-3, pink line) and CSE-NaDES (WPE-4, dark green line).

4.7 General Considerations

A comparative overview of the results obtained for all the studied AFW studied considering the extraction methods optimization, is reported in Table 63.

Despite NaDES are currently widely studied for the polyphenols' extraction as promising green solvents (Sharma et al., 2022; Gil Martìn et al., 2022), some drawbacks limited their use, as the need to isolate/purify the analytes after their extraction or their difficult handling directly linked with their high viscosity (Ruesgas-Ramón et al., 2017). Effectively, NaDES extraction approaches are related to lower polyphenols recovery for all the investigated AFW (Table 63). This could be partially attributed to polyphenolic fraction isolation after the extraction processes, obtained with a solid-phase extraction (SPE) (as reported in section 3.3.2.1) which probably is not complete and needs more investigation. However, the selection of the most efficient washing and eluent phase could be a limiting step as compounds with different chemical features are present in the extracts and an optimization of the purification step is probably required. Nevertheless, the extraction yield obtained with NaDES was generally less than half of the yield obtained with hydroalcoholic solvents, and this unsatisfactory result could be only partially attributed to the optimization of the polyphenolic fraction step.

Hydroalcoholic solvents were responsible for the highest polyphenols recovery. Consistent with findings from other authors, a high ethanolic content in the extraction mixture was proved to be effective for CC (Lao et al., 2018) and RH (Das et al., 2018), while lower ethanol concentrations were more effective for the others AFW (Leichtweis et al., 2023).

The use of microwaves offered a significant advantage, not only in terms of extraction yield but also in timesaving. The extraction process time was remarkably reduced to 5 min, a significant saving compared to 60-90 min generally required for CSE (Table 63). The effectiveness of MAE could likely be attributed to the disruption of plant matrix cells induced by microwave irradiation. This disruption promoted the fast release of bioactive compounds. This hypothesis was corroborated by scanning electron microscopy (SEM) analysis on corn cob matrix before and after MAE process, as depicted in Figure 41. Notably, the material subjected to microwave treatment displayed evident pores and fractures, possibly stemming from the rapid heating and internal pressure fluctuations brought about by microwave power. Similar findings have been previously documented by other researchers for other matrices (Alara et al., 2018; Náthia Neves and Alonso, 2021; Sharma et al., 2022). In addition, MAE short extraction time allowed to use high extraction temperature avoiding thermal degradation of polyphenols (Pimientel-Moral et al., 2018). Indeed, the higher recovery of polyphenols is achieved using the MAE-HA extraction method for all waste matrices, except for melon, which

best yield was obtained after 30 minutes of CSE-HA (Table 63). This suggest that the extraction technique used is not dependent from the type of food matrix extracted.

Table 63. Summary of the principal characteristics of the optimized methods regarding all the AFW and the main results (yields).

	CORN COB EXTRACTS (CBE)				RICE HUSK EXTRACTS (RHE)				WHEAT BY-PRODUCTS EXTRACTS (WPE)			
FACTOR	**CSE**		**MAE**		**CSE**		**MAE**		**CSE**		**MAE**	
	HA	**NaDES ChCl:Urea**	**HA**	**NaDES ChCl:Gly**	**HA**	**NaDES ChCl:Urea**	**HA**	**NaDES ChCl:LA**	**HA**	**NaDES ChCl:LA**	**HA**	**NaDES ChCl:LA**
EtOH (%)	50.3	-	62.4	-	64.1	-	80	-	41	-	23.8	-
T (C°)	60	58.7	88	90	60	40	90	89.9	40	51	40	40
t (min)	89.9	78	5	5	60	90	5	5	90	80	5	5
SSR (g/mL)	1:33.8	1:20	1:42.8	1:20	1:40	1:10	1:35	1:20	1:26	1:24	1:24.5	1:21
Water (%)	-	26.4	-	20	-	50	-	45.3	-	51	-	50
Yields (mAu*S)	**242965.2 ± 3411.5**	**102634.2 ± 3364.6**	**283565.4± 3737.7**	**108000.2 ± 4530.0**	**130154.3± 3270.4**	**30617.6 ± 444.7**	**135852.3 ± 1989.8**	**55684.85± 4491.5**	**23560.5± 236.7**	**6547.1± 75.1**	**22129.3± 394.9**	**6516.4± 193.2**

	MELON PEEL EXTRACTS (MPE)				PUMPKIN PEEL EXTRACTS (PPE)				ASPARAGUS BOTTOM PARTS EXTRACTS (ABE)			
FACTOR	**CSE**		**MAE**		**CSE**		**MAE**		**CSE**		**MAE**	
	HA	**NaDES ChCl:Urea**	**HA**	**NaDES ChCl:Gly**	**HA**	**NaDES ChCl:Urea**	**HA**	**NaDES ChCl:Urea**	**HA**	**NaDES ChCl:Gly**	**HA**	**NaDES ChCl:Gly**
EtOH (%)	21.3	-	20	-	0	-	0	-	12	-	10	-
T (C°)	52.8	60	60	50	59,9	48,6	60	58,6	45	50	40	90
t (min)	30	30	5	5	30	68.9	5	5	41	88	5	5
SSR (g/mL)	1:51.5	1:30	1:50	1.30.6	1:40	1:20.1	1:50	1:30	1:50	1:21	1:50	1.20
Water (%)	-	50	-	41	-	48.6	-	50	-	51.5	-	40
Yields (mAu*S)	**206531.8± 6044.7**	**41098.7± 1932.6**	**179916.8± 2004.2**	**33853.6± 4203.6**	**239402.6± 3521.9**	**35532.12± 2208.1**	**238409.9± 5413.5**	**27805.0 ± 577.0**	**529761.0± 1149.7**	**56601.4± 1774.3**	**520668.0± 1337.3**	**52812.5± 1453.9**

*HA: hydroalcoholic
ChCl: choline chloride
LA: lactic acid
Gly: glycerol

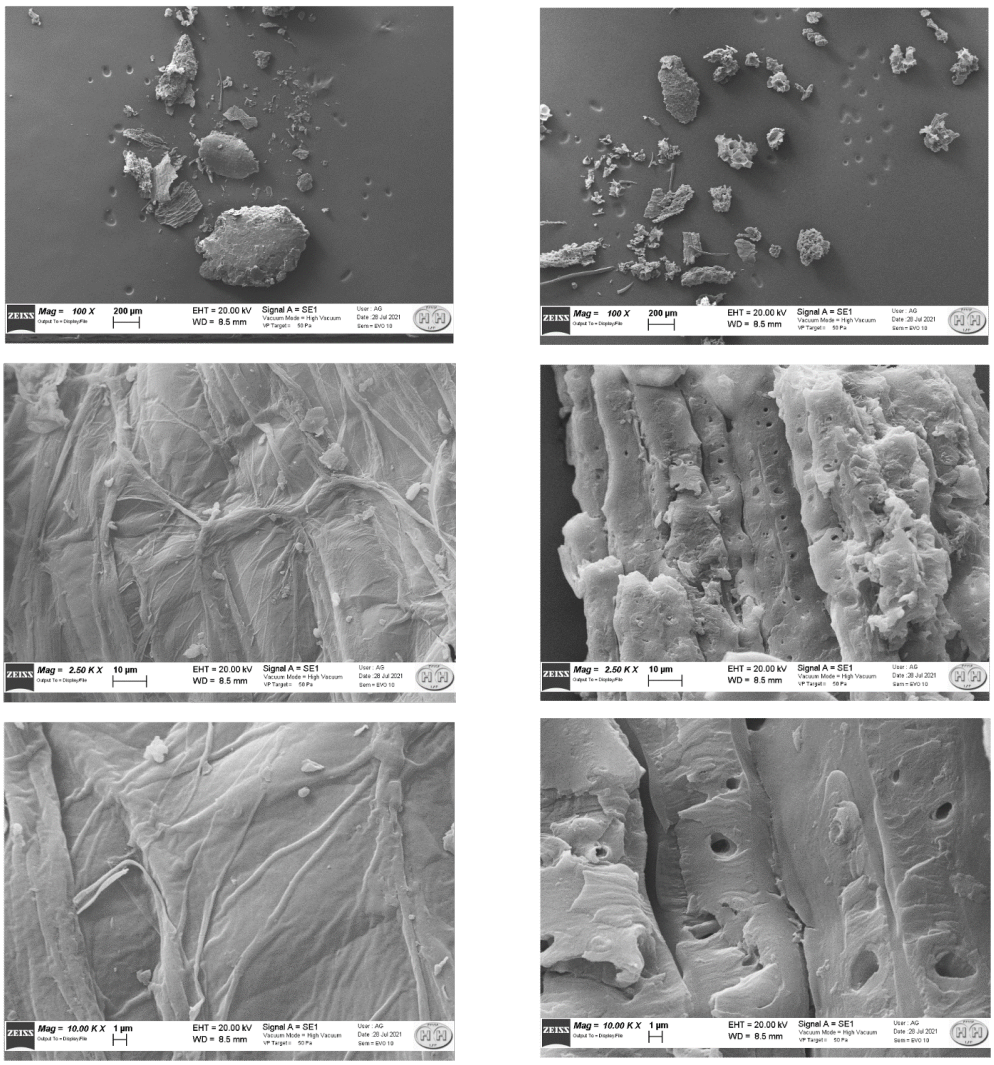

Figure 41. Scanning electron microscopy (SEM) images at different magnifications: for corn cob raw material (column a) and the material after MAE extraction (column b).

4.8 Evaluation of antiglycative activity

CBE-2, RHE-2, MPE-1, PPE-2, ABE-2, and WBE-2 were identified as the extracts yielding the highest TMC recovery and thus were tested for bioactivity assays.

The potential ability of the extracts to mitigate the non-enzymatic protein glycation (Maillard reaction) has been explored. Three different concentrations (0.5, 1 and 2.5 mg dry matter/mL) of each best AFW extracts were investigated to assess their antiglycative properties at various stages of non-enzymatic protein glycation (Figure 42).

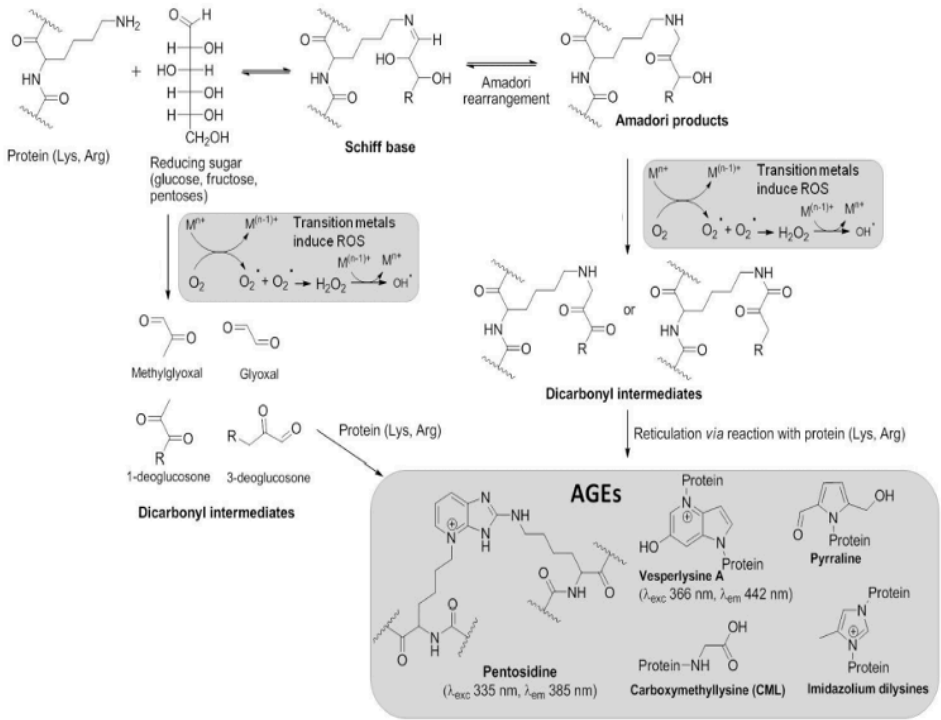

Figure 42. General scheme of the glycation starting from the reaction between the free amino group of a protein and the carbonyl group of a reducing sugar.

Their impact on the initial phase of the reaction was studied through the inhibition of fructosamine formation. Fructosamine, an Amadori product, is produced through the rearrangement of Schiff's bases originating from the reaction between sugar carbonyl groups and protein amino groups, followed by rearrangement, condensation, or oxidative modifications (Anwar et al., 2021). A system based on bovine serum albumin (BSA) and glucose (GLU) used as protein and sugar models, respectively, was used to monitor fructosamine formation using the NBT assay under mild conditions (see section 3.7.1) (Maietta et al., 2017). All the extracts had the capability to reduce the production of Amadori products, with the exception of ABE-2, that showed no activity (Figure 43). Considering the highest concentration

tested (2.5 mg/mL), CBE-2 and RHE-2 showed an inhibitory activity around 70% (CCE-1 72.5±4.7%; RHE-2 71.6±4.3%), followed by lower activities registered for PPE-2 (62.18±1.3 %), MPE-1 (60.3±3.2 %), and WPE-2 (59.7±0.1%).

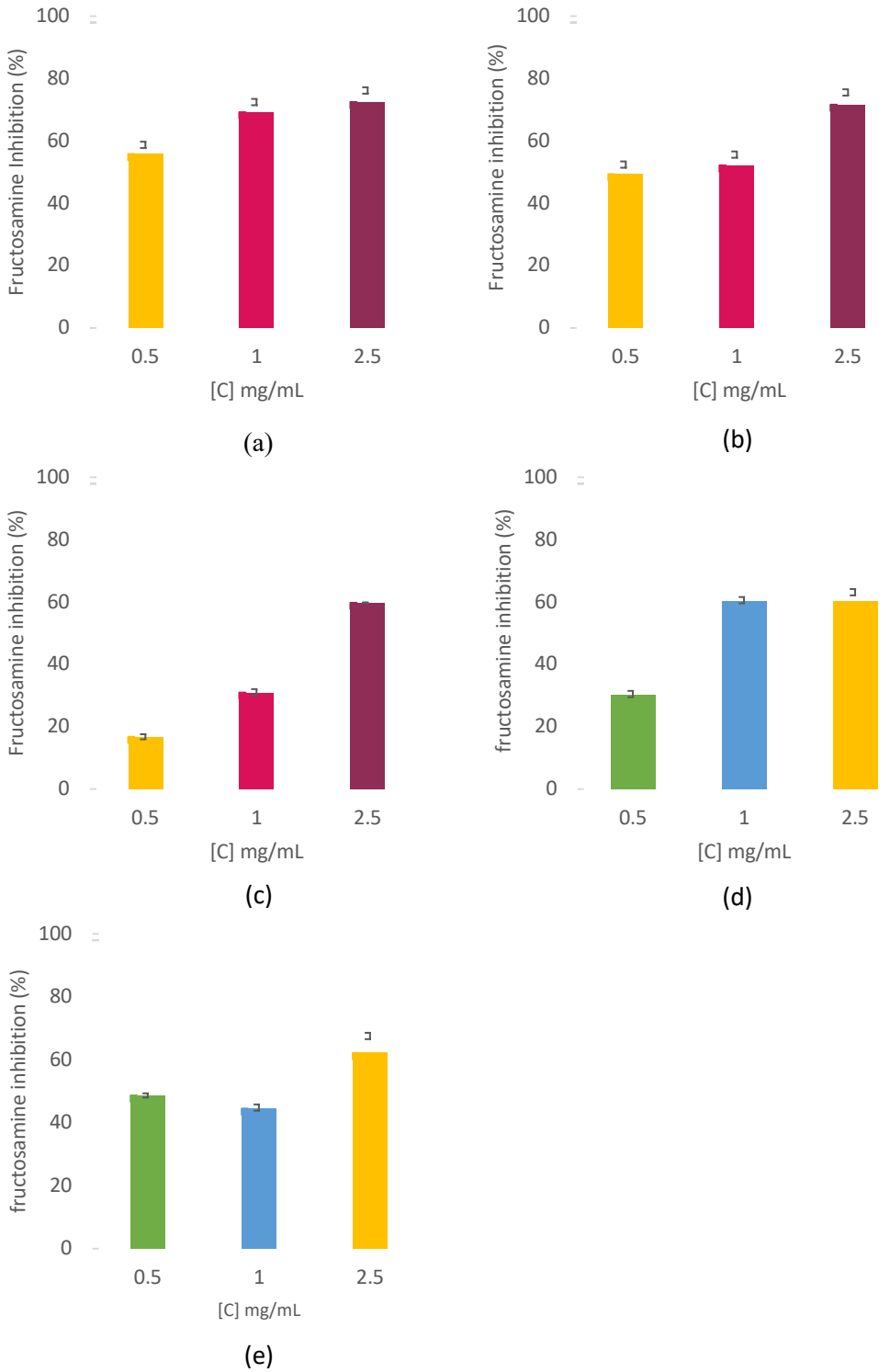

Figure 43. Inhibition of the fructosamine formation by CBE-2 (a), RHE-2 (b), WBE-2 (c), MPE-1 (d), PPE-2 (e) tested at different concentrations (0.5, 1, 2.5 mg dry matter/mL) in NBT assay.

Intermediate phases of the Maillard reaction exhibited a distinctive characteristic marked by the generation of dicarbonyl compounds. These compounds are recognized as precursors for advanced glycation end-products (AGEs) (Anwar et al., 2021). To investigate the impact of the AGW extracts during the middle stage of glycation, the BSA-MGO system was employed (see section 3.7.2). In this system, MGO reacted with BSA, playing an intermediate role in the formation of AGEs. The efficacy of the extracts in influencing this specific phase of protein glycation was probed by monitoring the formation of pentosidine- and argpyrimidine-like AGEs in BSA-MGO systems over 1, 4, and 7 days. In this phase, the activities of our extracts were compared with a standard, the aminoguanidine (AG, 0.5 mg/mL), a compound well-known for antiglycative abilities whose use is therapy is not recommended due to the numerous side effects.

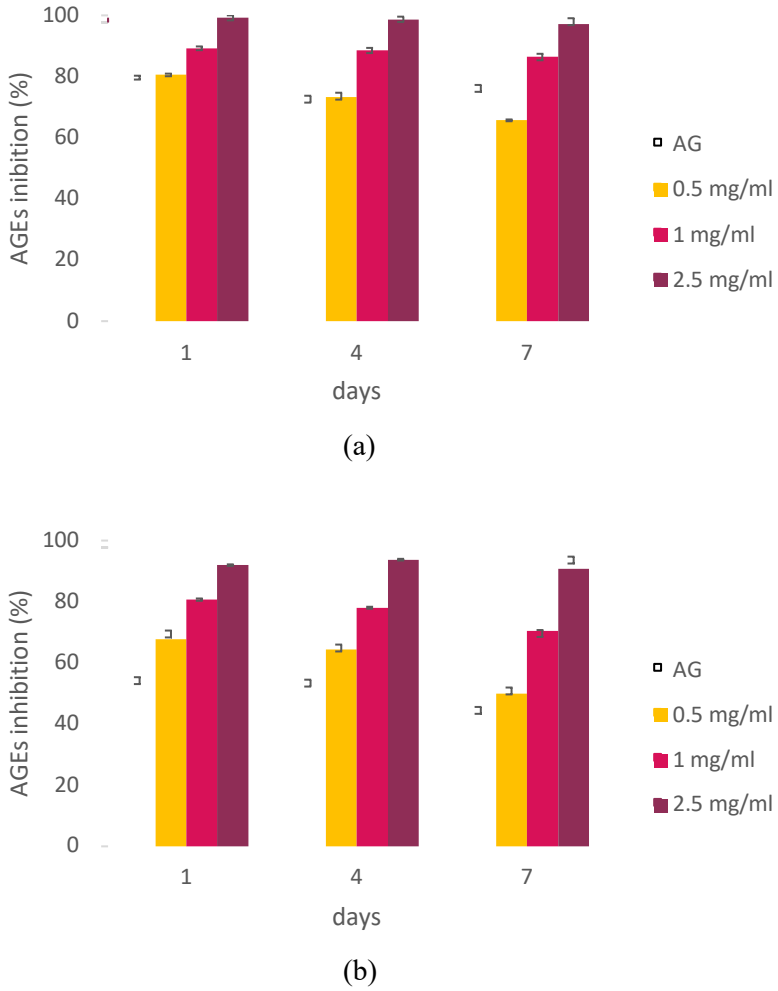

Figure 44. Inhibition of the pentosidine-like AGEs (a) and of argpyrimidine-like AGEs (b) by CBE-2.

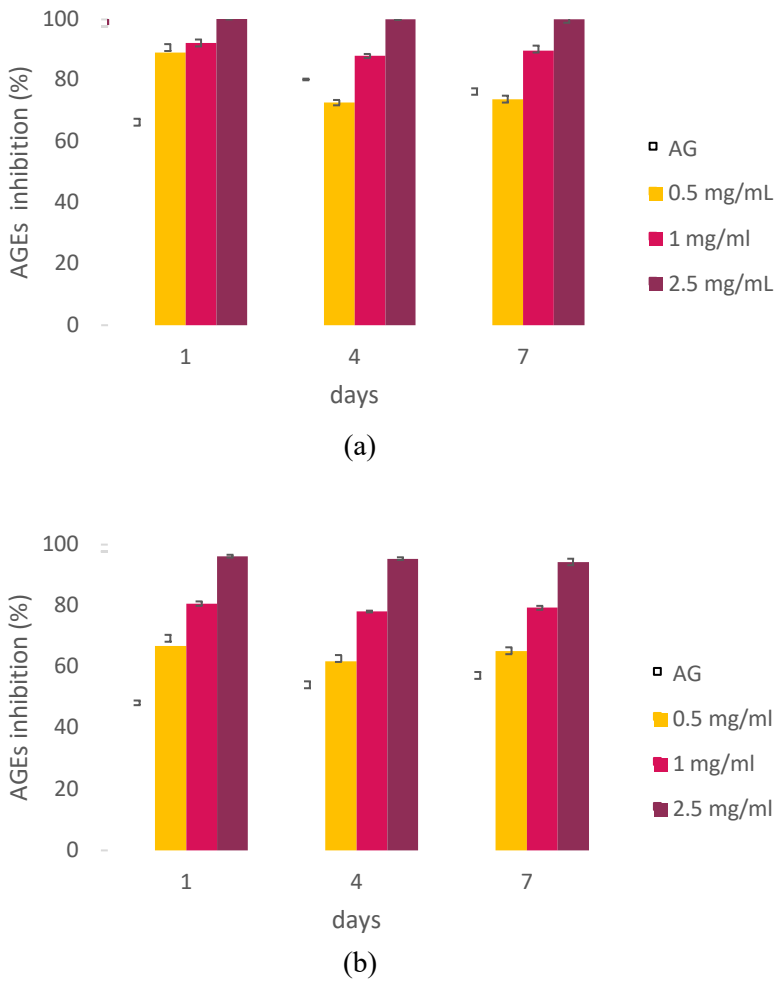

Figure 45. Inhibition of the pentosidine-like AGEs (a) and of argpyrimidine-like AGEs (b) by RHE-2.

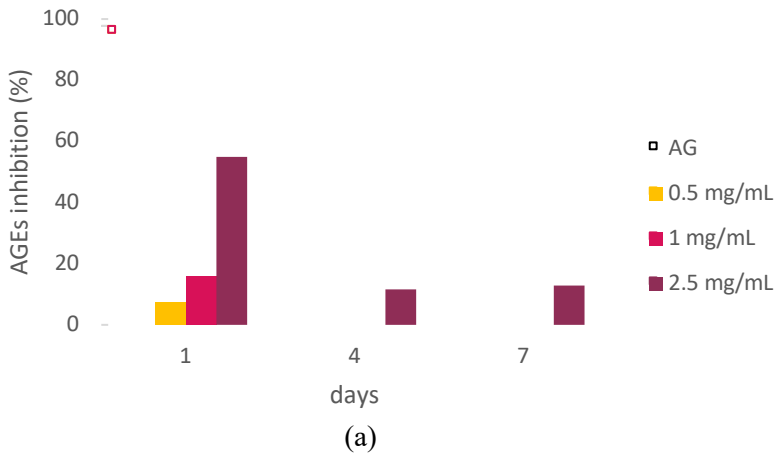

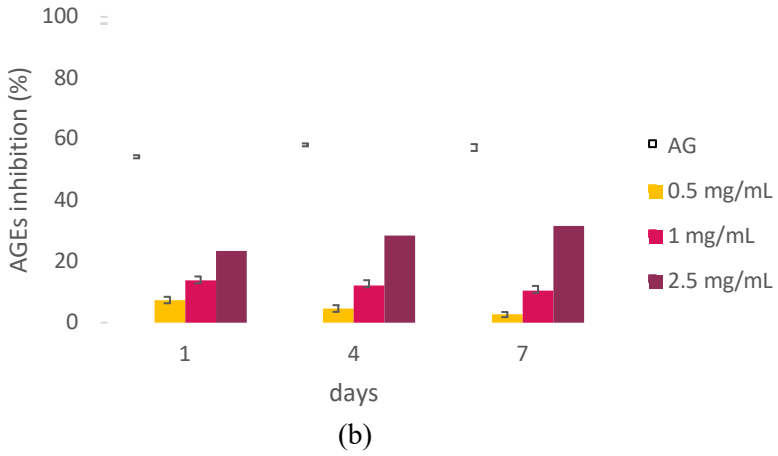

(b)

Figure 46. Inhibition of the pentosidine-like AGEs (a) and of argpyrimidine-like AGEs (b) by WPE-2.

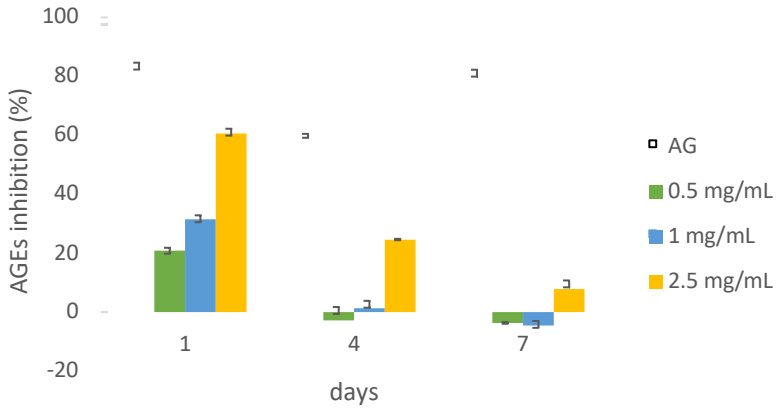

(a)

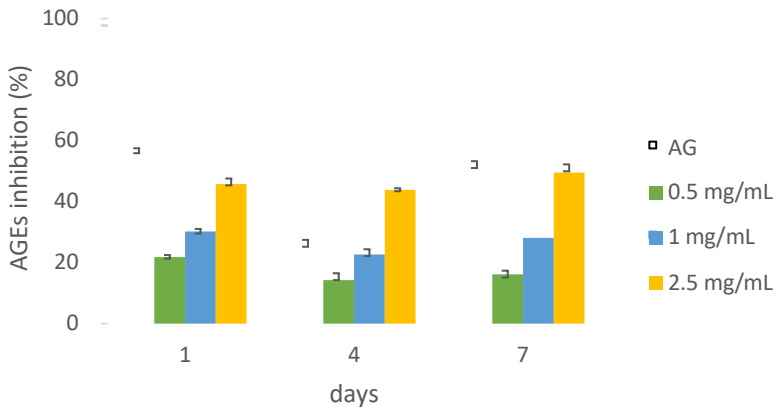

(b)

Figure 47. Inhibition of the pentosidine-like AGEs (a) and of argpyrimidine-like AGEs (b) by MPE-1.

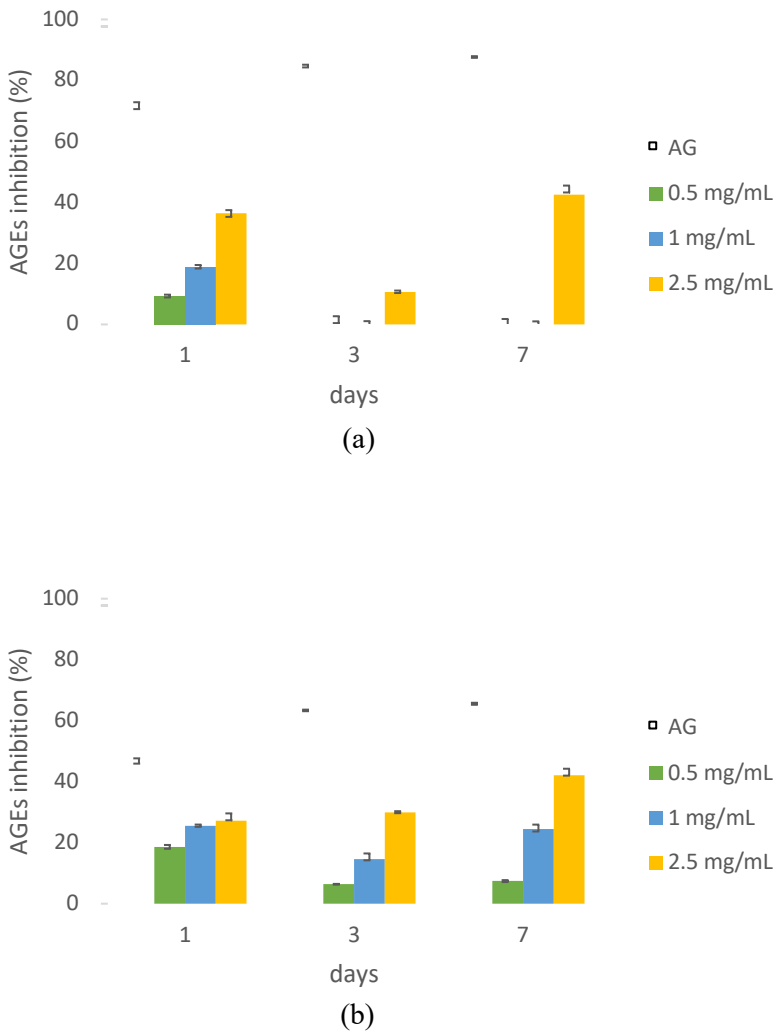

Figure 48. Inhibition of the pentosidine-like AGEs (a) and of argpyrimidine-like AGEs (b) by PPE-2.

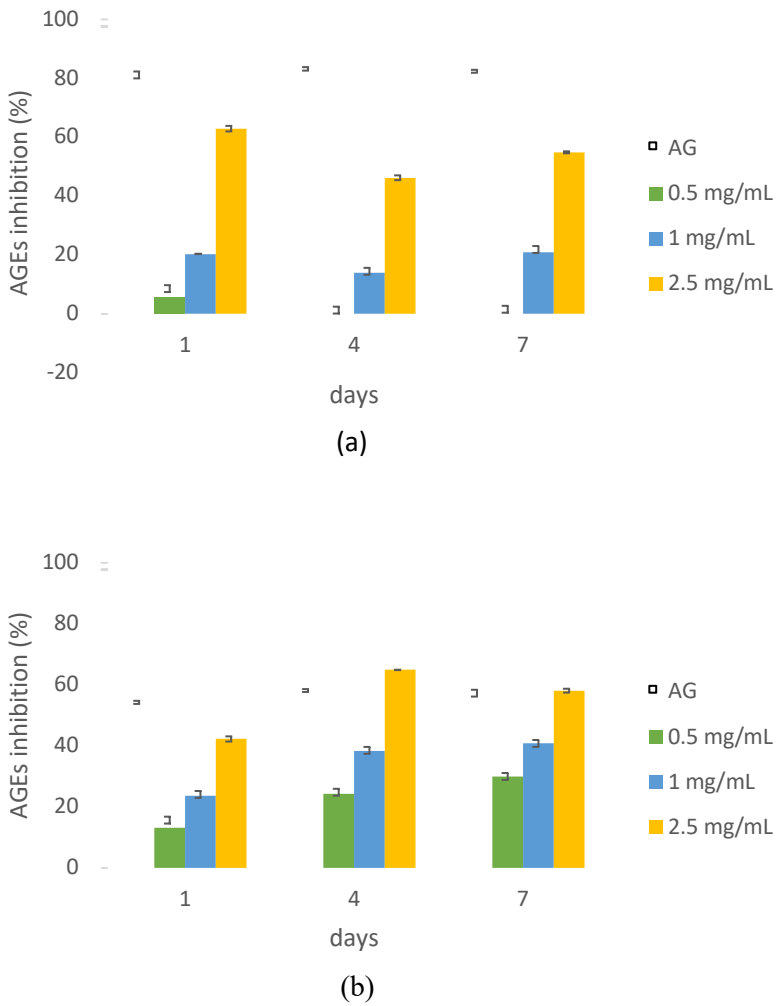

Figure 49. Inhibition of the pentosidine-like AGEs (a) and of argpyrimidine-like AGEs (b) by ABE-2.

As evident in Figures 44-45, CBE-2 and RHE-2 displayed very similar trends. The extracts activities were always equal or higher than the standard. The highest tested concentrations (2.5 mg/mL) were able to totally inhibit the formation of pentosidine-like AGEs and around the 90% of the argpyrimidine-like AGEs. On the other hand, the wheat extract was not very active in the 7 days monitored, with an activity that reached about 20-30% after 7 days for the highest concentration tested (Figure 46). The other extracts obtained from vegetable wastes material (Figures 47-49) have activities lower than those registered for cereals waste. Considering the inhibition of pentosidine-like AGEs, the activities recorded for MPE-1, PPE-2, and ABE-2 were always lower than the standard. MPE-1 was the least active extract, as the highest concentration tested can inhibit only about 8% of AGEs at the end of the monitoring period. PPE-2 and ABE-2 showed higher activities after 7 days, 42.5±2.97% and 54.9±0.3%, respectively.

Considering the argpyrimidine-like AGEs, ABE-2 and MPE-1 extracts tested at 2.5 mg/mL had activity values like that obtained for the standard (AG: 56.82±0.81; ABE-2: 58.11±0.63; and MPE1: 49.5±2.72%), while PPE-2 had decidedly lower values (42.29±2.05).

Polyphenols exert their antiglycative activity through several mechanism of action, including dicarbonyl compounds trapping, thus reducing the carbonyl stress (Anwar et al. 2021; Velinchova et al., 2021). In order to explore this possible mechanism at the intermediate stage of reaction, different model systems at different times (1h, 24h and 48h) were used to evaluate the extracts capacities to direct chelate dicarbonyl compounds, such as MGO and GO.

As illustrated in Figure 50, CBE-1 had the lowest trapping ability against MGO and no activity was registered for GO. This is probably because polyphenols present in the extract do not act preferentially with this mechanism. On the other hand, RHE-2 and WPE-2 have good chelating activities, especially wheat, with an almost total subtraction of MGO after 48h at the highest tested concentration (Figure 51 and 52).

In general, for all type of extracts the results obtained from the assay highlighted that the ability to trap MGO is higher compared to the ability to trap GO for all the extracts tested (Figure 53-55). This phenomenon, already documented in the literature, could be due to the easy polarization of GO in aqueous solutions, which limits its capture and separation from the solution (Sadowska-bartoz et a., 2014).

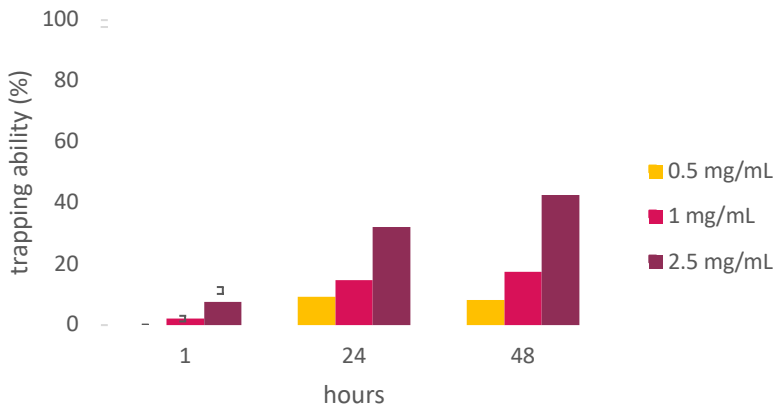

Figure 50. Trapping ability of CBE-2 against MGO.

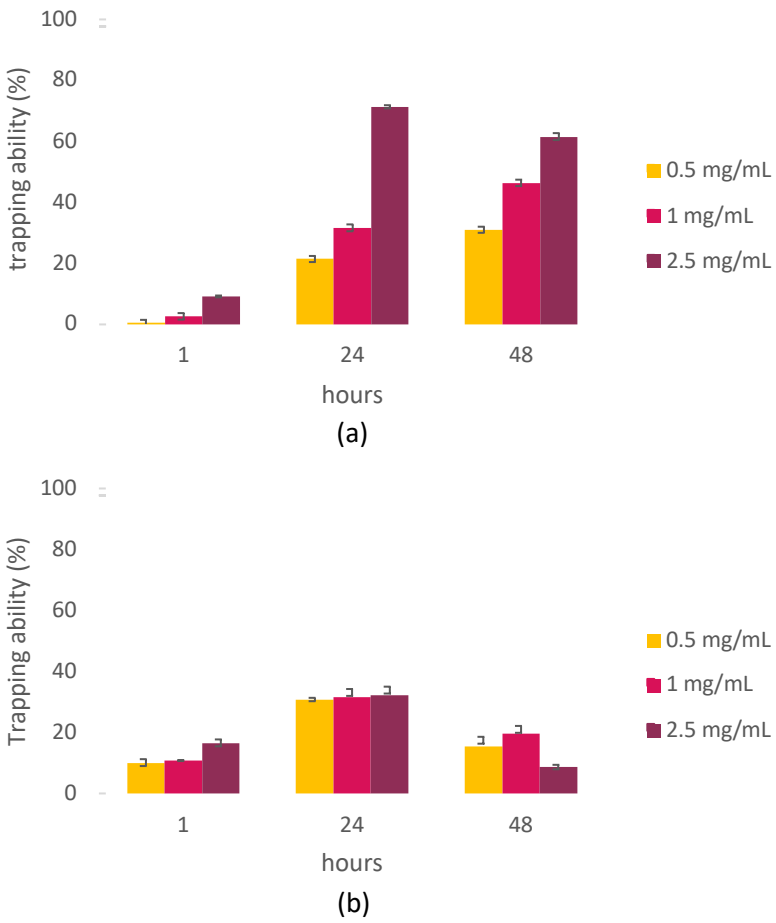

Figure 51. Trapping ability of RHE-2 against MGO (a) and GO (b).

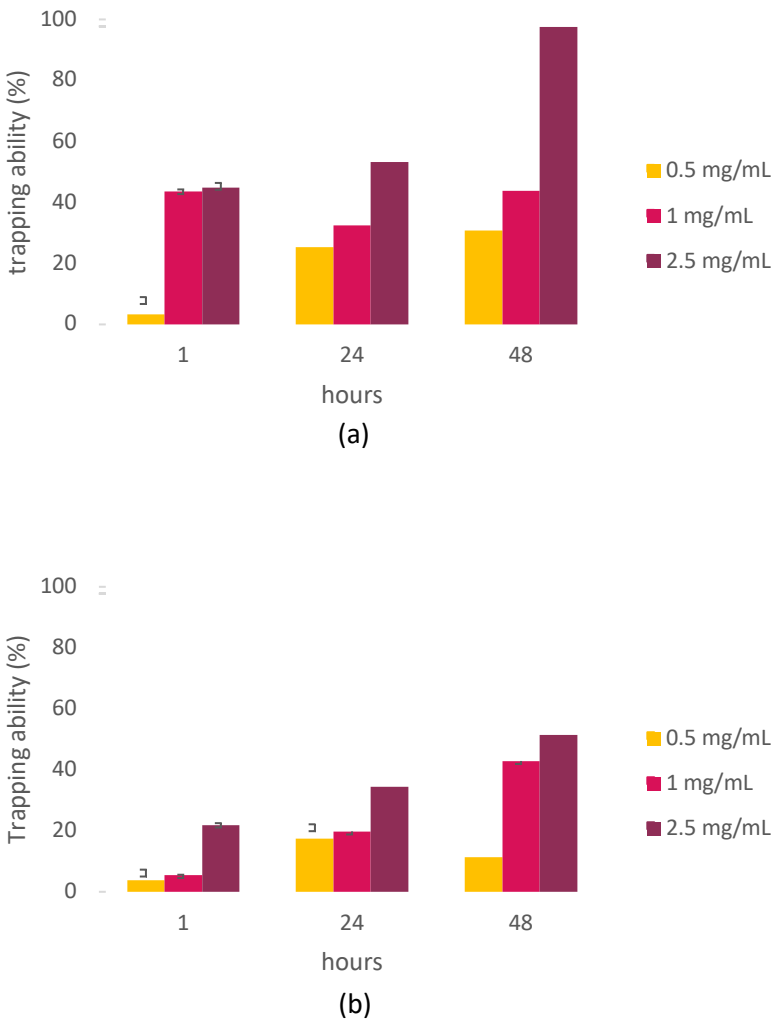

Figure 52. Trapping ability of WPE-2 against MGO (a) and GO (b).

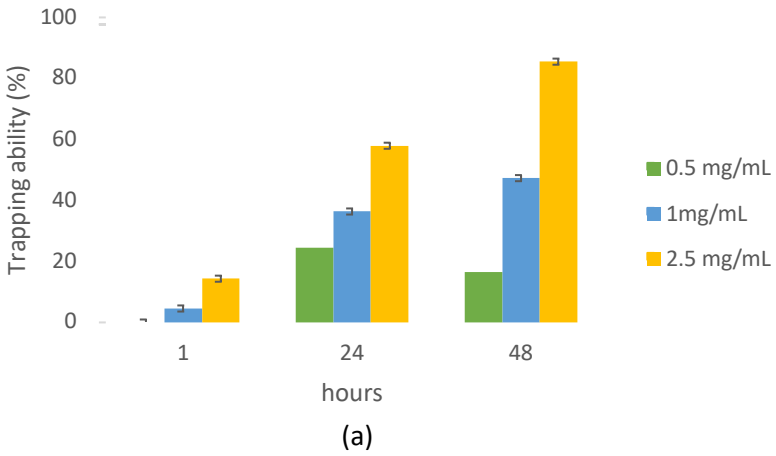

(a)

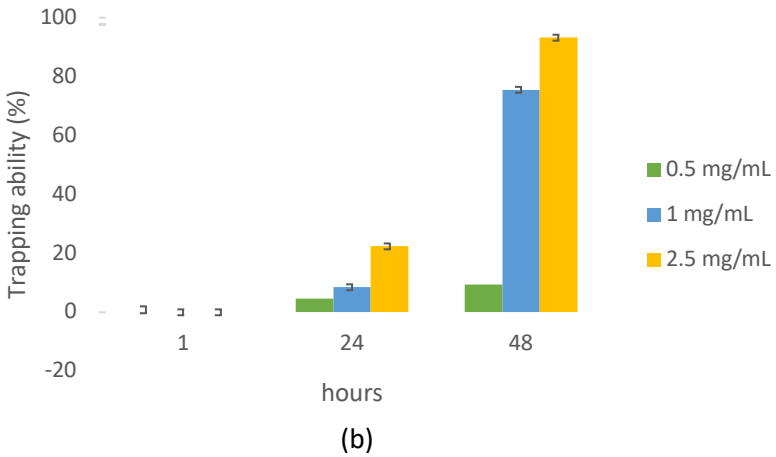

(b)

Figure 53. Trapping ability of MPE-1 against MGO (a) and GO (b).

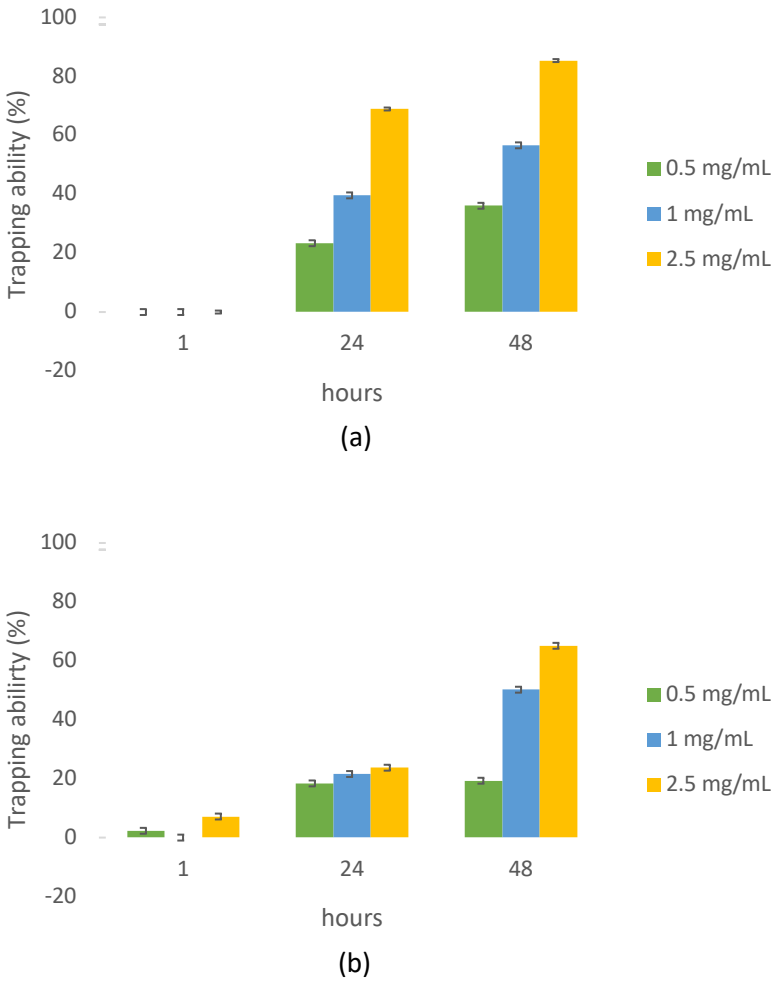

Figure 54. Trapping ability of PPE-2 against MGO (a) and GO (b).

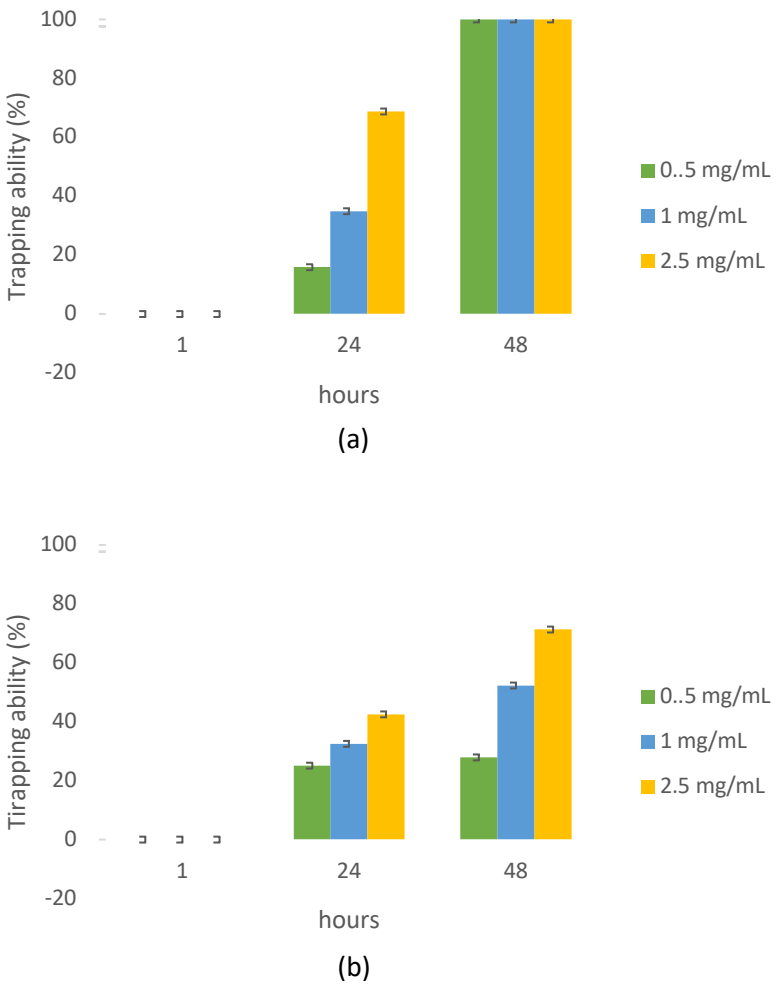

Figure 55. Trapping ability of ABE-2 against MGO (a) and GO (b).

In the context of the final stage of the glycation reaction, BSA-GLU systems was used to monitor the formation of argpyrimidine-like AGEs. Based on the reactivity of glucose, different time points, 7, 14, and 21 days, were selected for monitoring the AGEs formation, (Papetti et al., 2018, Maietta et al., 2017) (Figure 56). CBE-2 and RHE-2 displayed high activity in countering AGEs at this stage. Notably, corn cob exhibited the ability to inhibit approximately 80% of AGEs after 21 days, across all tested concentrations. Rice husk also had significant activity, with an inhibition rate of about 60% after 21 days for the 2.5 mg/mL. In contrast, wheat displayed noticeably lower activity, reaching only approximately 30% inhibition at the highest tested concentration by the end of the monitoring period. Considering the extracts obtained from vegetable waste matrices, not reproducible data were obtained over the monitoring period due to sample turbidity. The only assay that we were able to complete successfully was the one involving PPE-2, albeit with a high standard deviation. The extract

obtained from pumpkin peel appeared to be effective in countering AGEs at this final stage of the reaction.

(a)

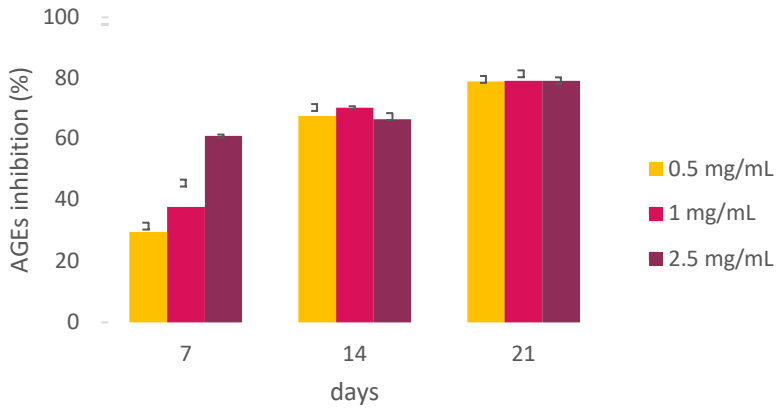

(b)

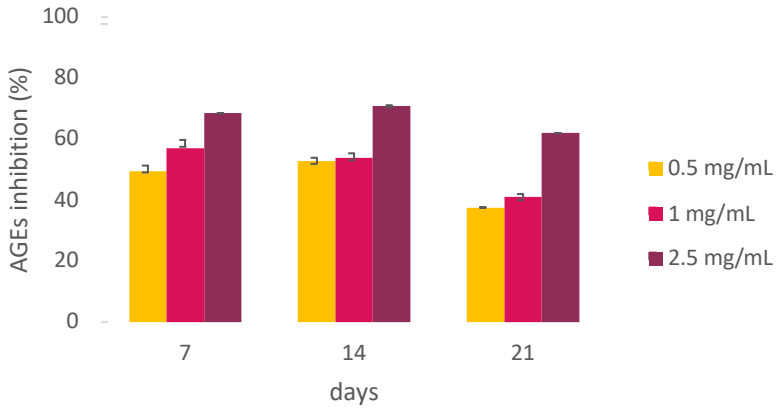

(c)

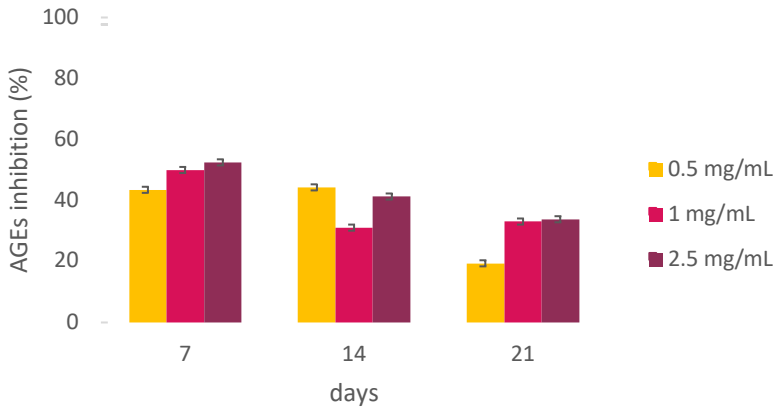

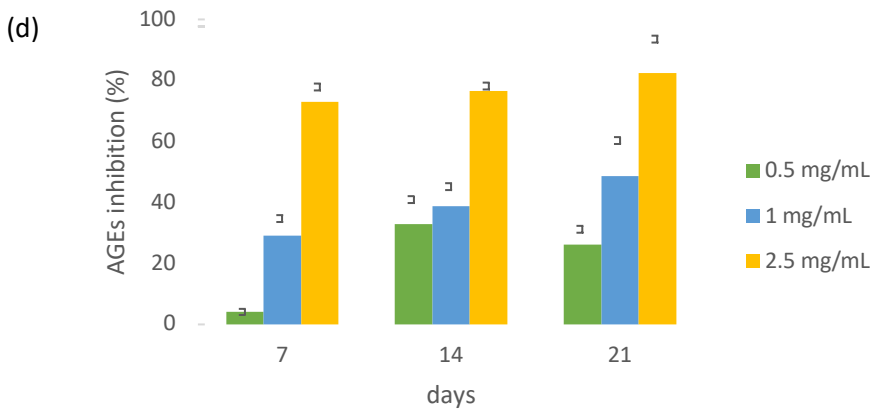

Figure 56. Inhibition of the AGEs formation in BSA-GLU system by CBE-2 (a), RHE-2 (b), WPE-2 (c), and PPE-2 (d) at different concentrations (0,5, 1, 2.5 mg/mL dry matter).

To gain deeper insights into the possible binding sites of polyphenols in AGEs formation, we selected RHE-2, one of the main active extracts obtained, and evaluate the early progression of the glycation reaction on the extract by measuring the levels of free lysine in BSA-GLU models after 7 days of incubation. This specific amino acid residue plays a critical role at the outset of the glycoxidation process through its covalent binding with reducing sugars (Wang et al., 2020). We estimated lysine residues in native BSA and glycated BSA (Gly-BSA) with and without the presence of RHE using the OPA assay. Figure 57 illustrates that Gly-BSA displayed a significant reduction in the percentage of free lysine content compared to the corresponding

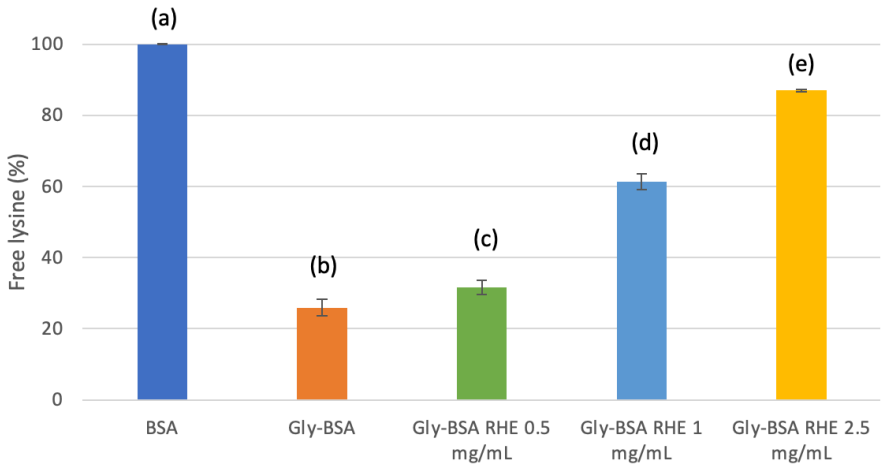

Figure 57. Free lysine levels in both the BSA-GLU and BSA-GLU-RHE systems following 7 days of incubation at various concentrations. Different superscript letters (a, b, c, d, e) are used to denote statistically significant differences ($p < 0.05$) in free lysine levels among the native bovine serum albumin (BSA), the glycated BSA systems (Gly-BSA), and the glycated BSA systems containing different concentrations of the tested extract (Gly-BSA RHE 0.5 mg/mL, Gly-BSA RHE 1 mg/mL, and Gly-BSA RHE 2.5 mg/mL).

value in native BSA. This reduction in lysine content percentage was further enhanced by varying the concentration of RHE added to Gly-BSA. The highest increase was observed at 2.5 mg/mL, with a substantial rise of 87.0±0.27%, followed by 1 mg/mL (61.3%) and 0.5 mg/mL (31.3%).

These findings provided evidence for the involvement of lysine in the glycation reaction, and they suggested that RHE-2 could effectively mitigate its interaction with reducing sugars in a concentration-dependent manner.

Numerous research studies highlighted the effectiveness of extracts derived from cereal by-products as agents against glycation, such as those sourced from rice bran (Aalim et al., 2018), purple corn cob (Ferron et al., 2020), sorghum buckwheat hulls (Senevirathne et al., 2021), and triticale bran (Chen et al., 2018). The inhibitory impact on advanced glycation end products (AGEs) during the middle stages of glycation observed in CBE-2 and RHE-2 is aligned to the outcomes reported for purple corn cob extract in BSA-MGO systems by Ferron et al. (Ferron et al., 2020), where AGEs formation was completely prevented. Our encouraging findings regarding the antiglycative potential of RHE-2 agree with the results presented by Rahman et al. (Rahman et al. 2014), who documented antihyperglycemic activity similar to that of glibenclamide in glucose-loaded mice using ethanolic extracts from rice husk and suggested their potential application for managing elevated glucose levels in diabetic individuals. Research about the *in vitro* antiglycative activity of white cereals is relatively limited, with the most promising studies predominantly concentrated on pigmented varieties, as highlighted by Premakumara et al. (2018) and Haldipur et al. (2018). Nevertheless, our findings for both CBE-2 and RHE-2 align with those observed in colored varieties. In their study, Premakumara et al. reported an impressive 80–90% inhibition of vesperlisine-like AGEs in BSA-GLU systems when utilizing red rice bran varieties. This inhibition rate significantly outperformed the outcomes observed for white rice bran varieties, which exhibited a modest 30% reduction in AGEs at the concentrations tested.

4.9 Evaluation of antioxidant activity

The second phase of the glycation reaction is characterized by the conversion of Amadori products into advanced glycation end products (AGEs), which involves the generation of reactive oxygen species (ROS) and reactive carbonyl species (RCS). As a result, antioxidant compounds may play a key role in counteracting the glycation process. To investigate the potential connection between antiglycative activity and antioxidant/antiradical properties, we performed two different assays: the ABTS cation radical scavenging activity and the DPPH free radical scavenging capacity test. In this thesis, we choose to present and discuss exclusively the results obtained from cereals, as they exhibited the highest level of activity (Figures 58), differently from vegetable wastes for which a very poor activity was registered. RHE-2 and CBE-2 exhibited remarkable capacities to scavenge ABTS radical cation. A dose-activity relationship was registered for RHE-2 which showed the highest antioxidant activity at 2.5 mg/mL (95.12±2.1%, TE = 379.77μM), followed by 1 mg/mL (65.57±2.3%, TE= 676.67 μM) and 0.5 mg/mL (41.55±0.3%, TE = 1041.94 μM). Similarly, CBE-2 at 2.5 mg/mL inhibited 97.0±0.5% (TE = 1041.17 μM) of ABTS radicals, followed by 1 mg/mL (58.1±2.4%, TE = 686.00 μM) and 0.5 mg/mL (33.9±1.5%, TE = 393.33 μM). However, both extracts displayed only a moderate capacity to scavenge the DPPH radical, even if this capacity increased in a dose-dependent manner. RHE-2 exhibited the highest DPPH inhibitory activity at the highest concentration tested (47.48±0.04%, TE = 858.40 μM), followed by 1 mg/mL (31.58±0.19, TE = 653.67 μM) and 0.5 mg/mL (20.89±0.09%, TE= 513.73 μM). Similarly, CBE-2 displayed the lowest activity at 0.5 mg/mL (13.51±0.46, TE = 212.07 μM), followed by 1 mg/mL (24.28±0.52%, TE = 324.80 μM) and 2.5 mg/mL (43.07±0.88%, TE = 507.13μM). On the contrary, WPE-2 showed lowest DPPH and ABTS-inhibiting activity, for all the concentration tested.

Furthermore, to evaluate the correlation between antioxidant and antiglycative activity, we then calculated the Pearson correlation coefficients for cereal waste extracts (Table 64). They always tend to 1 for RHE-2 and are generally always higher than 0.5 for CBE-2 and WPE-2, indicating a strong or moderate correlation between the two bioactivities, respectively. This underlines how the antioxidant species present in the extracts probably also have a role in counteracting the AGEs formation.

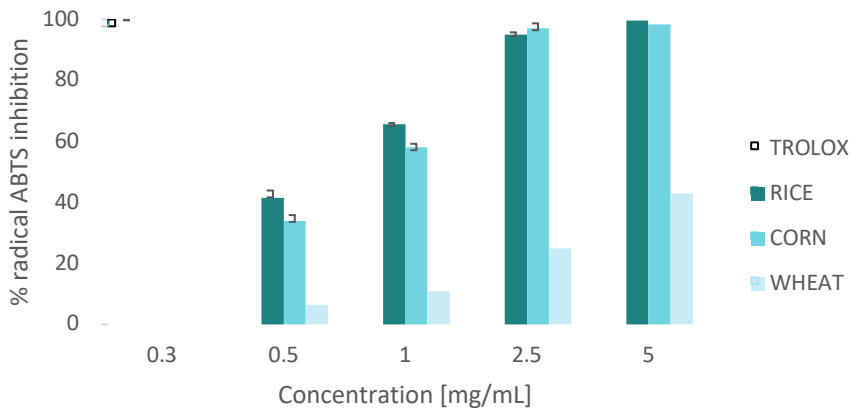

(a)

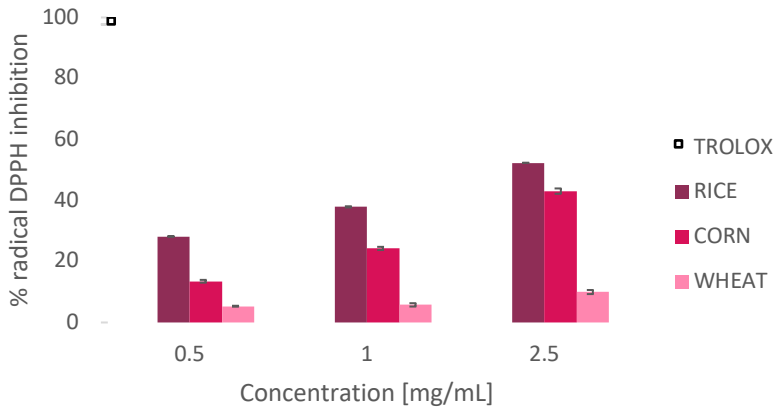

(b)

Figure 58. Inhibition of the $ABTS^{\bullet+}$ radical formation (a) and DPPH radical formation in BSA-GLU system by AFW extracts at different concentrations.

Table 64. The Pearson's correlation coefficients (R^2) were calculated to assess the relationship between the antiglycative activities observed at the end of the monitoring period in various assays and the antioxidant activities of RHE-2, CBE-2 and WPE-2 at the various concentrations tested.

	ASSAY	$DPPH^{\bullet}$ (R^2)	$ABTS^{\bullet+}$ (R^2)
RHE-2	NBT	0.9566	0.9399
	MGO	0.9705	0.9818
	GLU	0.9604	0.9443
CBE-2	NBT	0.9441	0.9512
	MGO	0.8812	0.8916
	GLU	0.5299	0.5486
WPE-2	NBT	0.9835	0.9993
	MGO	0.9704	0.9951
	GLU	0.6095	0.7180

Considering the antiglycative results, the AFW which globally had the highest activity was rice husk. Moreover, Pavia is the province with the highest percentage of rice cultivation in Italy and the first producer at national and European level. Thus, we decided to focus our attention on the characterization and formulation of RHE-2 as a promising innovative novel food ingredient.

4.10 Pectin extraction and characterization

In parallel to antiglycative studies, considering the limited bioaccessibility of AFW polyphenols under digestion, we investigated the possibility to obtain from the same AFW a carrier agent for the formulation of the food ingredient. Due to the increasing attention to pectin as carrier agent for intestinal targeted formulations (Frosi et al., 2023; Rehman et al., 2019), we decided to consider pumpkin peel (*Cucurbita maxima L.*, Mantua variety) as a possible source of pectin. A green extraction method assisted by microwaves using an acidic aqueous solution as medium (see MAE-WA, section 3.3.3) was optimized using a DOE approach. Water acidified with citric acid was used as solvent. The comprehensive experimental design, inclusive of observed pectin yield (YP) values, is outlined in Table 65. The considered experimental ranges (-1; +1) were: SSR 20-50 mL/g, pH of acidic water 1.5-3.5, T 45-95 °C, and 5-15 min of extraction.

The mathematical formula of the second-order polynomial equation derived from the response surface is as follows:

$$YP\ (\%) = -54{,}8662 + 2{,}03343*SSR + 35{,}8689*pH + 1{,}23813*T - 3{,}58301*t - 0{,}0203867*SSR^2 - 1{,}15128*SSR*pH + 0{,}00295733*SSR*T + 0{,}0209667*SSR*t - 2{,}04417*pH^2 - 0{,}8075*pH*T + 1{,}6025*pH*t - 0{,}00459067*T^2 + 0{,}00054*T*t + 0{,}04825*t^2 + 0{,}00967778*SSR^2*pH - 0{,}0000306667*SSR^2*T - 0{,}00028*SSR^2*t + 0{,}0763333*SSR*pH^2 + 0{,}00000773333*SSR*T^2 + 0{,}0815*pH^2*temperature - 0{,}2775*pH^2*t + 0{,}00232*pH*T^2 \quad (47)$$

Table 65. Box-Behnken Design for MAE-WA extraction of pectin from pumpkin peel. Actual variables. Extraction yields (YP %) are also reported.

Run No.	SSR (mL/g)	pH	T (°C)	T (min)	YP (%)
1	20	1.5	70	10	4.30
2	50	1.5	70	10	9.66
3	20	3.5	70	10	3.68
4	50	3.5	70	10	3.42
5	35	2.5	45	5	3.59
6	35	2.5	95	5	3.82
7	35	2.5	45	15	4.28
8	35	2.5	95	15	4.78
9	20	2.5	70	5	3.59
10	50	2.5	70	5	3.60
11	20	2.5	70	15	3.58
12	50	2.5	70	15	4.00
13	35	1.5	45	10	5.59
14	35	3.5	45	10	4.42
15	35	1.5	95	10	13.79
16	35	3.5	95	10	5.10
17	20	2.5	45	10	4.58
18	50	2.5	45	10	3.52
19	20	2.5	95	10	3.18
20	50	2.5	95	10	4.96
21	35	1.5	70	5	14.12
22	35	3.5	70	5	4.14
23	35	1.5	70	15	10.02
24	35	3.5	70	15	4.34
25	35	2.5	70	10	3.06
26	35	2.5	70	10	2.48
27	35	2.5	70	10	2.58

The YP obtained under various extraction conditions ranged from 2.48% and 14.12%.

Our findings were in line with those of other researchers who previously investigated the extraction of pectin from various waste materials (Pasandide et al., 2017; Jafari et al., 2017; Chaharbaghi et al., 2017). Notably from ANOVA results (Table 66), we identified pH as a crucial factor influencing pectin extraction ($p < 0.05$), with a negative impact on yield. In fact, we observed a significant increase in yield (YP) at lower pH values (i.e., 1.5). This phenomenon was attributed to the hydrolysis of polysaccharides under strong acidic conditions, which enhances the release and solubility of pectin. These results are consistent with other studies on pectin extraction from pistachio green hull (Chaharbaghi et al., 2017) and carrot pomace (Jafari et al., 2017) reported in literature. Furthermore, we observed a generally positive effect of increased SSR, T, and extraction time, even though their individual impacts were not statistically significant. A number of studies have reported increased YP as T increased; therefore, the highest YP were obtained at the highest extraction temperatures (Pasandide et al., 2017; Jafari et al., 2017). Indeed, we recorded the highest pectin recovery at highest temperatures (70-95 °C), likely due to enhanced solubility and diffusivity of pectin from plant tissues into the solvent with the increasing of temperature. Regarding SSR, it is well-documented that increased contact between the material and solvent, along with high water diffusivity into cells, leads to a higher yield, as reported in the extraction of polysaccharides from melon peel by Golbargi et al. (2021). Similarly, in terms of extraction time, it is generally advisable to keep irradiation times below 15 min to avoid decomposition, degradation, and hydrolysis of polysaccharides, which can reduce the yield (Golbargi et al., 2021). Our experiments demonstrated strong agreement with predicted values, as evidenced by high coefficients of determination (R^2: 96.71%; R^2adj: 78.59%).

Table 66. The analysis of variance of the Box-Behnken model for pectin extraction yield for MAE-WA process.

Source	Sum of squares	df	Mean square	F ratio	*P* value
A:SSR	0.05	1	0.05	0.02	0.8872
B:pH	61.31	1	61.31	30.26	0.0053
C:T	0.13	1	0.13	0.07	0.8103
C:t	0.68	1	0.68	0.34	0.5933
AA	0.35	1	0.35	0.17	0.6989
AB	7.65	1	7.65	3.77	0.1240
AC	2.02	1	2.02	1.00	0.3749
AD	0.04	1	0.04	0.02	0.8924
BB	67.50	1	67.50	33.32	0.0045
BC	14.14	1	14.14	6.98	0.0575
BD	4.62	1	4.62	2.28	0.2054
CC	4.56	1	4.56	2.25	0.2078
CD	0.02	1	0.02	0.01	0.9290
DD	7.76	1	7.76	3.83	0.1220
AAB	9.48	1	9.48	4.68	0.0965
AAC	0.06	1	0.06	0.03	0.8722
AAD	0.20	1	0.20	0.10	0.7699
ABB	2.62	1	2.62	1.29	0.3188
ACC	0.01	1	0.01	0.01	0.9460
BBC	8.30	1	8.30	4.10	0.1129
BBD	3.85	1	3.85	1.90	0.2401
BCC	4.21	1	4.21	2.08	0.2231
Errore totale	8.10	4	2.03		

The surface plots obtained for YP as a function of SSR and pH is reported in Figure 59.

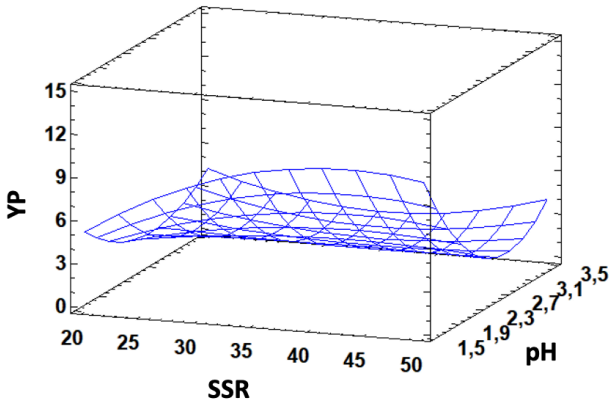

Figure 59. Response surface plot showing the effect of SSR and pH on pectin yield (YP) at 70 °C and 10 min extraction time.

Consequently, the optimal conditions for maximizing pectin yield (YP) were determined to be as follows: 94.8 °C, 5 min, pH 1.5, and a SSR of 46 mL/g. Under these conditions, the calculated YP was 18.05%, with a 95% confidence interval for the mean value ranging from 11.14% to 24.96%. Analyzing the results of three additional experiments performed under these optimal predicted conditions, the mean YP was 22.8 ±1.94 %, further confirming the accuracy of our fitted model. We have achieved higher yields compared to those obtained using the same extraction method (MAE) for pumpkin peel (11.3±0.2) (Yoo et al., 2012), grape pomace (11.23%) (Spinei et al., 2022) and Sentul peel (*Sandorium koetjape*)(12.66%) (Riza et al., 2021). Moreover, our yields are similar to those obtained with MAE in combination with citric acid from pistachio gene hull (22.1± 0.5%) (Chaharbaghi et al., 2017) and lime peel (19.63±0.78) (Rodsamran et al., 2019), supporting the validity of our results.

The polysaccharide obtained was characterized to investigate its structural ad tecno-functional properties together with its chemical characterization.

FT-IR spectrum (Figure 60) of the purified polysaccharide showed the typical bands of pumpkin peel pectin (PPP) already reported in literature (Torkova et al., 2018; Salima et al., 2022), confirming the pectin identity.

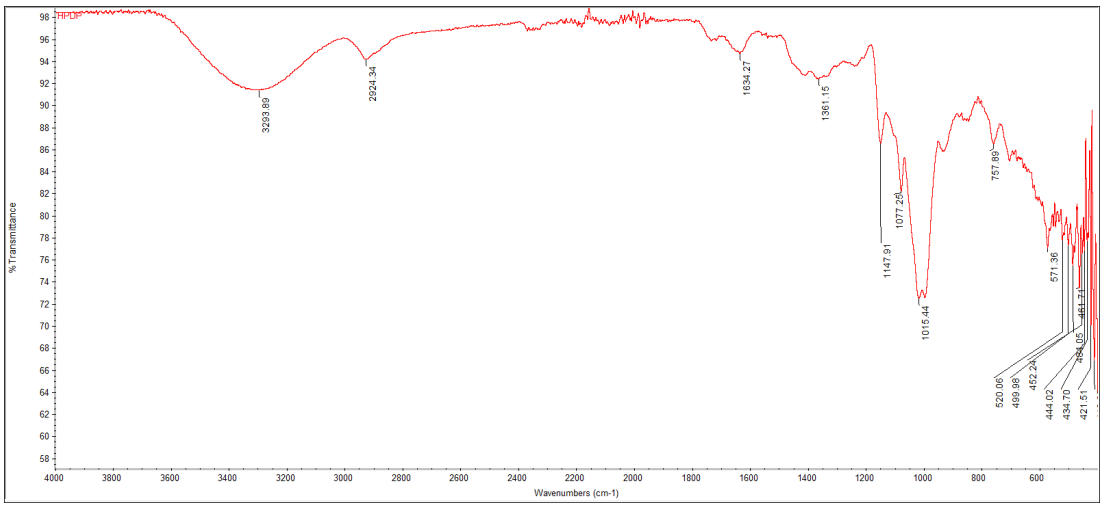

Figure 60. FT-IR spectrum of isolate pectin polysaccharide from pumpkin peel.

The band in the range of 3200-3600 cm^{-1} range corresponded to the oscillation of OH groups, both intra- and inter-hydrogen bonds within the pectin molecule. This vibration was particularly prominent at 3294 cm^{-1}. Another notable peak at 2924.3 cm^{-1} can be attributed to the stretching of C-H bonds in the methyl groups present on the sugar rings of the pectin molecule. Furthermore, two distinct absorption bands between 1770 cm^{-1} and 1600 cm^{-1} indicated the presence of C=O groups, specifically methyl-esterified (COO-R) and ionic carboxyl (COO-) groups. It's important to note that the relative intensity of the ester band increased according to the degree of esterification of the pectin (higher was the degree of esterification, higher was the increase in the ester band intensity), while the intensity of the carboxylic stretching band decreased (Torkova et al., 2018).

The region between 1200-1800 cm^{-1}, known as the fingerprint region, revealed distinct bands characteristics for PPP. Notably, the typical peaks at 1077 cm^{-1} and 1015 cm^{-1} were correlated with the vibration of neutral arabinose and galactose-based glycans within the pectin molecule (Torkova et al., 2018).

Additionally, thermal analysis using DSC (Figure 61a) supported the presence of physically bound water, which is released at temperatures below 100 °C and revealed multiple decomposition processes occurring up to 263.06 °C. TGA (Figure 61b) data confirmed a weight loss of 4.6%, corresponding to the removal of free water from the sample. A more significant loss of water was observed between 200-350 °C, indicative of the pyrolytic decomposition of the pectin chain and the cleavage of hydrolytic bonds. These processes continue until the complete decomposition of organic substances at 600 °C, leaving behind a carbon-based inorganic skeleton. These findings aligned with similar trends observed in the thermal performance of an ultrasound assisted extracted pectin (UAEP) from citrus peel by Panwar et

al. (2023). Their results also indicated greater thermal stability of UAEP compared to a commercial citrus pectin, highlighting the potential advantages of our pectin source (Panwar et al., 2023).

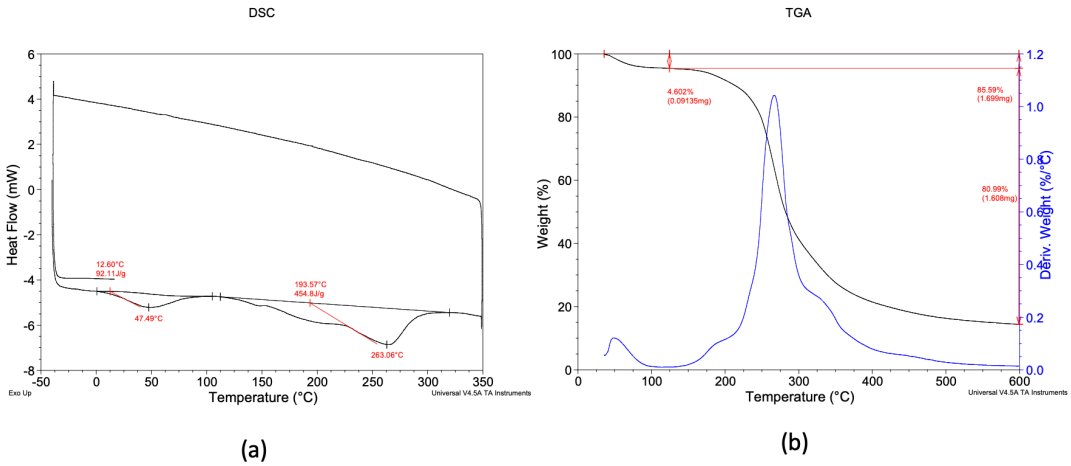

Figure 61. DSC (a) and TGA (b) analysis of the extracted pumpkin peel pectin.

Regarding the tecno-functional properties of the investigated polysaccharide, water holding capacity (WHC) and fat binding capacity (FBC) were examined to better understand the interaction between hydrophobic and lipophilic components of the molecule and the number of hydrophilic/lipophilic groups on the pectin's surface. A higher WHC was associated with a better suitability as texturizer, while a grater FBC was related to its use as an emulsifier and stabilizer. WHC referred to the amount of water held per gram of pectin, while FBC referred to the amount of oil bound per gram of pectin. The WHC of PPP was 1.55 ± 0.25 g water/g, a value was similar to those reported for melon peel pectin (1.88 g water/g) (Golbargi et al., 2021), but lower than that of citrus peel pectin (3.07 ± 0.09 g water/g) (Panwar et al., 2023). Conversely, the FBC of PPP was 2.51 ± 0.19 g oil/g, similar to the values observed for citrus peel pectin (2.37 ± 0.05 g oil/g) and pistachio green hull (2.02 ± 0.38 g oil/g) (Kazemi et al., 2019). PPP exhibited a higher proportion of hydrophobic regions, consistent with the trend observed in melon peel pectin by Golbargi et al. (2022). This reflected in the pectin polymer's increased ability to stabilize oil-in-water (O/W) emulsions. Various emulsions were prepared using different pectin concentrations (1% and 3% w/v) and different concentration of sunflower oil (35% and 60% v/v) (Figure 62) and their stability was monitored during 7 days at 4 °C.

Figure 62. Image of different emulsions prepared by using various concentration of pectin (1%-3% w/v) and sunflower oil (35%-60% w/v).

Interestingly, as shown in Table 67, the stability of the emulsions did not change significantly at 4 °C. In particular, the emulsions with the highest oil content (E2 and E3) exhibited the greatest stability, independently from the concentration of pectin used. When the water content was high compared to the oil content, separation of the oil phase may be observed on the surface of the emulsion. These findings were in line with those made by Mendez et al. (2021), where pectin extracted from watermelon rinds (from the same botanical family), resulted to be more effective at stabilizing emulsions with greater oil content.

Table 67. Emulsion stability (ES) after 1 and 7 days at 4 °C of the 4 different emulsions prepared with PPP.

ES (%)	Day 1	Day 7
E1) PP 1%, oil 35%	60.0±0.1	58.3±0.1
E2) PP 1%, oil 60%	90.0±3.3	91.7±2.3
E3) PP 3%, oil 35%	58.3±2.4	56.7±2.3
E4) PP 3%, oil 60%	98.3± 2.4	98.3±2.3

Preliminary rheological studies were also performed on PPP, in order to investigate the viscoelastic properties of pectin aqueous solution at different concentrations (0.5, 1, 2, and 3% w/v) by using shear-rate rheology. Figure 63a showed the mechanical properties of pectin

solution. The storage modulus (G') represented the stiffness and it increased by increasing pectin concentration (from 0.5 to 60 Pa). This behavior aligned with the typical pattern observed for soft hydrogel matrices, attributed to the formation of entanglements between pectin chains at highest concentrations, resulting in enhanced material stiffness. Consequently, these properties could be contingent upon the concentration of pectin in the solution. When analyzing the flow curves of apparent viscosity (Figure 63b), a non-Newtonian, shear-thinning, and pseudoplastic response was observed, indicating that the viscosity decreased as the applied shear rate increased. This phenomenon has been previously documented in pectin extracted from citrus peel using ultrasound techniques (Panwar et al., 2023).

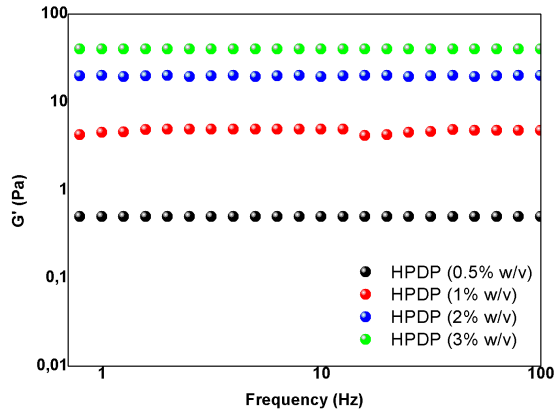

(a)

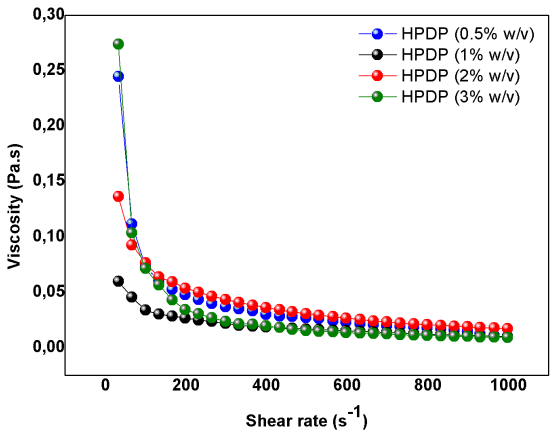

(b)

Figure 63. Rheological studies on PPP: frequency-dependent oscillatory rheology (0.1-100 Hz) (a) to test the mechanical properties and flow curves (b) to test the viscosity.

It was the result of the development of a robust pectin network at high concentrations, leading to increased pectin collision rates and, subsequently, a decrease in viscosity. This viscosity

profile underscored the potential of pectin as both a stabilizer and thickener, with potential applications in injectable formulations (Panwar et al., 2023).

The molecular weight (Mw) and degree of esterification (DE) are other factors that influence the application field of pectin and they were investigated to gain more insight on the chemical features of the polysaccharide. Size exclusion chromatography (SEC-RID-HPLC analysis) was used to investigate the distribution and size of PPP, after a calibration with pullulans (see section 3.9.1.1). Mendez et al. (2021) investigated the effect of various extraction conditions (in terms of different pH, extraction temperature, and time) on the variation of the molecular mass (MM) of the pectin extracted from watermelon rinds. They noted that under high-temperature (95 °C) and low-pH (about 1) conditions, the distribution became narrower. Indeed, our dispersity (PDI (Mw/Mn) = 2.67 ± 0.18) closely resembled that of commercial citrus pectin (PDI = 2.0 ± 0.0), which can be attributed to the high purity of pectins (Mendez et al., 2021). However, we observed a higher MM compared to that reported for pumpkin peel pectin by other researchers. Specifically, we identified a peak around 350 kDa (average Mn = 131.33 ± 3.53 kDa; average Mw = 351.55 ± 31.40 kDa) (Figure 64). Conversely, Torkova et al. (2018) reported values ranging from 72.2 ± 7.7 kDa to 169.1 ± 16.0 kDa, while Salima et al. (2022) found 171.25 ± 39.26 kDa. Our measured MM was also higher than that obtained by Mendez et al. in 2023 for watermelon rinds (same botanical family) under optimal extraction conditions, which measured 106 ± 2.69 kDa. Remarkably, our PPP exhibited a similar MM value to that reported by Salima et al. (2022) for pumpkin pulp (407.48 ± 8.45 kDa), as well as some commercial citrus pectin (389.3 ± 9.1) and sugar beet pulp pectin (590.3 ± 11) as documented by Saeidy et al. in 2023. Indeed, to the best of our knowledge, pectin extracted from Mantua pumpkin peel have never been investigated before.

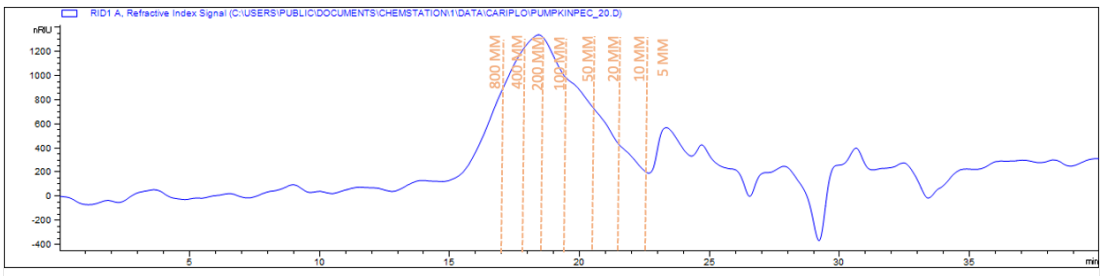

Figure 64. Molar mass (MM) distribution of PPP 1 mg/mL in NaCl 0.1M by SEC-RID system.

PPP exhibited a degree of esterification (DE) greater than 50% (DE = 56.19 ± 0.87), classifying it as a high methoxyl pectin (HMP). This result was in line with those reported for microwave-

assisted extraction of pumpkin pectin (DE= 55-63%) (Yoo et al., 2012; Cui et al., 2014). This classification implies and confirms a higher content of hydrophobic groups (Mendez et al., 2021). However, due to this feature, PPP was not suitable for a use as carrier agent, as low methoxyl pectins (LMP) were employed for this purpose (Frosi et al., 2023). In fact, LMP are characterized by the abundance of free carboxyl groups on the polysaccharide chains, which can interact with cations like Ca^{2+} and Zn^{2+} to form rigid gel structures that are well-suited for active entrapment (Tang et al., 2020).

Therefore, the type of pectin extracted from pumpkin peel is not suitable for our purpose of developing an intestinal targeted delivery of our extract. Nevertheless, we obtained promising results for its use as a stabilizer or emulsifying agent.

4.11 RHE-2 as possible novel food ingredient

4.11.1 Identification of phytochemicals

The qualitative analysis of RHE composition profile was conducted utilizing RP-HPLC-DAD-ESI/MS^n with data-dependent acquisition mode. The resulting base peak chromatogram, presented in Figure 65, was obtained through negative ionization mode.

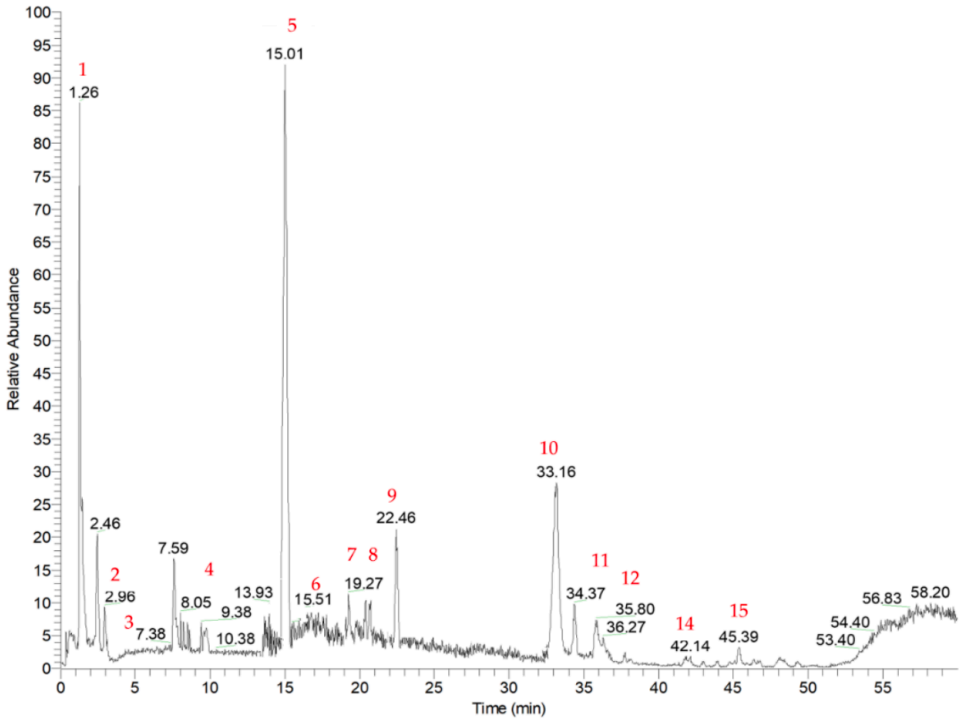

Figure 65. Base peak chromatogram of RHE-2 acquired under negative ionization mode using a reverse-phase high-performance liquid chromatography with diode array detection and electrospray ionization mass spectrometry (RP-HPLC-DAD-ESI-MS^n).

Through a comprehensive analysis of the acquired data, fifteen compounds were tentatively identified based on their molecular ion mass, retention time, MS fragmentation patterns, and references available in the scientific literature (Table 68). Within the RHE sample, two distinct hydroxycinnamic acids were detected and labeled as compounds 1 and 5. Compound 1 was identified as 1-caffeoyl-β-D-glucose (MM 342) and exhibited a formic acid adduct (*m/z* 387) in its MS spectrum. A noteworthy feature was the loss of the glucosyl moiety (162 Da), generating an ion at *m/z* 179, indicative of caffeic acid. Meanwhile, compound 5 displayed a molecular ion at *m/z* 163, which further fragmented to *m/z* 119 $[M\text{-}H\text{-}CO_2]^-$, leading to its identification as *p*-coumaric acid, as confirmed by the analysis of the pure standard compound. Additionally, two smaller organic molecules were assigned as quinic acid (*m/z* 191)

and vanillin (*m/z* 151), represented by compounds 3 and 4, respectively. Their identity was confirmed by the comparison with the standards analyzed in the same experimental conditions Compound 4 was notably characterized by the loss of a methyl moiety (15 Da), aligning with its identification as vanillin. Two C-glycoside derivatives, compounds 6 and 7, exhibited molecular ions at *m/z* 563 $[M-H]^-$ and displayed fragmentation patterns typical of this class, which included neutral losses of glucosyl and pentosyl residues. These compounds were putatively identified as isomers with the aglycone core represented by apigenin, with pentosyl and glucosyl moieties linked to positions 6 and 8. Another compound, labeled as compound 10, was tentatively identified as tricin. It presented distinctive characteristics in its fragmentation pattern, including the loss of two methyl groups giving an $[M-H]^-$ ion at *m/z* 329, and generating fragment ions at *m/z* 314 and 299. Compound 12 was also tentatively identified as a tricin derivative due to its unique fragmentation pattern. Compound 13 was putatively identified as 2,7-dihydroxy-4,5-dimethoxyisoflavone, as it exhibited a $[M-H]^+$ ion at *m/z* 315 under positive ionization mode. Among the hydroxybenzoic acid derivatives, compound 8 was tentatively assigned as hydroxygallic acid based on its molecular ion at *m/z* 187 and fragmentation pattern (MS2[187] = 125(100), 169(5), 97(5)). Additionally, compounds 2 and 15 were identified as levulinic acid and hydroxy-octodienoic acid, respectively. Lastly, compound 11 was tentatively attributed to a hydroxy oleic acid derivative, as suggested by its molecular ion at *m/z* 329 and the patterns observed in its fragmentation. These findings collectively contributed to a comprehensive understanding of the qualitative composition profile of RHE.

The relative abundance of ions detected by LC-MS/MS revealed that *p*-coumaric acid was the most abundant compound present in the extract. Its concentration was determined using a validated HPLC-DAD method (refer to the relevant section 3.10.2) and it was 245 µg/100 mg of dry extract (LOD values of 0.009 µg/mL and LOQ values of 0.03 µg/mL). For this reason, it was selected as the marker compound for calculating the encapsulation efficiency and bioaccessibility index of the extract, which will be discussed in the following paragraphs.

Table 68. HPLC-MS and MS^n data of identified compounds in RHE-2. The compounds are presented in the order of elution. *Positive ionization mode

Compound	Rt (min)	Precursor Ion (*m/z*)	HPLC-ESI-MS^n *m/z* (% of Base Peak)	Compound identity	Refs
1	1.26	387	MS2[387]: 341(100) MS3[341]: 179(100), 119(70), 113(50), 161(45), 143(40), 131(20)	1-Caffeoyl-β-D-glucose	(Goufo et al., 2020)
2	2.96	133	MS2[133]: 115(100), 71(10)	Levulinic Acid	(Lopez-Fernándes et al., 2022)
3	3.24	191	MS2[191]: 173(100), 111(50), 155(10)	Quinic acid	(Carrazzone et al., 2013)
4	10.38	151	MS2[151]: 136(100), 123(5), 107(5), 88(5)	Vanillin	(Ibrahim et al., 2015)
5	15.01	163	MS2[163]: 119(100)	*p*-Coumaric Acid	(Ibrahim et al., 2015)
6	17.20	563	MS2[563]: 443(100), 473(70), 353(40), 383(30)	Apigenin 8-C-arabinoside-6-C-glucoside	(Benjad et al., 2014; Righi et al., 2013)
7	17.27	563	MS2[563]: 473(100), 443(70), 353(65), 383(45)	Apigenin 6-C-arabinoside-8-C-glucoside	(Benjad et al., 2014; Righi et al., 2013)
8	20.70	187	MS2[187]: 125(100), 169(5), 97(5)	Hydroxy gallic acid	(Fathoni et al., 2016; Thepthanee et al., 2021)
9	22.46	355	MS2[355]: 337(100), 219(60), 325(20), 204(10), 176(5)	Unidentified	-
10	33.16	329	MS2[329]: 314(100), 299(5)	Tricin	(Poulev et al., 2018)
11	35.80	329	MS2[329]: 229(100), 211(90) 314(70), 311(20), 295(30), 171(10), 155(40)	tri-OH oleic acid derivative	(Li et al., 2016)
12	36.59	671	MS2[671]: 329(100), 314(30)	Tricin derivative	(Duarte-Almeida et al., 2007)
13	38.32	315*	MS2[315]:271(100), 269(10),199	2,7 dihydroxy-4,5-dimehoxyisoflavone	(Stochmal et al., 2004)
14	42.14	311	MS2[311]: 293(100), 171(50), 201(40), 211(30), 197(35)	Unidentified	-
15	45.39	295	MS2 [295]: 171(100), 277(80), 179(35), 195(30)	Hydroxy-octadienoic acid	(Tang et al., 2020; Fathoni et al., 2016)

4.11.2 Formulation of RHE-2-based ingredient

The bioavailability of polyphenols is usually highly affected by the fluids composition present in the gastrointestinal (GI) tract. To overcome this limitation, it is common to use a carrier agent that can stabilize them and facilitate their passage to the colon (Mouritzinos et al., 2019). Considering the impossibility to use the pectin isolated from melon peel as previously reported, a commercial LM pectin derived from citrus peel was selected as carrier for a preliminary investigation involving a rice husk-based ingredient.

To encapsulate RHE, pectin/zein hydrogel beads were formulated using the ionic gelation technique, as detailed in Section 3.10.3. Zein is a hydrophobic protein commonly found in corn kernels, and we chose to incorporate it together with pectin in our hydrogel bead formulation. The rationale behind this choice was to enhance the stability of the hydrogel beads, ensuring they reach their intended target in the small intestine. Zein plays a crucial role in preventing premature payload release, which can occur when pectin swells upon contact with gastrointestinal fluids. Furthermore, zein defends pectin from protease digestion, preserving its integrity during gastric transit (Tran et al., 2019).

A fixed concentration of 2.5 mg/mL of RHE was selected for the encapsulation because this concentration had previously demonstrated the highest bioactivity in antiglycative assays.

To optimize the formulation, response surface methodology (RSM) was used, focusing on pectin, zein, and $CaCl_2$ concentrations, with the encapsulation efficiency as the selected response variable.

For the experimental design, the Taguchi orthogonal array was used due to its suitability for achieving consistent reductions in time and the number of experiments. The selected ranges for experiments (scaled as -1 to +1) were as follows: pectin concentration (P) ranged from 0.5 to 3% w/v, zein concentration (Z) ranged from 1 to 10% w/v, and $CaCl_2$ concentration ranged from 0.5 to 4% w/v. Table 69 summarized the comprehensive experimental design, along with the observed encapsulation efficiency (EE), calculated as reported in section 3.10.4. Ten different formulations were tested, with two replicates performed at the central point of experimentation.

Table 69. Taguchi orthogonal array for the optimization of pectin/zein hydrogel beads. Actual variables.

Run No.	P (% w/v)	Z (% w/v)	$CaCl_2$ (% w/v)	EE (%)
1	0.50	1.0	0.50	4.54
2	1.75	1.0	2.25	11.01
3	3.00	1.0	4.00	15.57
4	0.50	5.5	2.25	8.02
5	1.75	5.5	4.00	25.91
6	3.00	5.5	0.50	17.27
7	0.50	10	4.00	38.05
8	1.75	10	0.50	48.33
9	3.00	10	2.25	61.54
10	1.75	5.5	2.25	31.27
11	1.75	5.5	2.25	34.88

The mathematical formula of the second-order polynomial equation derived from the response surface is as follows:

$$EE\ (\%) = -2{,}94695 + 26{,}7484*P + 1{,}53204*Z - 14{,}9672*CaCl_2 - 7{,}04373*P^2 - 1{,}21215*P*Z + 7{,}02705*P*CaCl_2^2 + 0{,}251235*Z^2 + 1{,}71534*Z*CaCl_2^2 - 1{,}73741*CaCl_2^2 \quad (48)$$

The EE obtained from the different formulation ranged from 4.54% and 61.54%.

The analysis of variance (ANOVA) results presented in Table 70 underlined the significant influence of zein concentration on the encapsulation of the extract ($p < 0.05$). This finding was visually represented in the Pareto chart (Figure 66), which clearly showed the positive impact of increasing zein concentration on encapsulation efficiency (EE). These findings are supported by the study of Liu et al. (2006), who developed pectin/zein beads for the colon delivery of indomethacin (I) as a representative low molecular weight drug and bovine serum albumin (BSA) as a protein drug model. Their research indicated a lower encapsulation efficiency for pectin beads (I = 180 ± 21 mg; BSA = 150 ± 9 mg), but the addition of increasing concentrations of zein significantly improved encapsulation (maximum values: I = 223 ± 11 mg for 5% w/v of zein; BSA = 210 ± 14 mg for 10% v/w of zein). Similar results were obtained by Mukhidinov et al. (2010) in the encapsulation of piroxicam in zein/pectin hydrogel microspheres. Once again, zein content was the crucial factor, with a minimum encapsulation without zein (1:1 ratio Z/P,

37% of piroxicam in the complex) and a notable increase as the zein fraction was raised in the complex (5:1 ratio Z/P, 93.9% of piroxicam encapsulated).

Table 70. The analysis of variance of the Orthogonal array model for the optimization of pectin/zein beads.

Source	Sum of squares	df	Mean square	F ratio	*P* value
A:P	364.39	1	364.39	55.92	0.0846
B:Z	1361.09	1	1361.09	208.88	0.0440
C:$CaCl_2$	6.28	1	6.28	0.96	0.5059
AA	223.62	1	223.62	34.32	0.1076
AB	30.99	1	30.99	4.76	0.2737
AC	157.52	1	157.52	24.17	0.1277
BB	47.78	1	47.78	7.33	0.2252
BC	121.65	1	121.65	18.67	0.1448
CC	52.27	1	52.27	8.02	0.2161
Total error	6.52	1	6.52		

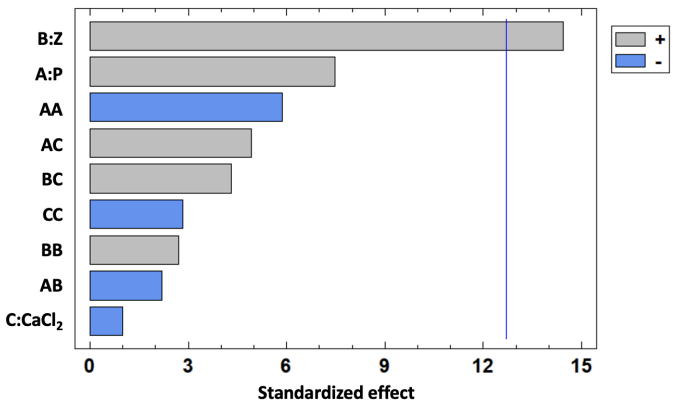

Figure 66. Standardized Pareto Chart effect for the encapsulation efficiency of RHE-2, considering the influence of zein (Z), pectin (P) and $CaCl_2$ concentrations. The positive and negative effect of the factors (reported as horizontal bars) on the response variable (TMC) is represented with grey and blue colors, respectively. The vertical line tests the significance of the effect at the 95% confidence level.

As a result, the optimal conditions for maximizing EE were determined to be as follows: 3% w/v of P, 10% w/v of Z and 4% $CaCl_2$ w/v. Under these conditions, the calculated EE reached an impressive 83.2%, with a 95% confidence interval for the mean value covering from 14.5% to 152.0%. To further validate the precision of our model, additional three experiments under

these optimal predicted conditions were performed and the EE mean was 51.77 ± 1.13%. This outcome reinforced the accuracy and reliability of our fitted model.

It is worth noting that our achieved encapsulation was estimable, especially when considering that we encapsulated at least half of the encapsulated concentration (1.25 mg/mL), which has demonstrated its antiglycative activity in previous reported bioactivity assays.

4.11.3 Bioaccessibility of RHE-2 and RHE-2-based ingredient

The raw and encapsulated extracts were digested using the Infogest digestion protocol 2.0, which simulate *in vitro* the oral, gastric, and intestinal phase of the digestion process using a mixture of electrolytes and enzymes (see section 3.11). An additional colon phase was added following the method proposed by Zhou et al. (2011), which contain the Pectinex® SP-L, a mixture of enzymes containing pectinases able to degrade pectin polymer.

2.5 mg/mL of extract, both as raw and encapsulated material, were digested. Thus, regarding the digestion of the raw extract: 12.5 mg of RHE-2 were solubilized in 5 mL water (fixed amount of sample volume of Infogest® protocol) to obtain a 2.5 mg/mL solution; considering the encapsulated one, 5 mL of a solution 2.5 mg/mL of RHE-2 were loaded in the beads, and then the formulation obtained was freeze-dried. At T0, the freeze-dried loaded beads were added to 5 mL of water and then subjected to the simulated digestion process. After each phase, the mixtures were stopped at 90 °C for 5 min to inactivate the gastrointestinal enzymes and then centrifuged. The supernatant was freeze-dried and the bioaccessibility calculated comparing the *p*-coumaric acid (*p*-CA) concentration before and after digestion.

We also performed the digestion protocol on raw extract without the enzymes (adding the equivalent volume of water or simulated gastrointestinal fluids), to estimate their influence on RHE-2 digestion. As can be seen in Figure 67, the instability of the extract was particularly evident at intestinal level, where the concentration of the marker increased notably compared to the control. This trend was probably due to the presence of the *p*-CA linked to protein or polysaccharide in the extract, which was then released during GI process by the action of the enzymes. Similar behavior was reported by Massarioli et al. (2023), who investigated the bioaccessibility of *p*-CA and coumaroyl-derivatives contained in a peanut extract using Infogest protocol. Free *p*-CA was the only compound that showed a significant increase at intestinal level ($p < 0.05$), with the highest bioaccessibility (around 370%). The outstanding results are expected and support our findings, since esterases present in the small intestine and colons of humans are able to cleave the ester bonds of the esterified hydroxycinnamic acids and

release a proportion of their free forms into the lumen (Massarioli et al., 2023). Our nominal results indicated an increase in *p*-CA concentration of about 46% more than the expected concentration (Table 71).

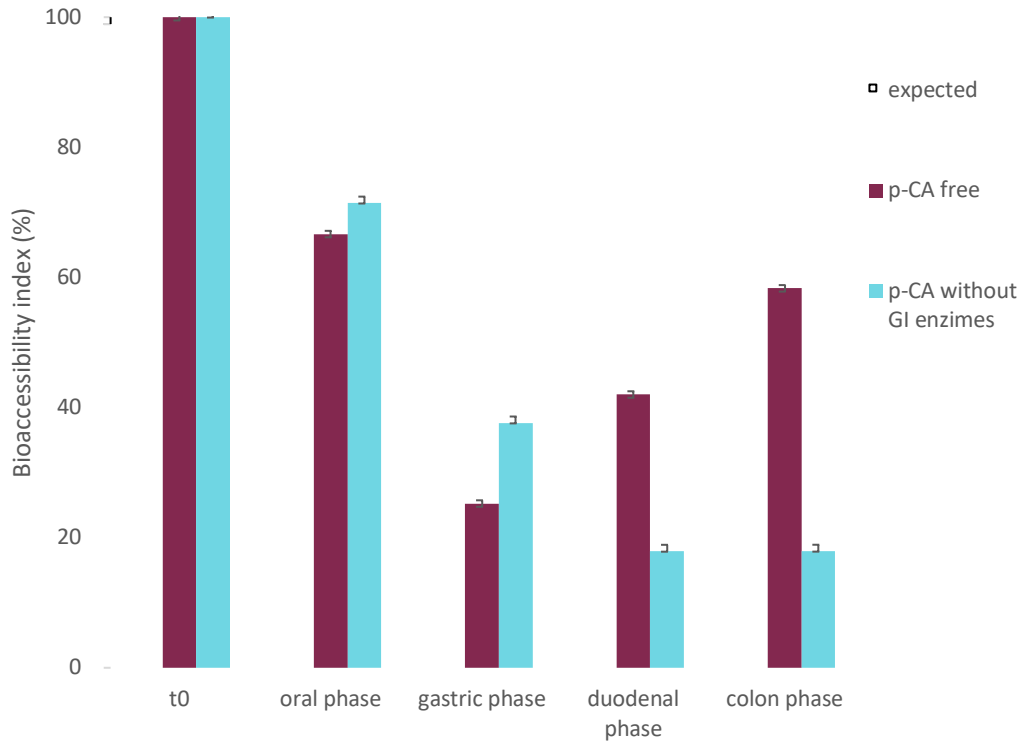

Figure 67. The bioaccessibility index of *p*-coumaric acid (*p*-CA) under the gastrointestinal tract is illustrated. The white bars represent the concentration of *p*-CA expected by the gradual dilution factor occurring during the process; The light blue bars show the concentration of *p*-CA detected at different digestion steps without the influence of gastrointestinal enzymes; finally, the violet bars indicate the concentration of *p*-CA found in the RHE-2 after undergoing digestion.

Table 71. Bioaccessibility index (BI) of *p*-CA after each gastrointestinal digestion step (oral, gastric, duodenal, colon). Nominal values.

Bioaccessibility Index (%)			
Digestion phase	**Expected *p*-CA**	**Free *p*-CA**	***p*-CA without GI enzymes**
T0	100	100	100
Oral phase	50	66.66±1.29	71.42±0.10
Gastric phase	25	25.24±0.16	37.62±0.14
Duodenal phase	12.5	42.00±2.02	17.90±0.01
Colon phase	12.5	58.32±0.84	17.91±0.01

Then, we evaluated the bioaccessibility of the encapsulated extract. The release of *p*-CA is shown in Figure 68. After encapsulation, about the 30% of *p*-CA was released within the first 2 h of gastric phase in acidic conditions, and about 80% at duodenal phase and then completed release at colon one. These results indicated the development of an intestinal-targeted formulation. In particular, at the end of the digestion it was possible to quantify all the *p*-CA amount present in the raw extract. These empirical results contradicted the encapsulation efficiency (EE) calculated for the optimal formulation, which was approximately 50%. This discrepancy was likely due to the partial efficiency of the method used to determine the encapsulation efficiency and the hypothesis of an incomplete release of *p*-CA from the formulation, resulting in an underestimation of its concentration. We established our EE determination method based on the study of Contado et al. (2020), with slight modifications, who compared two protocols for determining the concentration of resveratrol loaded in eudragit pectin/zein nanoparticles: prot-1 involved the use of DMSO as a solvent to dissolve the particles and UV-Vis measurements to assess concentration, while prot-2 involved the use of an aqueous methanolic solution (50:50 v/v) and HPLC measurements.

For our purposes, we opted for prot-2 due to its practicality and the availability of a validated HPLC-DAD method for determining *p*-CA concentration. However, authors underlined how prot-2 yielded encapsulation efficiency percentages lower than those obtained with UV-Vis, likely because DMSO was more efficient at dissolving all the particles. With prot-2, the particles were not completely dissolved, needing filtration prior to HPLC injection, which limited their quantification. Similarly, we observed that our beads were not fully dissolved in the aqueous methanolic solution, potentially leading to an underestimation of extract encapsulation. In fact, after digestion, the recovery of *p*-CA was complete and not halved due to the action pf pectinases at colon level which break down more efficiently the beads and favor the complete release of the *p*-CA (BI= 100.2±6.60%), supporting a total encapsulation of RHE-2.

Figure 68. The bioaccessibility index of encapsulated *p*-coumaric acid (*p*-CA) under the gastrointestinal tract is illustrated.

SECTION II: ENERGY

4.12 Rice bran biochar

Rice bran (RB) collected from the Italian paddy industry (Pavia province) was used as biomass source. RB was rinsed with distilled water to remove dust and dried in an oven at 80° C for 12 h to remove the excess of moisture. RB was ground sieved using a 1000-micron sieve. Particles less than 1000 μm were pyrolyzed in a tubular furnace under N_2 flux (50 mL/min). Two pyrolysis conditions were tested: 10°C/min up to 650°C or 950°C with an isothermal step of 12 h, followed by a cooling step at 10°C/min until room temperature. This set of samples was named RB-650 and RB-950. Pyrolyzed samples (RB-650 and RB-950) were mixed with KOH at different weight ratios KOH: Biochar (6:1 and 2:1). The KOH-activated samples were labelled as RB-650/2:1, RB-650/6:1, RB-950/2:1 and RB-950/6:1.

TGA was conducted on rice bran from 45 °C to 1000 °C. Figure 68 shows the TGA (wt.%) and DTG (wt. %/°C) curves of RB. The results show four main mass losses. In the first stage, 6.74 wt.% of the initial mass is loss due to the removal of moisture from RB. The second stage occurs between 130 °C to 230 °C, where 14.21 wt.% is loss due to the initial decomposition of lignin. Lignin is a biopolymer with an extensive network of aromatic rings crosslinked with different branches, the different nature of the chemical bonds in lignin, led to its degradation in a wide temperature range from 100–900 °C (Yang et al., 2007). For RB, the third main loss occurs in the temperature range from 230 °C to 600 °C where 58.75 wt.% of the mass is loss, which is attributed to the decomposition of both hemicellulose and cellulose. The decomposition of hemicellulose occurs at temperatures between 220 to 315 °C (Yang et al., 2007), while decomposition of cellulose mainly take place at temperatures between 315 °C to 400 °C (Weber et al., 2018; Shaaban et al., 2013). At temperatures higher than 400 °C a further decomposition of lignin is recorded (Shaaban et al., 2013). Finally, at temperatures from 600 °C to 1000 °C only a small weight loss is observed (6.39 wt. %). Based on the TGA analysis, 650 °C (constant mass) and 950 °C (maximum treatment temperature) were selected as the pyrolysis temperatures to produce biochar.

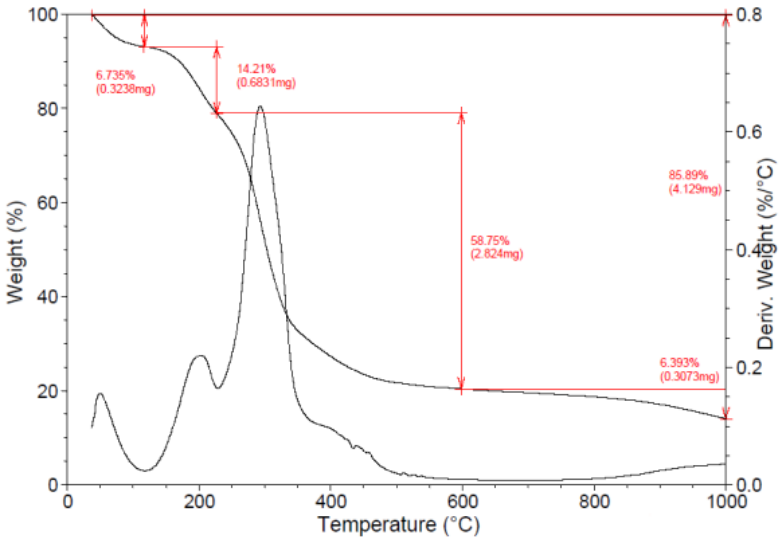

Figure 68. TGA and DTG curves of rice bran from 45 °C to 1000 °C.

Figure 69a show the FTIR spectra of the RB and the pyrolyzed biochar at 650 °C and 950 °C. As expected, the spectra of the pyrolyzed RB are more simplified due to the elimination of organic compounds and hence the loss of numerous functional groups during heat treatment (Wang et al., 2009). For the RB, the peaks at 850 cm^{-1} are due the vibrations of the Si-O-Si groups (Wang et al., 2009; Ellerbrock et al. 2002). The strong peak at 988 cm^{-1} corresponds to microcrystalline cellulose (Liu et al., 2021). The small peaks from 1240 to 1450 cm^{-1} are due to the C-O stretching from the esters and carboxylic groups in lignin. Vibrations in the frequency range from 1500 cm^{-1} to 1400 cm^{-1} reflects the stretching of the C-C bonds from the aromatic compounds. The peaks at 2849 cm^{-1} and 2918 cm^{-1} indicates the presence of methylene groups -CH_2- from hemicellulose, lignin, and cellulose. The former peaks are absent for the pyrolyzed samples, as these organic compounds decompose almost entirely at 600 °C, as discussed in the TGA results. The broad peak in RB at 3257 cm^{-1} is due to the O-H stretching vibration of water molecules adsorbed on the material. Figure 69b show the FTIR spectra of the ACs obtained by the chemical activation of RB-650 and RB-950 using different weight ratios KOH: Biochar (2:1 or 6:1), a series of small peaks from 1630 cm^{-1} to 1700 cm^{-1} indicates the presence C=O bonds from the carbon skeleton and the presence of small quantities of CO, CO_2 and K_2CO_3 as they are by-products from the activation process (Lozano-Castelló et al., 2007). These peaks are also visible in the RB and the pyrolyzed RB at 650 °C and 950 °C from the remaining and lignin. For all the samples, small vibrations from 2000 cm^{-1} to 2300 cm^{-1} can be ascribed to the C=C bonds (Mecozzi, et al. 2017).

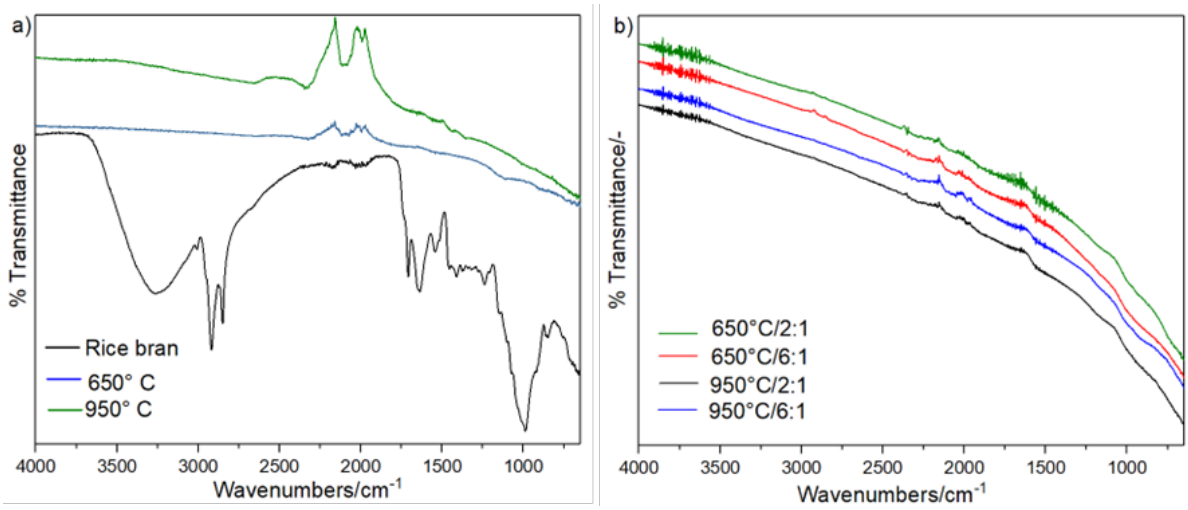

Figure 69. FTIR spectra of the: a) rice bran and the pyrolyzed samples at 650° C and 950° C; b) activated carbons obtained at different KOH: Biochar weight ratio.

The morphology and microstructure of the rice bran and the activated carbon samples was investigated by SEM: the results can be found in Figure 70. SEM micrographs of rice bran shows a non-porous morphology. After KOH activation on biochar samples at 650 °C and 950 °C, an evident porous structure is obtained. These results clearly show that KOH activation led to the production of mesopores and macropores in the pyrolyzed material. The formation of mesopores and micropores caused a significant increase in surface area. After pyrolysis at 650 °C, a surface area of 34 m^2/g was recorded, with average pore volume of 0.2 cm^3/g. The activation with a 6:1 ratio of KOH led to a surface area of 2500 m^2/g and pore volume of 1.3 cm^3/g. After the treatment at 950 °C, the surface area was 26 m^2/g, increasing to 1820 m^2/g (pores volume of 1.1 cm^3/g) after the 6:1 activation.

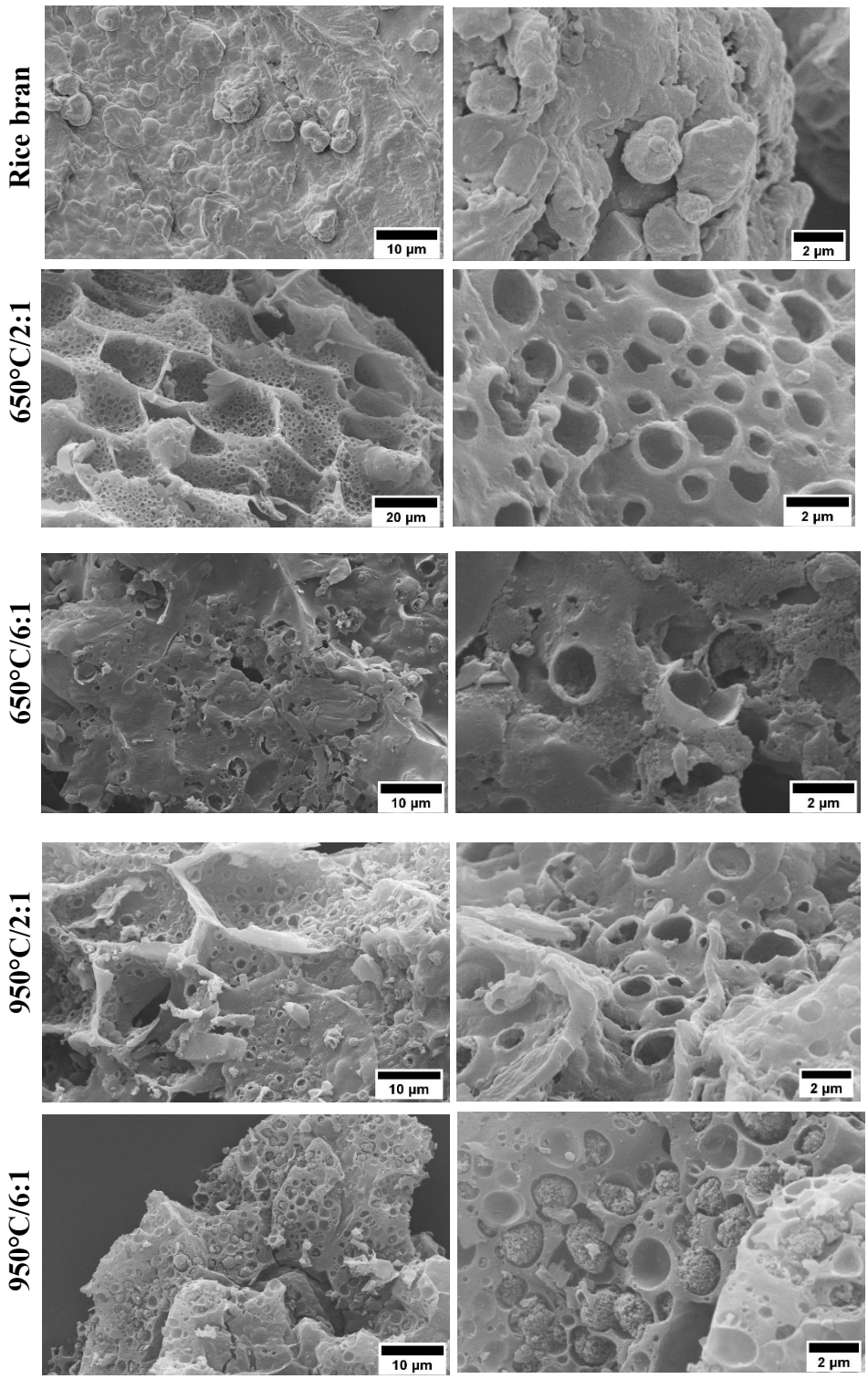

Figure 70. SEM micrographs of rice bran and the activated carbons obtained from pyrolyzed rice bran at 650 °C or 950 °C. Chemical activation was performed at a mass ratio KOH:Biochar (2:1 or 6:1).

Table 72 shows the EDS analysis of the rice bran and the ACs. The results indicate carbon and oxygen as the main components of RB; small quantities of other elements are present (K, Mg, P, Si, S and Cl). After pyrolysis and activation, carbon becomes the predominant component (93 wt.%), while the content of oxygen decreases up to 6 wt.%.

Table 72. SEM-EDS analysis of the activated carbon obtained by the chemical activation of biochar obtained from rice bran.

Elements	Elemental composition (wt.%)				
	Rice bran	650 °C KOH 2:1	650 °C KOH 6:1	950 °C KOH 2:1	950 °C KOH 6:1
C	47.0	93.48	93.4	89.63	91.28
O	47.48	6.21	6.46	9.54	8.31
Cl	0.14	0.30	0.15	0.83	0.41
P	2.08	-	-	-	-
K	2.06	-	-	-	-
Mg	0.75	-	-	-	-
S	0.24	-	-	-	-
Si	0.24	-	-	-	-

Hydrogen storage capacity was investigated at -196 °C (77 K) using biochar from rice bran after KOH activation. Figure 71a show the hydrogen storage capacity, expressed as wt.% against equilibrium pressure. The most performing ACs were achieved using the 6:1 ratio KOH: Biochar, regardless of the pyrolysis temperature. However, the sample 650 °C/6:1 showed a H_2 storage capacity of 4.7 wt.%. The second most performing sample was the 950 °C/6:1 with a H_2 storage capacity of 3.5 wt.%. For the two set of samples activated using a 2:1 ratio, the ACs pyrolyzed at 650 °C outperform the 950 °C with storage capacity values of 3.2 wt.% and 2.4 wt.%, respectively. Figure 71b shows the kinetic curves for the four ACs: the results outline a rapid hydrogen uptake within 2 min. Figure 71c shows the dehydrogenation curves for two selected samples (650 °C/2:1 and 650 °C/6:1). The results show H_2 was desorbed from these porous carbon materials within 2 min. These results demonstrate that the hydrogen storage on ACs takes place by a physisorption mechanism. Table 73 show the H_2 storage capacity of different biochar-based materials reported in the literature at 77 K and 298 K. The data show our material have a high H_2 storage capacity compared to other ACs produced from agricultural waste.

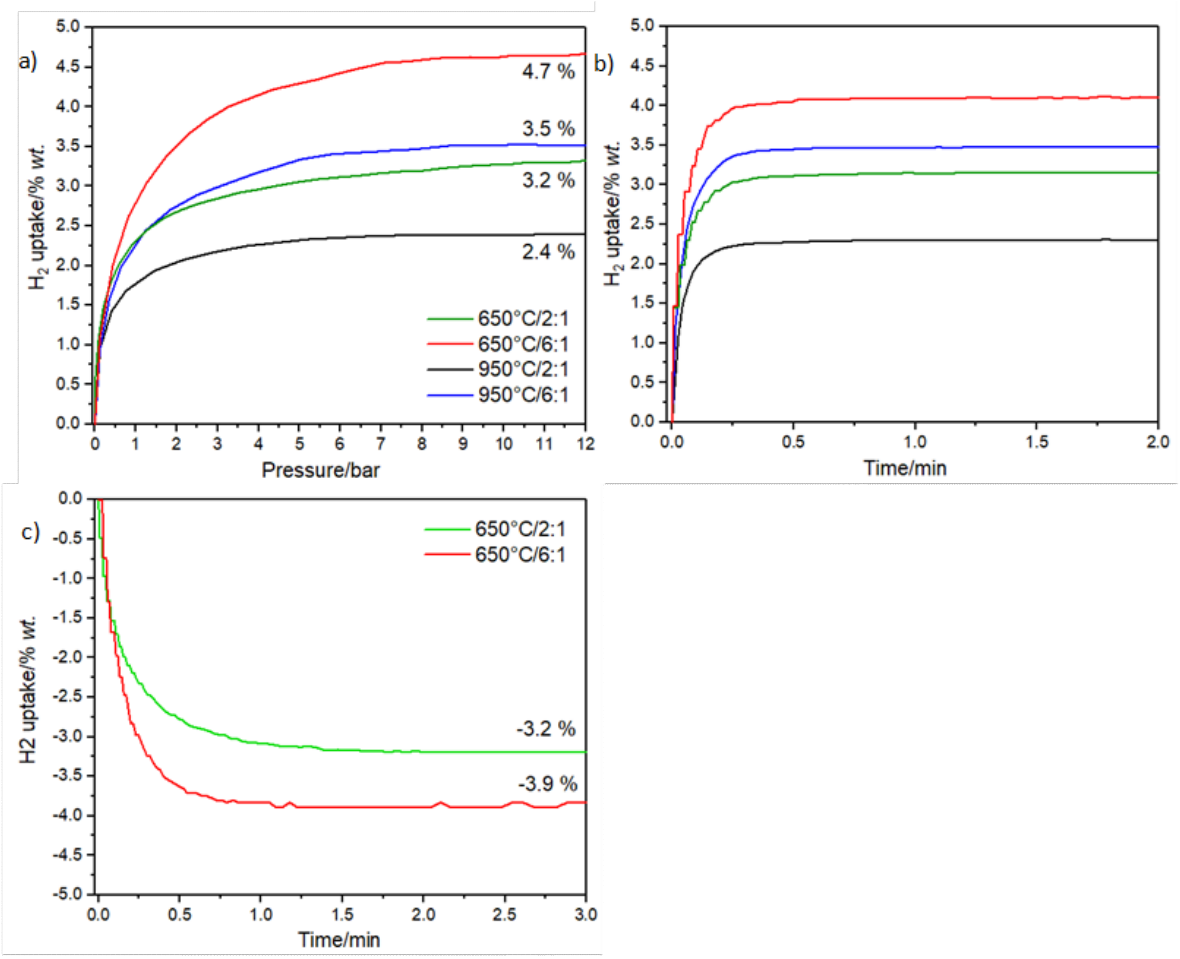

Figure 71. a) PCT measurements b) kinetic experiments c) Desorption measurement for the ACs obtained by the pyrolysis of RB at 650°C or 950° C and KOH activation KOH:biochar ratios (2:1 or 6:1).

Table 73. Biochar-based activated carbon for hydrogen storage

Type of biomass	Synthesis procedure		H_2 storage capacity		Ref.
	Pyrolysis	Activation	wt.%	Conditions	
Corncob	450 °C/2 h/N_2 atm	1 g biochar in 3 M KOH solution. Activation 850 °C/2h 3012 m^2/g	2.0 0.44	77 K, 0.1 MPa 298 K, 5MPa	(Sun et al., 2010)
Hemp stems	500 °C/2h/N_2 atm	800 °C/3.5 h KOH to biochar 4.5:1 (wt. ratio) 3241 m^2/g	3.28	77 K, 0.1 MPa	(Yang et al. 2012)
Coffee beans	Two-step steam activation a) steam at 45 g/min, 500 °C/1 h b) Steam/CO_2 (800 °C/2h)	850 °C/ 2h KOH to biochar 5:1 (wt. ratio) 2070 m^2/g	4.0 0.6	77 K, 4 MPa 298 K, 12 MPa	(Akasaka et al., 2011)
Cellulose acetate	Hydrothermal process (250 °C/2 h)	700 °C/ 2h KOH to biochar 4:1 (wt. ratio) 3800 m^2/g	8.9 1.2	77 K, 2 MPa 298 K, 3 MPa	(Blankenship et al., 2017)
Rice bran	650 °C/12 h/N_2 atm 950 °C/12 h/N_2 atm	KOH/ 6:1 KOH/6:1	4.7 3.5	77 K, 1.2 MPa	This study

The results demonstrate the micropore volume and distribution of pores are the most important factors for H_2 storage through a physisorption process. Rice bran pyrolyzed at 650 °C and activated with mass ratio 6:1 KOH/biochar showed the highest potential for hydrogen storage. The most performing AC had a SSA of 2 500 m^2/g and a hydrogen uptake of 4.7 wt.% at 77 K at 12 bar. The obtained value is close to the 5 wt.% hydrogen uptake objective set by the International Energy Agency. This result indicates the use of agricultural waste is a promising approach to produce high value-added materials for energy storage.

4.13 Rice husk biochar

The by-products of rice grown in Italy, Pavia province, Lombardia region, were used as primary biomass sources for this study. RH was washed with distilled water to remove impurities under natural conditions. The cleaned RH was placed in an oven at 80°C overnight to remove moisture. The dried RH was ground and sieved using a 1000-μm sieve. Particles less than 1000μm were used for the next step: the sieved samples were transferred to an alumina boat in the furnace and heated from 250C to 950°C at 10°C/min followed by a 12 h isothermal step under 200 ml/min N_2 airflow. The pyrolyzed sample (RH-950) was activated with KOH with a weight ratio 2: 1.

Biochar, derived from RH, was activated with KOH to form a porous structure and high surface area on the biochar. Activated biochar was washed overnight with HCl and then with distilled water until its pH was about 7. The activated samples were finally dried at 80°C in an oven for 24 h. The KOH-activated sample was labeled as RH-950/2:1.

Thermograms were obtained by TGA for RH before pyrolysis (950°C) as shown in Figure 72. Mass loss in RH is mainly divided into four stages. The removal of the sample's moisture content causes the first stage of weight loss, which is around 7.405% of the total weight, occurring at around 100°C. At 150°C -300°C, the second stage of weight loss occurs, resulting in a loss of around 9% of total mass owing to the elimination of structural water content and hemicellulose. Above 315°C, cellulose begins to decompose and around 400°C cellulose is converted into non-condensing gases and condensing organic vapors. Generally, lignin begins to decompose at around 160°C, but the process is sluggish, and the decomposition continues until the temperature reaches 900°C. Therefore, at 300°C-750°C, the third stage of weight loss occurs and 54% of total mass is released due to the removal of various types of carbonaceous components such as lignin and cellulose. The fourth stage of weight loss, accounting for a total 3 wt% of loss and whose end corresponds to a total 73.16% mass loss, occurs at around 750°C-1000^0C due to the continued elimination of various types of carbonaceous components (Ramesh et al., 2015; Yang et al., 2007). At 950°C all these processes are ended so this value was selected for pyrolysis: at this temperature only the carbon skeleton of the biochar starting material remains.

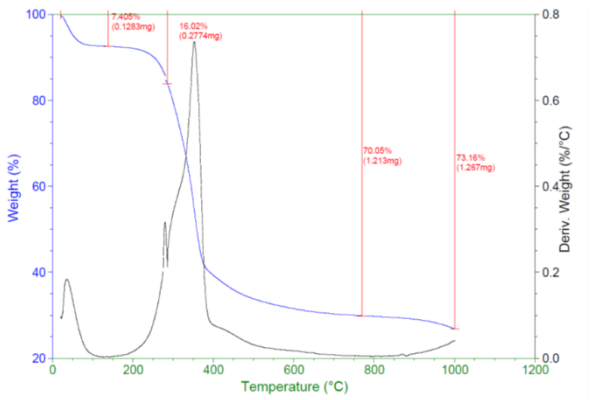

Figure 72: TGA of RH before pyrolysis

The crystallinity of the substance is shown by XRD examination. The XRD patterns for raw RH (before pyrolysis) and RH biochar produced at 950°C are shown in Figure 73. Two broad peaks at 16° and 21° and a smaller peak at 31° were detected before the pyrolysis (Figure 73). These might be attributed to crystalline cellulose while, according to (Sun et al., 2010; Aresta et al., 2012), both hemicellulose and lignin are amorphous in nature. Similar diffraction patterns were reported in (Shaaban et al., 2013) for rubberwood sawdust and in (Wang et al., 2009) for raw pine wood. The small peak at 35° was attributed to cellulose (Rambo et al., 2015). After pyrolysis, only the peak at 21° is retained, and a small signal at 43° is visible. This means that the cellulose structure is no longer present and only inorganic C can be recognized (Sun et al., 2010).

The identification of various functional groups on biochar surfaces formed at various temperatures is aided by FTIR. The FTIR spectra before and after pyrolysis (950°C) are shown in Figure 74. As expected, the spectrum of the activated C produced at 950°C differed from that of raw material, being more simplified, which might be attributed to the elimination of numerous functional groups and gradual carbonization (Wang et al., 2009). The O-H stretching vibration of water molecules adsorbed on the surface of carbon material is responsible for the peak at 3440cm^{-1} and disappeared when the temperature rose to 950°C. This signified dehydration of the biomass structure. The peak found in raw RH at 2929cm^{-1} indicating the methylene group -CH_2- in hemicellulose has been vanished after pyrolysis at 950°C, and -CH_2- is no longer present. There are some vibrations in the frequency range of 2000cm^{-1} to 2500cm^{-1} in raw RH that reflects peaks for C≡C and C≡N groups: their intensity is very small in the 950°C pyrolyzed sample. Near around 1653cm^{-1} the presence of the alkene groups and C=C bonds is evident for the raw material, and it has been vanished in pyrolyzed sample. The peak at around 1630cm^{-1}, indicating the presence of N-H bonds in raw RH, vanished at the pyrolysis temperature of 950°C. Vibration in the frequency range from 1500cm^{-1} to 1100cm^{-1} reflects

peaks for carbonate and carbonate-carboxyl groups: in the pyrolyzed sample these peaks are getting smooth. In raw RH, peaks around 1090cm^{-1} due to C-O stretching indicate the presence of ester or phenol: they are almost vanished in the 950°C pyrolyzed sample. Signals at around 794cm^{-1} indicate the aromatic C-H out-of-plane bend (Nandiyanto et al., 2019): these peaks show a declining trend in the pyrolyzed sample.

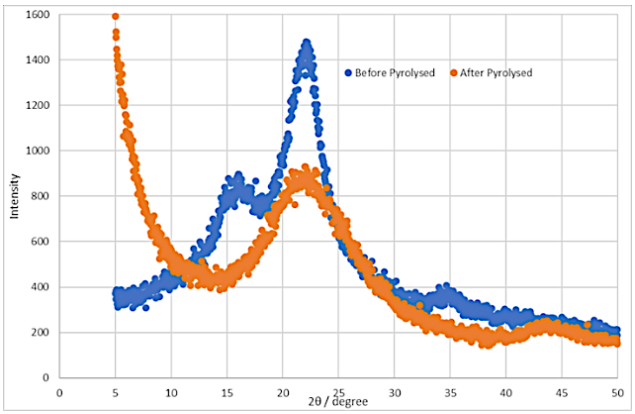

Figure 73: XRD analysis before and after pyrolysis

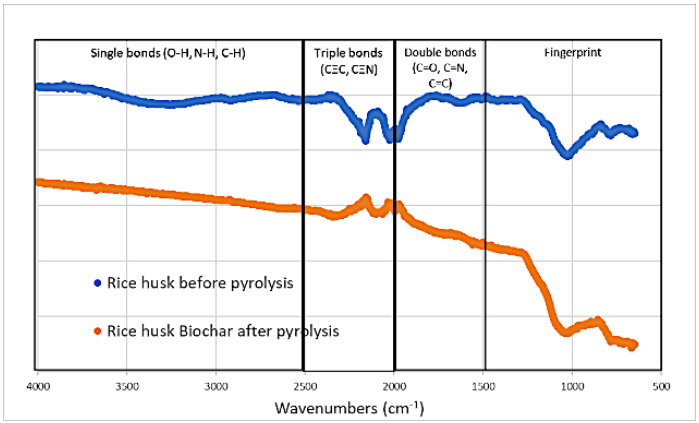

Figure 74: FTIR Spectrum of Rice Husk before pyrolysis and after pyrolysis

Morphological analysis of RH before pyrolysis, after pyrolysis, and after activation is shown in Figure 75. Prior to pyrolysis, the RH sample shows nodular fragments with a wavy structure (fig. 75a). It retains that structure after being pyrolyzed at 950°C (Figure 75d). After pyrolysis, it shows honeycomb shape and irregular pores (Figure 75e and f). Furthermore, following pyrolysis process at 950°C, the RH shape acquires a tubular-like channel structure (Figure 75). All the carbonized particles have similar morphology with different pore sizes. The variations in the micromorphology and microstructure of this RH biochar proved the importance of the thermal treatment and pre-carbonization stage in the development and stability of the exhibited honeycomb shape and irregular holes. After KOH activation, the hierarchical

structure is almost maintained with a smooth surface (Figure 75g and h). Furthermore, many new pores have been formed, while some old pores have been expanded (Figure 75h). This clearly shows that KOH activation introduces a large number of small pores on the carbon material (Figure 75). The formation of mesopores and micropores causes a significant increase in surface area and pore volume in the activated biochar. Also, mesopores can act as highways for rapid ion diffusion, and the presence of a large number of apertures contributes increasing the ratio of surface area to volume and its effect on the overall specific surface area of the structure (Bai et al., 2016).

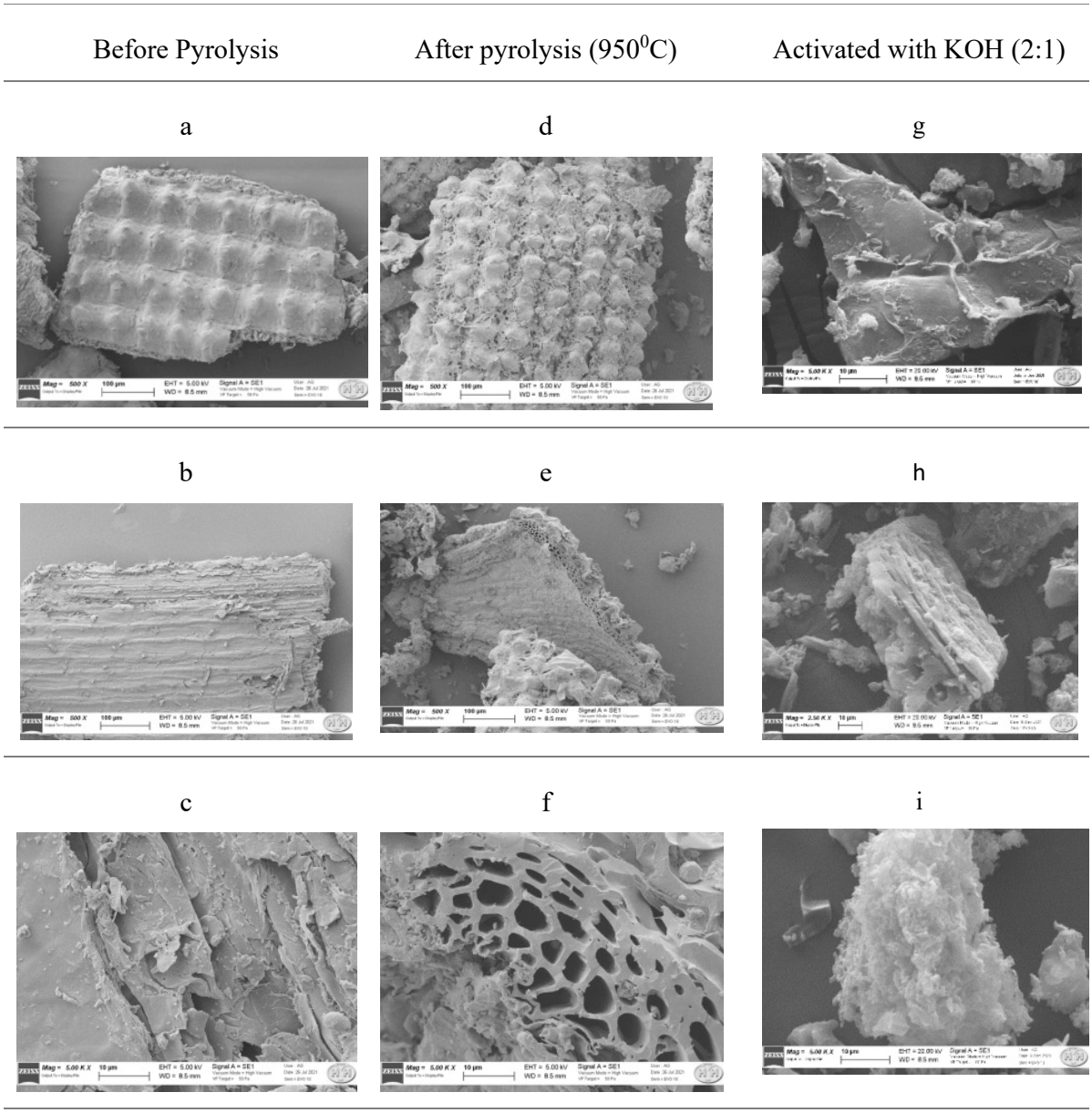

Figure 75: SEM morphology analysis of RH before pyrolysis and after pyrolysis and after activation.

EDX analysis was performed for RH samples before pyrolysis, after pyrolysis, and after

activation with KOH, as reported in Table 74. C, O, Si and K are predominant in the raw RH sample. After pyrolysis and after activation, the C content of the sample increased while the O, Si, and K content decreased significantly.

The BET instrument is used to evaluate the surface area of activated RH biochar samples as well as to analyze meso- and macropore volume. As the particle size of the biochar decreases, the surface area generally increases. The BET surface area of the biochar samples was analyzed by degassing for 6h at 53°C+14h at 80°C. Table 75 shows the specific surface area, and specific pore volume of activated carbon obtained from adsorption-desorption isotherms.

Table 74. EDX analysis of Rice husk samples

Elements	Average weight %		
	Before pyrolysis	Arter Pyrolysis	After activation
C	28.42	42.94	81.05
O	53.62	35.90	15.40
Si	16.98	17.93	3.27
K	3.66	0.77	0.00
Mg	0.05	0.30	0.00
S	0.11	0.00	0.03
Ca	0.46	1.69	0.00
Cl	0.03	0.00	0.23

Table 75. BET data after activation

Specific surface area	1508 m^2/g
Specific pore volume	0.81 cm^3/g

Considering the hydrogen storage capacity at -196°C, the potential of the activated RH biochar as a hydrogen storage material in physisorption mode was studied. For this reason, the samples in the experiments were immersed in a Dewar tank filled with liquid nitrogen under vacuum. The hydrogen uptakes of activated RH biochar were measured at 77K and up to 9 bars by PCT (Figure 76) and kinetic (Figure 77) measurements. The solid-gas interaction is significantly dependent on the physisorption mechanism caused by the textural features of the adsorbent materials (Dutta et al., 2014; Qiu et al., 2014; Xiao et al., 2014). In particular, for porous carbon,

hydrogen adsorption depends on the pore volume and pore size (Armandi et al., 2011; Stadie et al., 2010; Kim et al., 2008). According to the findings, the hydrogen adsorption of the activated RH biochar is shown to be +2.2 wt.% at 6 bars. The kinetics is very fast: after 0.5 min, all the hydrogen content is already adsorbed. The process was shown to be reversible in the frame of 5 sorption cycles.

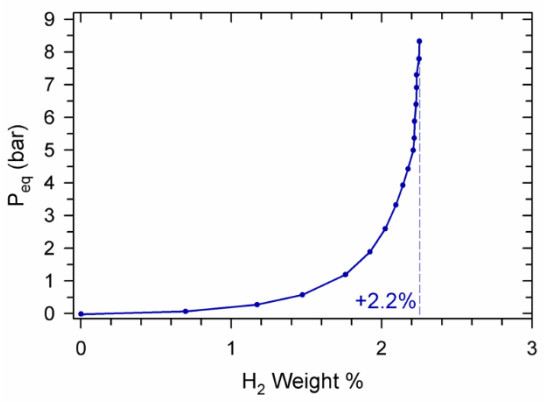

Figure 76: PCT measurement at 77K.

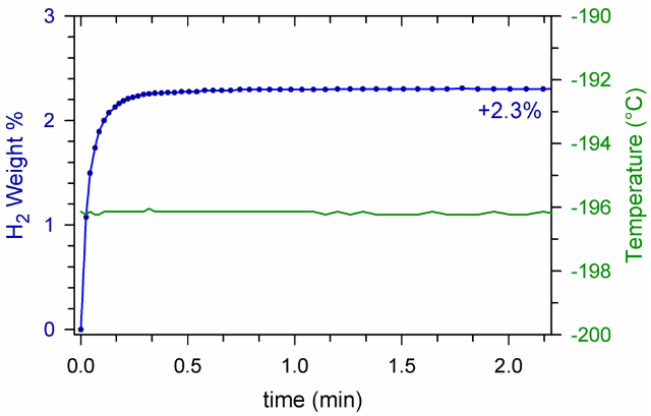

Figure 77: Kinetic measurement at 77K and 6 bar.

To sum up, the carbon content of activated carbon samples was greater than that of raw RH: it was 28.42% for raw material, grew to 42.94% in the biochar, and it climbed to 81.05% after activation with KOH. The micropore volume and distribution of pores are the most important factors for hydrogen storage through the physisorption process. Activated carbon with BET surface area of 1508 m^2/g and total pore volume of 0.81 cm^3/g is obtained, and the maximum

hydrogen uptake is 2.3 wt.% at 77K and 6 bar. On the other hand, in this study it was shown that it is possible to prepare activated carbons that have high microporosity using a small KOH amount, indicating that this study is relatively eco-friendly and economically profitable. Therefore, we indicate that the preparation of activated carbon from RH with a high specific surface area is a promising approach for the high-value conversion of abundant agricultural waste.

4.14 Melon peel biochar

The melon peels were collected during the summer period, dried under the sun and lyophilized for the storage in the freezer. The TGA curve (Figure 78) is quite complex: at the end of the release of adsorbed water at around 120 °C, a 5-stage decomposition is noted, evident from the DTG curve, which leads to a release of approximately 68% in mass within 650°C. A further decomposition stage takes place starting from approximately 720 °C and accounts for the loss of 10% in mass.

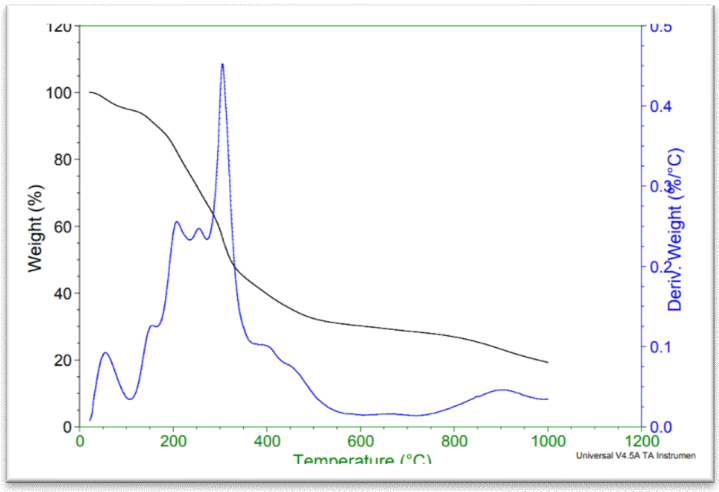

Figure 78. TGA of the lyophilized melon peels.

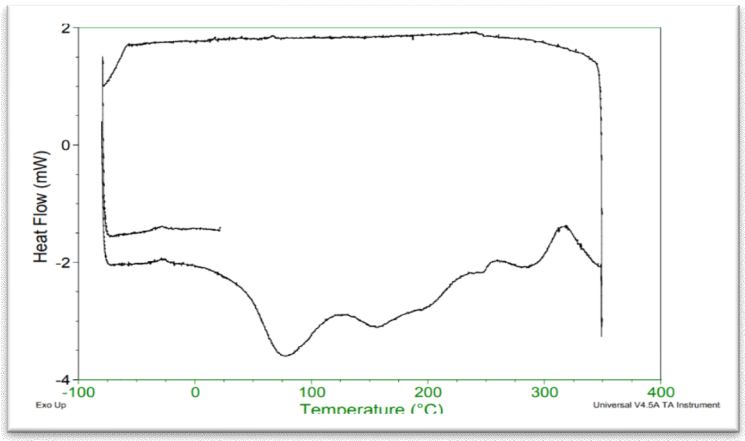

Figure 79. DSC of the lyophilized melon peels.

The melon calorimetric curve confirms the complexity of the decomposition mechanism highlighted by the DTG trace (Figure 79).

Considering the TGA described above, it was decided to pyrolyze the waste at 650°C, the temperature at which the main stages of decomposition of the organic part with the formation of inorganic carbon are terminated. Subsequently, the melon biochar was activated with KOH as described for rice wastes.

Concerning the SEM images (Figure 80), in the freeze-dried sample as it is, flakes ranging in size between 5 and 150 µm can be seen with a smooth surface covered by smaller fragments.

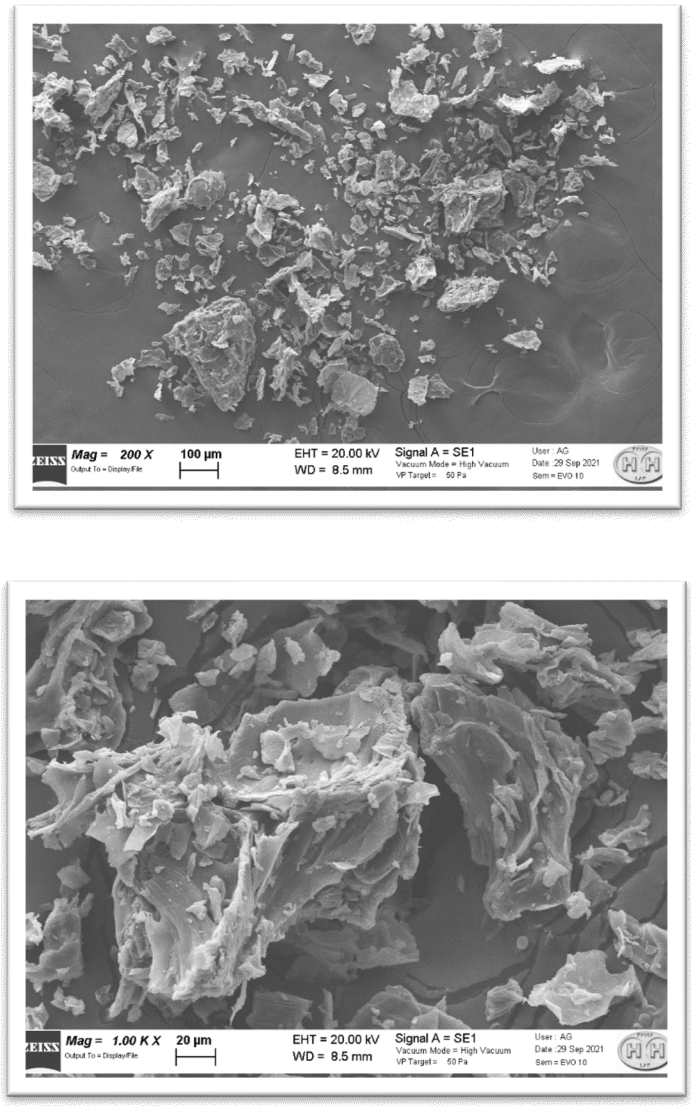

Figure 80. SEM images of the lyophilized melon peels.

After pyrolysis, the particle size was reduced and the particles appeared composed of sheet-like layers, with evident microporosity (Figure 81).

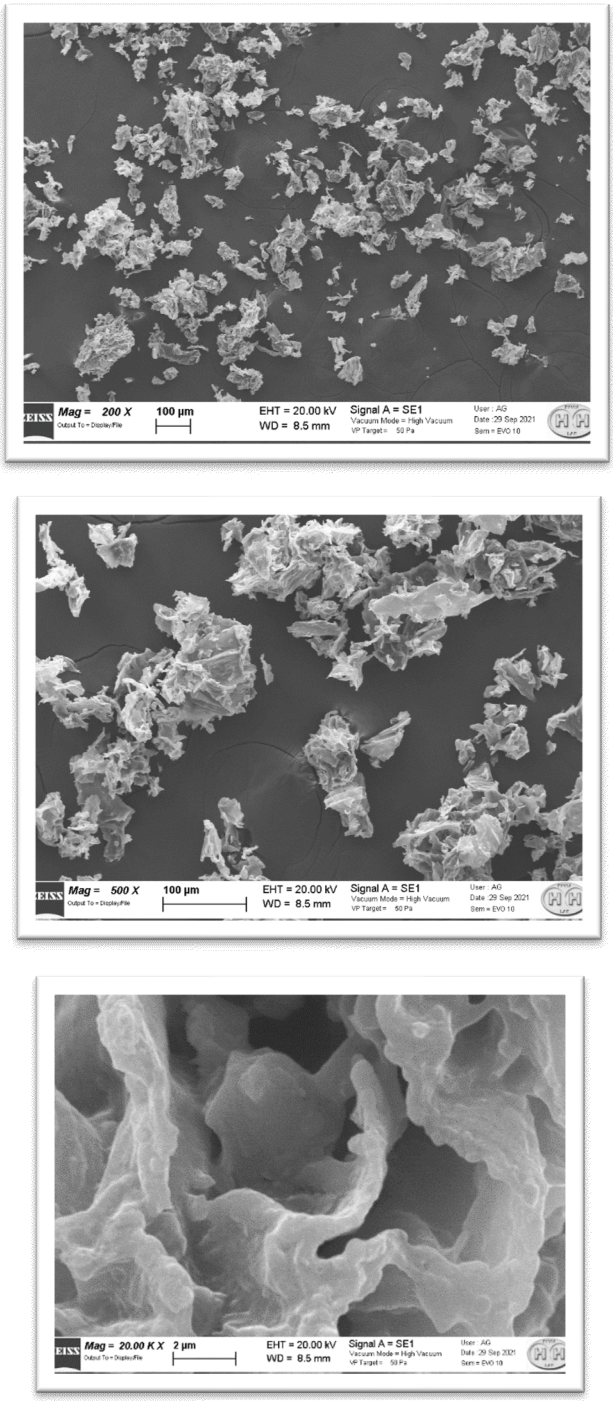

Figure 81. SEM images of the pyrolyzed melon peels.

After activation (Figure 82), the melon sample appears to consist of prismatic trapezoidal particles up to 200 mm in size. At higher magnification, surfaces with a morphology similar to crumpled sheets with macro and microscopic porosity can be seen.

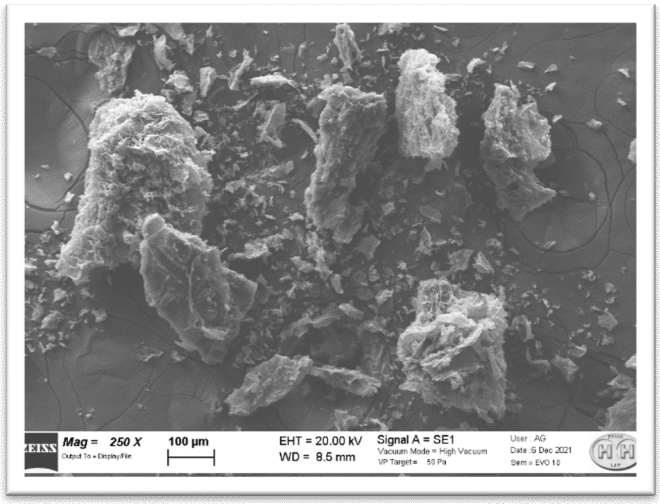

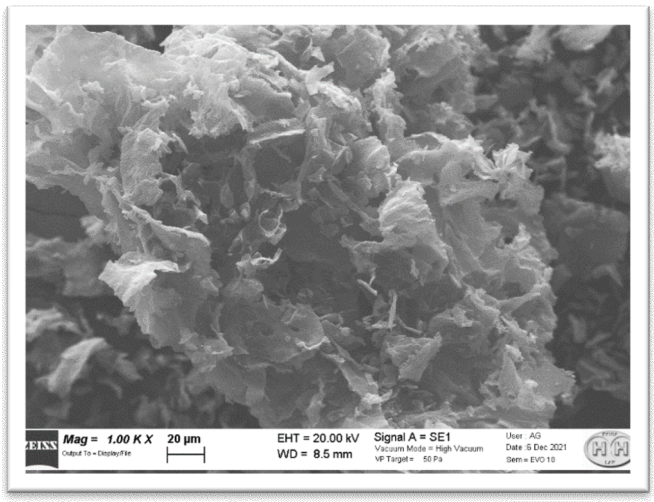

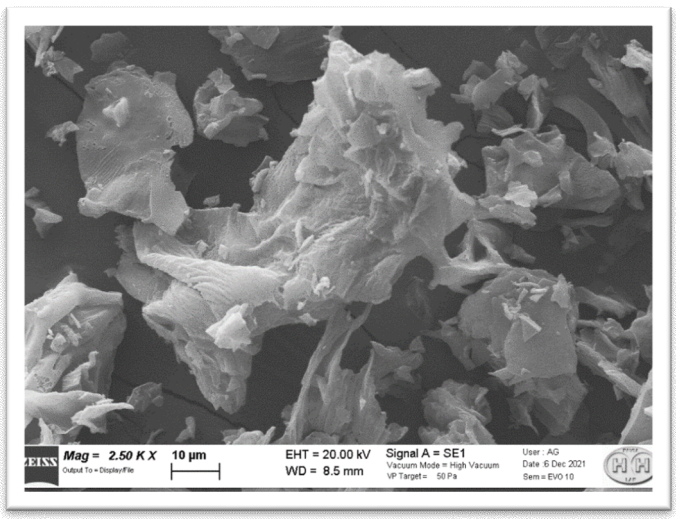

Figure 82. SEM images of the superactivated C from melon waste.

The IR spectrum of melon peels illustrated in Figure 83 shows the presence of the O-H bond band at 3278 cm^{-1}, the N-H bonds between 2850 and 2920 cm^{-1} and the C-C and C-O bonds at 1600, 1400 and 1000 cm^{-1}.

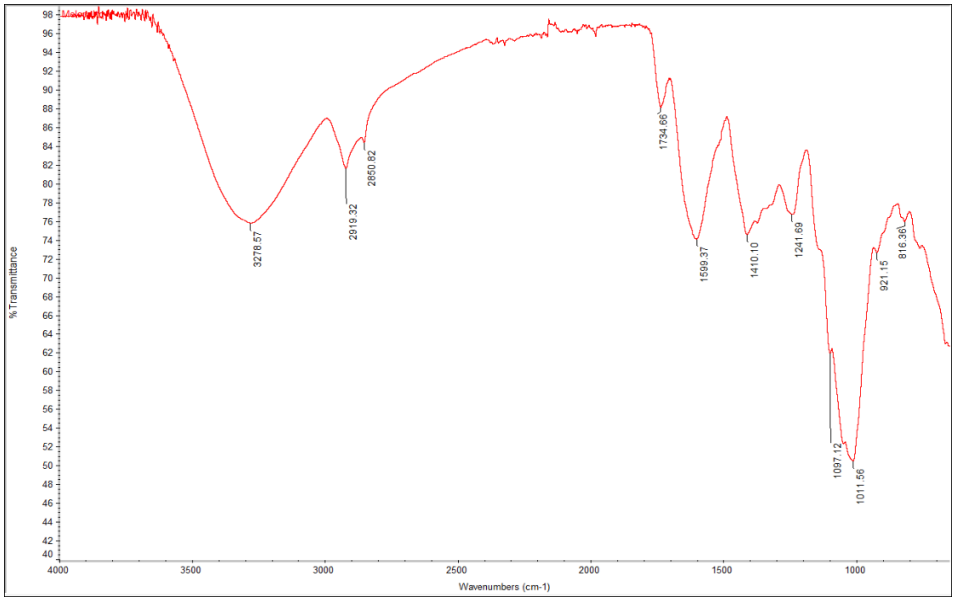

Figure 83. IR spectrum for melon peels.

These peaks disappear after pyrolysis (Figure 84), regardless of the treatment temperature.

Figure 84. IR spectrum for 2:1 melon peels.

The melon sample activated with KOH with a 2:1 ratio is the best performing sample and it shows, at 77K, a gravimetric storage capacity of the order of 4.2% (Figure 85). This value is already reached at 10 bar. Kinetic measurements presented in Figures 86 show that this amount is adsorbed in 40 seconds. Approximately 3.6% of hydrogen is released in 1.5 min (Figure 87).

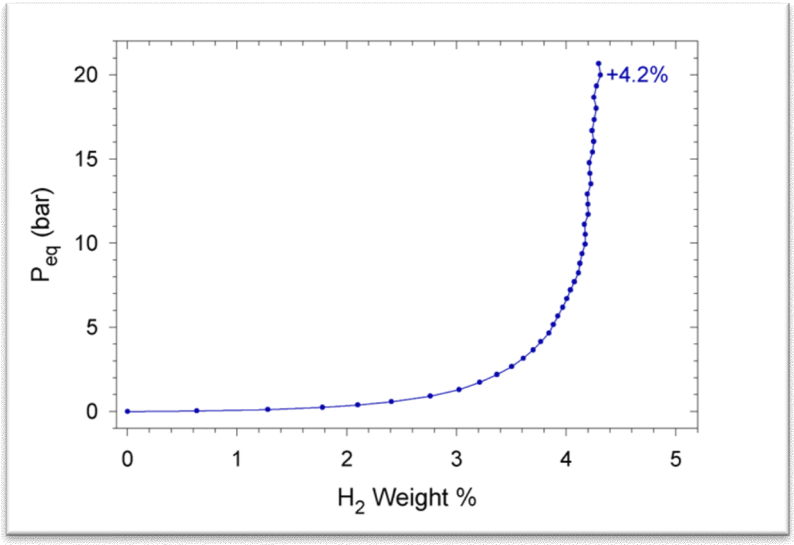

Figure 85. PCT for melon peels pyrolyzed at 650°C and activated with a KOH:waste ratio of 2:1.

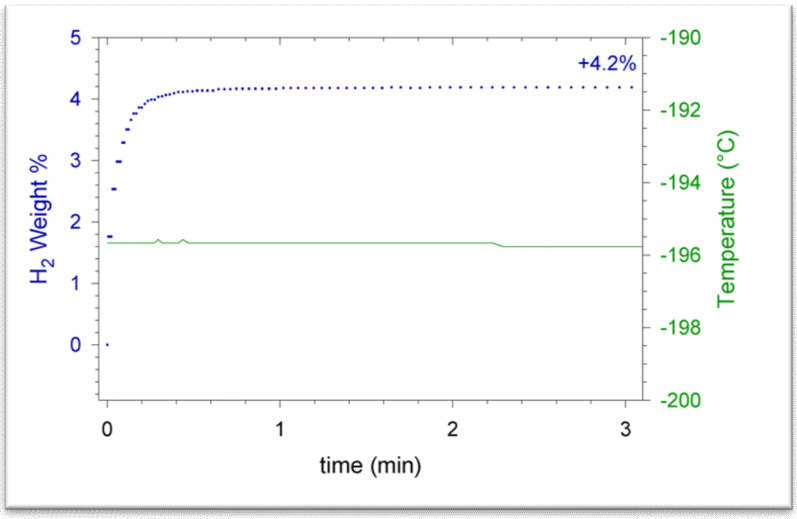

Figure 86. H_2 adsorption curve for the melon peels pyrolyzed at 650°C and activated with KOH:waste ratio of 2:1.

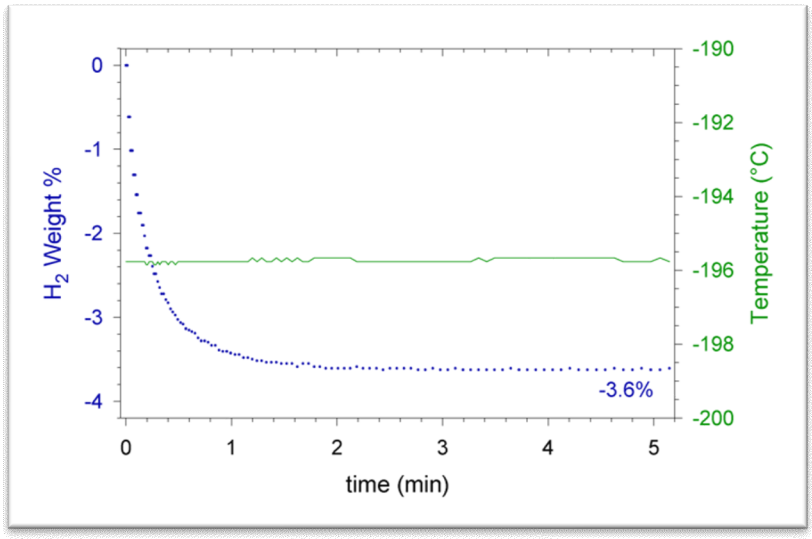

Figure 87. H_2 desorption curve for the melon peels pyrolyzed at 650°C and activated with a KOH:waste ratio of 2:1.

4.15 Asparagus bottom parts biochar

The asparagus bottom parts (or stems) were obtained from fresh asparagus edible vegetables, dried under the sun and in an oven at ambient pressure and 45°C and then cut in piece and pyrolyzed.

The IR spectrum of the dried stems shows several different peaks, as it is illustrated in Figure 88. In the area between 3100-3400 cm^{-1}, it is possible to observe a very widened absorption band relating to O-H vibrations and N-H stretching; this band can be traced back to some biomolecules present in the plant. In fact, there are high concentrations of asparagine at the level of amino acid composition in proteins, in addition to the presence of carotenoids and pectins. The width of the band indicates that the various functional groups responsible for the signal appear to be conjugated and not isolated. The signal at 2921 cm^{-1} concerns the C-H stretching of the methylene groups. At 1623 cm^{-1} it is possible to observe the stretching of the carbon-carbon double bond, and at 1033 cm^{-1} the signal is attributable to the stretching of the C-OH bond related to the alcoholic and carboxyl groups belonging to the biomolecules of the plant.

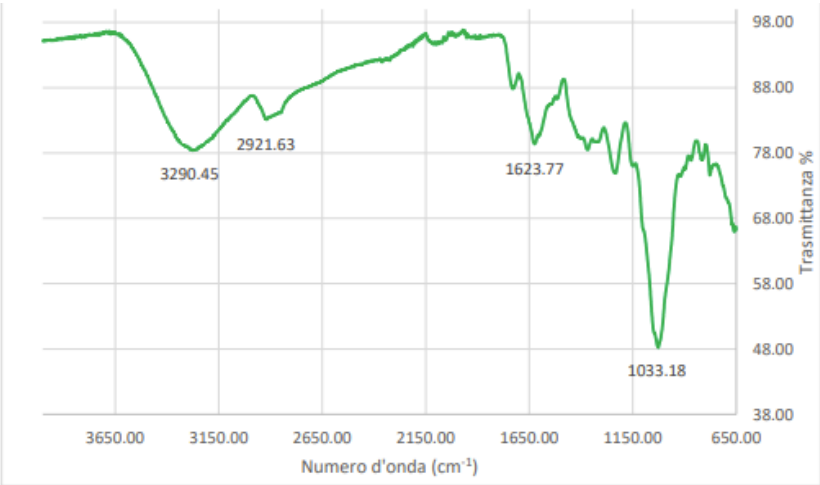

Figure 88. IR spectrum of asparagus stems

From the diffraction pattern (Figure 89) it is possible to note that the material does not show clear and precise peaks attributable to specific crystalline phases; therefore, it is plausible to consider this material as mainly amorphous. The very sloppy peak around 23° can be attributed from the literature to graphitic carbon (Deng et al., 2018).

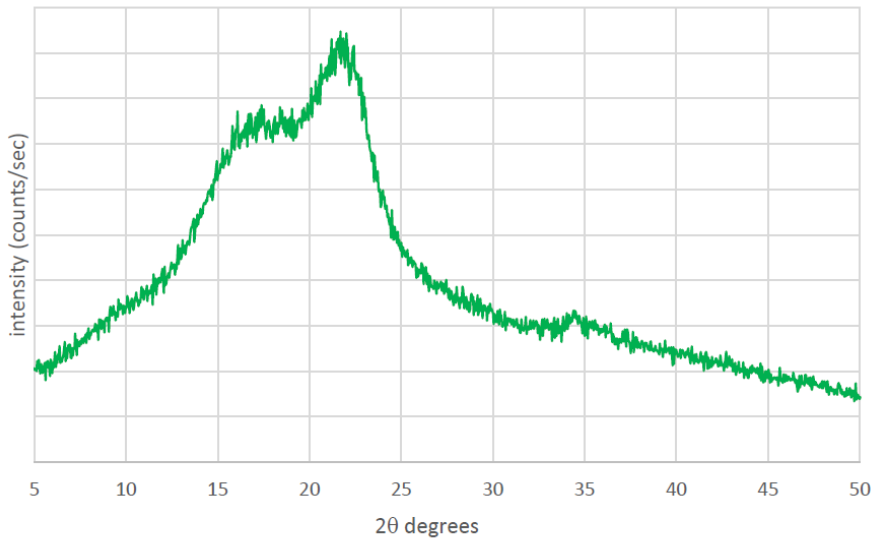

Figure 89. XRPD patterns of the asparagus stems

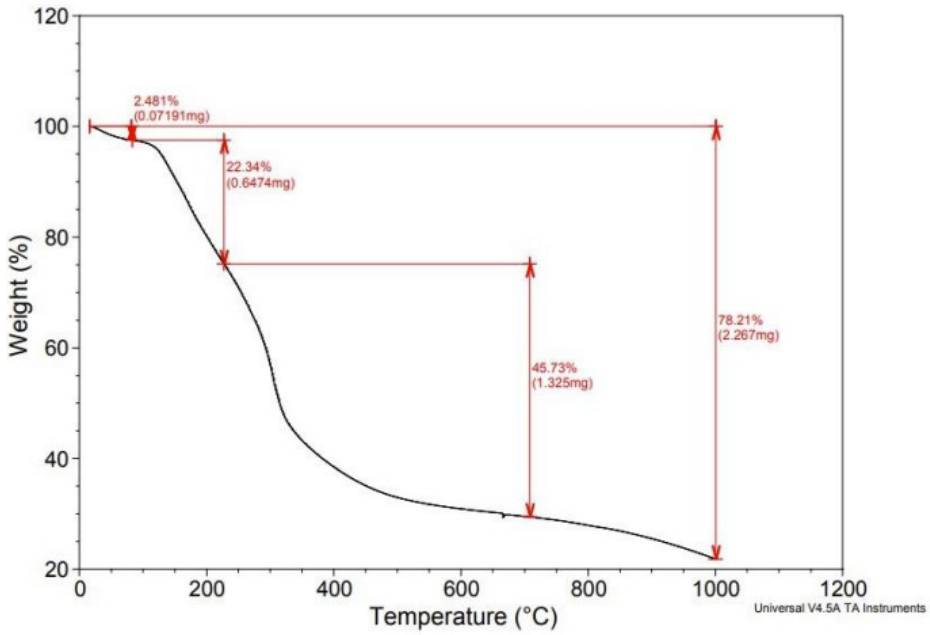

Figure 90. TGA curve of the asparagus stems

From the thermogram (Figure 90) it is possible to see that the sample had a total mass loss of 78.21%.

Around 100°C it is possible to visualize a variation in the slope, with a mass loss of 2.481%; this is attributable to the loss of water absorbed by the sample and other volatile substances.

In the temperature range between 150°C and 650°C, the sample lost a large part of its mass, in two stages of decomposition, one from 150°C up to 250°C and the other from 250°C up to 650°C.

Asparagus, like the other waste used, has a predominant component of cellulose, hemicellulose and lignin, and the variation in the slope of the line in the thermogram may be attributable to the various stages of decomposition of these substances, which occur at different temperatures based on their different composition.

However, it is possible to observe that beyond 600°C there are no longer significant mass losses, and this indicates that the residue contains substances that have sufficient thermal stability to resist temperatures equal to that value and up to the 1000°C investigated.

The temperature of 650°C was chosen as the pyrolysis temperature for the waste under consideration.

The pyrolyzed product was black in colour, very compact but easily grindable, and it was possible to observe that the pyrolysis reaction yield was around 30%, in line with the mass residue of the TGA analysis.

After pyrolysis, no bands were present in the FTIR spectra (Figure 91), attesting a good success of the decomposition of the organic compounds.

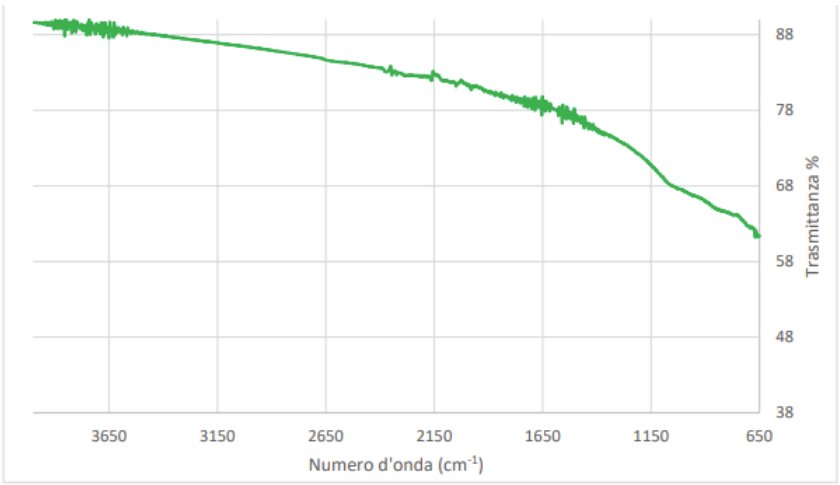

Figure 91. FTIR spectrum of the pyrolyzed asparagus stems

From the diffraction patterns (Figure 92) of the pyrolyzed sample it is possible to observe a peak falling at a diffraction angle of approximately 30°, one at approximately 31°, and another visible at diffraction angles of approximately 43°; all of these are attributable to graphitic carbon. The peak at 43° refers to the (100) plane of graphitic carbon (Deng et al., 2018). From the literature it is known that increasing the pyrolysis temperature leads to an increase in the intensity of the peaks and therefore an increase in the graphite structure of the carbon (Omar et al., 2021).

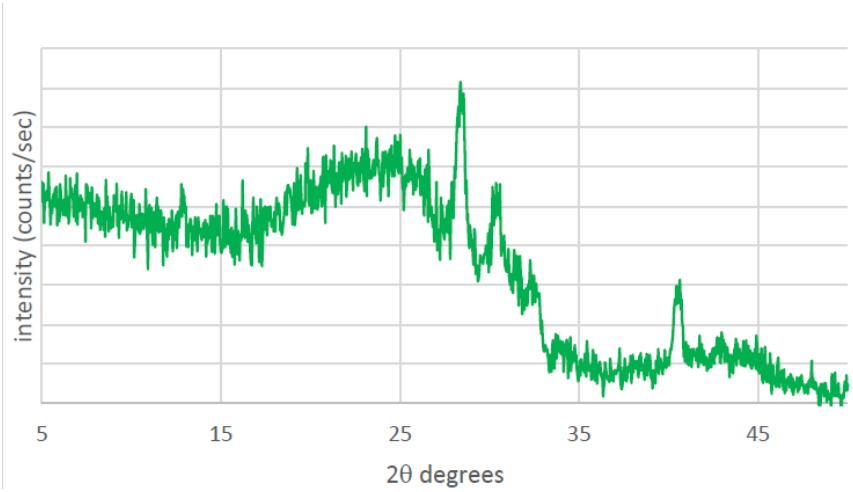

Figure 92. XRPD patterns of the pyrolyzed asparagus stems

The pyrolyzed sample was also subjected to thermo-gravimetric analysis, the thermogram can be observed in Figure 93, reported below.

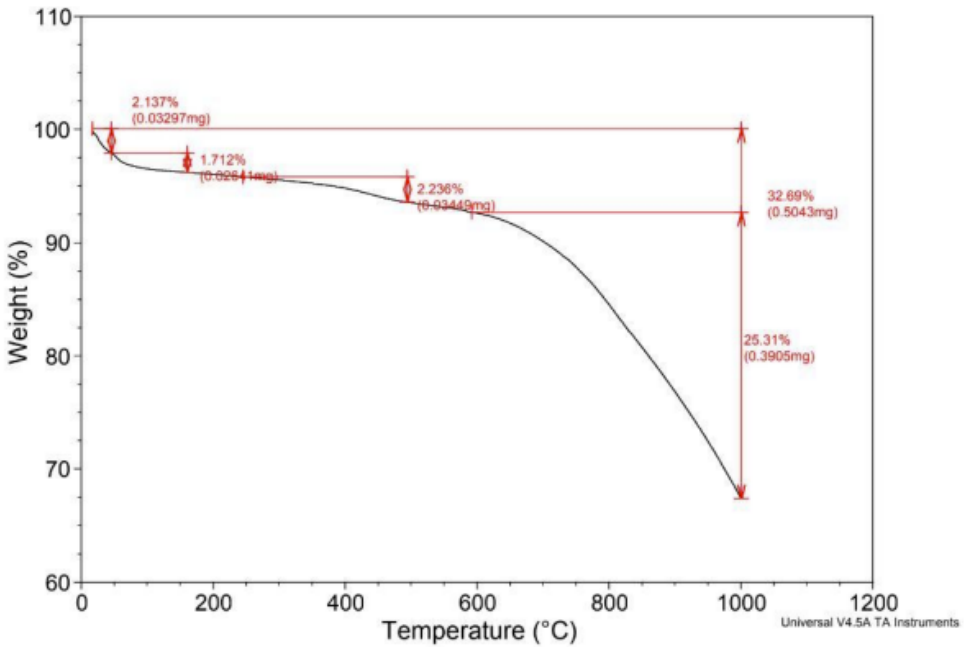

Figure 93. TGA analysis of the pyrolyzed asparagus stems.

A total mass loss of 32.69% is highlighted.

In the first part of the graph, around 100°C it is possible to observe a mass loss of 2.137%, attributable to the loss of humidity absorbed by the pyrolyzed sample. Up to approximately 650°C, no significant mass losses were found, which means that the pyrolysis process

eliminated all substances unstable at those temperatures; further confirmation comes from the IR spectrum, in which there are no peaks of characteristic functional groups.

In the part of the graph between 650°C and 1000°C the greatest mass loss is observed (25.31%); this is attributable to further decomposition of the material at temperatures higher than those of pyrolysis.

In the SEM images of non-pyrolyzed asparagus (Figure 94a), it is possible to observe its fibrous parts, with different shapes and geometries. The images of asparagus after pyrolysis (Figure 94b) highlight the effect of temperature on the structure, in fact the fibers appear to be damaged and the pores open and larger in size.

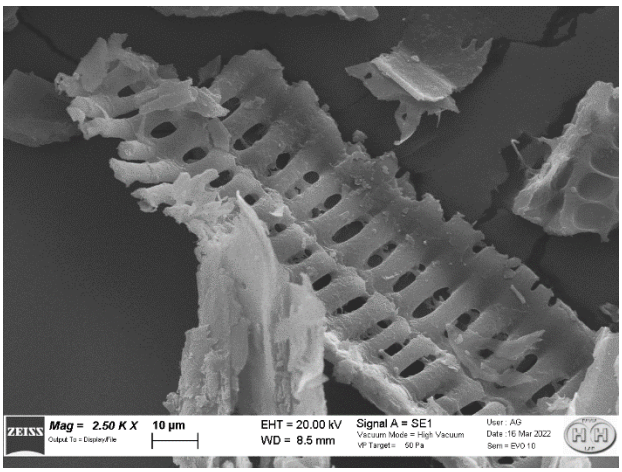

(a)

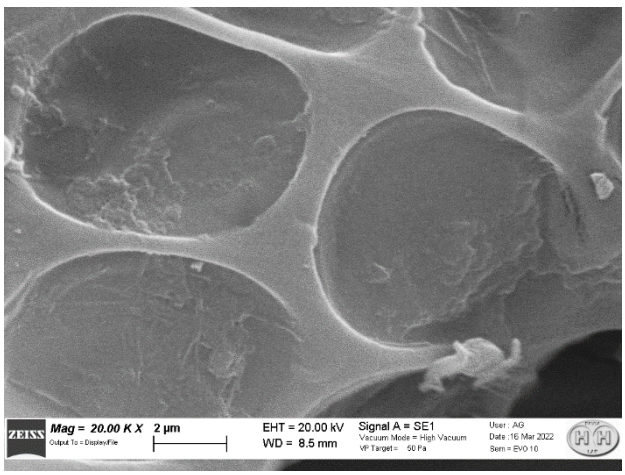

(b)

Figure 94. SEM images of the asparagus stems non-pyrolyzed (a) and pyrolyzed (b)

The images of asparagus after activation (Figure 95) highlight the effect of temperature and KOH on the structure, in fact the fibers appear to be damaged and the pores more numerous and with different size, from micro to macro.

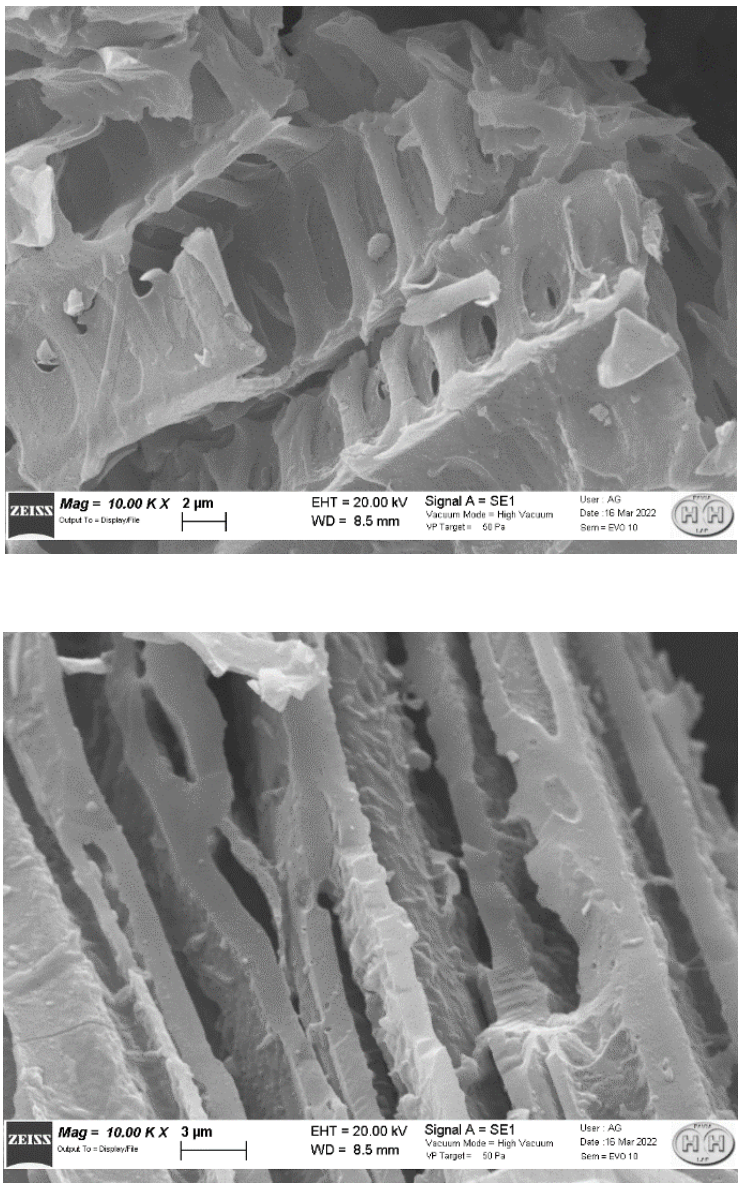

Figure 95. SEM images of the activated asparagus stems

An EDX analysis was conducted on the 6:1 activated asparagus sample to see the composition of the sample; the results are reported in the Figure 96.

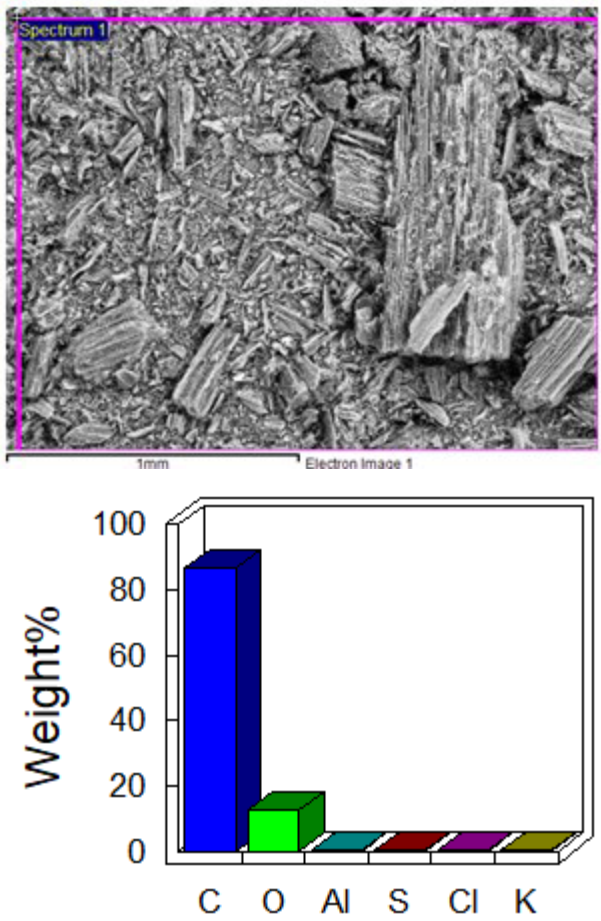

Figure 96. SEM and EDX characterization of the activated asparagus stems

From the histogram it is possible to observe that carbon is the most abundant element in activated biochar, with a weight % of approximately 85%, followed by oxygen with a weight % of approximately 20%. Al and S are probably present in the waste while K and Cl could be also due to the activation and washing procedure.

Considering PCT analysis (Figure 97), the activated sample shows a maximum hydrogen absorption of 3.9% at 20 bar and -196°C, therefore a very promising result in terms of quantity.

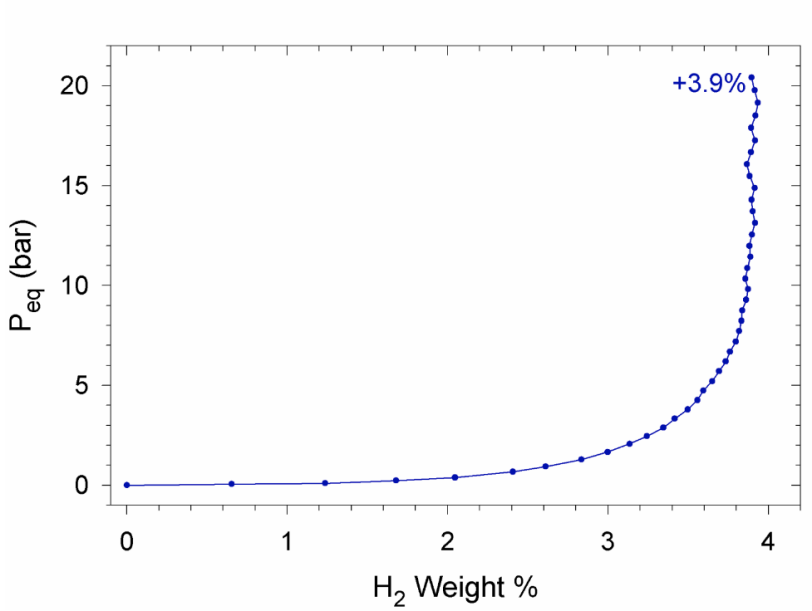

Figure 97. PCT of the activated asparagus stems.

The desorption curve shows reversibility of the process in the first cycle (Figure 98). 1.5 min is enough for full desorption, pointing for a very good kinetics.

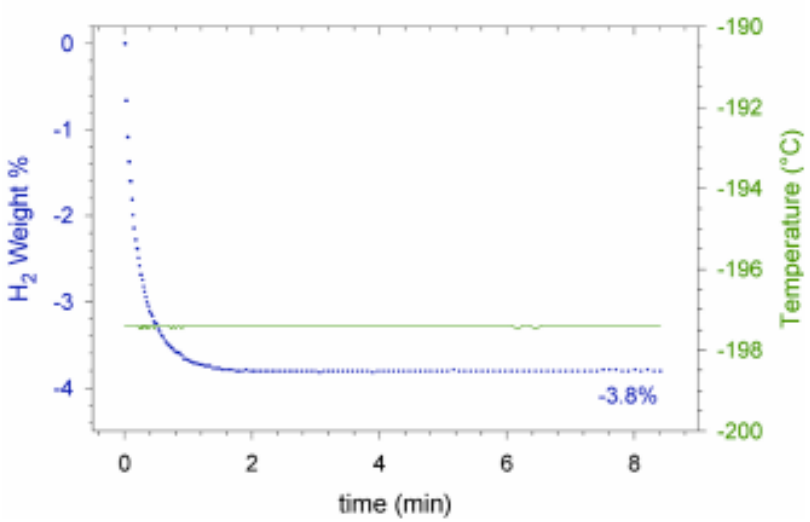

Figure 98. Desorption curve in kinetic mode for the activated asparagus stems.

Adsorption in the second cycle takes place in kinetics mode in 35 sec and shows almost full reversibility (the high pressure manometer used for evaluating adsorption is less sensitive and precise with respect to the low pressure manometer used in desorption) (Figure 99).

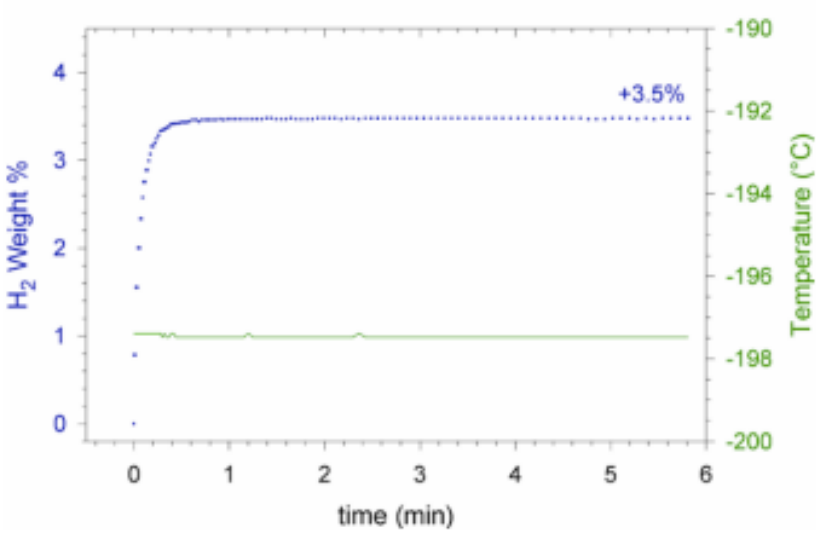

Figure 99. adsorption curve in kinetic mode for the activated asparagus stems

4.16 Corn cob biochar

The IR spectrum (Figure 100) of dried corn shows different peaks at different wave numbers, attributable to the functional groups present.

It is possible to find analogies with the IR spectrum of dried asparagus, although they are two plants belonging to different species. This is due to the fact that the treated parts of both plants, belonging to portions of non-edible plants, have a variable abundance of biopolymers, such as cellulose, hemicellulose and lignin aimed at giving specific physical properties to the plant. Effectively, these biopolymers are often used by nature to generate support structures, giving the plant a hard and resistant stem. It is possible to observe at 3309.73 cm^{-1} a broad peak belonging to the class of vibrations of the OH groups, and at 2919.22 cm^{-1} another peak belonging to the CH stretching of the methyl and methylene groups. At 1026.43 cm^{-1} there is an absorption peak relating to the OH stretching of the alcohol and carboxyl groups.

The XRPD patterns (Figure 101) is characteristic of an amorphous material, as evident from the two large bands present, centred at 16° and 21° (as graphitic C).

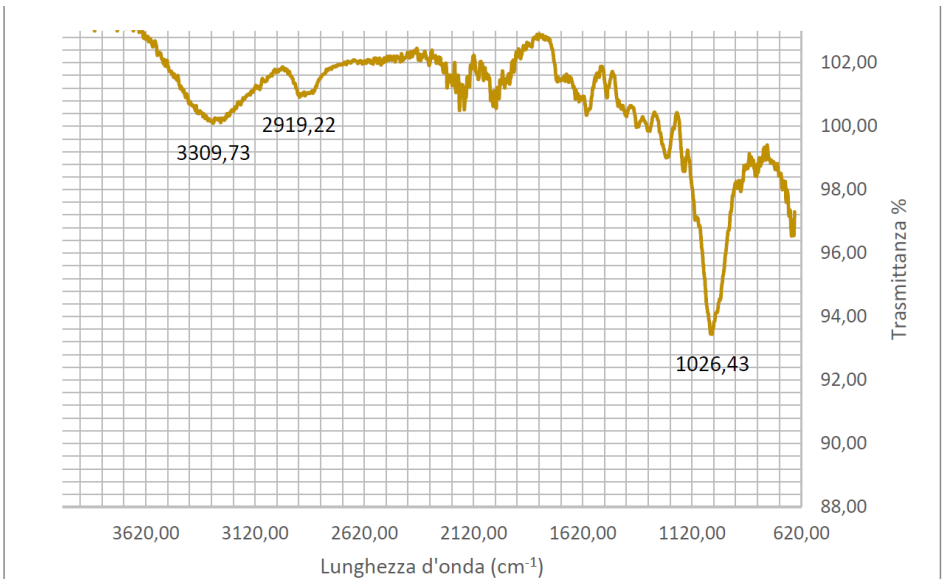

Figure 100. IR spectrum of the raw corn cob

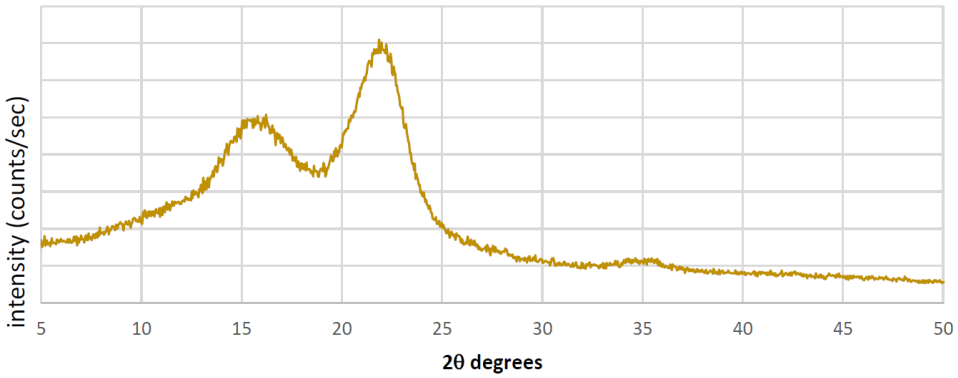

Figure 101. XRPD patterns of the raw corn cob

Concerning TGA analysis illustrated in Figure 102, the total mass loss for the corn sample was 87.05%. In the first area of the graph, a mass loss of 3.39% can be observed, attributable to the loss of adsorbed water.

In the second part of the graph, in a temperature range between 250°C and 650°C, a second important phenomenon of mass loss is observed, attributable to the decomposition of the corn; beyond 650°C, no further phenomena are appreciated of decomposition.

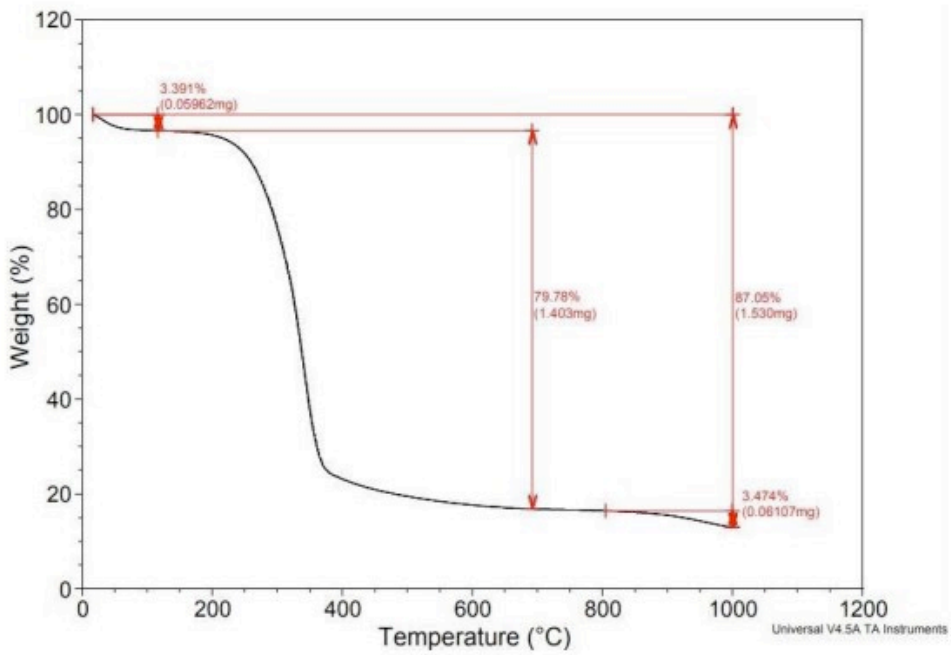

Figure 102. TGA curves for corn cob

Also in this case, the pyrolysis step was set according to the results obtained by TGA, setting a heating of 10 °C/min from room temperature up to 650°C, and maintaining an isotherm of 8 hours.

Once the sample was characterized in its dried form, it was possible to move on to the pyrolysis step, obtaining a product where the lowest density was found among all the samples investigated.

The yields of the pyrolyzed product were around 20-25%, completely in line with the result obtained by thermogravimetric analysis.

Below are reported the results of pyrolyzed corn biochar, obtained by IR (Figure 103) and XRD spectroscopy (Figure 104):

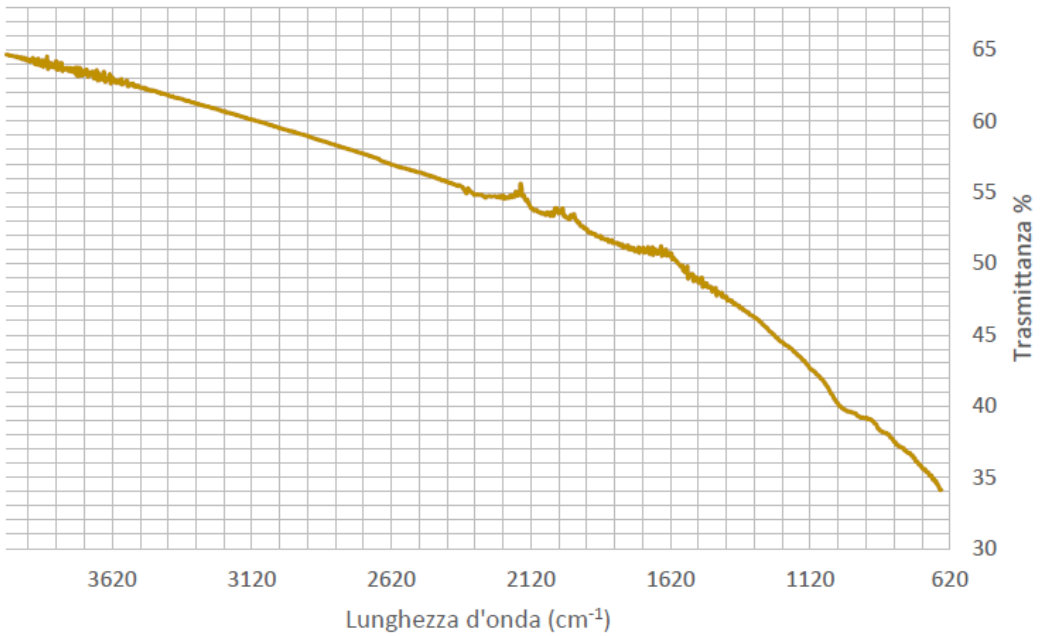

Figure 103. IR spectrum of the pyrolyzed corn cob

The IR spectrum shows an absence of the different functional groups, previously observable in the spectrum of the dried sample, which confirms the correct pyrolysis treatment.

The diffraction patterns of the pyrolyzed product present a peak with very low resolution between 20° and 25°, which could be attributable to graphitic carbon. However, it remains very difficult to interpret a diffraction pattern that appear in this way; therefore, this product can be considered as an amorphous compound. The pyrolyzed sample was subsequently activated, always following a chemical activation with KOH (in a 6:1 ratio), exploiting a solid state reaction in an oven and a nitrogen atmosphere.

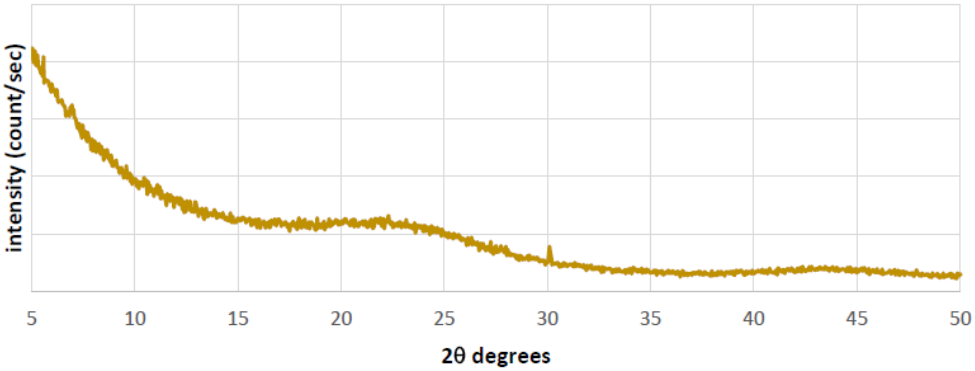

Figure 104. XRPD patterns of the pyrolyzed corn cob

The activated biochar was then treated with HCl for washing and dried in an oven.

From the histogram graph obtained through microanalysis, it is possible to observe that in the raw corn sample, there is an abundance of carbon and oxygen (Figure 105).

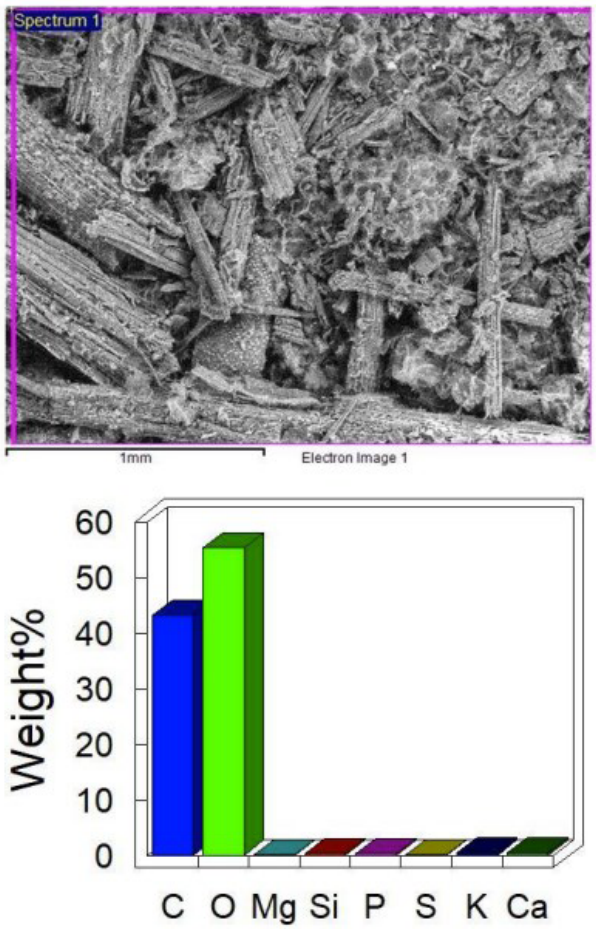

Figure 105. SEM image of the corn sample as it is and histogram obtained by microanalysis relating to the % abundance of the different elements contained in the corn sample as it is.

In the microanalysis conducted on the activated sample (Figure 106), it is possible to observe how the quantity of oxygen has significantly decreased compared to the raw sample. This is in agreement with the pyrolysis and activation processes, which favour the elimination of the different functional groups, leaving only a compound consisting almost exclusively from carbon atoms in inorganic form.

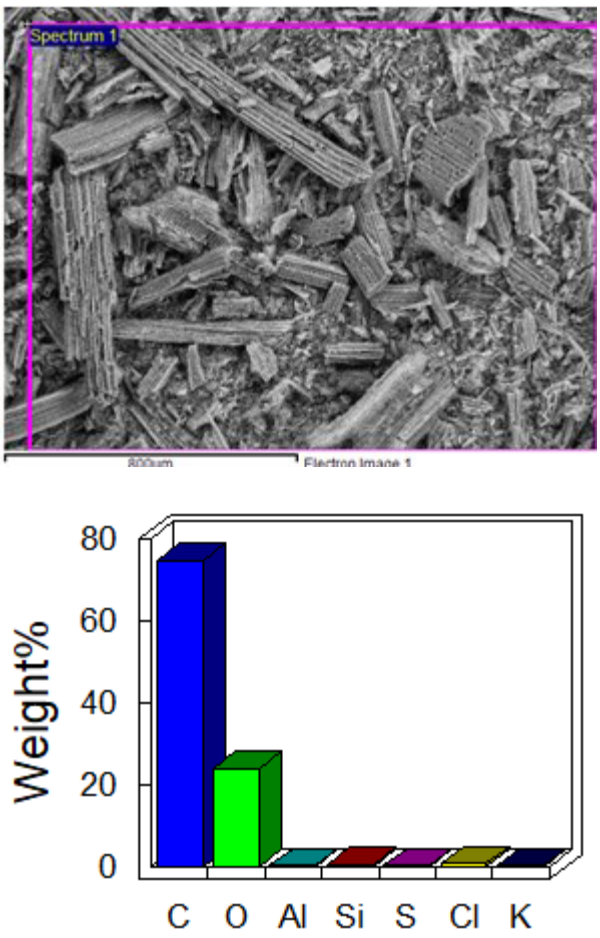

Figure 106. SEM image of the activated corn cob sample and histogram obtained by microanalysis relating to the % abundance of the different elements contained in the activated corn cob sample.

In the activated sample a maximum hydrogen adsorption of 2.7% at 77 K was observed in the PCT measurements (Figure 107). This value was confirmed in the kinetic desorption and adsorption analysis of the subsequent 5 cycles at 77 K (Figure 108). Adsorption takes place in around 30 sec and desorption in 1 min, very promising values for storage.

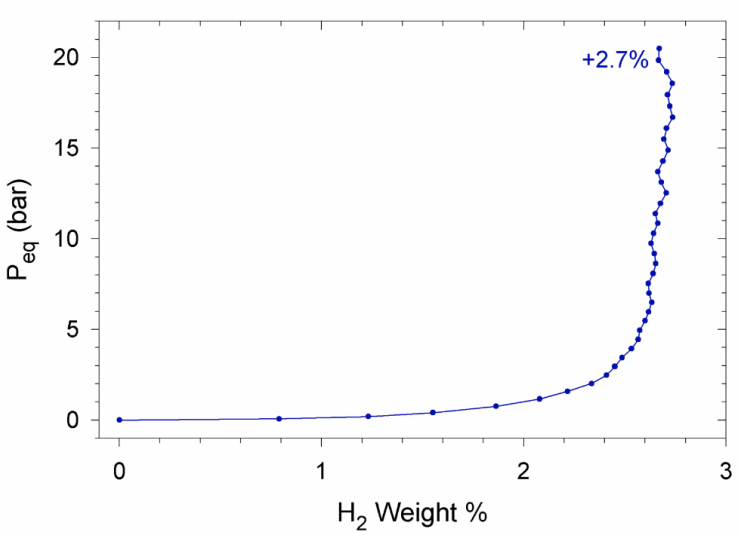

Figure 107. PCT curve of corn biochar activated with 6:1 KOH

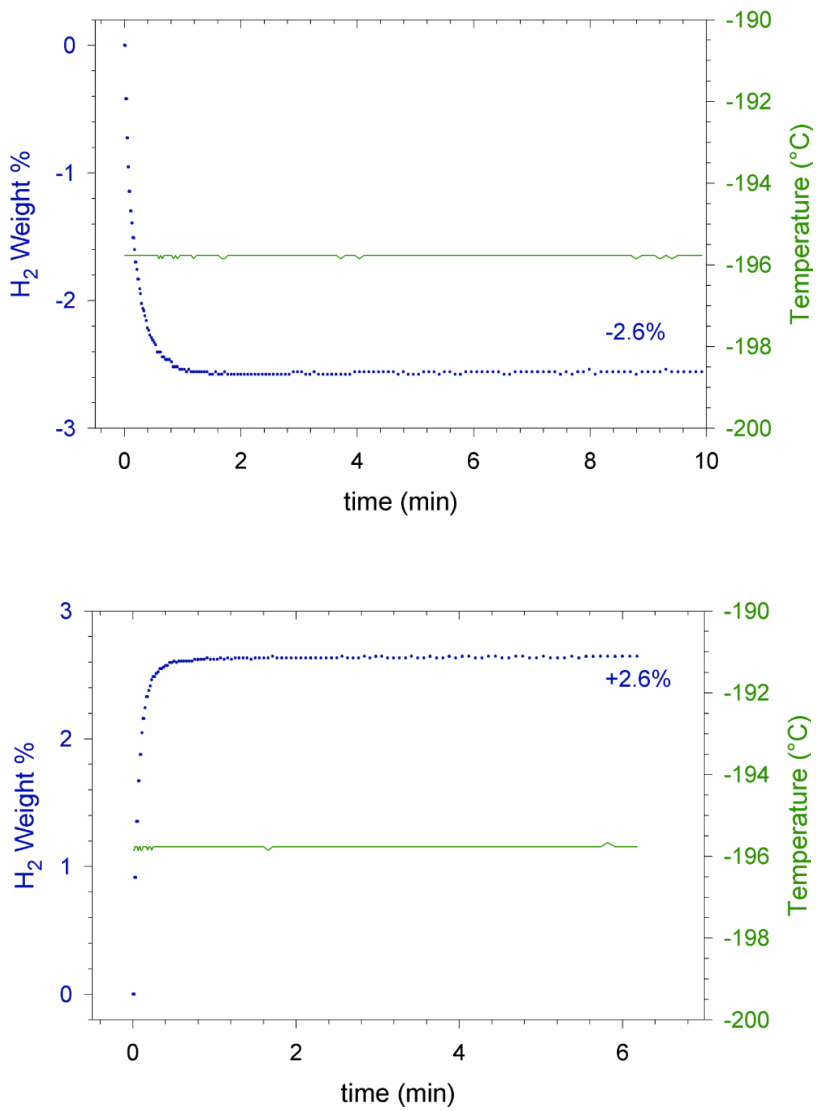

Figure 108. Kinetic curve of corn biochar activated with 6:1 KOH

4.17 Pumpkin peel biochar

The peel sample was freeze-dried to ensure better preservation and avoid the formation of mould, it was stored in the refrigerator at a temperature of 4°C and subsequently characterized and pyrolyzed, skipping the drying and grinding stage.

The IR, XRD and TGA analyses of the freeze-dried pumpkin peel are reported below.

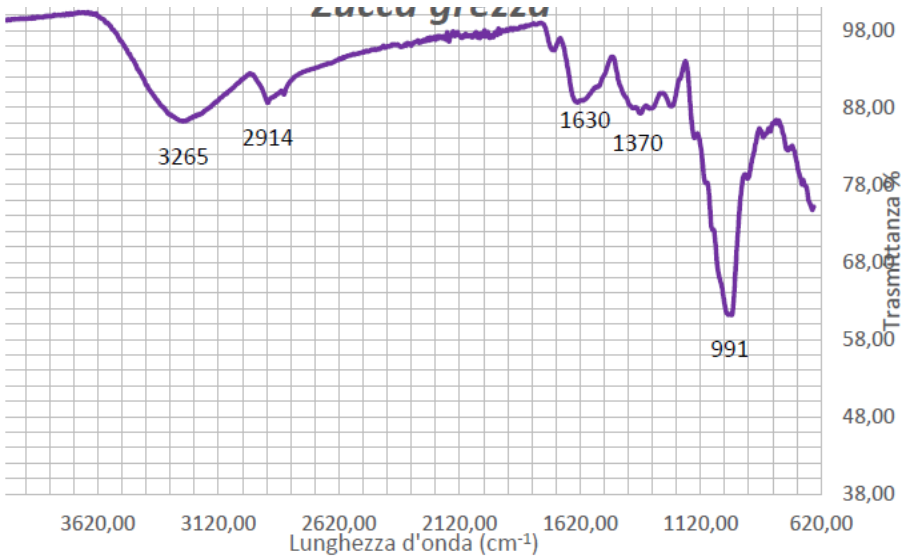

Figure 109. IR spectrum of the pumpkin peels

From the IR spectrum (Figure 109) of the freeze-dried sample there are many bands that fall at different wave numbers, this is in line with all the other samples in raw or freeze-dried form, confirming the presence of different functional groups belonging to the complex molecular structure of the vegetable.

It is possible to observe a peak at 3265 cm^{-1}, due to the vibration of OH and the stretching of the N-H group. At 2914 cm^{-1}, C-H stretching is visible. At 1630 cm^{-1} it is also possible to observe the stretching of the C=N groups. The band at 991 cm^{-1} confirms the presence of alcohol groups, as it is characteristic of C-OH stretching.

The diffraction patterns (Figure 110) confirm that the material is amorphous.

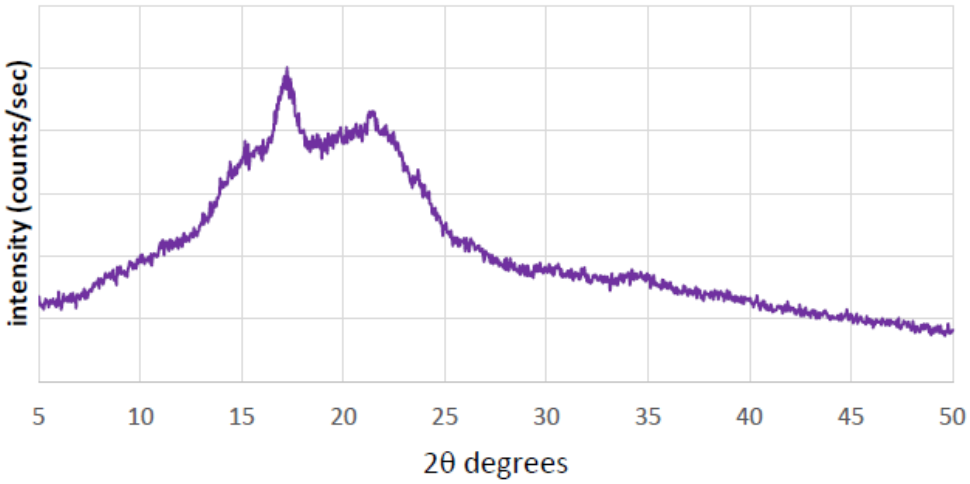

Figure 110. XRPD patterns of the pumpkin peels

The thermogram reported was obtained by setting the same setup as the other wastes. It is observable in the first part of the graph, in the temperature zone around 100-150 °C, a mass loss of 7.005% attributable to the evaporation of water and volatile substances. In this case there is an important amount of water loss probably since the freeze-dried sample has absorbed more humidity in the refrigerator.

In the pumpkin decomposition curve (Figure 111), two different processes are observable, one in a temperature range between 200-300°C, and one that reaches up to 650 °C; this can be explained by the fact that the vegetable has a complex molecular structure, with a large variety of chemical compounds, which have different thermostability.

As with any waste, beyond 650°C there are no longer appreciable mass losses, consequently the pyrolysis setup set for the oven was the same for each sample.

The total mass loss of the pumpkin sample is 81.37%.

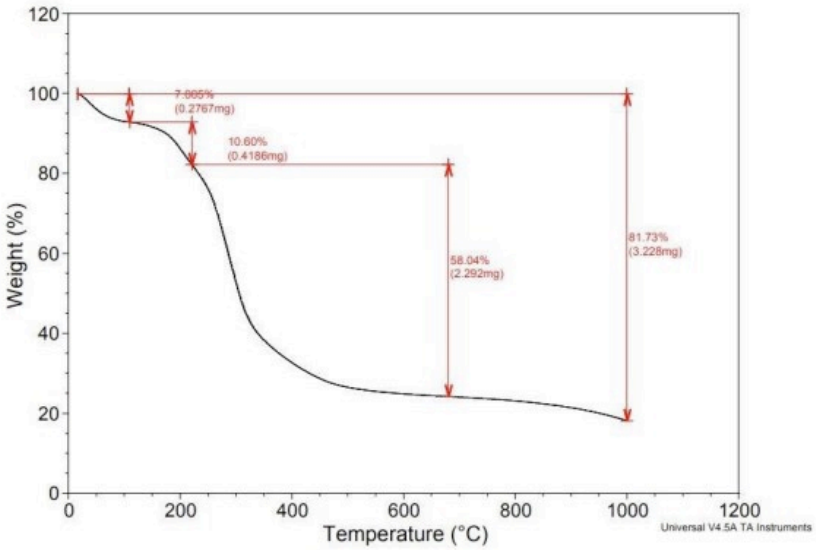

Figure 111. TGA curve for the pumpkin peels

The IR spectrum of the activated sample does not present any peak, as reported in Figure 112; this confirms that the activation process and subsequent washing were carried out without leaving impurities on the inorganic C skeleton.

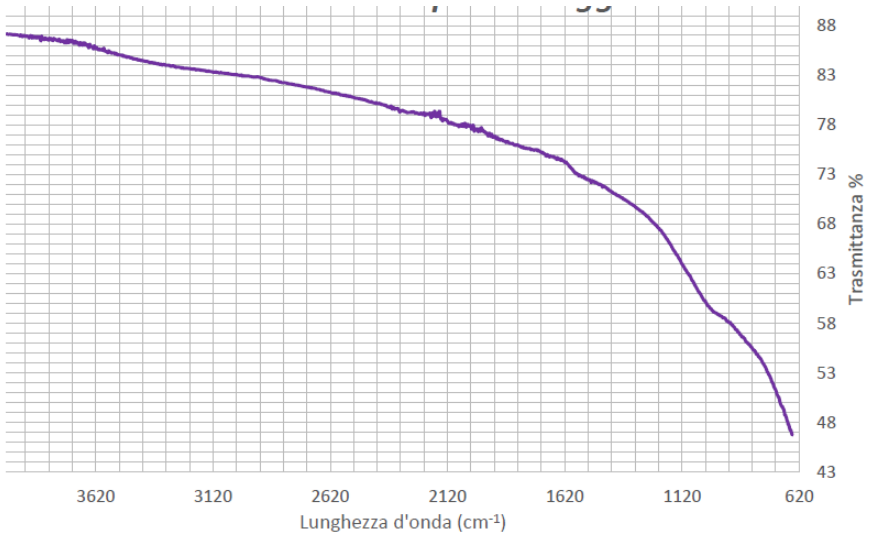

Figure 112. FTIR spectrum for the activated pumpkin peels

The diffraction patterns (Figure 113) does not show the presence of any peak, so it is plausible to consider the activated product as amorphous; at low scattering angles, it is possible to observe a shoulder trend; this identifies a high porosity of the material.

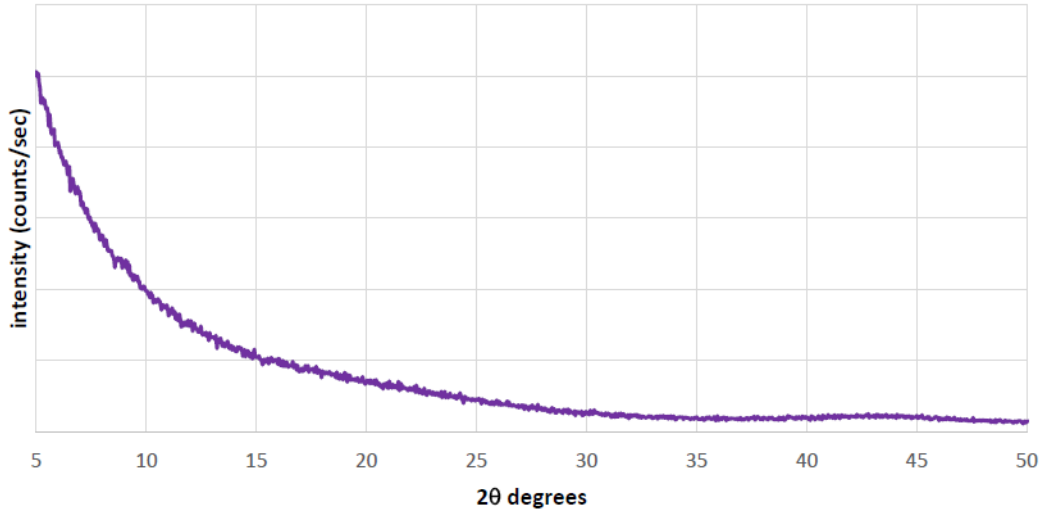

Figure 113. XRPD patterns for the activated pumpkin peels

From the PCT curve (Figure 114), it is possible to observe that the activated material gave a maximum absorption of 2.9% of hydrogen at a pressure of 20 bar and 77K. The subsequent cycles, realized in kinetic mode, confirm this trend (Figure 115a and b). Adsorption takes place in 1 min and desorption in around 2 min, attesting again the very good kinetic performance of the activated C obtained from organic wastes.

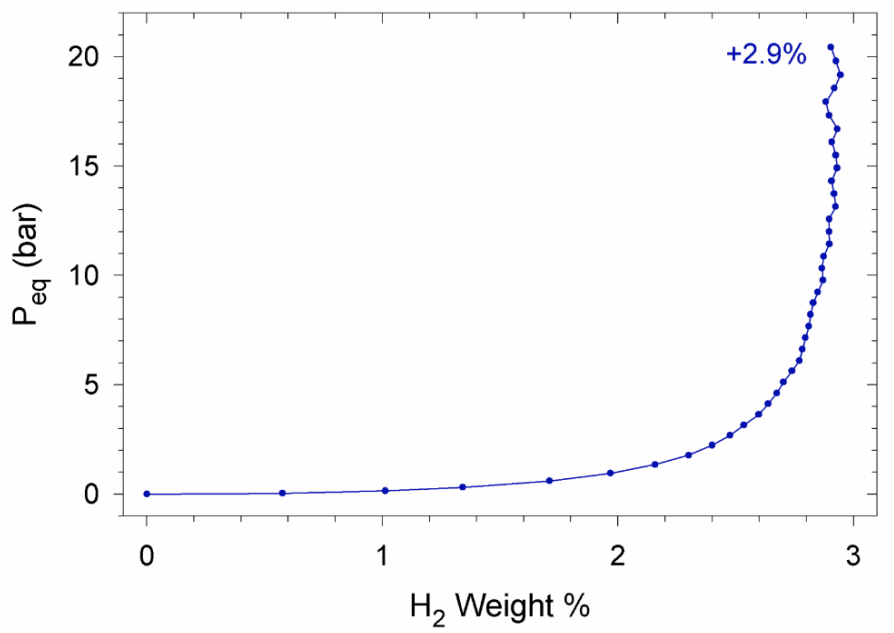

Figure 114. PCT for the activated pumpkin peels.

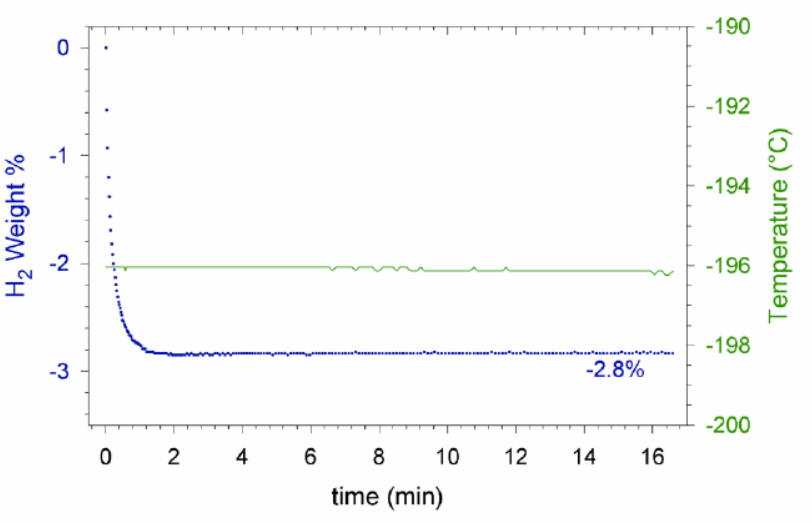

(a)

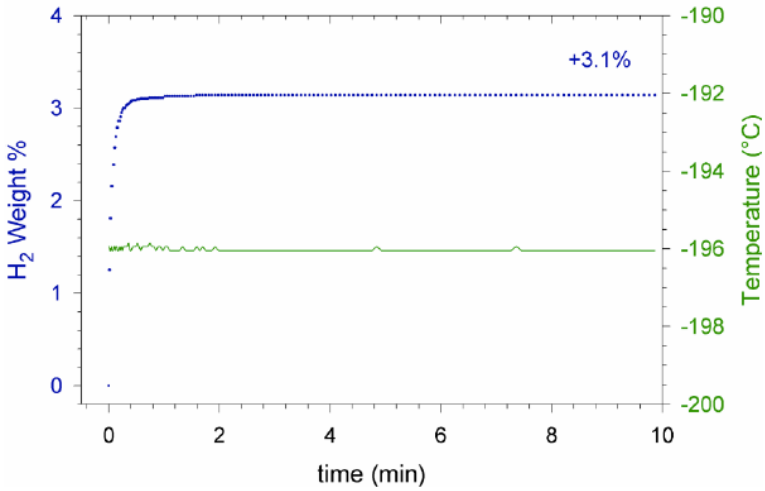

(b)

Figure 115. Kinetics curve for the activated pumpkin peels: desorption (a) and absorption (b) curves

4.18 Wheat processing by-products biochar

The wheat waste was washed with distilled water, dried in oven at 45°C overnight, milled with an electric miller for 2 min to reduce the macroscopic size and finally submitted to the physic-chemical characterization. The TGA of wheat as such presents a first stage of mass loss at 100 °C, due to the release of water absorbed, of 7.565% (Figure 116). The latter is followed by a stage of decomposition of the organic substances present between 220°C and 450°C; finally, at 500°C the mass of the sample remains constant. The total mass loss of grain waste as such is 87.55%. Also for this waste, the temperature of 650°C was chosen for the pyrolysis.

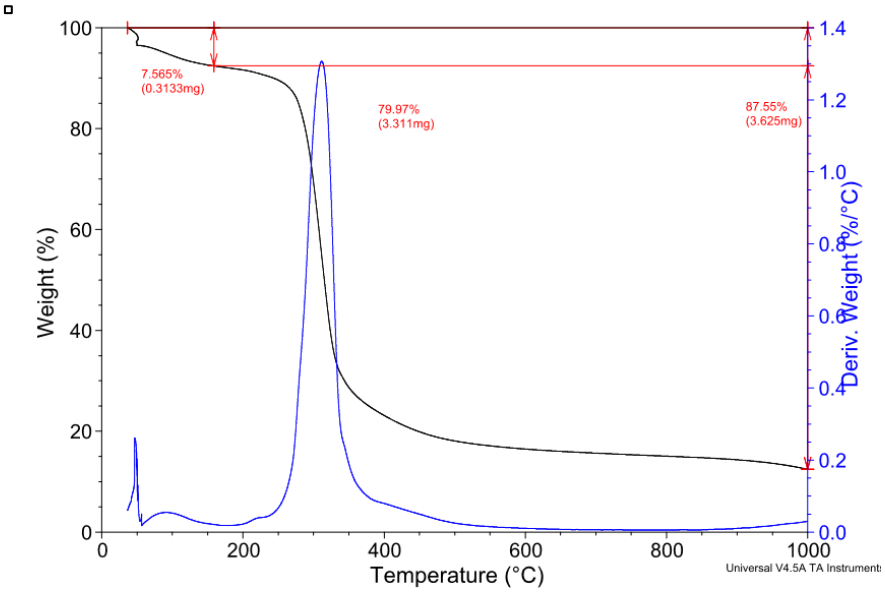

Figure 116. TGA for the dried and milled wheat waste

The IR spectrum of the grain as such is characterized by the presence of numerous peaks (Figure 117), indicators of the complexity of the structure of the material. Even in the latter case the presence of water, alcohols and aromatic organic compounds is predominant. The bands disappear after activation (Figure 118), proving the good action of the thermal and chemical treatment in obtaining an inorganic material.

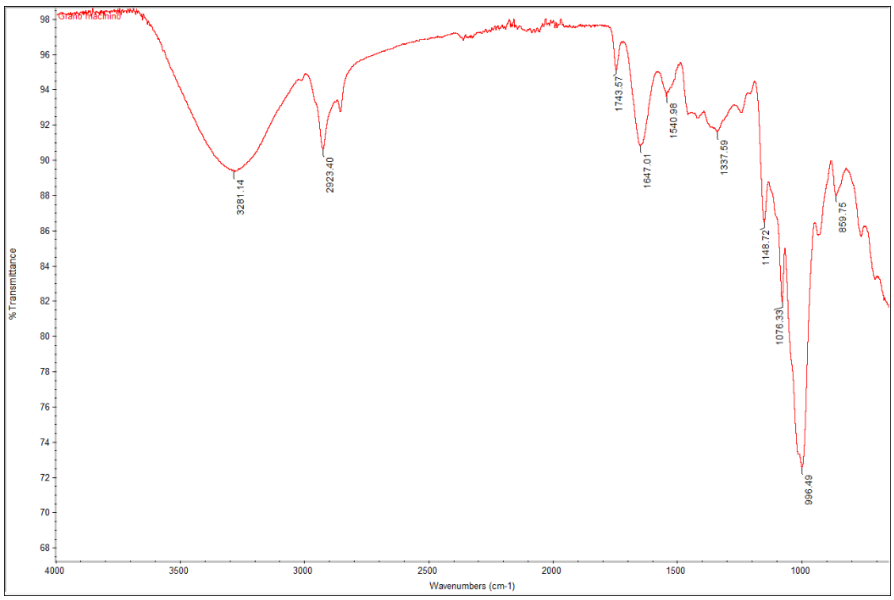

Figure 117. FTIR spectrum for the dried and milled wheat waste.

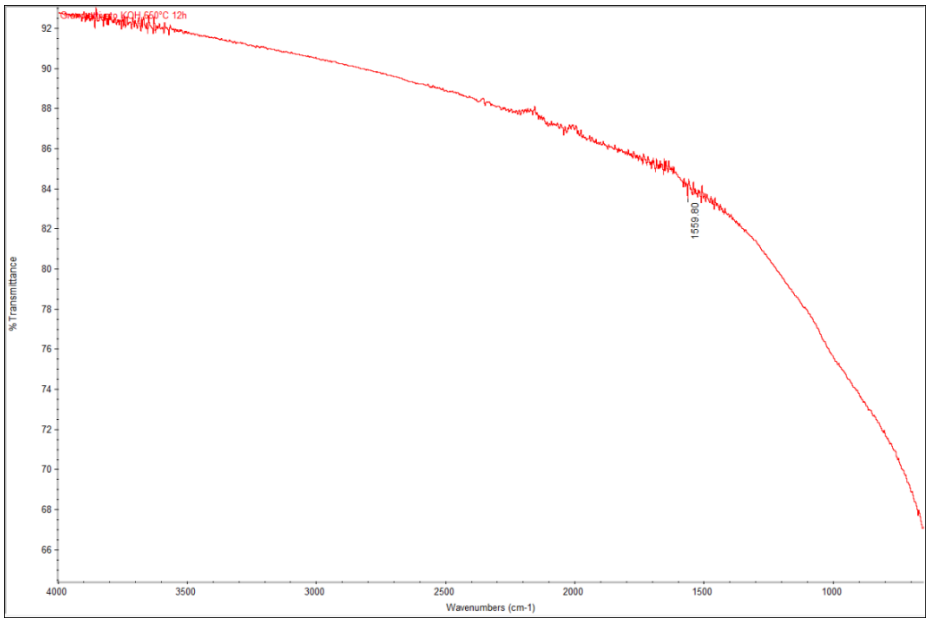

Figure 118. FTIR spectrum for the activated wheat waste.

The dried and milled sample gives an XRPD patterns characteristic of an amorphous material (Figure 119).

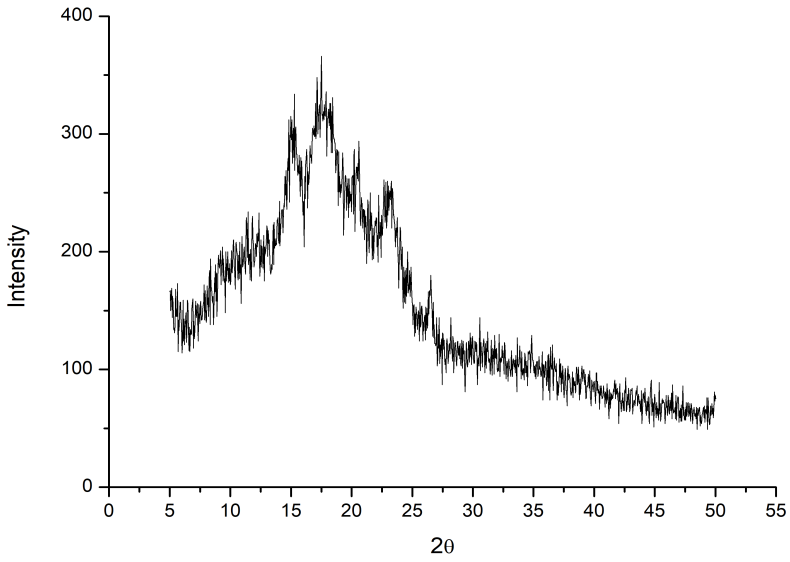

Figure 119. XRPD patterns for the dried and milled wheat waste.

The same applies for the activated sample (Figure 120), where a peak characteristic of the graphitic C at 26° is evident on the large halo.

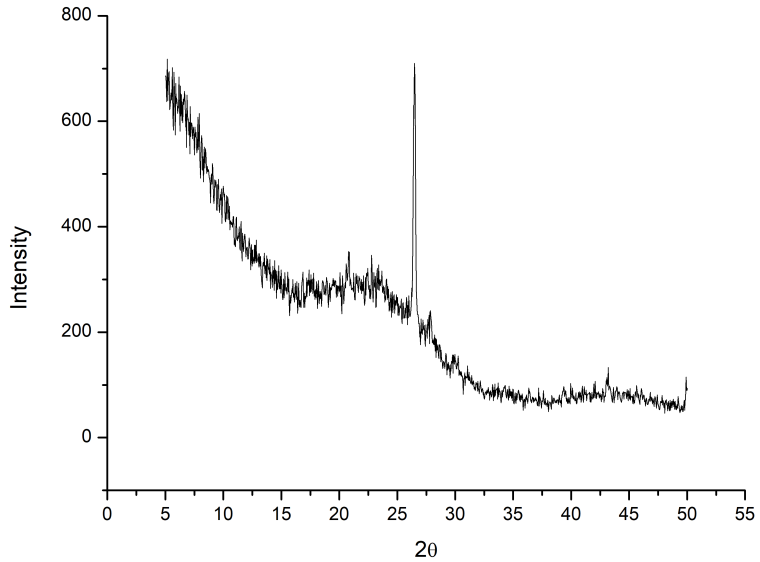

Figure 120. XRPD patterns for the activated wheat waste.

The images obtained from the SEM analysis for the grain as such (Figure 121) show irregularly shaped splinters of approximately 100 µm and made up of small particles of approximately 10

μm in size. They appear as bubbles or swellings on the surface, which create cavities underneath.

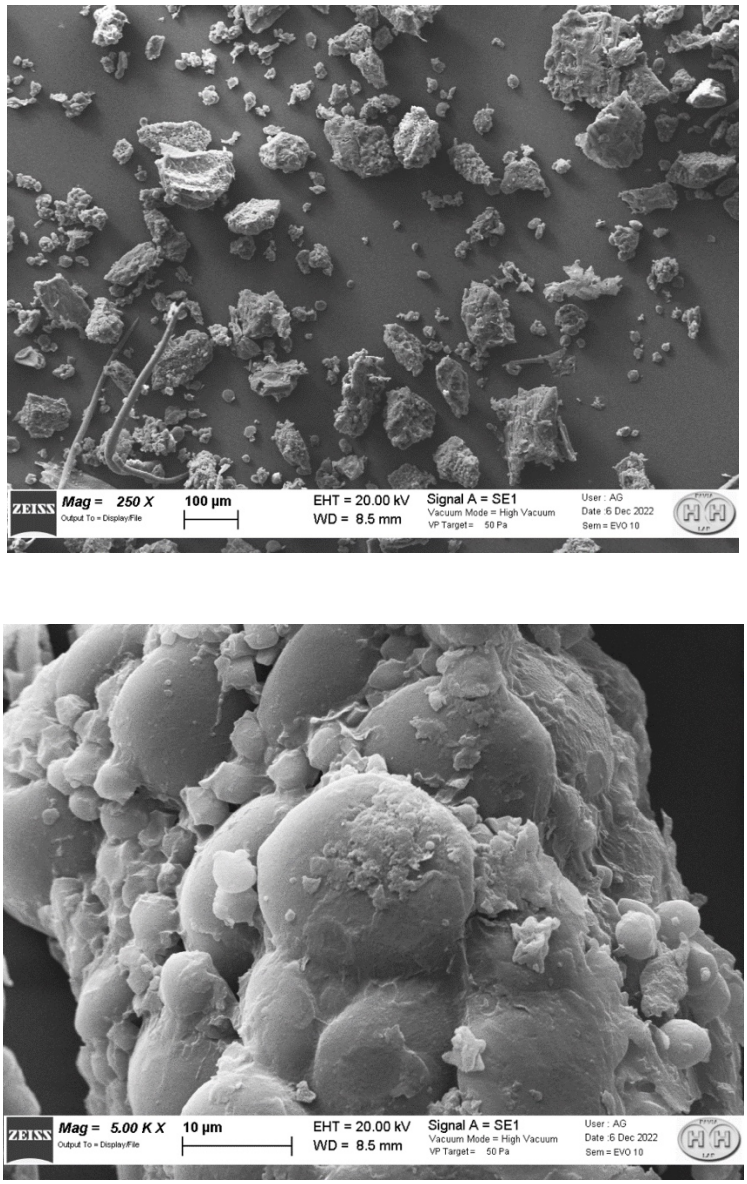

Figure 121. SEM images for the dried and milled wheat waste

After activation, the grain size decreases and some cavities are evident on the particles' surfaces (Figure 122).

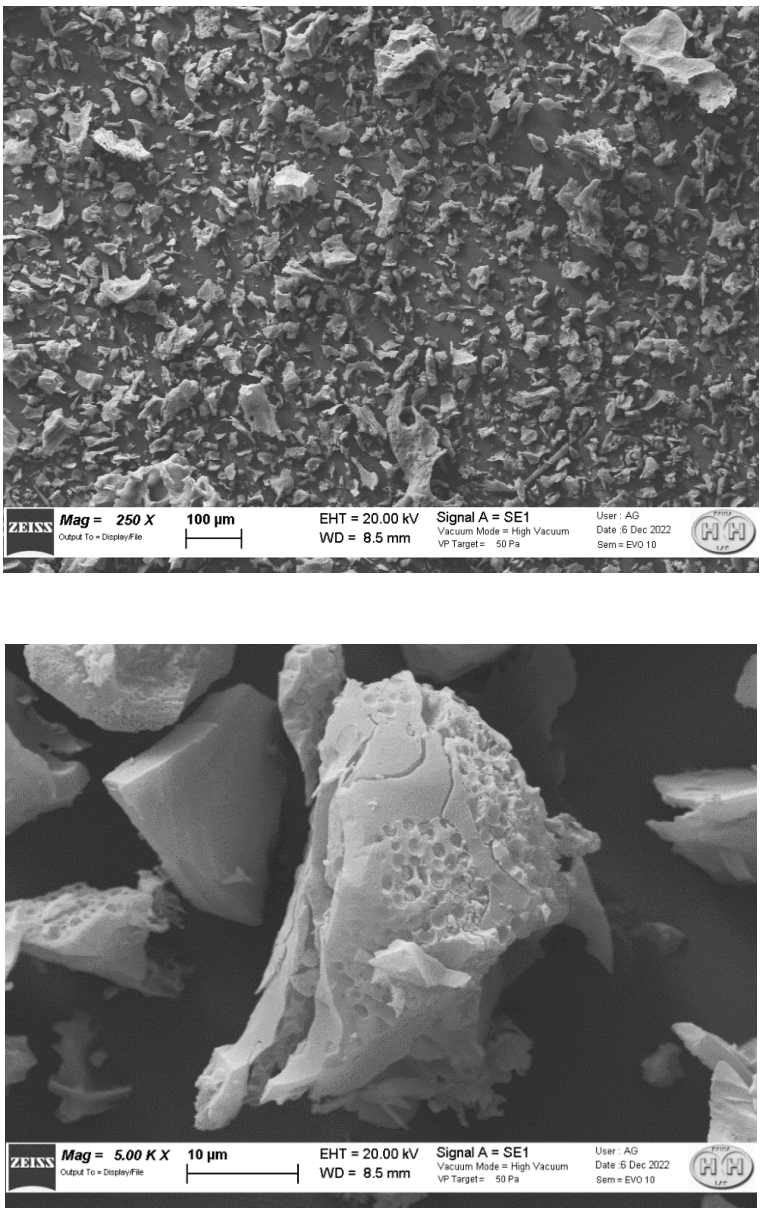

Figure 122. SEM images for the activated wheat waste.

Considering PCT analysis (Figure 123), the KOH 6:1 activated wheat sample showed a gravimetric reversible storage capacity of 2.6%. Full desorption takes place in 2 min (Figure 124).

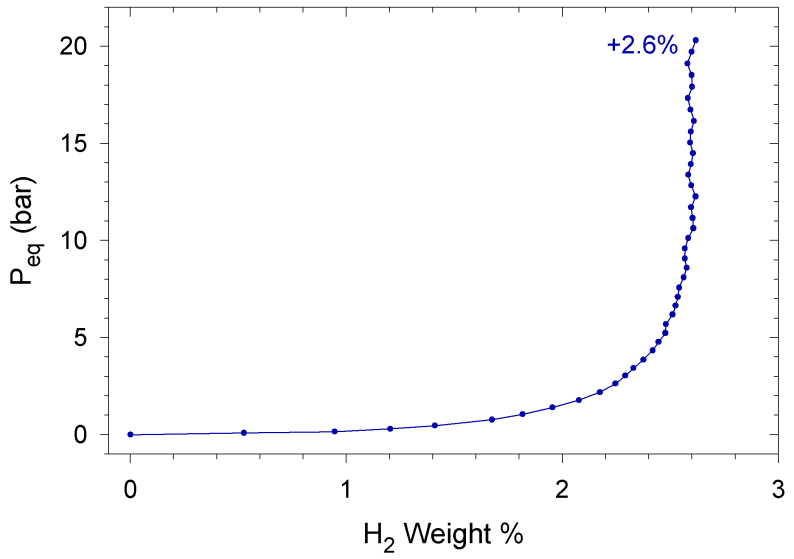

Figure 123. PCT for the activated wheat waste

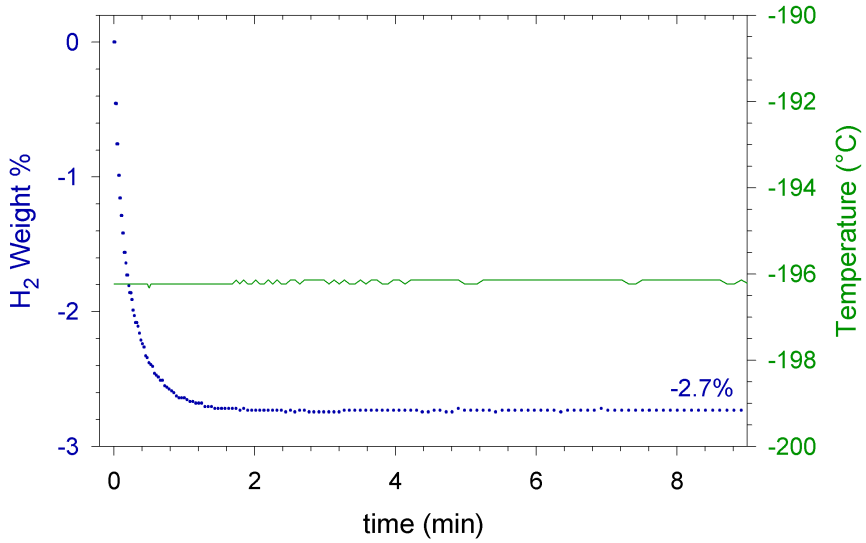

Figure 124. desorption curve for the activated wheat waste

4.19 Overview of the AFW biochar investigated.

The biochars obtained from the studied AFW resulted to be cheap and sustainable materials for stationary storage. Table 76 reports a summary of the main features of the biochar obtained from each AFW studied.

Table 76. Comparison between the main features of the biochar obtained from the AFW studied.

Absorption features	CORN CON	RICE BRAN	MELON PEEL	PUMPKIN PEEL	ASPARAGUS STEMS	WHEAT WASTE
Surface area (m2/g)	1220	1820	2600	1250	1750	1200
H_2 gravimetric capacity (%)	+2.7	+3.5	+4.1	+2.9	+3.9	+2.6
Adsorption rate (sec)	30	35	20	30	35	30
Desorption rate (s)	60	60	60	100	60	120

In general, the results obtained in term of gravimetric capacity and sorption kinetics are very promising, also considering the data reported in literature for graphitic C based materials (Figure 125) (Züttel, A., 2003; Nijkamp, M.G. et al., 2001). These latter have a linear H_2 adsorption trend in relation to their surface area (Figure 125). The maximum adsorption capacity measured for nanostructured graphitic carbon-based material was 2% mass (at 77K), for a surface area of 1315 m^2/g. Our ACs derived by waste display an ability to adsorb H_2 proportionated to their specific surface area too. In Figure 126 it can be noted that they show a capacity to adsorb hydrogen 1.8-2 times higher than the graphitic materials. This is enough to make them competitive for scientific research.

Among all, the biochar obtained from melon peel resulted to have a surface area of 2600 m^2/g and an ability to adsorb a huge amount of hydrogen (4.1% at 77K), with very fast kinetics to (less than 1 min).

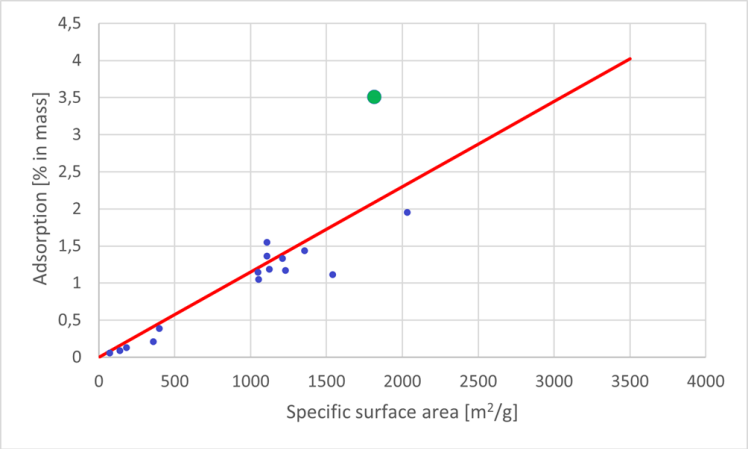

Figure 125. Plot of the hydrogen adsorbed by traditional graphene-based materials (blue spots), in relation to their specific surface area. They have a linear trend represented by the red line is evident.

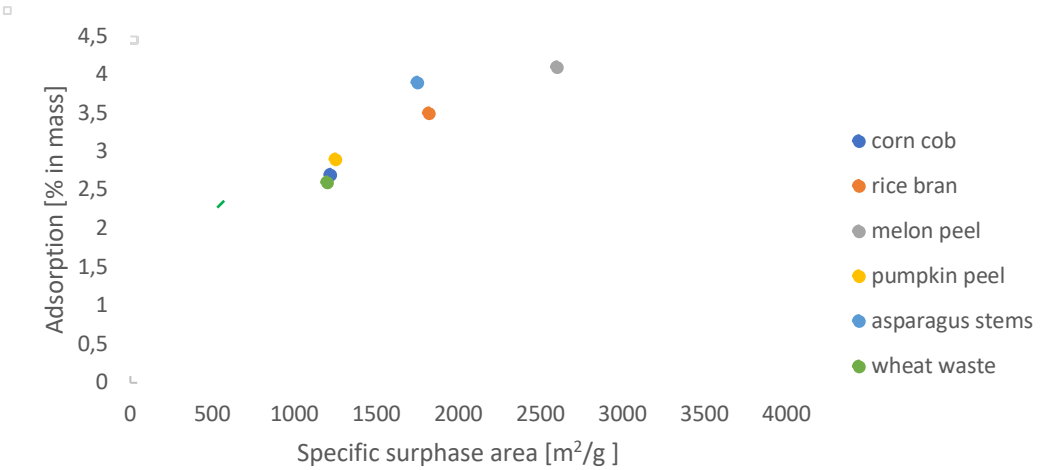

Figure 126. Plot of the hydrogen adsorption of our ACs derived by waste in relation to their specific surface area. Le linear trend is represented by the green line.

5. CONCLUSIONS

The research conducted during my PhD supported the idea that agri-food waste can be an effective sustainable source of new raw materials. In fact, considering food topic, we demonstrated that the extracts obtained from the different investigated AFW contained valuable bioactive compounds, as resulted by *in vitro* evidence of antioxidant and/or antiglycative activities at different level of the protein glycation reaction. CBE-2 and RHE-2 had the best antiglycative and antioxidant activities, while ABE-2 and WPE-2 were effective only in trapping some intermediates of glycation reaction, especially MGO. Further studies on their composition could be useful to identify trapping agents.

RHE-2 was the extract which globally exhibited the highest bioactivity, due to its composition. Different flavonoids, hydroxycinnamic and hydroxybenzoic acids were identified by LC-MS/MS, compounds well-known for their health benefits.

Thus, we decided to study a preliminary formulation of a RHE-2 based ingredient for food application. Given the limited bioaccessibility of polyphenols under the gastro-intestinal tract, pectin-zein hydrogel beads were successfully developed to preserve the polyphenolic extract undamaged until the intestinal district. The research is ongoing with stability studies on the raw and encapsulated extract, to verify its suitability as food ingredient.

In parallel, we also investigate melon peel and pumpkin peel as sources of pectin. Although these AFW did not show strong bioactivity, pectin extracted from pumpkin peel had a good potential as an emulsifying agent.

Furthermore, our results collected by comparing different green extraction methods on different waste matrices gave us evidence that MAE is a valid technique to obtain rapid extraction with high yield. This is perfectly in line with the requirement of sustainable techniques, with low energy consumption. Conversely, NaDES, despite they are very easy to prepare and very stable in a wide range of temperature, had not an efficiency comparable to that of hydroalcoholic solvents. More investigations are needed to optimize a selective recovery procedure to separate polyphenols from the solvent after the extraction.

In the frame of hydrogen storage, countries around the world are planning strategies to radically reduce the production of GHG. The transition from fossil fuels to alternatives that produce smaller quantities of CO_2 will then be fundamental and in this, hydrogen will be decisive. This work tried to investigate new hydrogen trapping structures for energy storage: a substitute of organic origin and agricultural origin was sought, which came from production waste. Our biochars materials derived from AFW display a capacity to adsorb hydrogen 1.8-2 times greater compared to the traditional graphitic carbon-based materials. Among all, the

material obtained from melon peel was found to be the most promising, with a hydrogen adsorption rate of 4.1% and very rapid kinetics.

6. REFERENCES

Aalim, H.; Belwal, T.; Jiang, L.; Huang, H.; Meng, X.; Luo, Z. Extraction optimization, antidiabetic and antiglycation potentials of aqueous glycerol extract from rice (Oryza sativa L.) bran. Lebensm. Wiss. Technol. 2018, 103, 147–154.

Akasaka, H.; Takahata, T.; Toda, I.; Ono, H.; Ohshio, S.; Himeno, S.; Kokubu, T.; Saitoh, H. Hydrogen Storage Ability of Porous Carbon Material Fabricated from Coffee Bean Wastes. Int. J. Hydrog. Energy 2011, 36, 580–585, doi:10.1016/j.ijhydene.2010.09.102.

Al Jitan, S.; Alkhoori, S.A.; Yousef, L.F. Phenolic acids from plants: Extraction and application to human health. Stud. Nat. Prod. Chem. 2018, 58, 389–417.

Alara, O.R., Abdurahman, N.H., Ukaegbu, C.I., Kabbashi, N.A. Extraction and characterization of bioactive compounds in Vernonia amygdalina leaf ethanolic extract comparing Soxhlet and microwave-assisted extraction techniques. J. Taibah Univ. Sci. 2019, 13(1), 414-422. doi:10.1080/16583655.2019.1582460

Alirezalu, K., Pateiro, M., Yaghoubi, M., Alirezalu, A., Peighambardoust, S.H., Lorenzo, J.M. (2020). Phytochemical constituents, advanced extraction technologies and techno-functional properties of selected Mediterranean plants for use in meat products. A comprehensive review. Trends Food Sci. Technol., 100, 292-306. doi:10.1016/j.tifs.2020.04.010

Alves Filho, E.G.; Sousa, V.M.; Rodrigues, S.; de Brito, E.S.; Fernandes, F.A.N. Green ultrasound-assisted extraction of chlorogenic acids from sweet potato peels and sonochemical hydrolysis of caffeoylquinic acids derivatives. Ultrason. Sonochem. 2020, 63, 104911.

Ameer, K., Shahbaz, H.M., Kwon, J.H. Green Extraction Methods for Polyphenols from Plant Matrices and Their Byproducts: A Review. Compr. Rev. Food Sci. Food Saf. 2017, 16(2), 295-315. doi:10.1111/1541-4337.12253

Anticona, M.; Blesa, J.; Frigola, A.; Esteve, M.J. High biological value compounds extraction from citrus waste with non- conventional methods. Foods 2020, 9, 811.

Anwar, S.; Khan, S.; Almatroudi, A.; Khan, A.A.; Alsahli, M.A.; Almatroodi, S.A.; Rahmani, A.H. A review on mechanism of inhibition of advanced glycation end products formation by plants derived polyphenolic compounds. Mol. Biol. Rep. 2021, 48, 787–805.

Aresta, M.; Dibenedetto, A.; Dumeignil, F. Biorefinery. DE GRUYTER, 2012.

Armandi, M.; Bonelli, B.; Cho, K.; Ryoo, R.; Garrone, E. Study of hydrogen physisorption on nanoporous carbon materials of different origin. Int. J. Hydrog. Energy 2011, 36, 7937-7943. https//doi.org/10.1016/j.ijhydene.2011.01.049

Aschemann-Witzel, J.; Asioli, D., Banovic, M.; Perito, M.A.; Peschel, A.O.; Stancu, V. Defining upcycled food: the dual role of upcycling in reducing food loss and waste. Trends Food Sci. Technol. 2023, 132, 132-137.

Avanza, M.V., Álvarez-Rivera, G., Cifuentes, A., Mendiola, J.A., Ibáñez, E. Phytochemical and functional characterization of phenolic compounds from cowpea (Vigna unguiculata (l.) walp.) obtained by green extraction technologies. Agronomy 2021, 11, 162. doi:10.3390/agronomy11010162

Azmir, J., Zaidul, I.S.M., Rahman, M.M., Sharif, K.M., Mohamed, A., Sahena, F., Jahurul, M.H.A., Ghafoor, K., Norluaini, N.A.N., Omar, A.K.M. Techniques for extraction of bioactive compounds from plant materials: A review. J Food Eng. 2013, 117(4), 426-436. doi:10.1016/j.jfoodeng.2013.01.014

Bai, S.; Tan, G.; Li, X.; Zhao, Q.; Meng, Y.; Wang, Y.; Zhang, Y.; Xiao, D. Pumpkin-derived porous carbon for supercapacitors with high performance. Chem. Asian J. 2016, 11, 1828-1836. https//doi.org/10.1002/asia.201600303

Banožić, M.; Banjari, I.; Jakovljević, M.; Šubarić, D.; Tomas, S.; Babić, J.; Jokić, S. Optimization of ultrasound-assisted extraction of some bioactive compounds from tobacco waste. Molecules 2019, 24, 1611.

Bath, S.; Te, H.; Deutsch, J.; Jeong, H.; Zhang, J.; Suri, R. Food waste and upcycled foods: can a logo increase acceptance of upcycled food?. J. Food Prod. Mark. 2021, 27:4, 188-203. https://doi.org/10.1080/10454446.2021.1955798

Battistella Lasta, H.F., Lentz, L., Gonçalves Rodrigues, L.G., Mezzomo, N., Vitali, L., Salvador Ferreira, S.R. Pressurized liquid extraction applied for the recovery of phenolic compounds from beetroot waste. Biocatal. Agric. Biotechnol. 2019, 21, 101353. doi:10.1016/j.bcab.2019.101353

Belwal, T., Bhatt, I.D., Rawal, R.S., Pande, V. Microwave-assisted extraction (MAE) conditions using polynomial design for improving antioxidant phytochemicals in Berberis asiatica Roxb. ex DC. leaves. Ind. Crops Prod. 2017, 95, 393-403. doi:10.1016/j.indcrop.2016.10.049

Benjad, Z.; Gómez-Cordovés, C.; Es-Safi, N.E. Characterization of flavonoid glycosides from fenugreek (Trigonella foenum-graecum) crude seed by HPLC-DAD-ESI/MS analysis. Int. J. Mol. Sci. 2014, 15, 20668–20685.

Bicil, Z.; Doğan, M. Characterization of Activated Carbons Prepared from Almond Shells and Their Hydrogen Storage Properties. Energy & Fuels 2021, 35, 10227–10240, doi:10.1021/acs.energyfuels.1c00795.

Blankenship, L.S.; Balahmar, N.; Mokaya, R. Oxygen-Rich Microporous Carbons with Exceptional Hydrogen Storage Capacity. Nat. Commun. 2017, 8, 1545, doi:10.1038/s41467-017-01633-x.

Brodkorb, A.; Egger, L.; Alminger, M.; Alvito, P.; Assunção, R.; Ballance, S.; Bohn, T.; Bourlieu-Lacanal, C.; Boutrou, R.; Carrière, F.; Clemente, A.; Corredig, M.; Dupont, D.; Dufour, C.; Edwards, C.; Golding, M.; Karakaya, S.; Kirkhus, B.; Le Feunteun, S.; Lesmes, U.; Macierzanka, A.; Mackie, A.R.; Martins, C.; Marze, S.; McClements, D. J.; Ménard, O.; Minekus, M.; Portmann, R.; Santos, N. C., Souchon, I.; Singh, R. P.; Vergarud, G. E.; Wickham, M. S. J.; Weitschies, W.; Recio, I. Infogest static in vitro simulation of gastrointestinal food digestion, Nat. Protoc. 2019, 14, 991–1040.

Caballero-Galván, A.S.; Restrepo-Serna, D.L.; Ortiz-Sánchez, M.; Cardona-Alzate, C.A. Analysis of extraction kinetics of bioactive compounds from spent coffee grounds (Coffea arábica). Waste Biomass Valorization 2018, 9, 2381–2389.

Capanoglu, E.; Nemli, E.; Tomas-Barberan, F. Novel approaches in the valorization of agricultural wastes and their applications. J. Agric. Food Chem. 2022, 70, 6787-6804. https://doi.org/10.1021/acs.jafc.1c07104

Carazzone, C.; Mascherpa, D.; Gazzani, G.; Papetti, A. Identification of phenolic constituents in red chicory salads (Chichorium intybus) by high-performance liquid chromatography with diode array detection and electrospray ionization tandem mass spectrometry. Food Chem. 2013, 138, 1062–1071.

Carciochi, R.A.; Sologubik, C.A.; Fernández, M.B.; Manrique, G.D.; D'Alessandro, L.G. Extraction of antioxidant phenolic compounds from brewer's spent grain: optimization and kinetics modeling. Antioxidant 2018, 7, 45, https://doi.org/10.3390/antiox7040045

Castro-López, C., Ventura-Sobrevilla, J.M., González-Hernández, M.D., Rojas, R., Ascacio-Valdés, J.A., Aguilar, C.N., Martínez-Ávila, G.C.G. Impact of extraction techniques on antioxidant capacities and phytochemical composition of polyphenol-rich extracts. Food Chem. 2017, 237, 1139-1148. doi:10.1016/j.foodchem.2017.06.032

Cha, J.C.; Park, S.H.; Jung, S.-C.; Ryu, C.; Jeon, J.-K.; Shin, M.-C.; Park, Y.-K. Production and utilization of biochar: a review. J. Ind. Eng. Chem. 2016, 40, 1-15. https://dx.doi.org/10.1016/j.jiec.2016.06.002

Chaharbaghi, E.; Khodaiyan, F.; Hosseini, S.S. Optimization of pectin extraction from pistachio green hull as a new source. Carbohydr. Polym. 2017, 173, 107–113.

Chaharbaghi, E.; Khodaiyan, F.; Hosseini, S.S. Optimization of pectin extraction form pistachio green hull as a new source. Carbohydr. Polym. 2017, 173, 107-113. http://dx.doi.org/10.1016/j.carbpol.2017.05.047

Chemat, F., Rombaut, N., Sicaire, A.G., Meullemiestre, A., Fabiano-Tixier, A.S., Abert-Vian, M. Ultrasound assisted extraction of food and natural products. Mechanisms, techniques, combinations, protocols and applications. A review. Ultrason Sonochem. 2017, 34, 540-560. doi:10.1016/j.ultsonch.2016.06.035

Chen, G.; Madl, R.L.; Smith, J.S. Cereal bran extracts inhibit the formation of advanced glycation end products in bovine serum albumin/glucose model. Cereal Chem. 2018, 95, 625–633.

Christou, A., Stavrou, I.J., Kapnissi-Christodoulou, C.P. Continuous and pulsed ultrasound-assisted extraction of carob's antioxidants: Processing parameters optimization and identification of polyphenolic composition. Ultrason Sonochem. 2021, 76, 105630. doi:10.1016/j.ultsonch.2021.105630

Cimbala, J.M. Taguchi Orthogonal Arrays. 2014

Cohen, Y., M. Levi, U. Lesmes, M. Margier, E. Reboul, and Y. D. Livney. Re-assembled casein micelles improve in vitro bio- availability of vitamin D in a Caco-2 cell model. Food Funct. 2017, 8 (6):2133–41. doi: 10.1039/c7fo00323d.

Collivignarelli, M.C.; Sorlini, S.; Milanese, C.; Illankoon, W.A.M.A.N.; Caccamo, F.M.; Calatroni, S. Rice Industry By-Products as Adsorbent Materials for Removing Fluoride and Arsenic from Drinking Water—A Review. Appl. Sci. 2022, 12, 3166, doi:10.3390/app12063166.
Contado, C.; Caselotto, L.; Mello, P.; Maietti, A.; Marvelli, L.; Marchetti, N.; Dalpiaz, A. Design an formulation of Eudragit-coated zein/pectin nanoparticles for the colon delivery of resveratrol. Eur. Food Res. Technol. 2020, 246, 2417-2441. https://doi.org/10.1007/s00217-020-03586-w

Cui et al., S.C.; Chang, Y.H. Emulsifying and structural properties of pectin enzymatically extracted from pumpkin. LWT 2014, 58, 396-403.

Dai, Y., Spronsen, J.V., Witkamp, G.-J., Verpoorte, R., Hae Coi, Y. Natural deep eutectic solvents as new potential media for green technology. Anal. Chim. 2013, 766, 61–68. http://dx.doi.org/10.1016/j.aca.2012.12.019.

Das, A. K., Dewanjee, S. Optimization of Extraction Using Mathematical Models and Computation. Comput. Chem., Elsevier 2018, 75–106. https://doi.org/10.1016/B978-0-12-812364-5.00003-1.

Daud, N.M., Putra, N.R., Jamaludin, R., Norodin N.S.M, Sarkawi, N.S., Hamzah, M.H.S., Mohd Nasir, H., Abang Zaidel, D.N., Che Yunus, M.A., Salleh L.M. Valorisation of plant seed as natural bioactive compounds by various extraction methods: A review. Trends Food Sci. Technol. 2021, 119, 201-214. doi:10.1016/j.tifs.2021.12.010

Deng, J.; Li, M.; Wang, Y. Biomass-Derived Carbon: Synthesis and Applications in Energy Storage and Conversion. Green Chem. 2016, 18 (18), 4824–4854. https://doi.org/10.1039/c6gc01172a.

Deng, L.; Zhao, Y.; Sun, S.; Feng, D.; Zhang, W. Thermochemical methods for controlling pore structure to enhance hydrogen storage capacity of biochar. Int. J. Hydrog. energy 2023, 48, 21799-21813. https://doi.org/10.1016/j.ijhjdene.2023.03.084

Deng, P.; Lei, S.; Wang, W.; Zhou, W.; Ou, X.; Chen, L.; Xiao, Y.; Cheng, B. Conversion of Biomass Waste to Multi-Heteroatom-Doped Carbon Networks with High Surface Area and Hierarchical Porosity for Advanced Supercapacitors. J. Mater. Sci. 2018, 53 (20), 14536–14547. https://doi.org/10.1007/s10853-018-2630-8.

Dib, T., H. Pan, and S. Chen. Recent advances in pectin-based nanoencapsulation for enhancing the bioavailability of bioactive compounds: Curcumin oral bioavailability. Food Rev. Int. 2022, :1–19. doi: 10.1080/87559129.2021.2012796.

Dogan, M.; Sabaz, P.; Bï cï l, Z.; Koçer Kizilduman, B.; Turhan, Y. Activated carbon synthesis from tangerine peel and its use in hydrogen storage, J. Energy Inst. 2020, 93 (6), 2176–2185.

Domínguez-Rodríguez, G., Marina, M.L., Plaza, M. Enzyme-assisted extraction of bioactive non-extractable polyphenols from sweet cherry (Prunus avium L.) pomace. Food Chem. 2021, 339, 128086. doi:10.1016/j.foodchem.2020.128086

Dou, Y.; Sun, L.; Ren, J.; Dong, L. Opportunities and Future Challenges in Hydrogen Economy for Sustainable Development. In Hydrogen Economy; Elsevier 2017; pp. 277–305.

Duarte-Almeida, J.M.; Negri, G.; Salatino, A.; de Carvalho, J.E.; Lajolo, F.M. Antiproliferative and antioxidant activities of a tricin acylated glycoside from sugarcane (Saccharum officinarum) juice. Phytochem. 2007, 68, 1165–1171.

Dutta, S. A review on production, storage of hydrogen and its utilization as an energy source. J. Industr. Engineer. Chem. 2014, 20, 1148-1156. https//doi.org/10.1016/j.jiec.2013.07.037

Dzah, C.S., Duan, Y., Zhang, H., Wen, C., Zhang, J., Chen, G., Ma, H. The effects of ultrasound assisted extraction on yield, antioxidant, anticancer and antimicrobial activity of polyphenol extracts: A review. Food Biosci. 2020, 35, 100547. doi:10.1016/j.fbio.2020.100547

Ellerbrock, R.; Stein, M.; Schaller, J. Comparing Amorphous Silica, Short-Range-Ordered Silicates and Silicic Acid Species by FTIR. Sci. Rep. 2022, 12, 11708, doi:10.1038/s41598-022-15882-4.

Essien, S.O., Young, B., Baroutian, S. Recent advances in subcritical water and supercritical carbon dioxide extraction of bioactive compounds from plant materials. Trends Food Sci. Technol. 2020, 97, 156-169. doi:10.1016/j.tifs.2020.01.014

EU Platform on Food Loss and Food Waste. Available at https://food.ec.europa.eu/safety/food-waste/eu-actions-against-food-waste/eu-platform-food-losses-and-food-waste_en

European Community (EC) Regulation No. 178/2002. Available at https://eur-lex.europa.eu/legal-content/EN/TXT/PDF/?uri=CELEX:02002R0178-20140630&rid=1#:~:text=This%20Regulation%20provides%20the%20basis,tioning%20of%20the%20internal%20market.

FAO (Food and Agriculture Organization of the United Nations). Food Wastage Footprint: Impacts on Natural Resources, 2013.

FAO (Food and Agriculture Organization of the United Nations). The State of Food and Agriculture 2019: Moving Forward on Food Loss and Waste Reduction; Rome, Italy, 2019.

FAO Global Hunger Report 2022, available at https://www.fao.org/newsroom/detail/un-report-global-hunger-SOFI-2022-FAO/en

Fathi, M., Á. Martín, and D. J. McClements. Nanoencapsulation of food ingredients using carbohydrate based delivery systems. Trends Food Sci. Technol. 2014, 39 (1):18–39. doi: 10.1016/j. tifs.2014.06.007.

Fathoni, A.; Saepudin, E.; Cahyana, A.H.; Rahayu, D.U.C.; Haib, J. Identification of Nonvolatile Compounds in Clove (Syzygium aromaticum) from Manado. In Proceedings of the AIP Conference, Pizzo Calabro, Italy, 19–25 September 2016; Volume 1862, p. 030079.

Fayle, S.E.; Healy, J.P.; Brown, P.A.; Reid, E.A.; Gerrard, J.A.; Ames, J.M. Novel approaches to the analysis of Maillard reaction proteins. Electrophoresis 2011, 22, 1518–1525.

Ferron, L.; Colombo, R.; Mannucci, B.; Papetti, A. A new Italian purple corn variety (Moradyn) byproduct extract: Antiglycative and hypoglycemic in vitro activities and preliminary bioaccessibility studies. Molecules 2020, 25, 1958.

Florez, N.; Conde, E.; Dominguez, H. Microwave assisted water extraction of plant compounds. J. Chem. Technol. Biotechnol. 2015, 90, 590–607.

Frosi, I., Vallelonga, D., Colombo, R., Milanese, C.; Papetti, A. Valorization of Rice Husk (Oryza sativa L.) as a Source of In Vitro Antiglycative and Antioxidant Agents. Foods 2023, 12, 529. https://doi.org/10.3390/foods12030529.

Frosi, I.; Ferron, L.; Colombo, R.; Papetti, A. Natural carriers: Recent advances in their use to improve the stability and bioaccessibility of food active compounds, Crit. Rev. Food Sci. Nutr. 2022. DOI: 10.1080/10408398.2022.2157371

Frosi, I.; Montagna, I.; Colombo, R.; Milanese, C.; Papetti, A. Recovery of chlorogenic acids from agri-food wastes: Updates on green extraction techniques. Molecules 2021, 26, 4515.

Galan, A.M.; Calinescu, I.; Trifan, A.; Winkworth-Smith, C.; Calvo-Carrascal, M.; Dodds, C.; Binner, E. New insights into the role of selective and volumetric heating during microwave extraction: Investigation of the extraction of polyphenolic compounds from sea buckthorn leaves using microwave-assisted extraction and conventional solvent extraction. Chem. Eng. Process. 2017, 116, 29–39.

Garofulić, I.E., Kruk, V., Martić, A., Zorić, Z., Pedisić, S., Dragović, S., Dragović-Uzelac, V. Evaluation of polyphenolic profile and antioxidant activity of Pistacia lentiscus L. Leaves and fruit extract obtained by optimized microwave-assisted extraction. Foods 2020, 9(11), 1556. doi:10.3390/foods9111556

Gil Martín, E., Forbes-Hernández, T., Romero, A., Cianciosi, D., Giampieri, F., Battito, M. Influence of the extraction method on the recovery of bioactive phenolic compounds from food industry by-products. Food Chem. 2022, 378, 131910. https://doi.org/10.1016/j.foodchem.2021.131918.

Gligor, O., Mocan, A., Moldovan, C., Locatelli, M., Crișan, G., Ferreira, I.C.F.R. Enzyme-assisted extractions of polyphenols – A comprehensive review. Trends Food Sci Technol. 2019, 88, 302-315. doi:10.1016/j.tifs.2019.03.029

Global Energy Review: CO_2 Emissions in 2021; 2022;

Goëlo, V., M. Chaumun, A. Gonçalves, B. N. Estevinho, and F. Rocha. Polysaccharide-based delivery systems for curcumin and tur- meric powder encapsulation using a spray-drying process. Powder Technol. 2020, 370:137–46. doi: 10.1016/j.powtec.2020.05.016.

Golbargi, F.; Gharibzahedi, S.M.T.; Zoghi, A.; Mohammadi, M.; Hashemifesharaki, R. Microwave-assisted extraction of arabinan- rich pectic polysaccharides from melon peels: Optimization, purification, bioactivity, and techno-functionality. Carbohydr. Polym. 2021, 256, 117522.

Goufo, P.; Singh, R.K.; Cortez, I. A reference list of phenolic compounds (including stilbenes) in grapevine (Vitis vinifera L.) roots, woods, canes, stems and leaves. Antioxidants 2020, 9, 398.

Habeebullah, S.F.K., Alagarsamy, S., Sattari, Z., Al-Haddad, S., Fakhraldeen, S., Al-Ghunaim, A., Al-Yamani, F. Enzyme-assised extraction of bioactive compounds from brown seaweeds and characterization. J. Appl. Phycol. 2020, 32, 615-629.

Haldipur, A.C.; Srividya, N. Multi-mechanistic in vitro evaluation of antihyperglycemic, antioxidant and antiglycation activities of three phenolic-rich Indian red rice genotypes and in silico evaluation of their phenolic metabolites. Foods 2018, 10, 2818.

Hannah Ritchie; Max Roser Energy Production and Consumption Available online: https://ourworldindata.org/energy-production-consumption (accessed on 6 January 2023). https://www.upcycledfood.org/the-standard-1

Hu, Y., W. Zhang, Z. Ke, Y. Li, and Z. Zhou. In vitro release and antioxidant activity of Satsuma mandarin (Citrus reticulata Blanco cv. unshiu) peel flavonoids encapsulated by pectin nanoparticles. Int. J. Food Sci. Technol. 2017, 52 (11):2362–73. doi: 10.1111/ijfs.13520.

Huang, Y., Feng, F., Jiang, J., Qiao, Y., Wu, T., Volgmeir, J., Chen, Z.-G. Green and efficient extraction of rutin from tartary buckwheat hull by using natural deep eutectic solvents. Food Chem 2017, 221, 1400-1405. https://doi.org/10.1016/j.foodchem.2016.11.013.

Hydrogen Available online: https://www.irena.org/Energy-Transition/Technology/Hydrogen (accessed on 29 January 2023).

Ibrahim, R.M.; El-Halawany, A.M.; Saleh, D.O.; El Naggar, E.M.B.; El-Shabrawy, A.E.R.O.; El-Hawary, S.S. HPLC-DAD-MS/MS profiling of phenolics from Securigera securidaca flowers and its anti-hyperglycemic and anti-hyperlipidemic activities. Rev. Bras. Farmacogn. 2015, 25, 134–141.

ICH guidelines Q2(R1) Validation of analytical procedures: text and methodology (2005).

Illankoon W.A.M.A.N.; Milanese, C.; Girella, A.; Medina-Llamas, M.; Magnani, G.; Pontiroli, D.; Ricco, M.; Collivignarelli, M. C.; Sorlini, S. Biochar derived from the rice industry by-products as sustainable energy storage material. In Proceedings of the 30th European Biomass Conference and Exhibition (EUBCE); P.-F. CHEVET, N. SCARLAT, A. GRASSI, Eds.; ETA-Florence Renewable Energies: Florence, May 2022.

Ismal, I.S.; Othman, M.F.H.; Rashidi, N.A.; Yusup, S. Recent progress on production technologies of food waste-based biochar and its fabrication method as electrode materials in energy storage application. Biomass Convertion and Biorefinery 2022. https://doi.org/10.1007/s13399-023-03763-3

Ivanović, M., Razboršek, M. I., Kolar, M. Innovative extraction techniques using deep eutectic solvents and analytical methods for the isolation and characterization of natural bioactive compounds from plant material. Plants 2020, 9 (11), 1–29. https://doi.org/10.3390/plants9111428.

Jafari, F.; Khodaiyan, F.; Kiani, H.; Hosseini, S.S. Pectin from carrot pomace: optimization of extraction and physicochemical properties. Carbohydr. Polym. 2017, 157, 1315-1322.

Jyoti, A.; Singh, R.K.; Kumar, N.; Aman, A.K.; Kar, M. 'Synthesis and Properties of Amorphous Nanosilica from Rice Husk and Its Composites. MSEB 2021, 263, 114871, doi:10.1016/j.mseb.2020.114871.

Kaderides, K.; Papaoikonomou, L.; Serafim, M.; Goula, A.M. Microwave-assisted extraction from pomegranate peels: Optimization, kinetics, and comparison with ultrasound extraction. Chem. Eng. Process. 2019, 137, 1–11.

Kazemi, M.; Khodaiyan, F.; Hosseini, S.S.; Najari, Z. An integrated valorization of industrial waste of eggplant: Simultaneous recovery of pectin, phenolics and sequential production of pullulan. Waste Manag. 2019, 100, 101–111.

Kim, B.-J.; Lee, Y.-S.; Park, S.-J. A study on the hydrogen storage capacity of Ni-plated porous carbon nanofibers. Intern. J. Hydrog. Energ. 2008, 33, 4112-4115. https//doi.org/10.1016/j.ijhydene.2008.05.077

Kim, D.O., Lee, C.Y. Extraction and isolation of polyphenolics. Curr. Protoc. Food Anal. Chem. 2002, 6, I1–I2. https://doi.org/10.1002/0471142913.fai0102s06.

Komatsu, K.; Li, H.; Kanma, Y.; Zhu, J.; Toda, I.; Tsuda, Y.; Saitoh, H. Increase in H2 Storage Capacity of Nanoporous Carbon Fabricated from Waste Rice Husk via Improving the Mode of the Reaction Mixture Cooling Down. J. Mater. Res. Technol. 2021, 12, 1203–1211, doi:10.1016/j.jmrt.2021.03.060.

Krishna, R.; van Baten, J.M. A Comparison of the CO2 Capture Characteristics of Zeolites and Metal–Organic Frameworks. Sep. Purif. Technol. 2012, 87, 120–126, doi:10.1016/j.seppur.2011.11.031.

Kumar, M.; Barbhai, M. D.; Hasan, M.; Punia, S.; Dhumal, S.; Radha, Nadeem Rais, Chandran, D.; Pandiselvam, R.; Kothakota, A.; Tomar, M.; Satankar, A.; Senapathy, M.; Anitha, T.; Dey, A.; Sayed, A.A.S.; Gadallah, F.M.; Amarowicz, R.; Mekhemar, M. Onion (Allium cepa L.) peels: A review on bioactive compounds and biomedical activities, Biomed. Pharmacother. 2022, 146, 112498. https://doi.org/10.1016/j.biopha.2021.112498.

Lao, F., Sigurdson, T., Giusti, M. M. Extraction of purple corn (Zea mays L.) cob pigments and phenolic compounds using food-friendly solvents, J. Cereal. Sci. 2018, 80, 87–93. https://doi.org/10.1111/1541-4337.12249.

Lee, T.; Chang, Y.H. Structural, physicochemical, and in-vitro release properties of hydrogel beads produced by oligochitosan and de-esterified pectin from yuzu (Citrus junos) peel as a quercetin delivery system for colon target. Food Hydrocoll. 2020, 108, 106086.

Lefebvre, T., Destandau, E., Lesellier, E. Selective extraction of bioactive compounds from plants using recent extraction techniques: A review. J. Chromatogr. A. 2021, 1635, 461770. doi:10.1016/j.chroma.2020.461770

Leichtweis MG, Molina AK, Petropoulos SA, Carocho M, Pires TCSP, Dias MI, Calhelha R, Oliveira MBPP, Pereira C, Barros L. Valorization of Pumpkin Peel as a Source of Bioactive Compounds: Optimization of Heat- and Ultrasound-Assisted Extraction. Molecules 2023, 28(7), 3168. doi: 10.3390/molecules28073168.

Li, M.; Pu, Y.; Yoo, C.G.; Ragauskas, A.J. The occurrence of tricin and its derivatives in plants. Green Chem. 2016, 18, 1439–1454.

Liang, X.; Cheng, W.; Liang, Z.; Zhan, Y.; McClements, D.J.; Hu, K. Co-Encapsulation of Tannic Acid and Resveratrol in Zein/Pectin Nanoparticles: Stability, Antioxidant Activity, and Bioaccessibility. Foods 2022, 11, 3478.

Liazid, A.; Palma, M.; Brigui, J.; Barroso, C.G. Investigation on phenolic compounds stability during microwave-assisted extraction. J. Chromatogr. A 2007, 1140, 29–34.

Lin, X., Wu, L., Wang, X., Yao, L., Wang, L. Ultrasonic-assisted extraction for flavonoid compounds content and antioxidant activities of India Moringa oleifera L. leaves: Simultaneous optimization, HPLC characterization and comparison with other methods. J. Appl. Res. Med. Aromat. Plants. 2021, 20, 100284. doi:10.1016/j.jarmap.2020.100284

Liu, L.; Fishman, M.L.; Hicks, K.B.; Kende, M.; Ruthel, G. Pectin-zein beads for potential colon-specific drug delivery: synthesis and in vitro evaluation. Drug Deliv. 2006, 13:6, 417-423. DOI: 10.1080/10717540500394935

Liu, X.; Renard, C.M.G.C.; Bureau, S.; le Bourvellec, C. Revisiting the Contribution of ATR-FTIR Spectroscopy to Characterize Plant Cell Wall Polysaccharides. Carbohydr. Polym. 2021, 262, 117935, doi:10.1016/j.carbpol.2021.117935.

Lopez-Fernández, O.; Domínguez, R.; Pateiro, M.; Munekata, P.E.S.; Rocchetti, G.; Lorenzo, J.M. Determination of polyphenols using liquid chromatography-tandem mass spectrometry technique (LC-MS/MS): A review. Antioxidants 2022, 9, 479.

Lozano-Castelló, D.; Calo, J.M.; Cazorla-Amorós, D.; Linares-Solano, A. Carbon Activation with KOH as Explored by Temperature Programmed Techniques, and the Effects of Hydrogen. Carbon 2007, 45, 2529–2536, doi:10.1016/j.carbon.2007.08.021.

Ma, L.; Bi, Z.; Xue, Y.; Zhang, W.; Huang, Q.; Zhang, L.; Huang, Y. Bacterial Cellulose: An Encouraging Eco-Friendly Nano-Candidate for Energy Storage and Energy Conversion. J. Mater. Chem. A. 2020, 8, 5812–5842, doi:10.1039/C9TA12536A.

Maietta, M.; Colombo, R.; Corana, F.; Papetti, A. Cretan tea (Origanum dictamnus L.) as a functional beverage: An investigation on antiglycative and carbonyl trapping activities. Food Funct. 2018, 9, 1545–1556.

Maietta, M.; Colombo, R.; Lavecchia, R.; Sorrenti, M.; Zuorro, A.; Papetti, A. Artichoke (Cynara cardunculus L. var. scolymus) waste as a natural source of carbonyl trapping and antiglycative agents. Food Res. Int. 2017, 100, 780-790.

Mallek-Ayadi, S.; Bahloul, N.; Kechau, N. Characterization, phenolic compounds and functional properties of Cucumis melo L. peels. Food Chem. 2017, 221, 1691-1697. http://dx.doi.org/10.1016/j.foodchem.2016.10.117

Massarioli, A.P.; De Oliveira Sartori, A.G.; Francetto Juliano, F.; Pedroso Gomes do Amaral, J-E-; Cavalcanti dos Santos, R.; De Lima, L.M.; De Alencas, S.M. Simulated gastrointestinal digestion/Caco-2 cell model to predict bioaccessibility and intestinal permeability of *p*-coumaric acid and *p*-coumaroyl derivatives in peanut. Food Chem. 2023, 400, 134033.

McClements, D. J. Nanoscale nutrient delivery systems for food applications: Improving bioactive dispersibility, stability, and bio- availability. J. Food Sci. 2015, 80 (7), 1602–1611. doi: 10.1111/1750-3841.12919.

Mecozzi, M.; Sturchio, E. Computer Assisted Examination of Infrared and Near Infrared Spectra to Assess Structural and Molecular Changes in Biological Samples Exposed to Pollutants: A Case of Study. J. Imaging 2017, 3, 11, doi:10.3390/jimaging3010011.

Mecozzi, M.; Sturchio, E. Computer Assisted Examination of Infrared and Near Infrared Spectra to Assess Structural and Molecular Changes in Biological Samples Exposed to Pollutants: A Case of Study. J. Imaging 2017, 3, 11, doi:10.3390/jimaging3010011.

Medina-Llamas, M.; Speltini, A.; Profumo, A.; Panzarea, F.; Milella, A.; Fracassi, F.; Listorti, A.; Malavasi, L. Preparation of Heterojunctions Based on Cs3Bi2Br9 Nanocrystals and G-C3N4 Nanosheets for Photocatalytic Hydrogen Evolution. Nanomaterials 2023, 13, 263, doi:10.3390/nano13020263.

Medvedkov, Y.B.; Yerenova, B.Y.; Pronina, Y.G.; Penov, N.D.; Belozertseva, O.D.; Kondratiuk, N.V. Extraction and characteristics of pectins from melon peel: Experimental review. J. Chem. Technol. 2021, 9, 650–659.

Mellinas, A.C.; Jiménez, A.; Garrígos, M.C. Optimization of microwave-assisted extraction of cocoa bean shell waste and evaluation of its antioxidant, physicochemical and functional properties. LWT-Food Sci. Technol. 2020, 127, 109361.

Mena-García, A.; Rodríguez-Sánchez, S.; Ruiz-Matute, A.I.; Sanz, M.L. Exploitation of artichoke byproducts to obtain bioactive extracts enriched in inositols and caffeoylquinic acids by microwave assisted extraction. J. Chromatogr. A 2020, 1613, 460703.

Mendez, D.A.; Fabra, M.J.; Gómez-Mascaraque, L.; López-Rubio, A.; Martinez-Abad, A. Modelling the extraction of pectin towards the valorization of watermelon rind waste. Foods 2021, 10, 738. https://doi.org/10.3390/foods10040738

Mendez, D.A.; Fabra, M.J.; Martínez-Abad, A.; Martínez-Sanz, A.; Gorria, M.; López-Rubio, A. Understanding the different emulsification mechanisms of pectin: Comparison between watermelon rind and two commercial pectin sources. Food Hydrocoll. 2021, 120, 106957.

Mesías, M.; Navarro, M.; Gökmen, V.; Morales, F.J. Antiglycative effect of fruit and vegetable seed extracts: Inhibition of AGE formation and carbonyl-trapping abilities. J. Sci. Food Agric. 2013, 93, 2037–2044.

Mir-cerdà, A.; Nuñez, O.; Granados, M.; Sentellas, S.; Saurina, J. An overview of the extraction and characterization of bioactive phenolic compounds from agri-food waste within the framework of circular bioeconomy. Trends Analyt. Chem. 2023, 161, 116994. https://doi.org/10.1016/j.trac.2023.116994

Mohan, M.; Sharma, V.K.; Kumar, E.A.; Gayathri, V. Hydrogen storage in carbon materials—a review, Energy Storage 2019, 1 (2), e35.

Mosić, M., Dramićanin, A., Ristivojević, P., Milojković-Opsenica, D. Extraction as a critical step in phytochemical analysis. J. AOAC Int. 2021, 103(2), 365-372. doi:10.5740/jaoacint.19-0251

Mouritzinos, I. and Goula, A. Polyphenols in agricultural byproducts and food waste. Polyphenols in Plants 2019, 2, 23-43. https://doi.org/10.1016/B978-0-12-813768-0.00002-5

Mukhidinov, Z.M.; Kasimova, G.F:; Bobokalonov, D.T.; Khalikov, D. Kh.; Teshavev, Kh.I.; Khalikova, M.D.; Liu, L.-S. Pectin-zein microspheres as drug delivery systems. Pharm. Chem. J. 2011, 44, 10.

Nadar, S.S., Rao, P., Rathod, V.K. Enzyme assisted extraction of biomolecules as an approach to novel extraction technology: A review. Food Res Int. 2018, 108, 309-330. doi:10.1016/j.foodres.2018.03.006

Nagavekar, N., Singhal, R.S. Supercritical fluid extraction of Curcuma longa and Curcuma amada oleoresin: Optimization of extraction conditions, extract profiling, and comparison of bioactivities. Ind. Crops Prod. 2019, 134, 134-145. doi:10.1016/j.indcrop.2019.03.061

Nandiyanto, A.B.D.; Oktiani, R.; Ragadhita, R. How to read and interpret FTIR spectroscope of organic material. Indonesian J. Sci. Technol. 2019, 4, 97. https//doi.org/10.17509/ijost.v4il.15806

Náthia-Neves, G.; Alonso, E. Valorization of sunflower by-product using microwave-assisted extraction to obtain a rich protein flour: Recovery of chlorogenic acid, phenolic content and antioxidant capacity. Food Bioprod. Process. 2021, 125, 57–67.

Nguyen, H.C., Nguyen, H.N.T., Huang, M.Y., Lin, K.H., Pham, D.C., Tran, Y.B., Su, C.H. Optimization of aqueous enzyme-assisted extraction of rosmarinic acid from rosemary (Rosmarinus officinalis L.) leaves and the antioxidant activity of the extract. J Food Process Preserv. 2021, 45, 15221. doi:10.1111/jfpp.15221

Nijkamp, M.; Raaymakers, J.; van Dillen, A; De Jong, K.P. Hydrogen storage using physisorption – materials demands. *Appl. Phys. A.* 2001, 72, 619–623. https://doi.org/10.1007/s003390100847

Ninčević Grassino, A.; Ostojić, J.; Miletić, V. Application of high hydrostatic pressure and ultrasound-assisted extractions as a novel approach for pectin and polyphenols recovery from tomato peel waste. Innov. Food Sci. Emerg. Technol. 2020, 64, 102424.

Noreen, A., Z. I. H. Nazli, J. Akram, I. Rasul, A. Mansha, N. Yaqoob, R. Iqbal, S. Tabasum, M. Zuber, and K. M. Zia. Pectins func- tionalized biomaterials; a new viable approach for biomedical applications: A review. Int. J. Biol. Macromol. 2017, 101:254–72. doi: 10.1016/j.ijbiomac.2017.03.029.

Novel Food Regulation (EU) 2015/2283. Available at https://eur-lex.europa.eu/legal-content/EN/TXT/PDF/?uri=CELEX:32015R2283

Okolie, C.L., Akanbi, T.O., Mason, B., Udenigwe, C.C., Aryee, A.N.A. Influence of conventional and recent extraction technologies on physicochemical properties of bioactive macromolecules from natural sources: A review. Food Res. Int. 2019, 116, 827-839. doi:10.1016/j.foodres.2018.09.018

Omar, N.; Abdullah, E. C.; Petrus, A. A.; Mubarak, N. M.; Khalid, M.; Agudosi, E. S.; Numan, A.; Aid, S. R. Single-Route Synthesis of Binary Metal Oxide Loaded Coconut Shell and Watermelon Rind Biochar: Characterizations and Cyclic Voltammetry Analysis. Biomass Convers. Biorefinery 2021. https://doi.org/10.1007/s13399-021-01367-3.

Otowa, T., Nojima, Y., Miyazaki, T.: Development of KOH activated high surface area carbon and its application to drinking water purification. Carbon 1997, 35, 1315–1319. https://doi.org/10.1016/S0008-6223(97)00076-6

Otowa, T.; Tanibata, R.; Itoh, M. Production and Adsorption Characteristics of MAXSORB: High-Surface-Area Active Carbon. Gas Sep. Purif. 1993, 7, 241–245, doi:10.1016/0950-4214(93)80024-Q.

Padma Ishwarya, S.; Sandhya, R.; Nisha, P. Advances and prospects in the food application of pectin hydrogels. Crit. Rev. Food Sci. Nutr. 2022, 62 (16), 4393–4417. doi: 10.1080/10408398.2021.1875394.

Pagano, I.; Piccinelli, A.L.; Celano, R.; Campone, L.; Gazzerro, P.; Russo, M.; Rastrelli, L. Pressurized hot water extraction of bioactive compounds from artichoke by-products. Electrophoresis 2018, 39, 1899–1907.

Pamunuwa, G., N. Anjalee, D. Kukulewa, C. Edirisinghe, F. Shakoor, and D. N. Karunaratne. Tailoring of release properties of folic acid encapsulated nanoparticles via changing alginate and pec- tin composition in the matrix. Carbohydrate Polymer Technologies and Applications 2020, 1:100008. doi: 10.1016/j.carpta.2020.100008.

Panja, P. Green extraction methods of food polyphenols from vegetable materials. Curr. Opin. Food Sci. 2018, 23, 173-182. doi:10.1016/j.cofs.2017.11.012

Panwar, D.; Panesar, P.S.; Chopra, H.K. Ultrasound-assisted extraction of pectin from Citrus limetta peels: optimization, characterization, and its comparison with commercial pectin. Food Bioscience 2023, 51, 102231.

Paritosh, K.; Kushwaha, S. K.; Yadav, M.; Pareek, N.; Chawade, A.; Vivekanand, V. Food waste to energy: an overview of sustainable approaches for food waste management and nutrient recycling. BioMed. Res. Int. 2017, 2017, 1–19.

Pasandide, B.; Khodaiyan, F.; Mousavi, Z.E.; Hosseini, S.S. Optimization of aqueous pectin extraction from Citrus medica peel. Carbohydr. Polym. 2017, 178:27-33. doi: 10.1016/j.carbpol.2017.08.098.

Pellicanò, T.M.; Sicari, V.; Loizzo, M.R.; Leporini, M.; Falco, F.; Poiana, M. Optimizing the supercritical fluid extraction process of bioactive compounds from processed tomato skin by-products. Food Sci. Technol. 2020, 40, 692–697.

Picot-Allain, M.C.N.; Ramasawmy, B.; Emmambux, M.N. Extraction, Characterisation, and Application of Pectin from Tropical and Sub-Tropical Fruits: A Review. Food Rev. Int. 2022, 38, 282–312.

Pimentel-Moral, S., Borrás-Linares, I., Lozano-Sánchez, J., Arráez-Román, D., Martínez-Férez, A., Segura-Carretero, A. Microwave-assisted extraction for Hibiscus sabdariffa bioactive compounds. J. Pharm. Biomed. Anal. 2018, 156, 313–322. https://doi.org/10.1016/j.jpba.2018.04.050.

Pontillo, A.R.N., Papakosta-Tsigkri, L., Lymperopoulou, T., Mamma, D., Kekos, D., Detsi, A. Conventional and enzyme-assisted extraction of rosemary leaves (Rosmarinus officinalis l.): Toward a greener approach to high added-value extracts. Appl. Sci. 2021, 11, 3724. doi:10.3390/app11083724

Poulev, A.; Chen, M.-H.; Cherravuru, S.; Raskin, I.; Belanger, F.C. Variation in levels in the flavone tricin in bran from rice genotypes varying in pericarp color. J. Cereal Sci. 2018, 79, 226–232.

Premakumara, G.A.S.; Abeysekera, W.K.S.M.; Ratnasooriya, W.D.; Chandrasekharan, N.V.; Benota, A.P. Antioxidant, anti-amylase and anti-glycation potential of brans of some Sri Lankan traditional and improved rice (Oryza sativa L.) varieties. J. Cereal Sci. 2018, 58, 451–456.

Priyangini, F.; Walde, S.G.; Chidambaram, R. Extraction optimization of pectin from cocoa pod husks (Theobroma cacao L.) with ascorbic acid using response surface methodology. Carbohydr. Polym. 2018, 202, 497–503.

Provisional State of the Global Climate in 2022. Available online: https://public.wmo.int/en/our-mandate/climate/wmo-statement-state-of-global-climate (accessed on 6 January 2023).

Qadir, R., Anwar, F., Gilani, M.A., Zahoor, S., Rehman, M.M., Mustaqeem, M. RSM/ANN based optimized recovery of phenolics from mulberry leaves by enzyme-assisted extraction. Czech J. Food Sci. 2019, 37(2), 99-105. doi:10.17221/147/2018-CJFS

Qiu, N.; Tian, Z.; Guo, Y.; Zhang, C.; Luo, Y.; Xue, Y. A first-principle study of calcium-decorated BC2N sheet doped by boron or carbon for High Hydrogen Storage. Int. J. Hydrogen Energy 2014, 39(17), pp. 9307–9320

Qu WH, Xu YY, Lu AH, Zhang ZQ, Li WC. Converting biowaste corncob residue into high value added porous carbon for supercapacitor electrodes. Bioresour. Technol. 2015, 189:285–91.

Rahman, S.; Jahan, R.; Rahmatullah, M. Effect of paddy husk extracts on glucose tolerance in glucose-induced hyperglycemic mice. World J. Pharm. Pharm. Sci. 2014, 8, 111–120.

Raji, Z.; Khodaiyan, F.; Rezaei, K.; Kiani, H.; Hosseini, S.S. Extraction optimization and physicochemical properties of pectin from melon peel. Int. J. Biol. Macromol. 2017, 98, 709–716.

Rambo, M.K.D.; Shmidt, F.L.; Ferreira, M.M.C. Analysis of the lignocellulosic components of biomass residues for biorefinery opportunities. Talanta 2015, 144, 696-703. https://doi.org/10.1016/j.talanta.2015.06.045

Ramesh, T.; Rajalakshmi, N.; Dhathathreyan, K.S. Activated Carbons Derived from Tamarind Seeds for Hydrogen Storage. J Energy Storage 2015, 4, 89–95, doi:10.1016/j.est.2015.09.005.

Rana, A.; Samtiya, M.; Dhewa, T.; Mishra, V.; Aluko, R.E. Health benefits of polyphenols: a concise review. J. Food Biochem. 2022, 46, e14264. Hppts://doi.org/10.1111/jfbc.14264

Rawat, S.; Wang, C.-T.; Lay, C.-H-; Hotha, S.; Bhaskar, T. Sustainable biochar for advanced electrochemical/energy storage applications. J. Energy Storage 2023, 63, 107115.

Re, R.; Pellegrini, N.; Proteggente, A.; Pannala, A.; Yang, M.; Rice-Evance, C. Antioxidant activity applying an improved ABTS radical cation decolorization assay. Free Radic. Biol. Med. 1999, 26, 1231–1237.

Rehman, A., T. Ahmad, R. M. Aadil, M. J. Spotti, A. M. Bakry, I. M. Khan, L. Zhao, T. Riaz, and Q. Tong. Pectin polymers as wall materials for the nano-encapsulation of bioactive compounds. Trends Food Sci. Technol. 2019, 90:35–46. doi: 10.1016/j.tifs.2019.05.015.

Righi, A.A.; Negri, G.; Salatino, A. Comparative chemistry of propolis from eight brazilian localities. Evid. Complement. Alternat. Med. 2013, 2013, 267878.

Rivadeneira, J.P.; Wu, T.; Ybanez, Q. Microwave-assisted extraction of pectin from "Saba" banana peel waste: Optimization, characterization, and rheology study. Int. J. Food Sci. 2020, 2020, 8879425.

Riza, M. and Dewi, M.I.Z.R. Pectin isolation from Sentu peel (*Sandorium Koetjape*) with microwave assisted extraction. Adv. Eng. Res. 2021, 203, 533-537.

Rodríguez Amado, I.; Franco, D.; Sánchez, M.; Zapata, C.; Vázquez, J.A. Optimization of antioxidant extraction from Solanum tuberosum potato peel waste by surface response methodology. Food Chem. 2014, 165, 290–299.

Rodríguez Robledo, V., and L. I. Castro Vázquez. 2020. Pectin - Extraction, Purification, Characterization and Applications. In M. A. Masuelli (Eds.), Pectins - Extraction, Purification, Characterization and Applications, 1–19. London, UK: ItechOpen. doi: 10.5772/intechopen.85588.

Rodsamran, P. and Sothornvit, R. Microwave heating extraction of pectin from lime peel: characterization and properties compared with the conventional heating method. Food Chem. 2019, 278, 364-372. https://doi.org/10.1016/j.foodchem.2018.11.067

Ruesgas-Ramón, M., Figueroa-Espinoza M. C., Durand, E. Application of Deep Eutectic Solvents (DES) for Phenolic Compounds Extraction: Overview, Challenges, and Opportunities. J. Agric. Food Chem. 2017, 65 (18), 3591–3601. doi:10.1021/acs.jafc.7b01054.

Saad, N., Louvet, F., Tarrade, S., Meudec, E., Grenier, K., Landolt, C., Ouk, T.S., Bressollier, P. Enzyme-Assisted Extraction of Bioactive Compounds from Raspberry (Rubus idaeus L.) Pomace. J. Food Sci. 2019, 84(6), 1371-1381. doi:10.1111/1750-3841.14625

Sadowska-Bartosz, I.; Galiniak, S.; Bartosz, G. Kinetics of glycoxidation of bovine serum albumin by glucose, fructose and ribose and its prevention by food components. Molecules 2014, 19, 18828–18849.

Saeidy, S.; Omidi, P.; Nasirpour, A.; Keramat, J. Physicochemical and functional properties of cross linked and high pressure homogenized sugar beet pectin: a comparative study. Food Hydrocoll. 2023, 134, 108041. https://doi.org/10.1016/j.foodhyd.2022.108041

Salima, B.; Seloua, D.; Djamel, F.; Samir, M. Structure of pumpkin pectin and its effect on its technologial properties. Appl. Rheol. 2022, 31, 34-55.

Samikannu, A.; Konwar, L.J.; Mäki-Arvela, P.; Mikkola, J.-P. Renewable N-Doped Active Carbons as Efficient Catalysts for Direct Synthesis of Cyclic Carbonates from Epoxides and CO2. Appl. Catal. B 2019, 241, 41–51, doi:10.1016/j.apcatb.2018.09.019.

Schaefer, S.; Jeder, A.; Sdanghi, G.; Gadonneix, P.; Abdedayem, A.; Izquierdo, M.T.; Maranzana, G.; Ouederni, A.; Celzard, A.; Fierro, V. Oxygen-promoted hydrogen adsorption

on activated and hybrid carbon materials, Int. J. Hydrog. Energy 2020, 45 (55, 30767–30782.

Senevirathne, I.G.N.H.; Abeysekera, W.K.S.M.; Abeysekera, W.P.K.M.; Jayanath, N.Y.; Premakumara Galbada Arachchige, S.; Wijewardana, D.C.M.S.I. Antiamylase, antiglucosidase, and antiglycation properties of millets and sorghum from Sri Lanka. Evid. Based Complemt. Alternat. Med. 2021, 2021, 5834915.

Senthil, C. and L., C.W. Biomass-derived biochar materials as sustainable energy sources for electrochemical energy storage devices. Ren. And Sust. Energ. Rew. 2021, 137, 110464.

Shaaban, A.; Se, S.-M.; Mitan, N.M.M.; Dimin, M.F. Characterization of Biochar Derived from Rubber Wood Sawdust through Slow Pyrolysis on Surface Porosities and Functional Groups. Procedia Eng. 2013, 68, 365–371, doi:10.1016/j.proeng.2013.12.193.

Shaaban, A.; Se, S.-M.; Mitan, N.M.M.; Dimin, M.F. Characterization of Biochar Derived from Rubber Wood Sawdust through Slow Pyrolysis on Surface Porosities and Functional Groups. Procedia Eng. 2013, 68, 365–371, doi:10.1016/j.proeng.2013.12.193.

Sharma, P., Vishvakarma, R., Gautam, K., Viman, A., Gaur, V. K., Farooqui, A., Varjani, S., Younis, k. Valorization of citrus peel waste for the sustainable production of value-added products. Bioresour. Technol. 2022, 351, 127064. https://doi.org/10.1016/j.biortech.2022.127064.

Shen, N.; Wang, T.; Gan, Q.; Liu, S.; Wang, L.; Jin, B. Plant flavonoids: classification, distribution, biosynthesis, and antioxidant activity. Food Chem., 2022, 383, 132531. https://doi.org/10.1016/j.foodchem.2022.132531

Shet, S.P.; Shanmuga Priya, S.; Sudhakar, K.; Tahir, M. A review on current trends in potential use of metal-organic framework for hydrogen storage, Int. J. Hydrog. Energy 2021, 46 (21), 11782–11803.

Shishir, M.R.I.; Karim, N.; Gowd, V.; Xie, J.; Zheng, X.; Chen, W. Pectin-chitosan conjugated nanoliposome as a promising delivery system for neohesperidin: Characterization, release behavior, cellular uptake, and antioxidant property. Food Hydrocoll. 2019, 95, 432–444.

Singh, G.; Maria Ruban, A.; Geng, X.; Vinu, A. Recognizing the Potential of K-Salts, Apart from KOH, for Generating Porous Carbons Using Chemical Activation. J. Chem. Eng. 2023, 451, 139045, doi:10.1016/j.cej.2022.139045.

Spinei, M. and Oroian, M. Microwave-assisted extraction of pectin from grape pomace. Scientific report 2022, 12, 12722. https://doi.org/10.1038/s41598-022-16858-0

Spratt, O.; Suri, R.; Deutsch, J. Defining upcycled food products. J. Culin. Sci. Technol. 2020. https://doi.org/10.1080/15428052.2020.1790074

Sreńscek-Nazzal, J.; Kiełbasa, K. Advances in Modification of Commercial Activated Carbon for Enhancement of CO2 Capture. Appl. Surf.. Sci 2019, 494, 137–151, doi:10.1016/j.apsusc.2019.07.108.

Stadie, N.P., purewall, J.J.; Ahn, C.C.; Fultz, B. Measurments of hydrogen spillover in platinum doped superactivated carbon. Langimur 2010, 15481-15485. https//doi.org/10.1021/la9046758

Stochmal, A.; Simonet, A.M.; Marcias, F.A.; Oleszek, W. Alfalfa (Medicago sativa L.) flavonoids. 2. Tricin and chrysoeriol glycosides from aerial parts. J. Agric. Food Chem. 2001, 49, 5310–5314.

Sun, Y.; Webley, P.A. Preparation of Activated Carbons from Corncob with Large Specific Surface Area by a Variety of Chemical Activators and Their Application in Gas Storage. J. Chem. Eng. 2010, 162, 883–892, doi:10.1016/j.cej.2010.06.031.

Taamalli, A.; Arráez-Román, D.; Abaza, L.; Iswaldi, I.; Fernández-Gutiérrez, A.; Zarrouk, M.; Segura-Sarretero, A. LC-MS- based metabolite profiling of methanolic extracts from medicinal and aromatic species Mentha pulegium and Origanum majorana. Phytochem. Anal. 2015, 26, 320–330.

Tan, X-f.; Liu, Y-g.; Gu, Y-l.; Zeng, X.-jiang, H.; Wang, X.; Liu, S.-h.; Jiang, L-h. Biochar as potential sustainable precursors for activated carbon production: multiple application in environmental protection and energy storage. Biores. Techn. 2017, 227, 359-372.

Tang, J.; Dunshea, F.R.; Suleria, H.A.R. LC-ESI-QTOF/MS characterization of phenolic compounds from medicinal plants (hops and juniper berries) and their antioxidant activity. Foods 2020, 9, 7.

Tapia-Quirós, P.; Montenegro-Landívar, M.F.; Reig, M.; Vecino, X.; Cortina, J.L.; Saurina, J.; Granados, M. Recovery of polyphenols from agri-food by-products: the olive oil and winery industries cases. Foods 2022, 11, 362. https://doi.org/10.3390/foods11030362

Thepthanee, C.; Liu, C.-C.; Yu, H.-S.; Huang, H.-S.; Yen, C.-H.; Li, Y.-H.; Lee, M.-R.; Liaw, E.-T. Evaluation of phytochemical contents and in vitro antioxidant, anti-inflammatory, and anticancer activities of black rice leaf (Oryza sativa L.) extract and its fractions. Foods 2021, 10, 2987.

Tian, Q.; Wang, X.; Xu, X.;Zhang, M; Wang, L.; Zhao, X.:,An, Z.; Yao, H.;,Gao, J. A novel porous carbon material made from wild rice stem and its application in supercapacitors. Mater. Chem. Phys. 2018, 213, 267–76.

Torkova, A.A; Lisitskaya, K.V.; Filimonov, I.S.; Glazunova, O.A.; Kachalova, G.S.; Golubev, V.N.; Fedorova, T.V. Physicochemical and functional properties of Cucurbita maxima pumpkin pectin and commercial citrus and apple pectins: a comparative evaluation. PLoS ONE 2018, 13 (9), e0204261. https://doi.org/10.1371/journal.pone.0204261

Torkova, A.A.; Lisitskaya, K.V.; Filimonov, I.S. Physicochemical and functional properties of Cucurbita maxima pumpkin pectin and commercial citrus and apple pectins: A comparative evaluation. PLoS ONE 2018, 13, e0204261.

Tran, P.H.I.; Duan, W.; Lee, B.-J.; Tran, T.T.D. Drug stabilization in the gastrointestinal tract and potential applications in the colonic delivery of oral zein-based formulations. Int. J. Pharm. 2019, 569, 118614. https:/doi.org/10.1016/j.ijpharm.2019.118614

Tranfić Bakić, M.; Pedisić, S.; Zorić, Z.; Dragović-Uzelac, V.; Ninčević Grassino, A. Effect of microwave-assisted extraction on polyphenols recovery from tomato peel waste. Acta Chim. Solv. 2019, 66, 367–377.

Týskiewicz, K., Konkol, M., Rój, E. The Application of Supercritical Fluid Extraction in Phenolic Compounds Isolation from Natural Plant Materials. Molecules 2018, 23(10), 2625. doi: 10.3390/molecules23102625.

United nation site(https://www.un.org/en/global-issues/population#:~:text=Our%20growing%20population&text=The%20world%27s%20population%20is%20expected,billion%20in%20the%20mid%2D2080s

United Nations Environment Programme. Food Waste Index Report; 2021, Nairobi.

Upcycled food association and Upcycled food foundation, Impact Report; 2022. Accelerating the upcycled food economy.

Uwineza, P.A., Waśkiewicz, A. Recent advances in supercritical fluid extraction of natural bioactive compounds from natural plant materials. Molecules 2020, 25(17), 3847. doi:10.3390/molecules25173847

Velinchova, S.; Foubert, K.; Pieters, L. Natural products as a source of inspiration for novel inhibitors on advanced glycation end products (AGEs) formation. Planta Med. 2021, 87, 780–802.

Vella, F.M.; Cautela, D.; Laratta, B. Characterization of polyphenolic compounds in Cantalupe melon by-products. Foods 2019, 8, 196. doi:10.3390/foods8060196

Vieira, V.; Prieto, M.A.; Barros, L.; Coutinho, J.A.P.; Ferreira, O.; Ferreira, I.C.F.R. Optimization and comparison of maceration and microwave extraction systems for the production of phenolic compounds from Juglans regia L. for the valorization of walnuts leaves. Ind. Crops Prod. 2017, 107, 341–352.

Vilas-Boas,A.A.;Pintado, M.; Oliveira, A.L.S. Natural Bioactive Compounds from Food Waste: Toxicity and Safety Concerns. Foods 2021,10,1564. https://doi.org/ 10.3390/foods10071564

Waldbauer, K.; McKinnon, R.; Kopp, B. Apple pomace as potential source of natural active compounds. Planta Med. 2017, 83, 994-1010. https://doi.org/10.1055/s-0043-111898

Wang Z.; Shen, D.; Wu, C.; Gu, S. State of the art on the production and application of carbon nanomaterials from biomass. Green Chem. 2018, 20, 5031–57.

Wang, D.; Jiang, P.; Zhang, H.; Yuan, W. Biochar Production and Applications in Agro and Forestry Systems: A Review. Sci. Total Environ. 2020, 723, 137775, doi:10.1016/j.scitotenv.2020.137775.

Wang, G.; Liang, R.; Liu, L.; Zhong, B. Improving the specific capacitance of carbon nanotubes-based supercapacitors by combining introducing functional groups on carbon nano- tubes with using redox-active electrolyte. Electrochim. Acta 2014, 115, 183–188.

Wang, R.; Khalifa, I.; Du, X.; Li, K.; Xu, Y.; Li, C. Effects of anthocyanins on β-lactoglobulin glycoxidation: A study of mechanisms and structure-activity relationship. Food Funct. 2021, 12, 10550–10562.

Wang, Z.; Cao, J.; Wang, J. Pyrolytic Characteristics of Pine Wood in a Slowly Heating and Gas Sweeping Fixed-Bed Reactor. J. Anal. Appl. Pyrolysis 2009, 84, 179–184, doi:10.1016/j.jaap.2009.02.001.

Wang, Z.; Li, C.; Domen, K. Recent Developments in Heterogeneous Photocatalysts for Solar-Driven Overall Water Splitting. Chem. Soc. Rev. 2019, 48, 2109–2125, doi:10.1039/C8CS00542G.

Weber, K.; Quicker, P. Properties of Biochar. Fuel 2018, 217, 240–261, doi:10.1016/j.fuel.2017.12.054.

Wongkaew, M.; Chaimongkol, P.; Leksawasdi, N. Mango peel pectin: Recovery, functionality and sustainable uses. Polymers 2021, 13, 3898.

Wu XL, Wen T, Guo HL, Yang S, Wang X, Xu AW. Biomass-derived sponge-like carbonaceous hydrogels and aerogels for supercapacitors. ACS Nano 2013;7: 3589–97.

Xia B., Yan, D., Bai, Y., Xie, J., Cao, Y., Liao, D., Lin, L. Determination of phenolic acids in Prunella vulgaris L.: A safe and green extraction method using alcohol-based deep eutectic solvents. Anal. Methods 2015, 7 (21), 9354–9364. https://doi.org/10.1039/C5AY02035B.

Xiao, Y.; Dong, H.; Long, C.; Zheng, M.; Lei, B.; Zhang, H.; Liu, Y. Melaleuca bark based porous carbons for hydrogens storage. Int. J. Hydrog. Energy 2014, 39, 11661-11667.https://doi.org/10.1016/j.ijhydene.2014.05.134

Xie, F.; Zhang, W.; Lan, X.; Gong, S.; Wu, J.; Wang, Z. Effects of high hydrostatic pressure and high pressure homogenization processing on characteristics of potato peel waste pectin. Carbohydr. Polym. 2018, 196, 474–482.

Xu, D.P., Li, Y., Meng, X., Zhou, T., Zhou, Y.; Zheng, J.; Zhang, J.-J., Li, H.-B. Natural antioxidants in foods and medicinal plants: Extraction, assessment and resources. Int. J. Mol. Sci. 2017, 18(1), 96. doi:10.3390/ijms18010096

Yan, W., X. Jia, Q. Zhang, H. Chen, Q. Zhu, and L. Yin. 2021. Interpenetrating polymer network hydrogels of soy protein isolate and sugar beet pectin as a potential carrier for probiotics. Food Hydrocoll. 2021, 113, 106453. doi: 10.1016/j.foodhyd.2020.106453.

Yang, H.; Yan, R.; Chen, H.; Lee, D.H.; Zheng, C. Characteristics of Hemicellulose, Cellulose and Lignin Pyrolysis. Fuel 2007, 86, 1781–1788, doi:10.1016/j.fuel.2006.12.013.

Yang, H.; Yan, R.; Chen, H.; Lee, D.H.; Zheng, C. Characteristics of Hemicellulose, Cellulose and Lignin Pyrolysis. Fuel 2007, 86, 1781–1788, doi:10.1016/j.fuel.2006.12.013.

Yang, R.; Liu, G.; Li, M.; Zhang, J.; Hao, X. Preparation and N2, CO2 and H2 Adsorption of Super Activated Carbon Derived from Biomass Source Hemp (Cannabis Sativa L.) Stem. Microporous and Mesoporous Mater. 2012, 158, 108–116, doi:10.1016/j.micromeso.2012.03.004.

Yeboah, M.L.; Li, X.; Zhou, S. Facile fabrication of biochar from palm kernel Shell waste and its novel application to magnesium-based materials for hydrogen storage, Materials 2020, 13, 625.

Yoo,S.-H.; Lee, B.-H.; Lee, H.; Lee, S.; Bae, I.Y.; Lee, H.G.; Fishman, M.L.; Chau, H.K., Savary, B.J., Arland, T.; Hotchkiss, J. Structural characteristics of pumpkin pectin extracted by microwave heating. J. Food Sci. 2012, 77, 11. DOI: 10.1111/j.1750-3841.2012.02960.

Yuan X.; Dissanayake P.D.; Gao B.; Liu W.J.; Lee K.B.; Ok, Y.S. Review on upgrading organic waste to value-added car- bon materials for energy and environmental applications. J Environ. Manage 2021, 296, 113128.

Zhang, J.Q.; Hou, Q.H.; Guo, X.T.; Yang, X.L. Modified MgH2 hydrogen storage properties based on grapefruit Peel-derived biochar, Catalysts 2022, 12 (5).

Zhang, L.-S.; Wang, X.; Dong, L.-L. Antioxidant and antiglycation of polysaccharides from Misgurnus anguillicaudatus. Food Chem. 2011, 124, 183–187.

Zhang, Q.; Han, K.; Li, S.; Li, M.; Li, J.; Ren, K. Synthesis of garlic skin-derived 3D hierarchical porous carbon for high-performance supercapacitors. Nanoscale 2018, 10, 2427–37.

Zuorro, A.; Lavecchia, R.; González-Delgado, Á.D.; García-Martinez, J.B.; L'Abbate, P. Optimization of enzyme-assisted extraction of flavonoids from Corn Husks. Processes 2019, 7,11. doi:10.3390/pr7110804

Züttel, A. Materials for hydrogen storage. Materials today 2003, 25-33.

7. PUBLICATIONS

1. Colombo, R.; Ferron, L.; Frosi, I.; Papetti, A. Advances in static *in vitro* digestion models after the COST action Infogest consensus protocol. *Food & Funct.* 2021, 12, 7619.

2. Frosi, I.; Montagna, I.; Colombo, R.; Milanese, C.; Papetti, A. Recovery of chlorogenic acids from agri-food wastes: updates on green extraction techniques. *Molecules* 2021, 26, 4515.

3. Frosi, I.; Ferron, L.; Colombo, R.; Papetti, A. Natural carriers: recent advances in their use to improve the stability and bioaccessibility of food active compounds. *Crit. Reviews Food Sci. Nutr.* 2022.

4. Marchetti, L.; Truzzi, E.; Frosi, I.; Papetti, A.; Cappellozza, S.; Saviane, A.; Pellati, F.; Bertelli, D. In vitro bioactivity evaluation of mulberry leaf extracts as nutraceutucals for the management of diabetes mellitus. *Food Funct.* 2022, 13, 4344-4359.

5. Frosi, I., Vallelonga, D., Colombo, R., Milanese, C.; Papetti, A. Valorization of Rice Husk (Oryza sativa L.) as a Source of In Vitro Antiglycative and Antioxidant Agents. *Foods* 2023., 12, 529. https://doi.org/10.3390/foods12030529.

6. Colombo, R.; Paolillo, M.; Ferron, L.; Frosi, I.; Papetti, A. Effect of the simulated digestion process on the chlorogenic acid trapping activity against methylglyoxal. *Food & Funct.* 2023, 14, 541.

7. Frosi, I.; Balduzzi, A.; Moretto, G.; Colombo, R.; Papetti, A. Towards valorization of food-derived pectin: recent advances on their characterization and application. *Molecules* 2023, 28, 6390.

8. Papetti, A.; Colombo, R.; Valleloonga, D.; Frosi, I.; Milanese, C. Methods in ethnopharmacology: phytochemical extraction, isolation and detection techniques. In Adnan, M.; Patel, M.; Snoussi, M. *Ethnobotany and ethnopharmacology of medicinal and aromatic plants* 2023*,* pp. 229-255.

9. Colombo, R.; Cavalloro, V.; Papetti, A.; Frosi, I.; Rossi, D.; Collina, S.; Martino, E.; Linciano, P. Chapter 20, Evolving challenges and opportunities in plant-based drug discovery and development. *E* In Adnan, M.; Patel, M.; Snoussi, M. *Ethnobotany and ethnopharmacology of medicinal and aromatic plants* 2023*,* pp. 379-413.

10. Frosi, I.; Balduzzi, A.; Colombo, R.; Milanese, C.; Papetti, A. recovery of polyphenols from corn cob (Zea mays L.): optimization of different green extraction methods and efficiency comparison. *Food and Bioprod. Process.* 2024, 143, pp.212-220.

11. Colombo, R.; Pellicorio, V.; Barberis, M.; Frosi, I.; Papetti, A. Recent advances in the valorization of seed wastes as source of bioactive peptides with multifunctional properties. *Trends in Food Sci. & Technol.* 2024, 144, 104322.

12. Colombo, R.; Moretto, G:; Barberis, M.; Frosi, I.; Papetti, A. Rice by-product compounds: from green extraction to antioxidant properties. *Antioxidant*, 2024, 13, 35.

13. Burlacchini, G.; Sandri, A.; Papetti, A.; Frosi, I.; Boschi, F.; Lleo, M.M.; Signoretto, C. Evaluation of antibacterial and antibiofilm activity of rice husk extract against *Staphylococcus aureus*. *Pathogens* 2024, 13, 80.

Submitted

14. Frosi, I.; Colombo, R.; Milanese, C.; Papetti, A. Preliminary studies on the bioaccessibility of a rice husk-based ingredient. Submitted to *J. Food Sci. and Technol.*

15. Colombo, R.; Frosi, I.; Papetti, A. Chapter, "Food protein digestion by in vitro static approaches" in book "Protein digestion-derived peptides", *Elsevier,* in press.

This project is founded by Cariplo Foundation, GHELF project 2019-2125